Sequence Stratigraphy, Porosity, and Primary Producers of the Middle to Late Devonian Canol Formation, Northwest Territories, Canada

by

Maya Tessalie LaGrange Rao

A thesis submitted in partial fulfillment of the requirements for the degree of

Doctor of Philosophy

Department of Earth and Atmospheric Sciences

University of Alberta

Abstract

The Devonian Canol Formation of the Northwest Territories (NWT) is an organic-rich mudstone interval deposited in a tropical marine setting along the west coast of Ancestral North America. This unit preserves a record of local marine conditions in the Middle to Late Devonian, a time characterized by successive global marine biodiversity crises and widespread deposition of fine-grained, organic-rich sediment. The Canol Formation is also of economic significance because it sourced the oil conventionally produced from the carbonate units at Norman Wells (NWT) and has potential as an unconventional reservoir. This thesis dissertation contributes to our understanding of the local oceanographic conditions at the time the Canol Formation was deposited and of the unconventional resource potential of this interval. Data was collected from cores in the Central Mackenzie Valley (NWT) and outcrops in the Mackenzie Mountains (NWT) where the Canol Formation is included in the Horn River Group (HRG), which also comprises the underlying Hare Indian and Ramparts Formations.

Chapter 1 introduces the Canol Formation and the research objectives. Chapter 2 investigates the stable C and N isotopic profile of the Canol Formation and surrounding units. Through the interpretation of $\delta^{13}C_{org}$ ($\delta^{13}C$ of organic matter) and $\delta^{15}N_{bulk}$ (whole rock $\delta^{15}N$) values, I show that primary producers were dominantly diazotrophic (N_2 fixing) throughout deposition of the HRG and that biological productivity varied through time as the Canol Formation accumulated. Through a synthesis of existing paleoredox interpretations and comparison to the modern, I also propose that episodic weak oxygenation of euxinic bottom waters during deposition of the Horn River Group could be produced by climatic variations causing periodic downwards migration of the upper OMZ boundary. These results contribute to

our understanding of marine conditions in the study area, which adds to the growing body of research focused on the Middle to Late Devonian oceans.

Chapter 3 is an evaluation of porosity in the HRG relating to resource evaluation. Pores are characterized through scanning-electron microscope (SEM) imaging and quantified by bulk porosity measurements and N_2 adsorption and desorption experiments. Relative to many other North American unconventional reservoirs, the Canol Formation and Bluefish Member of the Hare Indian Formation have similar bulk porosity, lower mesopore volume, and are dominated by mineral matrix pores, rather than organic matter pores. A comparison of porosity with mineralogy, lithofacies, and total organic carbon (TOC) shows that high quartz and low clay content are the best predictors of high porosity. Ultimately, this chapter further characterizes the properties and distribution of potential reservoir units in the HRG of the Central Mackenzie Valley.

In Chapter 4, I review the application of chemostratigraphic datasets to sequence stratigraphic interpretations in organic-rich, marine mudstone units. A synthesis of previous studies shows that the maximum flooding surface (MFS) and maximum regressive surface (MRS) have distinct chemostratigraphic signatures, allowing for delineation of the transgressive systems tract (TST) and regressive systems tract (RST). This review concludes that chemostratigraphic datasets are useful for the identification of transgressive-regressive (T-R) cycles. However, chemostratigraphic criteria do not yet exist to identify the basal surface of forced regression or the correlative conformity, which precludes subdivision of normal and forced regressions. The implications are that the highstand systems tract, lowstand systems tract, and forced regressive systems tract cannot be distinguished from one another based on chemostratigraphy alone.

Chapter 5 presents a sequence stratigraphic framework for the Horn River Group, primarily based on high-resolution chemostratigraphic profiles of Al, Si, and Ti. This interpretation comprises six complete T-R cycles from the base of the Horn River Group to the lower section of the overlying Imperial Formation. Redox-sensitive trace metals Mo and V are most enriched at or near MFS, suggesting that the most reducing conditions in the sediment and bottom waters coincided with the highest rates of relative sea level rise. I further demonstrate that this pattern in Mo and V is associated with unrestricted marine settings, supporting the preexisting hypothesis that the Horn River Group depositional setting was oceanographically open. The framework presented in Chapter 5 allows for mapping of higher reservoir quality (more siliceous) MFS and illustrates fluctuations in sedimentation, accommodation, and redox as the HRG was deposited. Chapter 6 summarizes the key conclusions and future research directions.

Preface

This is a journal-article-style dissertation, with chapters 2–5 comprising original research in the form of published articles and manuscripts in preparation. For all chapters, I was the primary researcher responsible for literature synthesis, project design, data collection, analysis, interpretation, and manuscript preparation. Drs. Murray Gingras and Kurt Konhauser provided supervision and guidance for all chapters of this thesis. Bibliographic information and details about each article are outlined below.

Chapter 2 will be submitted to *Palaeogeography, Palaeoclimatology, Palaeoecology* in August of 2022. The authors are as follows: LaGrange, M.T., Li, K., Li, L., Kabanov, P., Konhauser, K.O, Harris, B.S., Biddle, S.K., Terlaky, V., and Gingras, M.K. I oversaw project design, sample collection and preparation, data analysis, and interpretation. K. Li helped with data collection for one of the cores and the dataset for the other core was contributed by P. Kabanov from the Geological Survey of Canada. B.S. Harris, R. Ignacio, and M. Kehler helped with sample preparation. The manuscript text and figures were drafted by me, and all co-authors contributed to the manuscript preparation.

Chapter 3 has been published in *Marine and Petroleum Geology* as: LaGrange, M.T., Atienza, N.M.M., Biddle, S.K., Harris, B.S., Fiess, K.M., Terlaky, V., Konhauser, K.O. and Gingras, M.K., 2022. The nature, origin, and predictors of porosity in the Middle to Late Devonian Horn River Group of the Central Mackenzie Valley, Northwest Territories, Canada. Mar. Pet. Geol. 142, 105738. My responsibilities included project design, data collection and analysis, interpretation, and manuscript preparation. As an undergraduate, N.M.M Atienza assisted with a subset of the data collection and data analysis for her directed study project. Sara Biddle helped with scanning electron microscope data collection. B.S. Harris and S.

Dhiman assisted with multivariate statistical analysis. The X-ray diffraction mineralogical dataset was donated by Husky Energy. All authors contributed to the manuscript.

Chapter 4 has been published in *Earth-Science Reviews* as: LaGrange, M.T., Konhauser, K.O., Catuneanu, O., Harris, B.S., Playter, T.L. and Gingras, M.K., 2020. Sequence stratigraphy in organic-rich marine mudstone successions using chemostratigraphic datasets. Earth-Sci. Rev. 203, 103137. For this review paper, I summarized the existing literature on the topic, synthesized the key findings to date, and provided suggestions for future research directions. I prepared the manuscript with contributions from all co-authors.

Chapter 5 will be submitted to the AAPG Bulletin in Autumn 2022. The authors will be as follows: LaGrange, M.T., Harris, B.S., Biddle, S.K., Dhiman, S. Catuneanu, O., Konhauser, K.O., Terlaky, V., and Gingras, M.K. I was responsible for project design, sample collection including fieldwork, sample preparation, data collection and analysis, interpretation, and preparation of the manuscript. S. Lybbert, N. Atienza, R. Ignacio, M. Kehler, S. Sigstad, and D. Baker assisted with sample preparation. B.S. Harris and D. Frayn assisted with data collection and S. Dhiman helped with multivariate statistical analysis in R. The manuscript was prepared by me with contributions from all co-authors.

For Grandma Wendy, whose bowl of rocks and curiosity about the world inspired my interest in Earth sciences, and for Grandma Annette, who showed me that this is possible.

Acknowledgments

First, I am incredibly grateful to Murray and Kurt for their immeasurable support throughout this process. I cannot thank them enough for their guidance at every step of the way. I am also appreciative of the help from Long Li, Octavian Catuneanu, Tiffany Playter, and John Duke. Working as a field assistant for Dave Herbers inspired me to pursue a graduate degree and I am grateful for his mentorship. Thank you to the NTGS crew (Kathy, Viktor, and Jonathan) for their collaboration on my project. Fieldwork would not have been the same without Viktor and Jonathan's careful planning, contributions to Fieldopoly, and assistance in consuming the accidental twelve lbs of bananas (which led to the discovery of orzapony). Thank you to Pavel Kabanov from the GSC, his collaboration on my second chapter was immensely helpful. I am also forever indebted to those who spent time powdering samples: thank you so much Skye Lybbert, Nicole Atienza, Rizal Ignacio, Marcus Kehler, Sheridan Sigstad, Adam LaRivere, and Daniel Baker.

There are so many students who have impacted my Ph.D. experience, and I will name just a few. Sara, you are a wonderful person and inspiring colleague, thank you for your contributions to my Ph.D. and for so many fun times at conferences and on fieldwork. Scott, I have greatly appreciated our office/field conversations over the years and will be eternally grateful for the time you spent making the oreo ranking spreadsheet. Brette, I seriously don't know where to begin. There is so much to say, most of which I will save for another time, but here are a few of my thoughts. You are the best person to chat with over a beer, a great scientist, and an exceptional friend. Working together has made every grad school hurdle more manageable, and most importantly, more fun. Thank you for all your advice, empathy, and help over the past six years.

I am also grateful to everyone in the lunch group (and particularly Murray, Brette, and Scott) for participating in endless food-centric debates about the best type of oreo, pie, or pizza topping. Because of these lunches, I look forward to coming into the office every single day. Thank you to the 2016 IRG crew for welcoming me into their group (Dave, Eric, Carolyn, Aimee, Donald, and Derek) and to Sara, Scott, Matt, Cole, Dan, Jared, and Brette for keeping the IRG lively over the past few years. It is so exciting to be part of the new ichnology Geobiology Observational Division alongside Arzu, Maria, Dani, Baptiste, Jen, Kelly, Cody, Jason, Drew, Katey (and her baking), Riley, Scott, Brette, and many others. The iGod Casseroff was unforgettable and impressively delicious! Thanks to all these people, I will look back on these years as some of the best of my life.

My friends and family have shown me unwavering support, without which I would not be writing this thesis. Nicole, Ashley, Alex, Celine, Jamie, Alia, Jenny, Anna, and Dani: your intelligence and humour are inspiring, and you keep things in perspective by reminding me that there is a world beyond grad school. The tremendous support I felt from my parents (Dad, Olivia, Mom), my sister Stella, my grandparents, and aunts and uncles gave me the strength to pursue this degree. My Mom also deserves a massive thank you for all the applications she has edited over the past six years.

Lastly and maybe most importantly, thank you to Murray for showing me that nobody is too busy for lunch, and to Kurt for showing me that nobody is too busy for Friday beers. Having supervisors who cultivate such a strong sense of lab group community has made all the difference.

Table of Contents

List of Tables

List of Figures

Chapter 1: Introduction

1.1 Organic-rich mudstone intervals

The term 'black shale' is often used to describe dark-coloured, organic-rich, fine-grained sedimentary intervals, with organic content commonly ranging from 1–15 wt. % (Stow et al., 1996; Nichols, 2009). In this thesis, 'organic-rich mudstone' will be used instead, as 'shale' has been used with a wide variety of meanings, sometimes referring to fine-grained sedimentary rocks in general and other times used specifically for fissile fine-grained intervals (Wignall, 1994; Lazar et al., 2015). Here, 'mudstone' is used as a general term referring to all fine-grained sedimentary rocks and is defined as a rock composed of greater than fifty percent silt and clay size grains following Lazar et al. (2015).

Organic-rich mudstone intervals are geographically and temporally widespread and of economic significance because they are the primary source of oil and gas worldwide (Tourtelot, 1979; Klemme and Ulmishek, 1991; Wignall, 1994). Historically, organic-rich mudstone successions were studied for their macrofossil content or to understand their hydrocarbon source rock potential, which involved assessing thermal maturity, kerogen type, and total organic carbon (TOC), as well as the correlation of migrated oils through organic geochemistry (e.g., Peters and Cassa, 1994). Because these units typically lack features such as large-scale sedimentary structures or trace fossils, and they may not exhibit variations in grain size that can readily be observed at core or outcrop scale, these units were until recently viewed as largely homogenous intervals with little variation in character or composition. Moreover, it has commonly been assumed that organic-rich mudstone intervals accumulate by slow suspension settling of particles in environments characterized by low hydraulic energy, significant water depth, and an absence of dissolved O_2 (Schieber, 2003; Macquaker and Bohacs, 2007; Lazar et

al., 2015). Owing to advances in drilling technology and analytical techniques used to study mudstone successions, this view has shifted in recent years (Egenhoff and Fishman, 2013; Turner et al., 2015; Lazar et al., 2015).

The development of horizontal drilling and hydraulic fracturing has allowed fine-grained, organic-rich sedimentary units to be viewed as hydrocarbon reservoirs rather than only oil sources and reservoir trapping seals, thus sparking new academic and industry interest in the properties of these units. Organic-rich mudstone units have also generated interest because they can provide insight into past oceanography (e.g., paleoredox, paleoecology) and carbon cycling (e.g., Meyers, 2006; Scott et al., 2008; Kendall et al., 2010). Moreover, several advances in analytical technology have allowed for more detailed studies of mudstone intervals. Advances in energy-dispersive x-ray fluorescence (ED-XRF) allowing for better detection limits and instrument portability permitted quantitative whole-rock geochemical composition to be obtained rapidly, in-situ and at a high-resolution (Rowe et al., 2012).

Recently developed methods for investigating mudstone intervals also include chemostratigraphy, which involves characterization and correlation of sedimentary units based on whole-rock geochemical properties (Pearce et al., 1999; Ratcliffe et al., 2010), and micro-scale facies and ichnological analysis conducted through petrographic observations and scanning electron microscopy (e.g., Biddle et al., 2021; Egenhoff and Fishman, 2013). Today, such techniques are used to provide insight to the environmental conditions under which organic-rich intervals accumulate and enable detailed lithostratigraphic and sequence stratigraphic mapping of these units (Schieber, 1994; Egenhoff and Fishman, 2013; Zhou et al., 2011; Sano et al., 2013; Borcovsky et al., 2017).

1.2 The Canol Formation

This thesis focuses on the Devonian Canol Formation, an organic-rich mudstone present in the Central Mackenzie Valley and Mackenzie Mountains, Canada (Fig. 1.1), which was deposited along the margin of Ancestral North America in the tropics near the equator (Fig. 1.2; Cocks and Torsvik, 2011; Scotese, 2014; Scotese and McKerrow, 1990). The Canol Formation is the source rock for the oil produced conventionally from the reef buildups of the Devonian Ramparts Formation at Norman Wells, Northwest Territories (Snowdon et al., 1987). Within the past decade, interest has shifted to the unconventional reservoir potential of the Canol Formation, with a preliminary estimate by the National Energy Board and the Northwest Territories Geological Survey reporting 145 billion barrels of oil in place (NEB and NTGS, 2015). The Canol Formation also preserves a record of oceanographic conditions in the Middle to Late Devonian, a time in Earth history characterized by the widespread deposition of fine-grained, organic-rich sediment and a series of global biodiversity crises in the marine realm (e.g., Becker et al., 2020; Klemme and Ulmishek, 1991; Walliser, 1996).

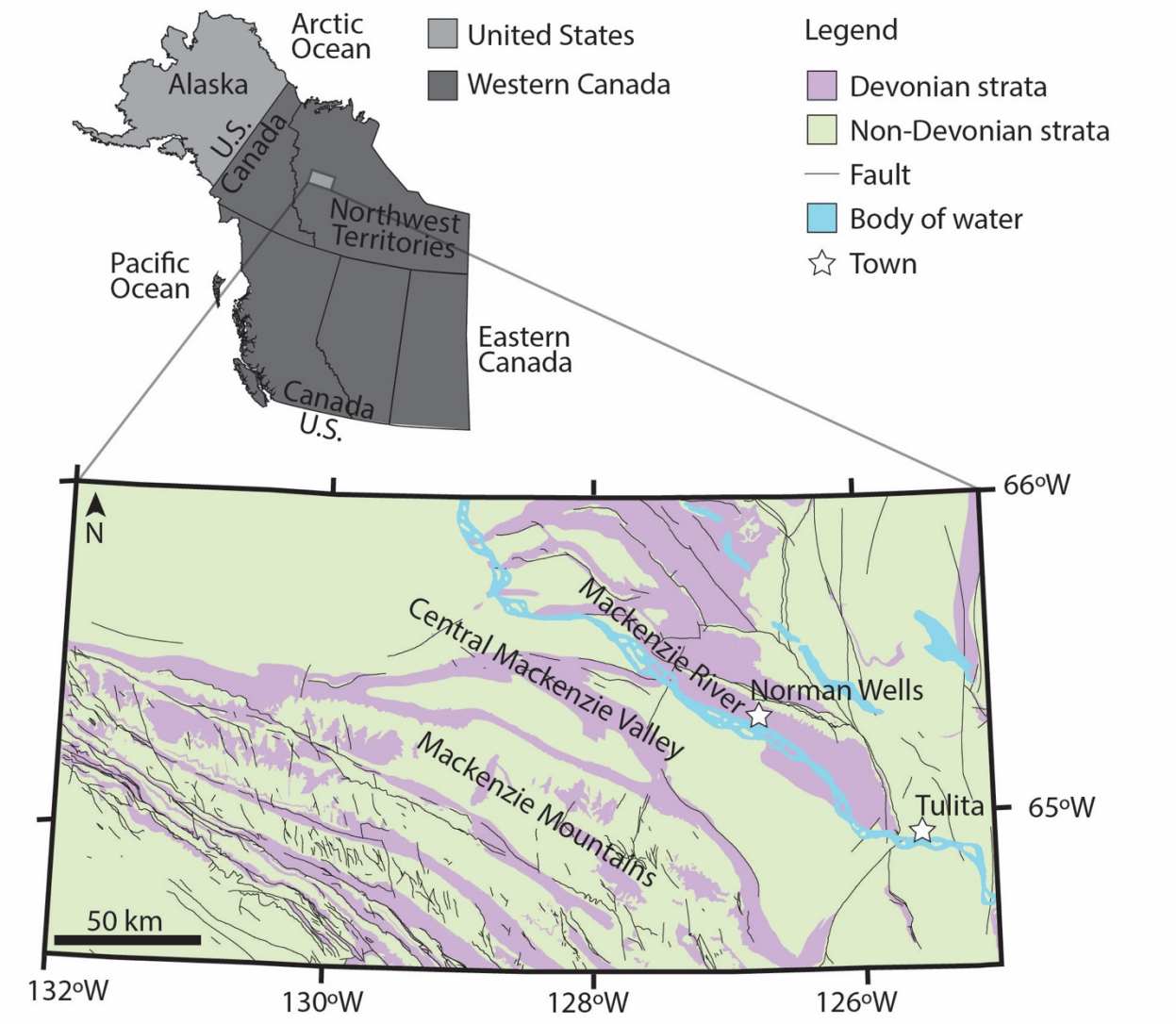

Figure 1.1 Geological map of the study area in the Central Mackenzie Valley and adjacent Mackenzie Mountains of the Northwest Territories, Canada. Modified from Irwin (2020).

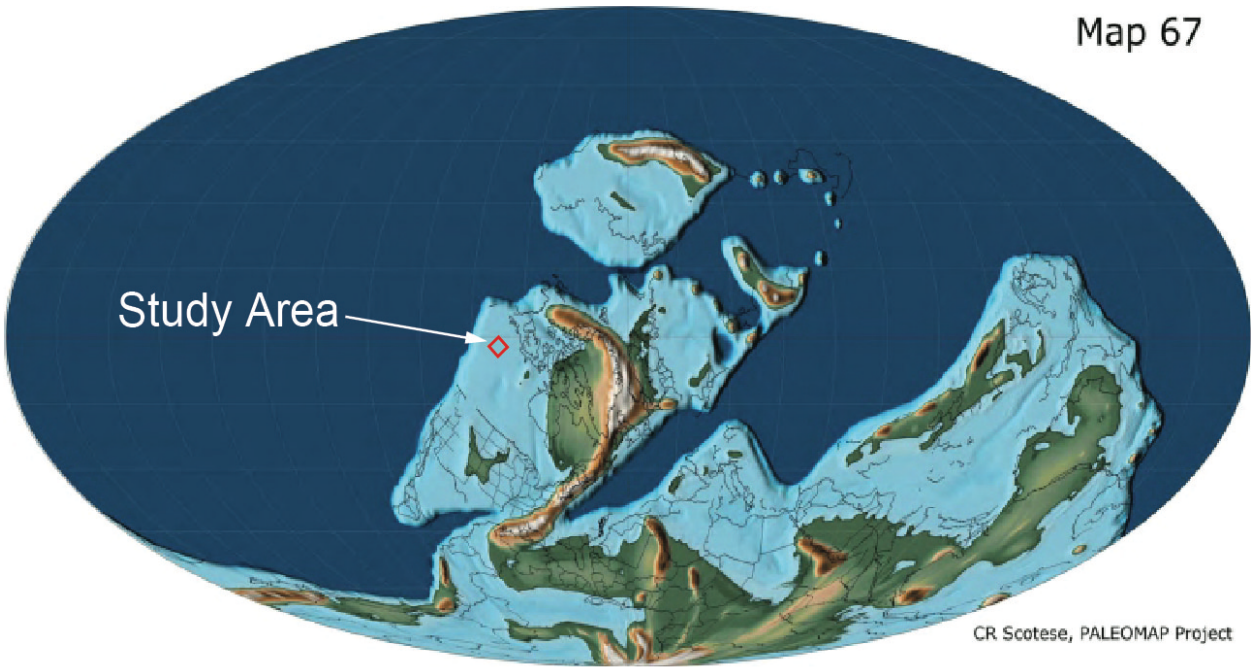

Figure 1.2 A global paleogeographic reconstruction for the Late Devonian, which illustrates the position of the study area just south of the equator. Modified from (Scotese, 2014).

The Canol Formation is included in the Middle to Late Devonian Horn River Group, which consists of a mixed mudstone and carbonate succession that comprises the Hare Indian, Ramparts, and Canol Formations (Fig. 1.2; Pugh, 1983; Pyle and Gal, 2016). Laterally, the Canol Formation has been observed northward up to approximately 68 °N, south to Ram River in the Northwest Territories (~60 °N). It has an erosional edge to the east of the Mackenzie River in the Northwest Territories (~127 °W) and can be traced westward to Snake River in the Yukon (~132 °W), after which the formations present in the Horn River Group become difficult to differentiate (Basset, 1961; Pugh, 1983). The Canol Formation was first named and defined by Basset (1961)

as the formation that overlies the Ramparts Formation. However, with two exceptions: (a) in some locations where the Ramparts Formation is thickest, the Canol Formation may not be present, (b) the Canol Formation directly overlies the Hare Indian Formation where the Ramparts Formation is absent (Basset, 1961).

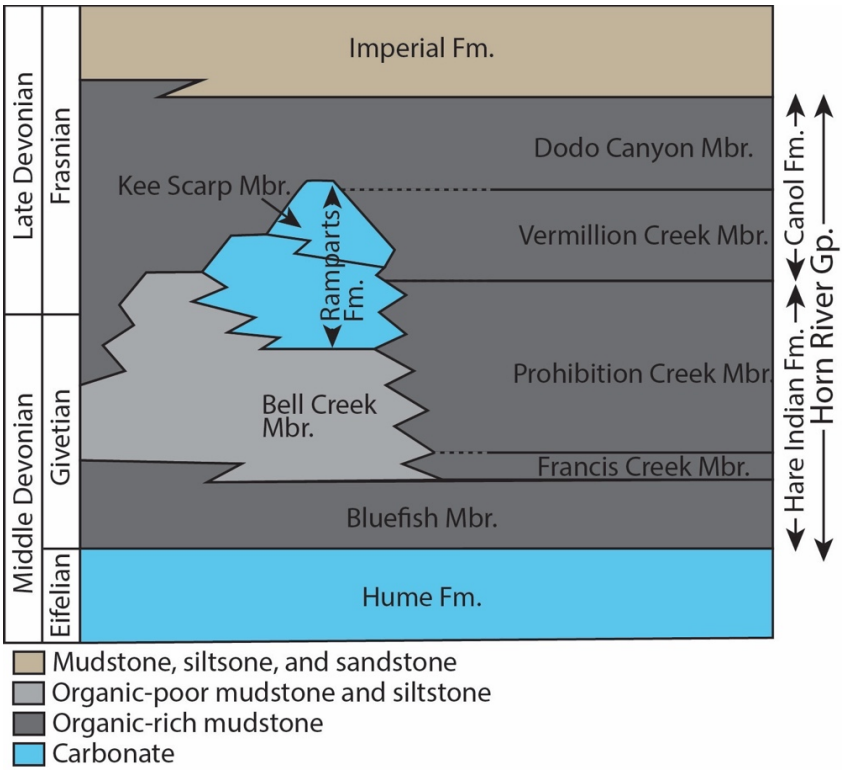

Figure 1.3 Stratigraphic column for the Horn River Group of the Central Mackenzie Valley and the Mackenzie Mountains of the Northwest Territories, Canada showing the Horn River Group and surrounding formations.

The lithology of the Canol Formation comprises dominantly planar laminated siliceous dark grey to black mudstone with carbonate and siltstone interbeds (Basset, 1961; Tassonyi, 1969; Pyle and Gal, 2016; Kabanov and Gouwy, 2017). Fine-grained matrix pyrite and pyrite nodules are common (Al-Aasm et al., 1996; Pyle and Gal, 2016; Kabanov and Gouwy, 2017). Reported fossils include rare ammonoid aptychi (Norris, 1967; Tassonyi, 1969), conodonts, sponge spicules, siliceous spheres from radiolarians, and *Tentaculites* (Basset 1961; Norris, 1967; Tassonyi 1969). Micro-scale bioturbation has been observed in thin section (Biddle et al., 2021), but bioturbation observable at the outcrop or core scale is absent. In locations where the Hare

Indian Formation is thickest, the Ramparts Formation underlies the Canol Formation and comprises limestone and calcareous mudstone deposited in a ramp and platform setting, with localized reef units (Muir et al., 1985). The Hare Indian Formation includes organic-rich and organic-poor mudstone, with intervening limestone and siltstone beds (e.g., Pugh, 1983; Pyle and Gal, 2016).

The 1920 discovery of oil at Norman Wells initiated a series of regional geological mapping projects in the central Northwest Territories, which continued until the 1980s (e.g., Kindle and Bosworth, 1920; Hume, 1922; Pugh, 1983) and include some of the first descriptions of the formations comprising the Horn River Group. These reports were later accompanied by preliminary stratigraphic, sedimentological, and geochemical characterizations of the Horn River Group (e.g., Basset, 1961; Tassonyi, 1969; Muir et al., 1985; Al-Aasm et al., 1996) along with source rock evaluations of the Canol and Hare Indian formations (e.g., Snowdon et al., 1987; Feinstein et al., 1988, Issler et al., 2005). Interest in Middle to Late Devonian marine conditions, along with the possibility of unconventional production from the Horn River Group, generated renewed research leading to resource assessments, more detailed lithostratigraphy, and higher-resolution sedimentological and geochemical characterization of these Devonian strata (e.g., Biddle et al., 2021; Harris et al., 2022; Kabanov and Gouwy, 2017; Kabanov, 2019; Kabanov and Jiang, 2021; Pyle and Gal, 2016).

The depositional system of the Canol Formation is interpreted as a distal marine shelf setting (Biddle et al., 2021), with bottom water paleoredox conditions fluctuating between euxinic and weakly oxygenated as evidenced by redox-sensitive trace metal enrichment, biomarkers for green sulfur bacteria, the presence of hyalosponge spicules, and micro-scale bioturbation (Biddle et al., 2021; Kabanov and Jiang, 2021). Assessments of unconventional resource potential in the

Canol Formation have focused on patterns in thermal maturity, kerogen type, total organic carbon (TOC) content and distribution, and SiO_2 abundance to assess brittleness (e.g., Hadlari et al., 2015; Pyle et al., 2015, Pyle et al., 2018; Terlaky et al., 2020) in addition to preliminary oil in place estimates (NEB and NTGS, 2015). Previous sequence stratigraphic interpretations of the Canol Formation were at a coarse scale: a study of the Ramparts Formation by Muir et al. (1985) included the Canol Formation in one of two Middle to Late Devonian transgressive-regressive (T-R) cycles, while Morrow (2018) presented a sequence stratigraphic framework for the Devonian system of the entire North Canadian Mainland Sedimentary Basin, which included the Canol Formation. Muir et al. (1985) and Morrow (2018) both propose two T-R cycles for the Middle to Late Devonian of the west-central Northwest Territories as follows: (1) Hume Formation – Hare Indian Formation or lower Ramparts Formation, and (2) Hare Indian Formation or lower Ramparts Formation – Imperial Formation. The Canol Formation is included in the second of these Middle to Late Devonian T-R cycles, however, these previous studies do not clearly specify the boundary between transgressive and regressive components of each cycle and previous studies have not interpreted cycles within the Canol Formation itself.

1.3 Research objectives

Broadly speaking, this thesis aims to fill gaps in our understanding of; (1) the environmental conditions in the study area during the Middle to Late Devonian and how these conditions evolved with time, and (2) the resource potential of the Canol Formation. All chapters discuss the Canol Formation in the context of the entire Horn River Group to enable comparison between the Canol Formation and surrounding units and to allow for the interpretation of conditions leading up to and after deposition of the Canol Formation. Chapter 2 corresponds with

the first objective and investigates biological productivity in the marine water column at the time the Horn River Group was deposited. Chapter 3 focuses on porosity characterization and quantification to enable prediction of higher porosity intervals and possibly allow for more accurate estimates of hydrocarbon storage, relating to the second objective. The third chapter also compares the nature of porosity in the Horn River Group with other North American unconventional mudstone reservoirs. Chapter 4 reviews the chemostratigraphic signature of sequence stratigraphic surfaces and systems tracts in organic-rich mudstone units. The review in Chapter 4 facilitates the use of chemostratigraphy to establish a high-resolution sequence stratigraphic framework for the Canol Formation in the fifth chapter. The sequence stratigraphic interpretation of Chapter 5 relates to the first objective by interpreting the evolution of relative sea level and sediment supply with time and to the second objective because this framework allows for high-resolution correlation and mapping of the Canol Formation. Chapter 6 summarizes the findings and provides examples of potential future studies.

1.4 References

Al-Aasm, I.S., Morad, S., Durocher, S., Muir, I., 1996. Sedimentology, C–S–Fe relationships and stable isotopic compositions in Devonian black mudrocks, Mackenzie Mountains, Northwest Territories, Canada. Sediment. Geol., 106 (3–4), 279–298. https://doi.org/10.1016/S0037-0738(96)00018-8

Bassett, H.G., 1961. Devonian stratigraphy, central Mackenzie River region, Northwest Territories, Canada, in: G. Raasch (Ed.), Geology of the Arctic. Alberta Society of Petroleum Geologists and University of Toronto Press, pp. 481–498. https://doi.org/10.3138/9781487584979-043

Becker, R.T., Marshall, J.E.A., Da Silva, A.C., Agterberg, F.P., Gradstein, F.M., Ogg, J.G., 2020. The Devonian Period, in: Geologic time scale 2020. Elsvier, pp. 733–810. https://doi.org/10.1016/B978-0-12-824360-2.00022-X

Biddle, S.K., LaGrange, M.T., Harris, B.S., Fiess, K., Terlaky, V., Gingras, M.K., 2021. A fine detail physico-chemical depositional model for Devonian organic-rich mudstones: A petrographic study of the Hare Indian and Canol Formations, Central Mackenzie Valley, Northwest Territories. Sediment. Geol., 414, 105838. https://doi.org/10.1016/j.sedgeo.2020.105838

Borcovsky, D., Egenhoff, S., Fishman, N., Maletz, J., Boehlke, A., Lowers, H., 2017. Sedimentology, facies architecture, and sequence stratigraphy of a Mississippian black mudstone succession—The upper member of the Bakken Formation, North Dakota, United States. Am. Assoc. Pet. Geol. Bulletin, 101(10), 1625–1673. https://doi.org/10.1306/01111715183

Cocks, L.R.M., Torsvik, T.H., 2011. The Palaeozoic geography of Laurentia and western Laurussia: A stable craton with mobile margins. Earth-Sci. Rev. 106, 1–51. https://doi.org/10.1016/j.earscirev.2011.01.007

Egenhoff, S.O., Fishman, N.S., 2013. Traces in the dark—Sedimentary processes and facies gradients in the upper shale member of the Upper Devonian–Lower Mississippian Bakken Formation, Williston Basin, North Dakota, USA. J. Sediment. Res., 83(9), 803–824. https://doi.org/10.2110/jsr.2013.60

Feinstein, S., Brooks, P.W., Fowler, M.G., Snowdon, L.R., Williams, G.K., 1988. Families of oils and source rocks in the central Mackenzie corridor: a geochemical oil-oil and oil-source rock correlation, in: James, D.P., Leckie, D.A. (Eds.), Sequences, Stratigraphy,

Sedimentology: Surface and Subsurface. Canadian Society of Petroleum Geologists, Memoir 15, pp. 543–552.

Harris, B.S., LaGrange, M.T., Biddle, S.K., Playter, T.L., Fiess, K.M., Gingras, M.K., 2022. Chemostratigraphy as a tool for sequence stratigraphy in the Devonian Hare Indian Formation in the Mackenzie Mountains and Central Mackenzie Valley, Northwest Territories, Canada. Can. J. Earth Sci., 59(1), 29–45. https://doi.org/10.1139/cjes-2020-0198

Hume, G.C., 1922. Geology of the Norman Wells oil fields and a reconnaissance of a part of Liard River. Geological Survey of Canada, Summary Report Part B, Calgary, AB.

Irwin, D., 2020. Geology of the Northwest Territories. (NWT Open Report No. 2020-007).

Issler, D.R., Grist, A.M., Stasiuk, L.D., 2005. Post-Early Devonian thermal constraints on hydrocarbon source rock maturation in the Keele Tectonic Zone, Tulita area, NWT, Canada, from multi-kinetic apatite fission track thermochronology, vitrinite reflectance and shale compaction. Bull. Can. Pet. Geol. 53, 405–431. https://doi.org/10.2113/53.4.405

Kabanov, P., Gouwy, S.A., 2017. The Devonian Horn River Group and the basal Imperial Formation of the central Mackenzie Plain, N.W.T., Canada: multiproxy stratigraphic framework of a black shale basin. Can. J. Earth Sci. 54, 409–429. https://doi.org/10.1139/cjes-2016-0096

Kabanov, P., 2019. Devonian (c. 388–375 Ma) Horn River Group of Mackenzie Platform (NW Canada) is an open-shelf succession recording oceanic anoxic events. J. Geol. Soc. 176, 29–45. https://doi.org/10.1144/jgs2018-075

Kendall, B., Reinhard, C.T., Lyons, T.W., Kaufman, A.J., Poulton, S.W., Anbar, A.D., 2010. Pervasive oxygenation along late Archaean ocean margins. Nat. Geosci., *3*(9), 647. https://doi.org/10.1038/ngeo942

Kindle, E.M., Bosworth, T.O., 1921. Oil bearing rocks of lower Mackenzie River Valley. Thomas Mulvey, Ottawa, Ontario.

Klemme, H.D., Ulmishek, G.F., 1991. Effective Petroleum Source Rocks of the World: Stratigraphic Distribution and Controlling Depositional Factors. Am. Assoc. Pet. Geol. Bull. 75, 1809–1851. https://doi.org/10.1306/0C9B2A47-1710-11D7-8645000102C1865D

Hadlari, T., MacLean B.C., Pyle L.J., Fallas K.M., and Durbano, A.M. 2015. A combined depth and thermal maturity map of the Canol Formation, northern Mackenzie Valley, Northwest Territories. Geological Survey of Canada, Open File 7865, 1 .zip file. https://doi.org/10.4095/296460

Lazar, O.R., Bohacs, K.M., Macquaker, J.H.S., Schieber, J., Demko, T.M., 2015. Capturing key attributes of fine-grained sedimentary rocks in outcrops, cores, and thin sections: nomenclature and description guidelines. J. Sediment. Res. 85, 230–246. https://doi.org/10.2110/jsr.2015.11

Macquaker, J.H., Bohacs, K.M., 2007. On the accumulation of mud. Science, 318(5857), 1734–1735. https://doi.org/10.1126/science.1151980

Meyers, P.A., 2006. Paleoceanographic and paleoclimatic similarities between Mediterranean sapropels and Cretaceous black shales. Palaeogeogr., Palaeoclimatol., Palaeoecol., 235(1-3), 305–320. https://doi.org/10.1016/j.palaeo.2005.10.025

Morrow, D.W., 2018. Devonian of the Northern Canadian Mainland Sedimentary Basin: A Review. Bull. Can. Pet. Geol. 66, 623–694.

Muir, I., Wong, P., Wendte, J., 1985. Devonian Hare Indian-Ramparts (Kee Scarp) evolution, Mackenzie Mountains and subsurface Norman Wells, NWT: basin-fill and platform reef development, in: Longman, M.W., Shanley, K.W., Lindsay, R.F., Eby, D.E. (Eds.), Rocky Mountain Carbonate Reservoirs: A Core Workshop. SEPM (Society for Sedimentary Geology), pp. 311–341. https://doi.org/10.2110/cor.85.07

Norris, A.W., 1985. Stratigraphy of Devonian outcrop belts in northern Yukon Territory and northwestern District of Mackenzie (Operation Porcupine area) (Memoir No. 410). Geological Survey of Canada. https://doi.org/10.4095/120309

Northwest Territories Geological Survey (NTGS) and National Energy Board (NEB), 2015. An assessment of the unconventional petroleum resources of the Bluefish shale and the Canol shale in the Northwest Territories - energy briefing note. Canada: National Energy Board.

Nichols, G., 2009. Sedimentology and Stratigraphy. John Wiley & Sons., Chichester, UK.

Pearce, T.J., Besly, B.M., Wray, D.S., Wright, D.K., 1999. Chemostratigraphy: a method to improve interwell correlation in barren sequences—a case study using onshore Duckmantian/Stephanian sequences (West Midlands, UK). Sediment. Geol. 124(1–4), 197–220. https://doi.org/10.1016/S0037-0738(98)00128-6

Peters, K.E., Cassa, M.R., 1994. Applied source rock geochemistry, in: Magoon, L.B., Dow, W.G., (Eds.), The Petroleum System-from source to trap. AAPG Memoire 60, pp. 93–12.

Pugh, D.C., 1983. Pre-Mesozoic geology in the subsurface of Peel River map area, Yukon Territory and District of Mackenzie. Geological Survey of Canada, Memoir 401. https://doi.org/10.4095/119498

Pyle, L.J., Fiess, K.M., Rocheleau, J., Terlaky, V., 2018. Source rock characterization data from the Devonian Horn River Group, Imperial Formation, and Cretaceous Slater River Formation outcrops - NTS 96D, 96E, and 106H, Northwest Territories. Northwest Territories Geological Survey, NWT Open Report 2016-013, 42 pages and appendices.

Pyle, L.J., Gal, L.P., Hadlari, T., 2015. Thermal maturity trends for Devonian Horn River Group units and equivalent strata in the Mackenzie Corridor, Northwest Territories and Yukon (Geological Survey of Canada Open File Report No. 7850). https://doi.org/10.4095/296446

Pyle, L.J., Gal, L.P., 2016. Reference Section for the Horn River Group and Definition of the Bell Creek Member, Hare Indian Formation in central Northwest Territories. Bull. Can. Pet. Geol. 64, 67–98. https://doi.org/10.2113/gscpgbull.64.1.67

Ratcliffe, K., Wright, M., Montgomery, P., Palfrey, A., Vonk, A., Vermeulen, J., Barrett, M., 2010. Application of chemostratigraphy to the Mungaroo Formation, the Gorgon field, offshore northwest Australia. The APPEA Journal, 50(1), 371–388. https://doi.org/10.1071/AJ09022

Rowe, H., Hughes, N., Robinson, K., 2012. The quantification and application of handheld energy-dispersive x-ray fluorescence (ED-XRF) in mudrock chemostratigraphy and geochemistry. Chem. Geol., 324, 122–131. https://doi.org/10.1016/j.chemgeo.2011.12.023

Sano, J.L., Ratcliffe, K.T, & Spain, D.R., 2013. Chemostratigraphy of the Haynesville Shale, in: Hammes, U., Gale, J. (Eds.), Geology of the Haynesville Gas Shale in East Texas and West Louisiana, U.S.A., AAPG Memoir 105, pp.137-154. http://dx.doi.org/10.1306/13441847M1053602

Schieber, J., 2003. Simple gifts and buried treasures–implications of finding bioturbation and erosion surfaces in black shales. The Sedimentary Record, 1(2), 4–8.

Scotese, C.R., 2014. Atlas of Devonian Paleogeographic Maps, PALEOMAP Atlas for ArcGIS, volume 4, The Late Paleozoic, Maps 65-72, Molleweide Projection.

Scotese, C.R., McKerrow, W.S., 1990. Revised World maps and introduction. Geol. Soc. Lond. Mem. 12, 1–21. https://doi.org/10.1144/GSL.MEM.1990.012.01.01

Scott, C., Lyons, T.W., Bekker, A., Shen, Y.A., Poulton, S.W., Chu, X.L., & Anbar, A.D., 2008. Tracing the stepwise oxygenation of the Proterozoic ocean. Nature, 452(7186), 456–459. https://doi.org/10.1038/nature06811

Snowdon, L. R., Brooks, P. W., Williams, G. K., Goodarzi, F., 1987. Correlation of the Canol Formation source rock with oil from Norman Wells. Org. Geochem., 11(6), 529–548. https://doi.org/10.1016/0146-6380(87)90008-8

Stow, D.A.V., Reading, H.G., & Collinson J.D., 1996. Deep seas, in: Reading, H.G. (Ed.), Sedimentary Environments: Processes, Facies and Stratigraphy. Oxford: Blackwell Science, pp.395–453.

Tassonyi, E.J., 1969. Subsurface geology, lower Mackenzie River and Anderson River area, District of Mackenzie (Paper No. 68–25). Geological Survey of Canada.

Terlaky, V., Fiess, K.M., and Rocheleau, J., 2020. Outcrop description, lithogeochemical, and source-rock characterisation of the Devonian Horn River Group at the Arctic Red River

East and Flyaway Creek outcrops – NTS 106F and 106G, Northwest Territories; Northwest Territories Geological Survey, NWT Open Report 2019-004, 54 pages and appendices.

Tourtelot, H.A., 1979. Black shale—its deposition and diagenesis. Clays and Clay Miner., 27(5), 313–321. https://doi.org/10.1346/CCMN.1979.0270501

Turner, B.W., Molinares-Blanco, C.E., Slatt, R.M., 2015. Chemostratigraphic, palynostratigraphic, and sequence stratigraphic analysis of the Woodford Shale, Wyche Farm Quarry, Pontotoc County, Oklahoma. Interpretation, 3(1), SH1–SH9. https://doi.org/10.1190/INT-2014-0089.1

Walliser, O.H., 1996. Global events in the Devonian and Carboniferous, in: Walliser, O.H. (Ed.), Global Events and Event Stratigraphy in the Phanerozoic. Springer, Berlin, Heidelberg, pp. 225-250.

Wignall, P.B., 1994. Black shales (No. 30). Oxford: Clarendon Press.

Zhou, L., Su, J., Huang, J., Yan, J., Xie, X., Gao, S., Dai, M., 2011. A new paleoenvironmental index for anoxic events—Mo isotopes in black shales from Upper Yangtze marine sediments. Sci. China Earth Sci., 54(7), 1024-1033. https://doi.org/10.1007/s11430-011-4188-z

Chapter 2: Primary producers and biological productivity

2.1 Introduction

The Middle to Late Devonian was characterized by the widespread deposition of organic matter (OM)-rich mudstone (e.g., Klemme and Ulmishek, 1991; Ormiston and Oglesby, 1995) in conjunction with a series of global biotic crises (e.g., Becker et al., 2020; McGhee et al., 2013; Walliser, 1996). Successive episodes of globally expanded marine anoxia on continental shelves is generally accepted as the explanation for the occurrence of these Devonian OM-rich mudstone intervals and associated biotic events, although there is not yet consensus about the root cause (e.g., Carmichael et al., 2019; Lu et al., 2021; Walliser, 1996; Zambito et al., 2012). High biological productivity and associated high rates of OM sedimentation are commonly recognized as key factors leading to elevated OM content in sediment (e.g., Harris, 2005; Konhauser, 2007). Several triggers of high productivity in the Middle to Late Devonian have been proposed, including eutrophication of epeiric seas from volcanism (Racki et al., 2018) or increased terrestrial weathering associated with either land plant evolution (Algeo and Scheckler, 1998) or intense mountain building (Averbuch et al., 2005). Murphy et al. (2000) also argued that eutrophication was maintained by fluctuating redox conditions, which led to the recycling of biolimiting nitrogen and phosphorus from anoxic seafloors. Regarding the primary producers themselves, biomarker results have shown evidence of green sulfur bacteria (anaerobic phototrophs) in several Middle Devonian to Early Mississippian OM-rich mudstones globally (e.g., Brown and Kenig, 2004 and references therein; Kabanov and Jiang, 2020). Nonetheless, our understanding of the nature of primary producers in the Middle to Late Devonian and trends in the rate of biological production of OM remains incomplete. Moreover, far more studies have focused on the Late Devonian Frasnian –Famennian Kellwasser mass extinction event, with

significantly less focus on the Middle to Late Devonian (Eifelian to Frasnian) biotic crises, including the Kacak, Thaganic, Frasne, Middlesex, and Rhinestreet events. For these events and corresponding OM-rich mudstone units, the local, regional, and global patterns in biological productivity have not yet been fully untangled to understand how productivity trends coincide with ocean anoxic events and biotic crises. Additionally, there is not yet a clear global picture of the types of primary producers that thrived in the Middle to Late Devonian epeiric seas or whether the types of organisms shifted with fluctuating marine redox conditions. A better understanding of these patterns could provide clues to the ultimate local, global, or regional cause of marine anoxic events and elevated biological productivity in the Middle to Late Devonian.

One such Middle to Late Devonian OM-rich mudstone, the upper Eifelian to Frasnian Horn River Group, which also includes carbonate intervals, is present in the Mackenzie Mountains and adjacent Mackenzie Valley of the Northwest Territories, Canada. At its maximum, the thicknesses of this group exceeds 300 m (e.g., Kabanov and Deblonde, 2019), with total organic carbon (TOC) values up to approximately 16 wt.% (e.g., Kabanov, 2015; Pyle et al., 2015), and locally containing carbonate strata with significant thickness. The Horn River Group of the Northwest Territories comprises the Hare Indian, Ramparts, and Canol Formations (Fig. 2.1).

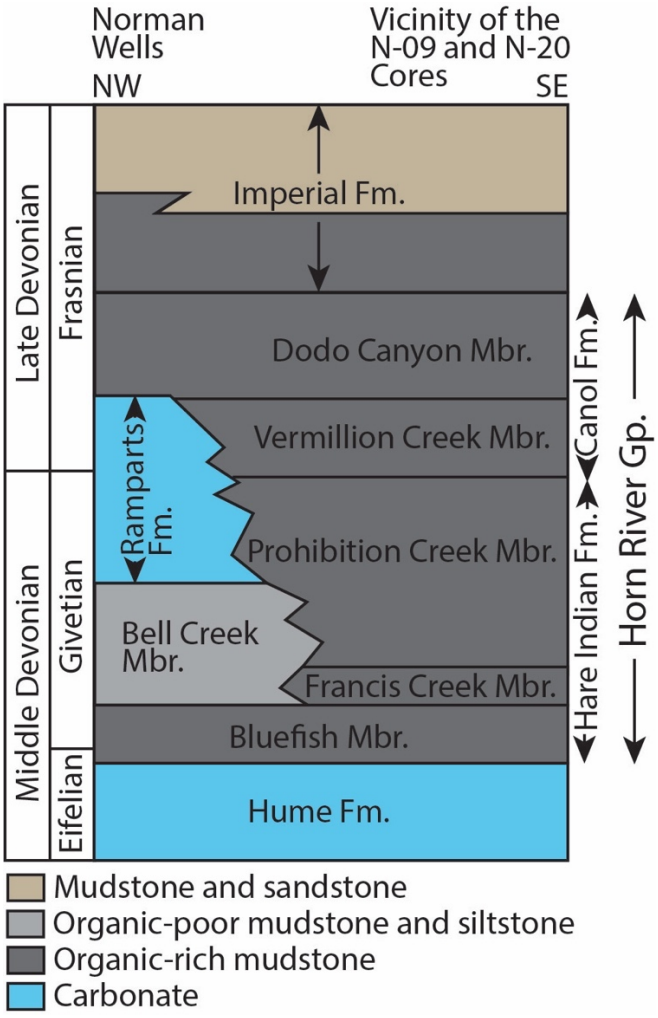

Figure 2.1 Schematic stratigraphic column showing the Middle to Late Devonian units present in the central Mackenzie Valley, Northwest Territories, Canada. Members are shown for the Hare Indian and Canol Formations. This column shows the difference in stratigraphic units present from the area near the town of Norman Wells compared to the location of the N-09 and N-20 cores to the southeast. Modified from Kabanov and Gouwy (2017). Abbreviations: Mbr–Member, Fm–Formation, Gp–Group. The nomenclature scheme of Lazar et al. (2015) is followed herein, with 'mudstone' used as the generic term for all sedimentary rocks with more than half of their grains classified as mud (clay and silt) size.

Initial depositional interpretations for the laminated organic-rich mudstones of the Horn River Group suggested deposition in anoxic to euxinic bottom waters in low energy "basinal" positions with localized development of thick (up to 200 m) organic-poor mudstones and siltstones, which were interpreted as basin margin or deltaic clinoforms (Al-Aasm et al., 1996; Muir and Dixon, 1984; Snowdon et al., 1987; Tassonyi, 1969). Since then, resource exploration and interest in the conditions associated with OM burial have encouraged new investigations of the depositional settings. Recent studies have focused on understanding specific physicochemical parameters and sedimentary processes. Ichnological, paleontological, and biomarker data have revealed that bottom water oxygenation fluctuated between weakly oxygenated and anoxic or euxinic (Biddle et al., 2021; Harris et al., 2021; Kabanov and Jiang, 2020). Moreover, petrographic facies analysis has provided evidence for sediment-gravity-driven deposition in many intervals of the Hare Indian and Canol Formations (Biddle et al., 2021). Characterizing the depositional setting of the Horn River Group is essential to understanding the conditions that produced OM burial in these strata. Despite these earlier studies, many paleoenvironmental parameters remain poorly constrained.

This paper seeks to resolve two questions; (1) what type of primary producers were dominant during Horn River Group deposition and (2), were there temporal variations in the types of primary producers or in biological productivity? We address these questions through the interpretation of $\delta^{13}C_{org}$ ($\delta^{13}C$ of OM) and $\delta^{15}N_{bulk}$ (whole rock $\delta^{15}N$) values. In the case of primary producer type, depending on the C or N sources (e.g., CO_2, HCO_3^- or CH_4 and N_2, NH_4^+ or NO_3^-) and the isotope fractionations associated with corresponding metabolic pathways, the isotopic signature of primary producers varies (e.g., Ader et al., 2016; Bauersachs et al., 2009; Lamb et al., 2006; Peters et al., 1978). Changes in biological productivity influence $\delta^{13}C_{org}$ and

$\delta^{15}N_{bulk}$ through the reservoir effect (whether C and N are growth-limiting). If biological productivity increases or dissolved CO_2 ($CO_{2\ (aq)}$) decreases, $\delta^{13}C$ values in primary producers shift toward heavier values (Falkowski, 1991; O'Leary, 1981). Likewise, higher N availability and/or slower growth rates are associated with higher fractionation and lighter $\delta^{15}N$ in primary producers (e.g., Hoch et al., 1994; Kessler et al., 2014; Pennock et al., 1996; Thunell et al., 2004; Wada et al., 1990).

Previously, C isotopic signatures of the Hare Indian and Canol Formations were used to explore the marine *versus* terrestrial source of OM (Al-Aasm et al., 1996) and representative $\delta^{13}C$ logs were also used for global correlations, in particular, the characterization of oceanographic events (Fraser and Hutchison, 2017; Kabanov and Jiang, 2020; Terlaky et al., 2020). However, the significance of $\delta^{13}C$ signatures and trends have not yet been considered in the context of biological productivity and $\delta^{15}N$ signatures have not yet been studied. This paper examines both $\delta^{13}C_{org}$ and $^{15}N_{bulk}$ at a high-resolution sampling interval through the Horn River Group in continuous cores from two exploration wells drilled a decade ago in the Central Mackenzie Valley. Furthermore, this contribution serves as an example of the types of primary producers and trends in productivity at one locality that spans a wide time range from the Middle to Late Devonian, which could be compared to similar results from age-equivalent OM-rich mudstone units to assess global patterns.

2.2 Geological background

The study area is located along the northwestern limit of Ancestral North America. Neoproterozoic supercontinental breakup was succeeded by the development of passive margins along the present-day northwest of Ancestral North America, which was followed by

convergence along the northern front (Franklinian margin) in the early Paleozoic (Dewing et al., 2019; Hadlari et al., 2014). Early to Middle Cambrian extension and graben development in the study area (MacLean, 2011) was succeeded by Late Cambrian to Middle Devonian subsidence and carbonate platform development (Fritz et al., 1991; MacLean et al., 2014). At this time, the study area was situated at tropical latitudes slightly to the south of the paleoequator (e.g., Cocks and Torsvik, 2011; Scotese and McKerrow, 1990) on the paleogeographic feature known as the Mackenzie Platform (Lenz, 1972; Norris, 1985; Fig. 2), which is also referred to as the Peel Platform or Peel Shelf by some authors (e.g., Kabanov and Jiang, 2020; Morrow, 2018). To the west, this platform was separated from the Porcupine Platform (or Yukon Stable Block) by the Richardson Trough (Jeletzky, 1975; Lenz, 1972; Pugh, 1983; Fig. 2.2). The Richardson Trough is interpreted to be an aulacogen produced by extensional tectonics in the Lower Cambrian or earlier (Jeletzky, 1975; Pugh, 1983) along with the other intracratonic topographic lows in the area at the time (the Selwyn Basin and Misty Creek Embayment; Morrow, 2018; Fig. 2.2).

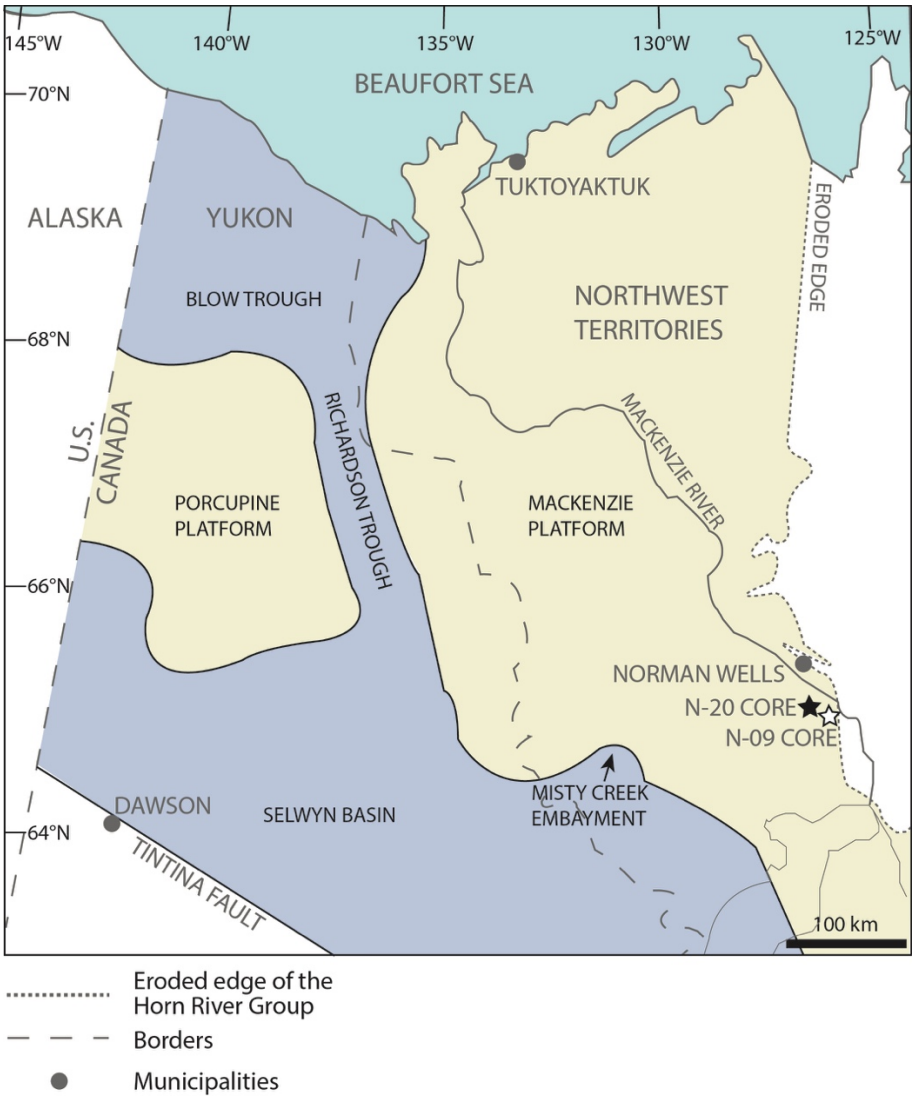

Figure 2.2 Middle to Late Devonian paleogeographic features in the northern Yukon and Northwest Territories, Canada. Grey lines and text are associated with modern-day geographic features, whereas black lines and text represent Middle to Late Devonian features. The locations of the ConocoPhillips Mirror Lake N-20 and Husky Little Bear N-09 cores are shown with black and white stars, respectively. Modified from LaGrange et al. (2022) after Pugh (1983), Al-Aasm et al. (1996) and Morrow (2018).

The Horn River Group of the west-central Northwest Territories is approximately time equivalent to the Horn River Group of British Columbia and the Woodbend Group of Alberta, which includes the Duvernay Formation. In the central-northern mainland Northwest Territories, the Horn River Group includes the Hare Indian, Ramparts, and Canol Formations (Fig. 1). Four members make up the Hare Indian Formation: the Bluefish (Pugh, 1983), Bell Creek (Pyle and Gal, 2016), Francis Creek, and Prohibition Creek Members (Kabanov and Gouwy, 2017). The Ramparts Formation is not formally subdivided, aside from the uppermost Kee Scarp Member comprising localized reef limestones (Hills et al., 1981), which is absent in our study area. The Canol Formation comprises the Vermillion Creek and Dodo Canyon Members (Kabanov and Gouwy, 2017; Fig. 1) and is the source rock for the hydrocarbons produced from the Kee Scarp Member in the area of Norman Wells (Snowdon et al., 1987). In the early 21st century, interest in the Canol Formation shifted to its unconventional petroleum reservoir potential, along with the Bluefish Member. These two intervals comprise OM-rich mudstone, with the locally intervening Ramparts Formation consisting of carbonate ramp, platform, and reef deposits (Muir et al., 1985; Pyle and Gal, 2016). The overlying Imperial Formation comprises mudstone and fine-grained silty sandstone (Pugh, 1983).

Leading up to the Middle Devonian, the Mackenzie Platform was characterized by shallow-water carbonate deposition (Norris, 1985; Pugh, 1983). Horn River Group deposition began in the late Eifelian with the accumulation of the OM-rich Bluefish Member of the Hare Indian Formation (Kabanov and Gouwy, 2017). The shift from Hume Formation carbonates to OM-rich mudstone deposition has been attributed to a relative sea-level rise (Gal et al., 2009; Morrow, 2018; Muir and Dixon, 1984) or to a rise in the oxygen minimum zone (Kabanov, 2019). Subsequent uplift to the northwest resulted in progradation of the Bell Creek Member

mudstone banks (Muir and Dixon, 1984; Tassonyi, 1969), interpreted as marine regression (Morrow, 2018). Meanwhile, the Francis Creek and Prohibition Creek Members of the Hare Indian Formation were deposited in off-bank settings (Kabanov and Gouwy, 2017) and deposition of the Ramparts Formation carbonates began where the Bell Creek Member mudstone bank was thickest (Kabanov, 2019). The onset of another marine transgression (Morrow, 2018; Muir et al., 1985) eventually led to drowning of the Ramparts Formation carbonates and onlapping of the OM-rich Canol Formation (Muir et al., 1985; Muir and Dixon, 1984; Yose et al., 2001). In the Late Devonian, the Ellesmerian orogeny along the northern margin of Ancestral North America produced a foreland basin in the study area, which ended Horn River Group deposition and initiated a shift to the siliciclastic Imperial Formation (Beranek et al., 2010; Garzione et al., 1997).

Much progress has been recently achieved in understanding the burial-exhumation history of the studied strata. Peak thermal conditions (~90 ºC – 190 º C) for the Horn River Group occurred prior to the Cretaceous (Issler et al., 2005; Powell et al., 2020). This was followed by the development of a regional sub-Cretaceous unconformity caused by cooling and uplift, subsequent burial, and finally, erosion associated with the North American Cordillera foreland basin (Powell et al., 2020). Beginning in the Miocene, the study area has experienced ongoing crustal shortening, produced by accretion of the Yakutat terrane to the North American craton in the Gulf of Alaska (Mazzotti and Hyndman, 2002). The studied cores are currently situated within the eastern Laramide Cordillera, in the gently deformed hanging wall of the presently active thrust sheet of the Mackenzie Valley synclinorium (Hadlari, 2015).

2.3 Samples and Analytical Methods

Samples for this study were collected from two vertical cores in the Central Mackenzie Valley of the Northwest Territories, Canada (Fig. 2.3): (1) the ConocoPhillips Mirror Lake N-20 core located at 64°59'40.55" N, 126°48'14.83" W (hereafter referred to as the N-20 core), and (2) the Husky Little Bear N-09 core at 64°58’55.2” N, 126°31’20.2” W (hereafter referred to as the N-09 core), which is approximately 13 km east of the N-20 core.

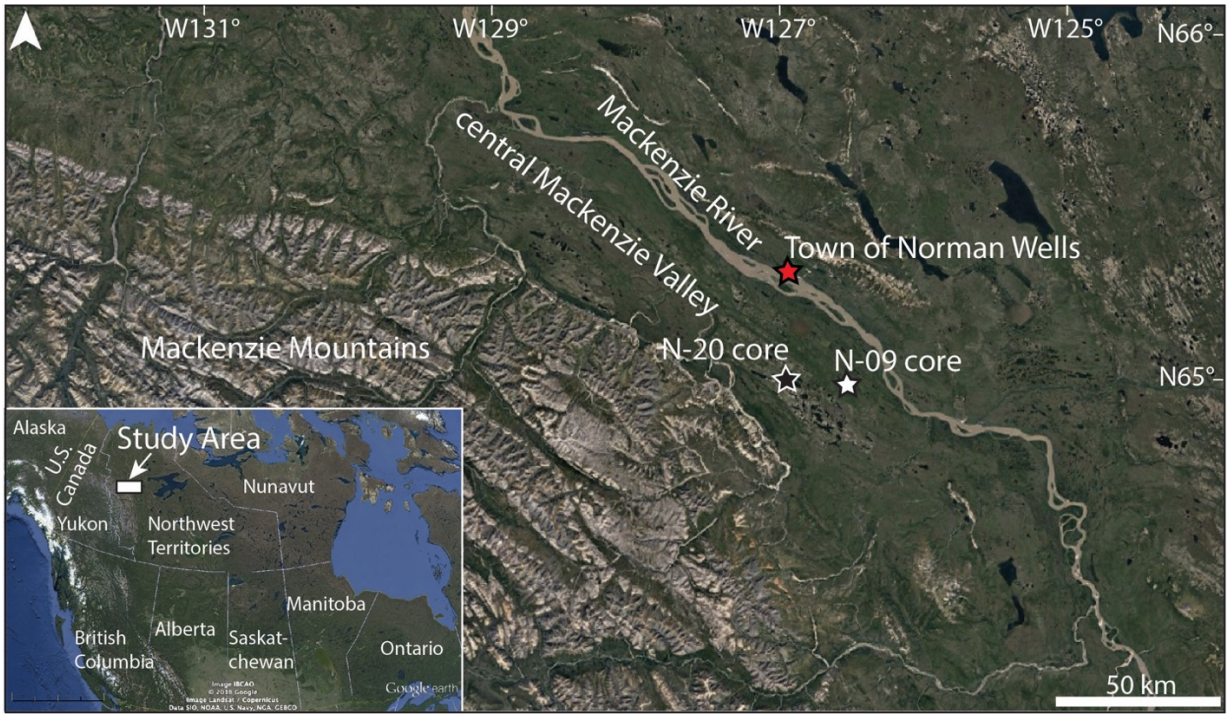

Figure 2.3 Map of the Central Mackenzie Valley and Mackenzie Mountains of the Northwest Territories, Canada, showing the location of the ConocoPhillips Mirror Lake N-20 and the Husky Little Bear N-09 core labelled with black and white stars, respectively. The study area is shown with a white box on the inset map. Image modified from Google Earth Pro 7.1.8.3036 (2018). Central Mackenzie Valley and Mackenzie Mountains, Northwest Territories, Canada.

64º58’56.91” N, 127º49’26.08” W, Eye alt 323.9 km. Data SIO, NOAA, U.S. Navy, NGA, GEBCO. (Accessed October 4, 2019).

The N-20 core is 216.5 m long and includes the top of the Hume Formation, the entire Hare Indian and Canol Formations, and the lowermost 50 m of the Imperial Formation. Samples from this core were collected throughout the Horn River Group and the Imperial Formation at 2 m intervals except where a significant interval of core was missing. Sample preparation and analyses for this core were completed at the University of Alberta. An automated mortar and pestle were used to crush the samples into fine powder. Homogenized powdered samples were immersed in 1 N HCl for 24 hours to dissolve the carbonate component. This solution was centrifuged for 30 minutes with an acceleration of 29,000 g and the resulting powder was washed three times with deionized water, freeze-dried, and then 11-12 mg of powder from each sample was weighed into tin capsules. A Thermo Scientific Flash 2000 Organic Elemental Analyzer was used for combustion extraction of C and N from samples. The produced CO_2 and N_2 were separated by gas chromatography and then introduced into a Thermo Scientific Delta V plus isotope ratio mass spectrometer for analysis of C and N isotopic composition. Both C and N isotopic results are reported using the delta notation whereby $\delta = (R_{sample}/R_{standard} - 1)$. The $\delta^{13}C_{org}$ values are reported relative to Vienna Pee Dee Belemnite (V-PDB) and the $\delta^{15}N_{bulk}$ values are reported relative to atmospheric N_2 (AIR). Two standards were used for calibration of isotopic measurements: OAS High Organic Content Sediment Standard ($\delta^{13}C$ = –28.9 ‰ and $\delta^{15}N$ = +4.3 ‰) and OAS Low Organic Content Soil Standard ($\delta^{13}C$ = –26.7 ‰ and $\delta^{15}N$ = 7.0 ‰). The analytical precision of these measurements was within 0.2 ‰ for both N and C isotopic compositions based on repeated measurements over the course of this study.

The N-09 core spans the uppermost Hume Formation to the lower Imperial Formation and is 167.8 m long. Samples were collected from the Bluefish, Francis Creek, and Prohibition Creek Members of the Hare Indian Formation and both members of the Canol Formation at an interval of 0.6 to 0.7 m. The $\delta^{13}C_{org}$ data for this core has been published by Kabanov and Jiang (2020). Methods for both $\delta^{13}C_{org}$ and $\delta^{15}N_{bulk}$ can be found in the supplementary materials of Kabanov and Jiang (2020).

Vitrinite is an organic maceral and its reflectance is commonly used as a proxy for thermal maturity, with higher reflectance indicating greater thermal maturity (Burnham and Sweeney, 1989; Tissot et al., 1987). Vitrinite reflectance measurements were collected by TerraTek (Schlumberger) for the N-20 core, and by Core Laboratories Canada for the N-09 core. Five vitrinite measurements from the N-09 core in the interval are considered: two from the Hare Indian Formation and three from the Canol Formation. Sampling density in the N-20 core was much higher, with 61 vitrinite reflectance measurements spanning the Hare Indian Formation to the Imperial Formation. Total organic carbon (TOC) data were collected using a LECO Analyzer by Core Laboratories Canada for the N-09 core and by Weatherford Laboratories for the N-20 core.

2.4 Results

The N-09 core is characterized by a large TOC range from 1.54 wt. % to 8.63 wt. % (Appendix 1 SI Table 1.1) and a vitrinite reflectance range from 1.02 % R_o to 1.29 % R_o (Appendix 1 SI Table 1.2). The N-20 core has similar TOC range from 0.15 wt. % to 7.46 wt. % (Appendix 1 SI Table 1.1), but a larger range of vitrinite reflectance from 0.04 % R_o to 1.46 % R_o (Appendix 1 SI Table 1.2). The N and C isotopic composition of samples from the N-20 core are presented in

Figure 2.4 A and C. In this core, $\delta^{13}C_{org}$ values range from –31.0 ‰ to –24.3 ‰ and $\delta^{15}N_{bulk}$ values are between –3.8 ‰ and +1.9 ‰. For the N-09 core, $\delta^{13}C_{org}$ values are between –31.0 ‰ and –27.2 ‰ with $\delta^{15}N_{bulk}$ values ranging from –2.0 ‰ to +5.9 ‰ (Fig. 2.4 B and D). A summary of the results for each core by formation is presented in Table 2.1.

When taken together, $\delta^{13}C_{org}$ from the N-20 and N-09 cores spans from –31.0 ‰ to –24.3 ‰. Trends in $\delta^{13}C_{org}$ are similar for both cores starting in the Bluefish Member with an initial decrease followed by an increase (Fig. 2.4). A noticeable $\delta^{13}C_{org}$ peak is present in the Hare Indian Formation near the Bluefish Member-Francis Creek Member contact, which is succeeded by a sharp decline throughout the Francis Creek Member. The $\delta^{13}C_{org}$ values remain relatively constant throughout the Prohibition Creek Member, after which there is an increasing trend with a $\delta^{13}C_{org}$ peak in the lower Vermillion Creek Member of the Canol Formation. The $\delta^{13}C_{org}$ values then decreases upwards throughout the Vermillion Creek Member to the contact with the Dodo Canyon Member. Only the N-20 core dataset extends significantly above this contact, where the $\delta^{13}C_{org}$ values steadily decrease extending up until an abrupt peak at 1954 m in the Imperial Formation, which is followed by a steady shift toward heavier $\delta^{13}C_{org}$ values. Following the system of Kabanov and Jiang (2020), the four noticeable peaks in this dataset are labelled A–D (Fig. 2.4).

Table 2.1 Carbon and nitrogen isotopic composition for samples from the N-20 and N-09 cores grouped by formation. $\delta^{13}C$ of organic matter ($\delta^{13}C_{org}$) is relative to Vienna Pee Dee Belemnite (V-PDB) and total $\delta^{15}N$ ($\delta^{15}N_{bulk}$) is relative to AIR. Abbreviations: Fm– Formation.

Core	**Interval**	**$\delta^{13}C_{org}$ range (‰)**	**Average $\delta^{13}C_{org}$ (‰)**	**$\delta^{15}N_{bulk}$ range (‰)**	**Average $\delta^{15}N_{bulk}$ (‰)**
N-20	Hare Indian Fm	–30.4 to –28.3	–29.3	–3.5 to +1.9	–2.0
N-20	Canol Fm	–30.1 to –28.2	–29.0	–3.7 to –0.4	–2.5
N-20	Imperial Fm	–31.0 to –24.3	–29.2	–3.8 to –0.2	–2.2
N-09	Hare Indian Fm	–31.0 to –27.9	–29.4	–2.0 to +5.9	–0.4
N-09	Canol Fm	–30.7 to –27.2	–28.7	–1.9 to +1.1	–1.1

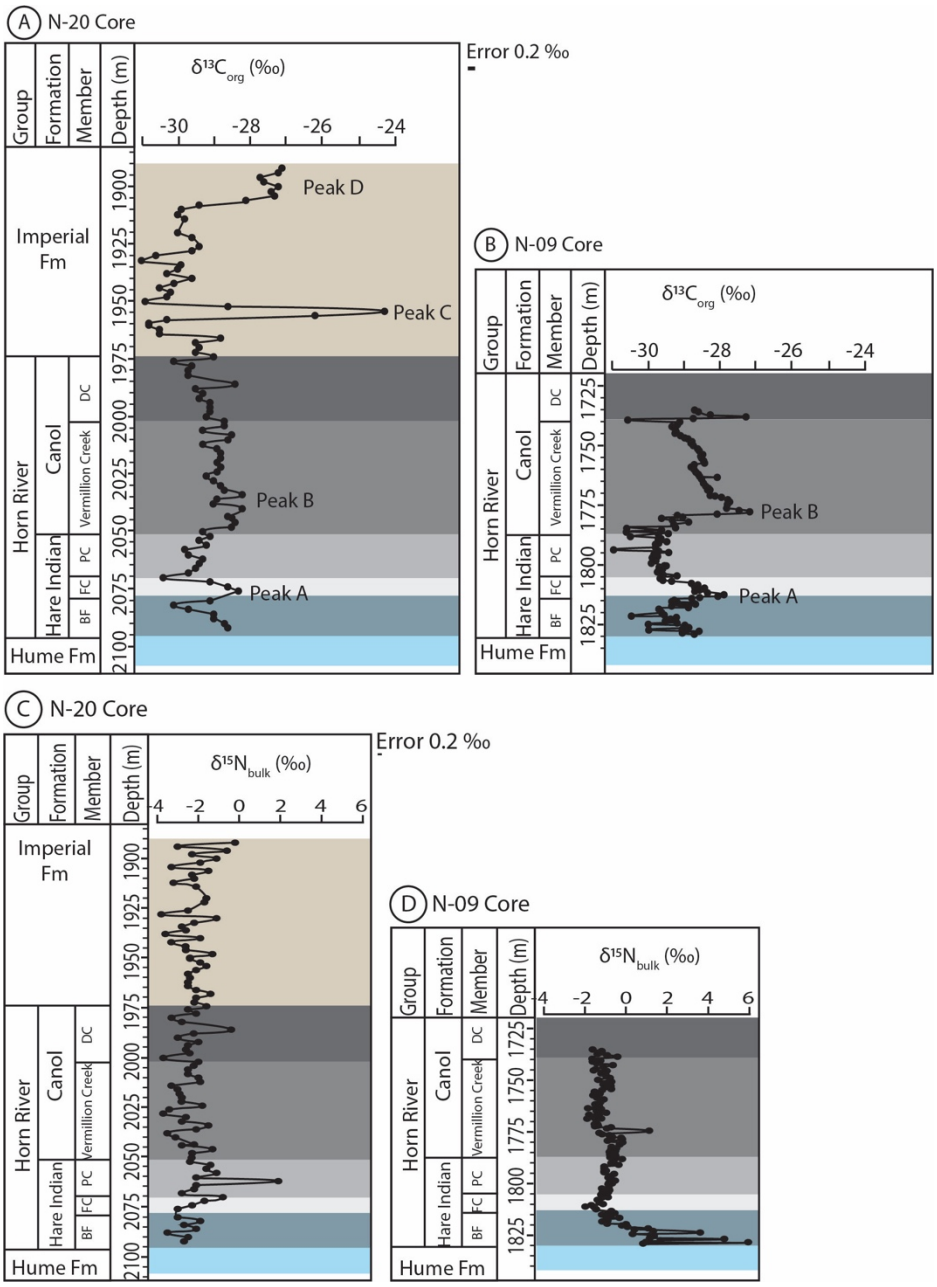

Figure 2.4 Carbon isotopic composition with depth in (A) the N-20 core and (B) the N-09 core and nitrogen isotopic composition in (C) the N-20 core and (D) the N-09 core. Colours correspond to the members. The letters A–D label the four noticeable peaks in $\delta^{13}C_{org}$. Abbreviations: Fm – Formation, BF – Bluefish, FC – Francis Creek, PC – Prohibition Creek, DC – Dodo Canyon.

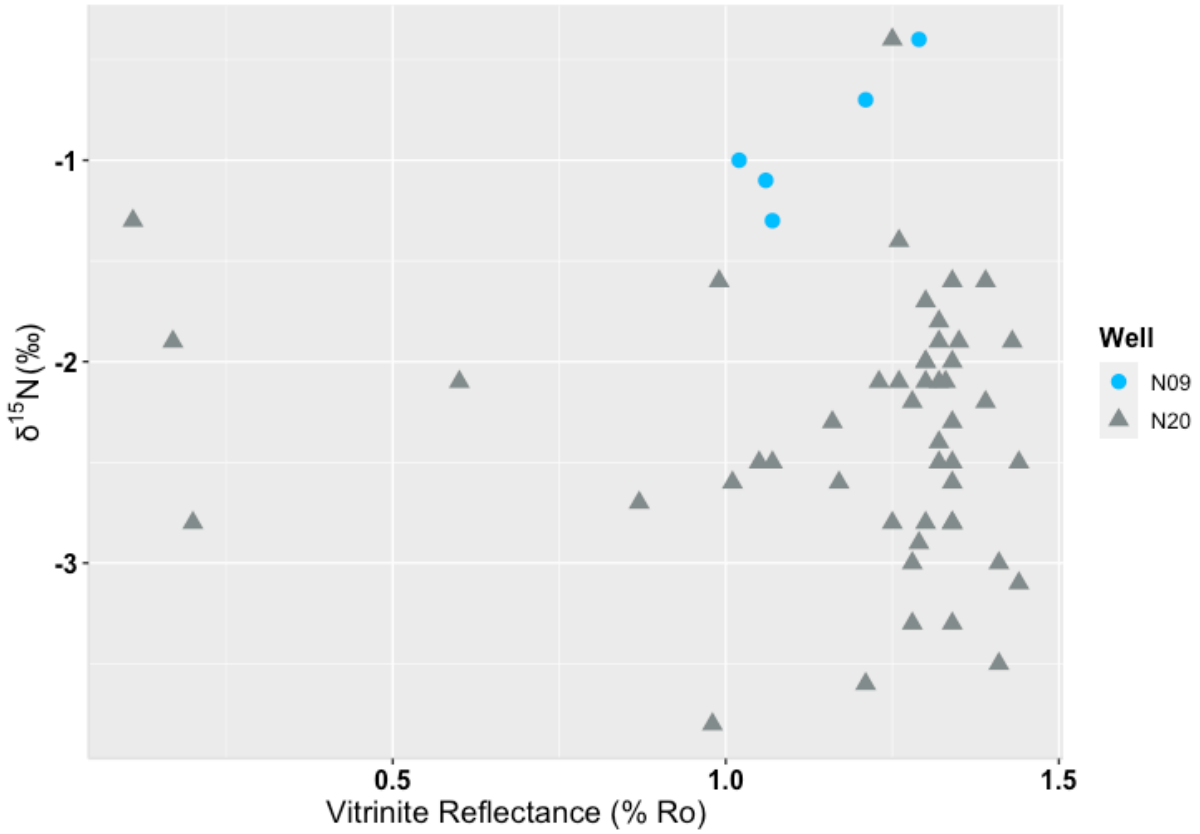

Figure 2.5 The relationship between vitrinite reflectance and $\delta^{15}N_{bulk}$ for the Horn River Group and Imperial Formation in the N-09 and N-20 cores. Definitions: % R_o–percent reflectance in oil.

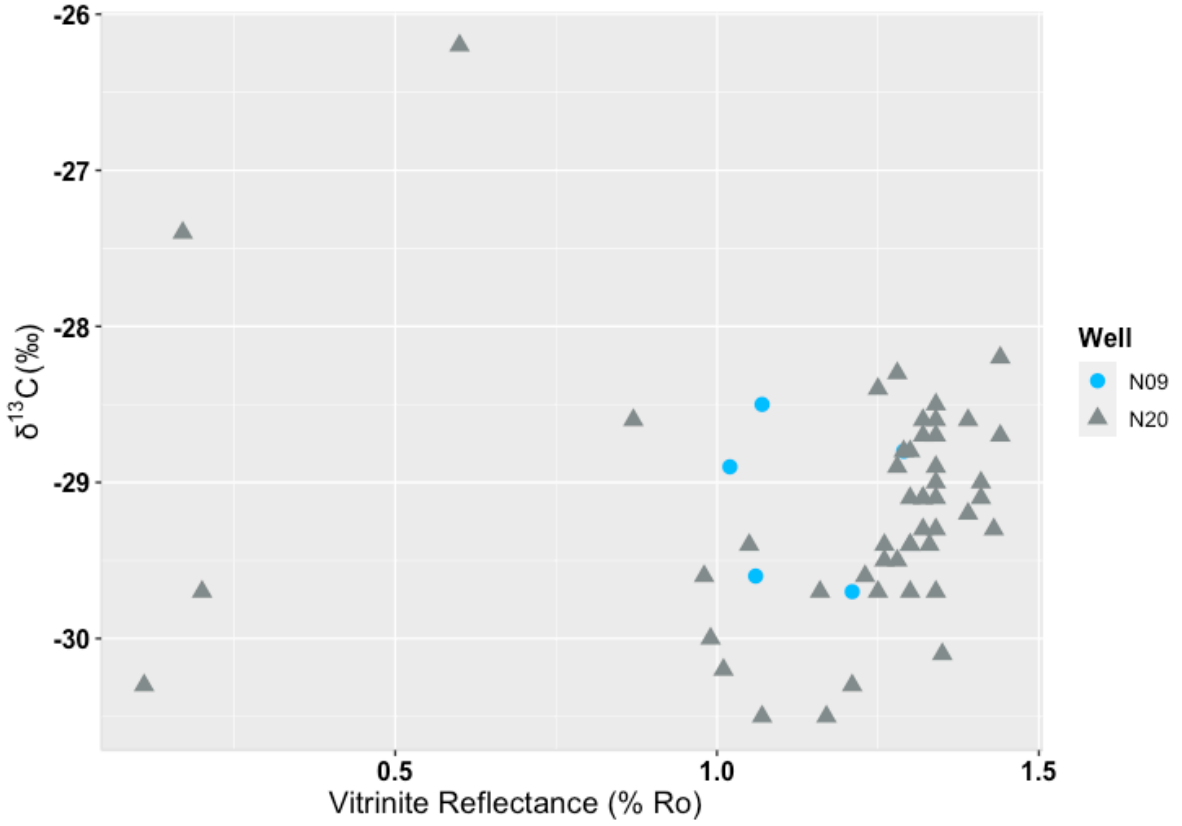

Figure 2.6 The relationship between vitrinite reflectance and $\delta^{13}C_{org}$ for the Horn River Group and Imperial Formation in the N-09 and N-20 cores. Definitions: % Ro–percent reflectance in oil.

The $\delta^{15}N_{bulk}$ values of the N-20 core are relatively constant with most falling into a narrow range from 0 ‰ to –4 ‰ throughout the Bluefish Member to the Imperial Formation (Fig. 2.4). In the Bluefish Member of the N-09 core, the $\delta^{15}N_{bulk}$ values show a peak at +6 ‰ followed by an up-core decrease. From the overlying Francis Creek Member to the Dodo Canyon Member, the $\delta^{15}N_{bulk}$ values of the N-09 core remain at relatively constant values from 0 ‰ to –2 ‰ (Fig. 2.4). A cross-plot of vitrinite reflectance and $\delta^{15}N_{bulk}$ values from the two cores considered was constructed by taking an average of the data at two-meter intervals (Fig. 2.5). A rough positive

trend is present in the limited N-09 dataset, whereas no trend is observed from the more abundant data points associated with the N-20 core (Fig. 2.5). Average $\delta^{13}C_{org}$ and vitrinite reflectance values were also cross-plotted at a two-meter interval and no relationship is observed (Fig. 2.6).

Figure 2.7 A–C shows the relationship between $\delta^{13}C_{org}$ and TOC with $\delta^{15}N_{bulk}$ – TOC shown in Figure 2.7 D–F. This plot was constructed by comparing isotopic results to TOC content at two-meter intervals for both the N-09 and N-20 cores (Fig. 2.7). Outliers in this plot were identified statistically using the interquartile range method and are labelled in Figure 2.7. There are two statistical outliers in $\delta^{15}N_{bulk}$ values, both in the Bluefish Member of the N-09 core: +1.7‰ in the 1822 m to 1824 m bin and +2.1 ‰ in the 1826 m to 1828 m bin. In the $\delta^{13}C_{org}$ dataset, there is one outlier of –26.2 ‰ at 1954 m to 1956 m in the Imperial Formation of the N-20 core. Finally, the TOC value of 8.63 wt. % in the N-09 core is also a statistical outlier. The geological significance of these outliers will be addressed in the discussion, but they were excluded from the linear regression because they fall outside the primary trends in the dataset (Fig. 2.7). Overall, the $\delta^{13}C_{org}$ – TOC relationship is weak, and data points plot in a cloud with a range of $\delta^{13}C_{org}$ values at any given TOC (Fig. 2.7 A). The coefficient of determination (r^2) for $\delta^{13}C_{org}$ – TOC does not change if only the Canol Formation (Fig. 2.7 B) or only the Vermillion Creek Member (Fig. 2.7 C) is considered in the linear regression ($r^2 = 0.1$). The $\delta^{15}N_{bulk}$ – TOC relationship shows a similarly low r^2 (Fig. 2.7 D), which does not change if only the Canol Formation is considered (Fig. 2.7 E) but does increase slightly to $r^2 = 0.2$ if only the Vermilion Creek Member is included (Fig. 2.7 F).

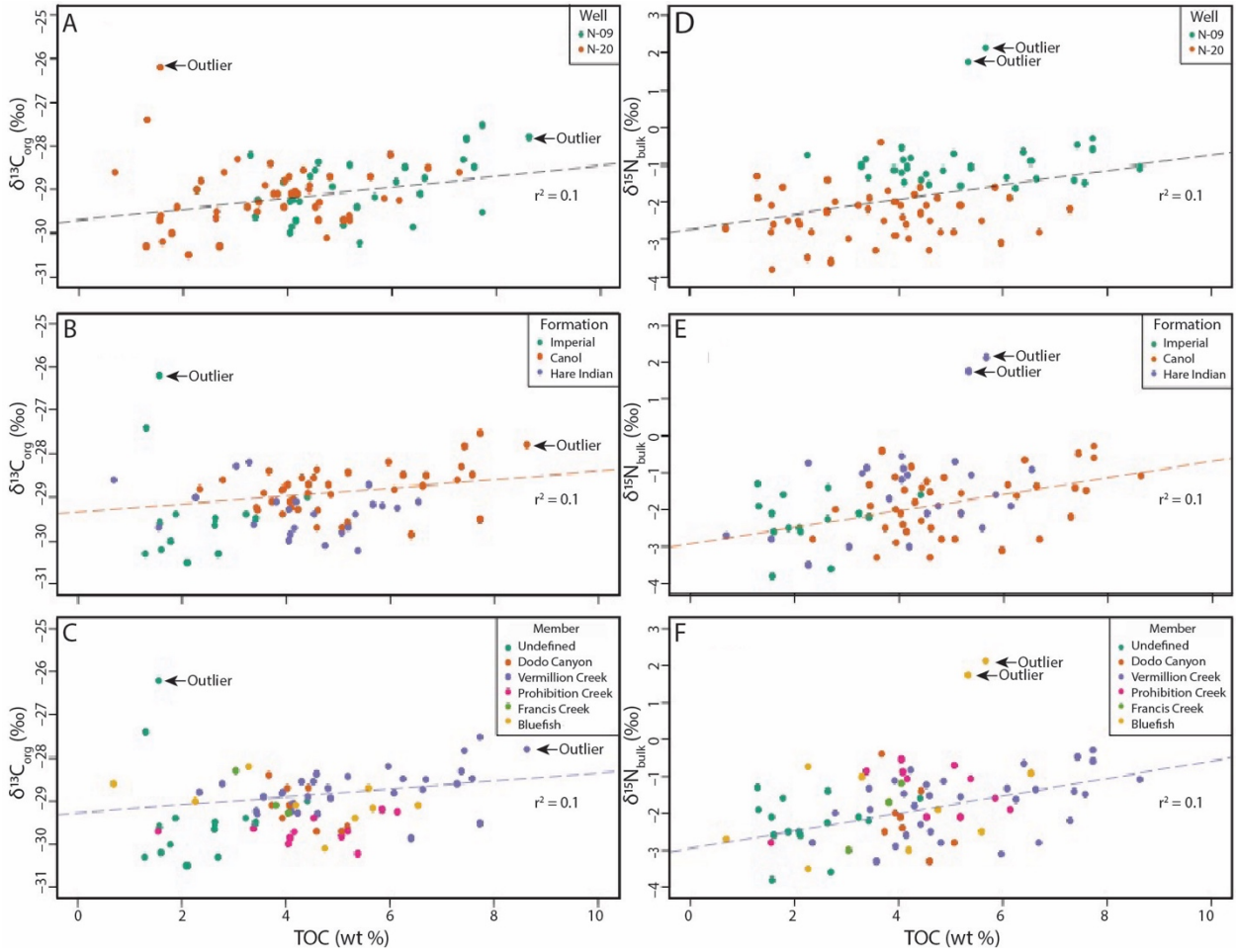

Figure 2.7 Cross plots of $\delta^{13}C_{org}$ and TOC coloured by (A) well, (B) formation, and (C) member and plots of $\delta^{15}N_{bulk}$ vs TOC coloured by (D) well, (E) formation, and (F) member. Outliers were not included in the linear regressions. In plots (B) and (E), the linear regression includes only data from the Canol Formation. In plots (C) and (F), the linear regression comprises solely data from the Vermillion Creek Member of the Canol Formation. For plots (C) and (F), the 'Undefined' member refers to the Imperial Formation because this unit was not subdivided into members herein.

2.5 Discussion

2.5.1 Paleoredox model

Nitrogen speciation and the fractionation of its isotopes are significantly influenced by redox conditions (e.g., Ader et al., 2016; Somes et al., 2010). Pyle and Gal (2016), Kabanov (2019), and Harris et al. (2021) observed enrichments of redox-sensitive trace metals (e.g., Mo, V, and U) throughout much of the Horn River Group, suggesting seawater or sediment anoxia at that time. Moreover, biomarkers for green sulphur bacteria in the Canol Formation and Bluefish Member indicate euxinia (anoxic and sulfidic conditions) within the photic zone (Kabanov and Jiang, 2020), whereas Mo abundance in the Hare Indian Formation is characteristic of intermittent euxinia in the water column overlying the depositional setting (Harris et al., 2021). On the other hand, micro-scale bioturbation (< 150 μm) observed in many horizons of the Horn River Group can only be explained by intermittent, mild bottom water oxygenation (dysoxic conditions, 0.0–0.1 ml/L O_2; Biddle et al., 2021) and the presence of benthic hyaline sponge spicules in several intervals also supports periodic if low oxygenation of bottom waters (Kabanov and Jiang, 2020). Collectively, these seemingly contrasting indicators are best reconciled by the Horn River Group water column having been euxinic with episodic weak oxygenation of bottom waters (Biddle et al., 2021; Harris et al., 2021; Kabanov and Jiang, 2020).

With reference to surface water oxygenation, biomarker evidence for photic zone euxinia (Kabanov and Jiang, 2020) paired with a scarcity of macrofossils or macrofossil imprints is best explained by limited dissolved oxygen in surface waters. Supporting this assertion, a low diversity and abundance of pelagic microfossils was observed in Horn River Group thin sections, indicating that some oxygen was present in surface waters, although limited (Biddle et al., 2021). Together, the above observations and interpretations indicate that dissolved oxygen in the water

column was likely restricted to the very surface (wave-mixed) layer of the photic zone, aside from episodic instances of bottom water oxygenation.

We consider the Cariaco Basin and the central Peruvian Margin as partial modern analogues to explain the mechanism of redox fluctuation in the Horn River Group depositional system. Both the Cariaco Basin and the central Peruvian Margin are in the tropics near the equator, as was our study area in the Middle to Late Devonian. Moreover, both are characterized by oxic surface waters, anoxic conditions at greater depths in the water column, and periodic bottom water oxygenation.

The Cariaco Basin of the Venezuelan continental shelf is a pull-apart basin with a maximum water depth exceeding 1,400 m, bordered by shallow sills which restrict exchange with the open ocean (e.g., Sigurdsson et al., 1997). The waters of the Cariaco Basin are oxic near the surface and transition to euxinic conditions at 200 m to 300 m depth (e.g., Astor et al., 2003; Zhang and Millero, 1993). The residence time of anoxic bottom waters has been estimated at 50–100 years with geochemical evidence suggesting that the most recent deep water oxygenation event occurred in approximately 1915, likely due to earthquake activity (e.g., Zhang and Millero, 1993 and references therein). Moreover, on several occasions, Astor et al. (2003) observed the presence of a secondary oxygen peak within the OMZ (i.e. water column) of the Cariaco Basin below the sill depth, which they attributed to the injection of water from the Caribbean Sea caused by cyclone activity. In certain years, several of these ventilation events were recorded whereas, in other years, none were present (*ibid*).

The central Peruvian Margin is an unrestricted shelf to basin system characterized by upwelling and high productivity (Pennington et al., 2006). An anoxic oxygen minimum zone (OMZ) is present with the upper boundary on the shelf (< 100 m water depth) and lower

boundary on the upper slope, meaning that much of the shelf is normally within the OMZ and bottom waters are anoxic (e.g., Emeis et al., 1991; Scholz et al., 2011). Moreover, results from Schunck et al. (2013) indicate that the Peruvian Shelf OMZ is episodically sulfidic. During warm El Niño Southern Oscillation (ENSO) events, coastal trapped waves move the upper OMZ boundary down by tens of meters, exposing a large portion of the previously anoxic shelf to oxygenated waters (Gutiérrez et al., 2008).

In our study area, the presence of a hydrographic barrier similar to the Cariaco Basin has not been identified, suggesting that the Horn River Group may have been deposited in an oceanographically open system (Kabanov, 2019) more like the central Peruvian Margin. Moreover, the water depth of the Horn River Group depositional setting is estimated at 250–300 m (Kabanov and Jiang, 2020), whereas the maximum water depth in the Cariaco Basin is much greater (<1400 m), with the oxic to anoxic transition at a depth of 200 m to 300 m (e.g., Astor et al., 2003; Zhang and Millero, 1993). The oxic to anoxic transition in the Horn River Group thus appears to have been at a depth closer to the central Peruvian Margin than the Cariaco Basin. Nonetheless, within the OMZ, the bottom waters of the Peruvian Margin shelf are most often anoxic and nitrate-reducing (Scholz et al., 2017), despite episodic events of euxinia (e.g., Schunck et al., 2013) or oxygenation (e.g., Gutiérrez et al., 2008). In contrast, the geochemical, paleontological, and ichnological evidence from the Horn River Group points to dominantly euxinic (rather than nitrate-reducing) bottom waters, punctuated by weak bottom water oxygenation (Biddle et al., 2021; Harris et al., 2021; Kabanov and Jiang, 2020), more like the Cariaco Basin.

In sum, neither of these modern analogues represents the Horn River Group depositional setting in every regard. Instead, they help understand the mechanisms that may have produced

periodic bottom water oxygenation events in the Horn River Group depositional environment. These can be distilled to three potential processes that might explain intermittent oxygenation of the Horn River Group seafloor: (1) a downward shift of the upper OMZ boundary, possibly caused by some high-frequency climatic periodicity comparable to ENSO; (2) episodic bypassing of oxic ocean waters over oceanographic barriers, such as sills; or (3) sediment gravity flows that carry sediment and oxic waters to the distal basin floor. Considering that a topographic barrier cannot be definitively identified, and an overall absence of discernible turbidites, a cyclic climatic effect best explains intermittent oxygenation of Horn River Group bottom waters.

2.5.2 $\delta^{15}N_{bulk}$ signatures

The $\delta^{15}N_{bulk}$ values of sediments or sedimentary rocks are weighted averages of the N isotopic compositions of organic N and mineral-bound N. Because the N in detrital minerals is low and the N in authigenic minerals is mainly sourced from organic degradation and thus has similar $\delta^{15}N$ value to that of OM (Y. Li et al., 2021; Williams et al., 1995), the $\delta^{15}N_{bulk}$ values of OM-rich sediments or sedimentary rocks are generally representative of the organic signatures of the samples. Before interpreting $\delta^{15}N_{bulk}$ values in the context of primary organic signatures, it is important to note that microbial degradation of OM during early diagenesis can produce $\delta^{15}N$ shifts. The magnitude of these changes is dependent on productivity, bottom water dissolved oxygen concentration, and sedimentation rate (Robinson et al., 2012). Accordingly, the $\delta^{15}N$ values of sediments from modern continental margin settings (shelf and slope; water depth < ~ 1,000 m) have been found to reflect the $\delta^{15}N$ signatures of photic zone NO_3^- and sinking particles, indicating negligible early-diagenetic $\delta^{15}N$ shifts (< 2 ‰), which contrasts with deeper water, open-ocean systems typically characterized by lower productivity and sedimentation rates

(Altabet et al., 1999; Freudenthal et al., 2001; Robinson et al., 2012; Thunell et al., 2004). A recent depositional interpretation of the Horn River Group points to a distal shelf setting (Biddle et al., 2021) with water depth coarsely estimated at 250– 300 m (Kabanov and Jiang, 2020), which according to the modern, would have been characterized minimal early-diagenetic $\delta^{15}N$ shifts in the sediment.

Thermal maturation is further expected to cause ^{15}N enrichment in the remaining OM as the lighter isotope is preferentially released during this process (Williams et al., 1995). Nonetheless, thermal maturation appears to have little effect on $\delta^{15}N_{bulk}$ and OM $\delta^{15}N$ values of sedimentary rocks (e.g., Boudou et al., 2008; Rivera et al., 2015), which could be explained by retention of released N through incorporation into authigenic clay minerals as fixed NH_4^+ (Ader et al., 2016; Williams et al., 1995) or minimal N isotope fractionation during thermal N loss (Boudou et al., 2008). A cross-plot of vitrinite reflectance (a proxy for thermal maturity) and $\delta^{15}N_{bulk}$ values shows that, while the few data from the N-09 core show a rough positive trend, more data from the N-20 core clearly show no relationship between $\delta^{15}N_{bulk}$ and R_o values (Fig. 2.5), suggesting that thermal maturation has not significantly affected $\delta^{15}N_{bulk}$ values in this case. Moreover, the N-20 core is located approximately 13 km to the WNW of the N-09 core and thus was buried deeper than the N-09 core, suggesting that the weak positive relationship between vitrinite reflectance and $\delta^{15}N_{bulk}$ in the N-09 core is unlikely to be indicative of a true thermal maturity – $\delta^{15}N_{bulk}$ relationship. Finally, vitrinite is classified into two types, and the classical vitrinite reflectance scale is based on type 1 vitrinite. However, it is not uncommon for other macerals to be misidentified as vitrinite, or the wrong type of vitrinite to be measured (Tissot et al., 1987), which may be the cause of the vitrinite reflectance outliers in Figure 2.5.

Considering the potential effects of microbial degradation and thermal maturation on the $\delta^{15}N_{bulk}$ values of the Horn River Group in the N-09 and N-20 cores, we conclude that the $\delta^{15}N_{bulk}$ signatures observed are representative of the primary organic signatures of the samples. The primary organic signature, in turn, is impacted by the type of inorganic N used by organisms that first introduce N into the food chain. We use the term inorganic N users (INUs) to refer to organisms that take up inorganic N (e.g., bacteria, algae) as opposed to organisms that obtain N by consuming other living things (e.g., animals).

Some organisms assimilate dissolved nitrate whereas other organisms, known as diazotrophs, obtain N by 'fixing' dissolved atmospheric N_2. Relative to atmospheric N_2 gas ($\delta^{15}N$ = 0 ‰), dissolved N_2 is slightly enriched in ^{15}N, with $\delta^{15}N$ value of approximately +0.7 ‰ (Emerson et al., 1999). Studies of modern diazotrophic cyanobacteria have shown that fractionation during N_2 fixation catalyzed by Mo (the most common catalyst in modern oceans) varies from ~ –2 ‰ to –3 ‰, resulting in biomass $\delta^{15}N$ values of –2‰ to 0‰ (e.g., Bauersachs et al., 2009; Carpenter et al., 1997; Minagawa and Wada, 1986; Montoya et al., 2002). Diazotrophic cyanobacteria with "alternative" vanadium (V)- and iron (Fe)-only nitrogenases can have larger magnitude of isotope fractionation and thus produce $\delta^{15}N$ as low as –6‰ to –7‰ (Zhang et al., 2014).

Processes that remove N from seawater and recycle N within the oceans can also modify the isotopic signature of the fixed N pool. In OMZs of modern oceans, non-quantitative loss of fixed N through denitrification and anammox results in large $\delta^{15}N$ enrichment of the remaining NO_3^-, producing heavy $\delta^{15}N_{NO3-}$ values exceeding +15 ‰ (e.g., Brandes et al., 1998; Cline and Kaplan, 1975). However, N isotopic enrichments produced by fixed N loss are not always this large. For denitrification and anammox zones in marine *sediments*, models suggest positive $\delta^{15}N$

shifts in overlying water column NO_3^- that range from only ~ 0 ‰ to +5 ‰ (e.g., Brandes and Devol, 2002; Kessler et al., 2014 and references therein) and settings characterized by water column anoxia (and thus quantitative denitrification) show very little resulting $\delta^{15}N$ enrichment of NO_3^- (e.g., Thunell et al., 2004). Nitrogen isotopic fractionation can also occur during mineralization of OM and nitrification (Ader et al., 2016), although associated shifts in $\delta^{15}N$ of the fixed N pool are minimal if these processes are near quantitative (e.g., Thunell et al., 2004).

Biological uptake of NO_3^- or NH_4^+ through assimilation by INUs can produce significant negative $\delta^{15}N$ shifts relative to the N source because the lighter ^{14}N is preferentially taken up in this process (e.g., decreases of up to ~ 9 ‰ for NO_3^- assimilation and up to ~ 25 ‰ for NH_4^+; Bauersachs et al., 2009; Pennock et al., 1996). The degree of fractionation depends on the availability of fixed N and the biological growth rate, with higher N availability and/or lower growth rates associated with higher fractionation and thus lighter $\delta^{15}N$ in primary producers (e.g., Hoch et al., 1994; Kessler et al., 2014; Thunell et al., 2004; Wada et al., 1990). The particulate OM (mostly from organisms using NO_3^- or NH_4^+) in modern global oceans mainly have positive values with an average $\delta^{15}N$ value of +5.1‰ (see data summary in Li et al., 2014).

In our Paleozoic samples, the $\delta^{15}N_{bulk}$ values are mostly between 0‰ and –4‰ in the N-20 core and 0‰ and –2‰ in the N-09 core (except for the Bluefish Member, which will be discussed below). These persistent negative $\delta^{15}N_{bulk}$ values could be possibly obtained in one or more of the following ways: (1) assimilation of abundant (non-limiting) NO_3^-, (2) assimilation of abundant (non-limiting) NH_4^+, or (3) N_2 fixation. First, NO_3^- assimilation from a NO_3^--unlimited reservoir is associated with a large isotopic effect and can result in a similar $\delta^{15}N$ range to the values observed in this study (Bauersachs et al., 2009). We discount this first possibility because the interpreted paleoredox conditions (regularly occurring photic zone euxinia) would have been

associated with intense denitrification and thus, it is unlikely that NO_3^- was abundant to the point that it was non-limiting for growth. Second, abundant (non-growth-limiting) NH_4^+ advected from deeper waters could lead to N isotopic fractionation during assimilation, producing ^{15}N-depleted biomass (Ader et al., 2016) and $\delta^{15}N$ values similar to those seen herein. For an interval of strata representing the Cenomanian–Turonian Ocean Anoxic Event II (OAE II), Junium and Arthur (2007) interpreted that $\delta^{15}N_{bulk}$ values of approximately –2‰ to –3‰ represent a period of chemocline rising and assimilation of ^{15}N-depleted NH_4^+. A scenario of abundant NH_4^+ is plausible for the Horn River Group given that reducing conditions in the water column would have been associated with lower levels of nitrification. However, in contrast to the highly fluctuating redox change in the OAE II case, the Horn River Group was deposited in dominantly reducing conditions. This would have caused the reduction of a majority of the dissolved NO_3^-. As a result, the NH_4^+ product should have high $\delta^{15}N$ values (close to that of initial NO_3^-) rather than low $\delta^{15}N$ values, and thus cannot be responsible for the low $\delta^{15}N$ values in the Horn River Group. In addition, a comparison of $\delta^{15}N_{bulk}$ to $\delta^{13}C_{org}$, which is discussed in detail in section 5.3, does not show any relationship (Fig. 2.8). This suggests a decoupling of the sources or processes that affect C and N in this interval. If phytoplankton used C and N both from dissolved ions, the $\delta^{13}C_{org}$ and $\delta^{15}N_{bulk}$ values should vary parallelly as primary productivity changes, but this covariance is not observed, which indicates primary producers instead derive N from atmospheric N_2 (e.g., Hodell and Schelske, 1998; Li et al., 2008). This leads us to the third possibility: N_2 fixation. The observed $\delta^{15}N_{bulk}$ range (–2‰ to 0‰) is consistent with the $\delta^{15}N$ signatures of diazotrophs. Although paleoredox conditions would have limited the presence of aerobic diazotrophs (e.g., the cyanobacteria *Trichodesmium*) to the upper oxygenated water column, anaerobic diazotrophs (e.g., the bacteria *Vibrio diazotrophicus*) could have occupied the

deeper shelfal waters, much like in the modern including the Costa Rica Dome OMZ (Cheung et al., 2016) and the Peru Margin OMZ (e.g., Loescher et al., 2014). The $\delta^{13}C_{org} - \delta^{15}N_{bulk}$ decoupling observed in this study (Fig. 2.8) also lends support to the third possibility (prevalence of diazotrophs) suggesting that atmospheric N_2 was most likely the dominant source of N to INUs during deposition of the Horn River Group in our study area. Interestingly, biomarker results point to the presence of green sulfur bacteria (anaerobic phototrophs) in the Bluefish Member of the Hare Indian Formation and the Canol Formation (Kabanov and Jiang, 2020) and many modern species of these bacteria are diazotrophic (e.g., Madigan, 1995).

The $\delta^{15}N_{bulk}$ values of the N-09 core show a peak in the Bluefish Member near the contact with the underlying Hume Formation (Fig. 2.4). This contact represents drowning of the underlying carbonate platform caused by marine transgression (Morrow, 2018), also interpreted as a drowning unconformity *sensu* W. Schlager (Kabanov and Gouwy, 2017). In the N-09 core, the interval at the base of the Bluefish Member is characterized by organic-rich, calcareous to argillaceous mudstone intercalated with limestone laminae and beds, which are commonly graded, and contain tentaculitids and fragments of other benthic fossils such as *Amphipora*, brachiopods, and ostracods (Kabanov et al., 2016). These characteristics of the limestone beds suggest that they comprise transported debris, possibly derived from an up-dip area where the carbonate factory was still operating following significant relative sea-level rise. The relatively high $\delta^{15}N_{bulk}$ values observed at the base of the Bluefish Member in the N-09 core likely correspond to these limestone beds. OM with higher $\delta^{15}N$ was likely transported along with carbonate debris from a more proximal area where higher dissolved oxygen in the water column meant that NO_3^- was available to primary producers. Statistical outliers in $\delta^{15}N_{bulk}$ from the N-09 core in Figure 2.7 also belong to this interval at the base of the Bluefish Member. The absence of

similarly high $\delta^{15}N$ readings in the N-20 core can be explained by two factors. First, in the N-09 core, the stratigraphically lowest sample was collected right at the Bluefish Member – Hume Formation contact, whereas the lowest sample from the N-20 core was collected 2.9 m above the Bluefish Member base. Secondly, the sampling spacing for the N-20 core (2 m) was somewhat coarser than for the N-09 core (0.6 – 0.7 m), making it more likely that the basal Bluefish limestone beds comprising transported debris were not sampled.

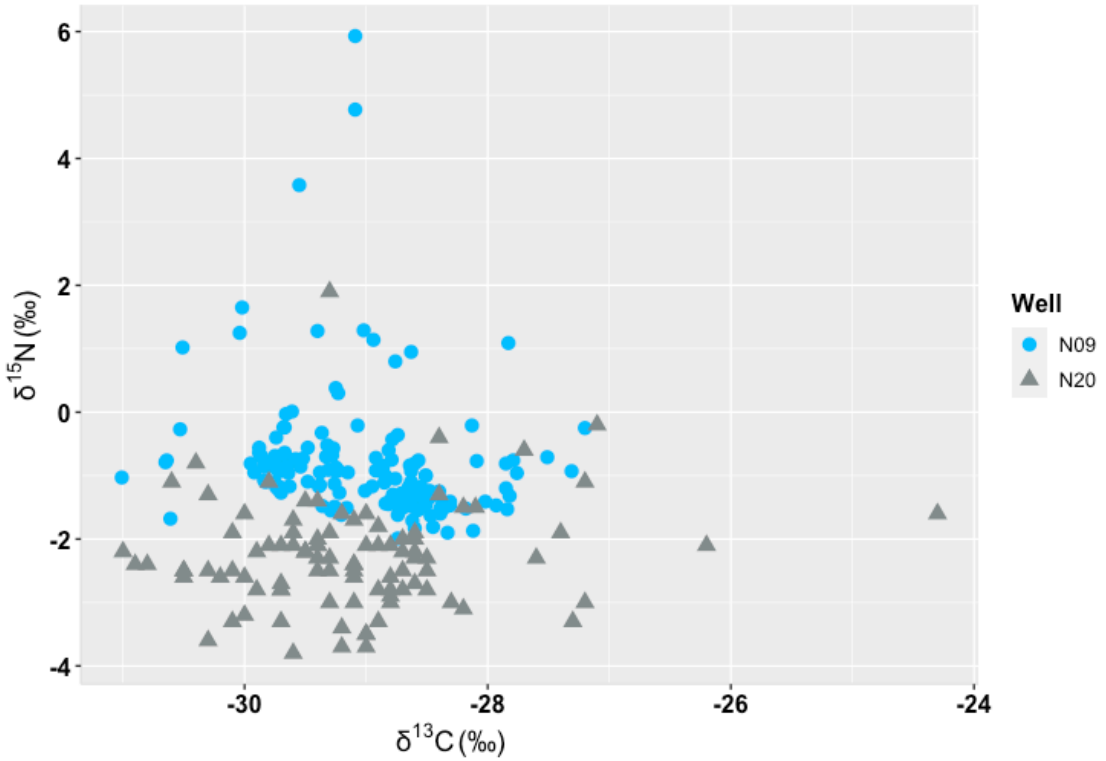

Figure 2.8 A crossplot of $\delta^{13}C_{org}$ and $\delta^{15}N_{bulk}$ for all Horn River Group and Imperial Formation samples in both the N-09 and N-20 cores.

Finally, relative to the N-09 core, the $\delta^{15}N_{bulk}$ signatures from the N-20 core are on average 1.4 ‰ lower in the Canol Formation and 1.6 ‰ lower in the Hare Indian Formation (Table 1; Fig.

2.7 and 2.8). Although a small inter-lab $\delta^{15}N$ discrepancy could occur, these large differences in $\delta^{15}N_{bulk}$ are more likely explained by somewhat differing marine conditions at the location of each core. While the $\delta^{15}N_{bulk}$ values in both cores indicates a dominance of diazotroph INUs, lower average $\delta^{15}N_{bulk}$ in the N-20 core is suggestive of a higher proportion of diazotrophs compared to the N-09 core, where there may have been a slightly higher contribution of DIN-assimilating INUs in the near surface oxygenated zone. The N-20 core is situated approximately 13 km to the WNW from the N-09 core, and thus was deposited in a seaward position relative to the N-09. It is possible that there were differences in the supply of nutrients or abundance of oxygen in surface waters between these two positions in the basin, affecting the abundance of DIN. If this difference were instead attributed to contrasting burial depth and thermal maturity between the two cores, this would mean that the N-09 core experienced a higher degree of thermal degradation of organic matter than the N-20 core. In fact, vitrinite reflectance values from the two cores are comparable (Fig. 2.5) and the N-20 was buried deeper, which discounts the possibility of variations in thermal maturity as the cause of the $\delta^{15}N_{bulk}$ differences.

2.5.3 $\delta^{13}C_{org}$ signatures

The factors that may affect $\delta^{13}C$ values of OM are similar to those that control $\delta^{15}N_{bulk}$, starting with the C isotopic signatures of primary producers. In the modern, $\delta^{13}C$ signatures of both land plants and phytoplankton vary depending on the species, within a range of approximately –20 ‰ to –30 ‰ for C_3 land plants (e.g., Fry and Sherr, 1984; Sackett, 1989; Wilson et al., 2005) and –10 ‰ to –30 ‰ for marine phytoplankton (e.g., Falkowski, 1991; Lamb et al., 2006; Wilson et al., 2005). The $\delta^{13}C_{org}$ values from the N-20 and N-09 cores range from –31.0 ‰ to –24.3 ‰ (Fig. 4), within the approximate range for both marine phytoplankton and C_3 land plants.

Previous petrologic analysis, Rock-Eval results, and biomarker results from the Bluefish Member and Canol Formation in the area indicated that OM is predominantly marine in both these units, with a high proportion of algal megaspores in the Bluefish Member and phytoplankton debris dominated-OM in the Canol Formation (Snowdon et al., 1987). When considered with the depositional interpretation for the Horn River Group (distal shelf; Biddle et al., 2021), the results from Snowdon et al. (1987) suggest that during deposition of the Horn River Group, primary producers comprised mostly marine phytoplankton (e.g., algae or bacteria, which is consistent with the $\delta^{15}N_{bulk}$ signatures indicative of diazotrophs) with possible minor contributions from land plants.

Microbial degradation can subsequently modify carbon isotopic signatures of OM. Studies from some areas have observed that microbial degradation does not significantly alter $\delta^{13}C$ signatures of OM (e.g., Chen et al., 2008; Galimov, 2004; Meyers and Eadie, 1993; Schelske and Hodell, 1995), whereas in other cases it has been concluded that these processes do result in small $\delta^{13}C_{org}$ shifts (e.g., Benner et al., 1987; Bottcher et al., 1998; Galimov, 2004; Lehmann et al., 2002; Prahl et al., 1997). For example, a decrease of 4 ‰ and 1.6 ‰ in $\delta^{13}C_{org}$ following microbial degradation was observed by Benner et al. (1987) and Lehmann et al. (2002), respectively. Microbial degradation should lead to decreased $\delta^{13}C_{org}$ because it results in enrichment of lignin in the remaining organic matter, which is ^{13}C poor relative to other components of organic matter (Benner et al., 1987; Lehmann et al., 2002). Nonetheless, these decreases may be counteracted by the in situ growth of heterotrophic microbial biomass enriched in ^{13}C compared to primary producers from the trophic effect (Chen et al., 2008). Finally, thermal maturation of organic matter during burial leads to increases in $\delta^{13}C_{org}$ of the residual OM (typically by < 2 ‰) because molecules with lower weight experience preferential thermal

cracking (Lewan, 1983; Tang et al., 2005; Tocqué et al., 2005). Even with C isotopic shifts of a few per mil associated with microbial degradation and thermal maturation (which may have counteracted one another), the $\delta^{13}C_{org}$ signatures observed are within the expected range for marine phytoplankton and C_3 plants (Falkowski, 1991; e.g., Fry and Sherr, 1984; Sackett, 1989; Wilson et al., 2005).

The $\delta^{13}C_{org}$ datasets shows trends throughout the Horn River Group and overlying Imperial Formation (Fig. 2.4), consisting most notably of four peaks in $\delta^{13}C_{org}$, labelled A–D following the system of Kabanov and Jiang (2020). Peak A is present in the Francis Creek Member of the Hare Indian Formation, while peak C and D are observed in the Imperial Formation. The statistical outlier in $\delta^{13}C_{org}$ from Figure 2.7 A–C corresponds to peak C. Through comparison of $\delta^{13}C_{org}$ to the Oxygen Index and visual core observations, Kabanov and Jiang (2020) interpreted that peaks A, C, and D can be explained by the presence of terrigenous OM. Following this interpretation, $\delta^{13}C_{org}$ peaks A, C, and D are best explained by a larger proportion of terrestrial OM than the rest of the Horn River Group, with the terrestrial OM characterized by higher $\delta^{13}C_{org}$ relative to the marine phytoplankton. The addition of terrestrially derived OM is typically expected to also influence $\delta^{15}N_{bulk}$ signatures, which is not observed (Fig. 2.4). However, it is possible that temporal variations in the proportion of terrestrial OM produced shifts in $\delta^{13}C_{org}$ but not $\delta^{15}N_{bulk}$. Terrestrial plants contain a similar proportion of C as aquatic plants, but much less N (e.g., Meyers, 1994). This mass difference led Algeo et al. (2014) to suggest that the addition of a small proportion (e.g., 10–20%) of terrestrial OM has little influence on the $\delta^{15}N_{bulk}$ of the marine sedimentary units. Thus, if the fraction of terrestrial OM compared to marine OM in horizons A, C, and D is small, this would explain the absence of corresponding $\delta^{15}N_{bulk}$ shifts.

Peak B in $\delta^{13}C_{org}$ values occurs in the Vermillion Creek Member of the Canol Formation. This horizon B marks the shift from overall increasing $\delta^{13}C_{org}$ moving from the Hare Indian Formation (Powell Creek Member) upwards into the lower Canol Formation to a trend of generally upwards decreasing $\delta^{13}C_{org}$ throughout the mid to upper Canol Formation into the base of the Imperial Formation (Fig. 2.4). It is not associated with an increase in Oxygen Index or the presence of terrigenous OM in core and instead coincides with a horizon characterized by proxies suggestive of a shift to more reducing conditions in the water column and/or sediment (Kabanov and Jiang, 2020). We explore the other possible causes of this spike in $\delta^{13}C_{org}$ values: (1) a difference in thermal maturity, and (2) a local and/or global change in biological productivity.

First, variations in the degree of thermal maturity with depth could cause trends in $\delta^{13}C_{org}$, with higher thermal maturity resulting in increased $\delta^{13}C_{org}$ (Tang et al., 2005; Tocqué et al., 2005). Average $\delta^{13}C_{org}$ and vitrinite reflectance values were cross-plotted at a two-meter interval and no relationship is observed (Fig. 2.6). As such, it is unlikely that thermal maturation is the cause of peak B in $\delta^{13}C_{org}$.

Secondly, trends in $\delta^{13}C_{org}$ could reflect variations in biological productivity. Biological uptake of C favours ^{12}C (Freeman, 2001) and photosynthesis in aquatic primary producers favours $CO_{2\,(aq)}$ over HCO_3^- (Degens et al., 1968). If growth rates increase, $\delta^{13}C$ values in primary producers shift toward heavier values (Falkowski, 1991; O'Leary, 1981). This heavier shift in $\delta^{13}C$ of primary producers can be explained by a switch to reliance on HCO_3^-, which is isotopically heavier, or because of a change in isotopic fractionation between dissolved inorganic C and primary producers (Hollander and Mackenzie, 1991). A peak in $\delta^{13}C_{org}$, as observed in peak B, would represent maximum biological productivity, with generally decreasing biological

productivity after the deposition of this horizon associated with decreasing $\delta^{13}C_{org}$ (Fig. 2.4). Moreover, the results presented herein indicate that diazotrophs are the dominant primary producers in this interval. Since the source of N (atmospheric N_2) was likely very large compared to demand by diazotrophs, variations in primary productivity would not have resulted in variations in the degree of N isotopic fractionation, which could explain why there is no corresponding peak in $\delta^{15}N_{bulk}$ (Fig. 2.4).

The relationship between $\delta^{13}C_{org}$ and TOC in the N-09 and N-20 cores is weak (Fig. 2.7 A) and the r^2 does not increase when the linear regression includes only samples from the Canol Formation (Fig. 2.7 B) or only samples from the Vermillion Creek Member of the Canol Formation, which contains peak B (Fig. 2.7 C). If $\delta^{13}C_{org}$ trends in the Canol Formation were produced by variations in biological productivity, effectively meaning that $\delta^{13}C_{org}$ is a proxy for productivity in the Canol Formation, one might expect a correlation between $\delta^{13}C_{org}$ and TOC. The observed lack of correlation between TOC and $\delta^{13}C_{org}$ in the Canol Formation (Fig. 2.7 B) thus suggests that biological productivity is not the dominant control on OM preservation in the Canol Formation. Results from Biddle et al. (2021) show higher TOC in Horn River Group samples deposited nearer to the shoreline, suggesting that sedimentation rates were one of the controls on OM preservation in the Horn River Group, although these results do not allow for the distinction between clastic and organic sediment supply. It is possible that other factors which also control OM deposition and preservation (e.g., clastic sedimentation rate) obscure the productivity – TOC relationship and thus the $\delta^{13}C_{org}$ – TOC relationship in the Canol Formation.

In summary, following Kabanov and Jiang (2020), we suggest that certain variations in $\delta^{13}C_{org}$ throughout the Horn River Group were produced by fluctuations in terrestrial OM abundance, specifically trends in the Imperial Formation and the Francis Creek Member of the

Hare Indian Formation (Fig. 2.4). For those two units, high $\delta^{13}C_{org}$ values are produced by an increased proportion of terrestrial OM compared to intervals displaying lower $\delta^{13}C_{org}$ values. The overall $\delta^{13}C_{org}$ trends present in the Canol Formation (increase up to peak B and then decrease; Fig. 2.4) are interpreted as the product of variations in biological productivity with high $\delta^{13}C_{org}$ values at peak B indicative of comparatively high growth rates.

Although changes in biological productivity during deposition of the Canol Formation may have occurred on a local scale, previous studies have suggested that trends in $\delta^{13}C_{org}$ from the Horn River Group may correspond with global $\delta^{13}C$ patterns. Positive $\delta^{13}C_{carb}$ and $\delta^{13}C_{org}$ excursions have been observed and correlated in Middle to Late Devonian sedimentary intervals worldwide, many of which have been correlated with biotic crises (e.g., Lash, 2019; Zhang et al., 2019). West of our study area, in the Richardson Mountains of the Yukon, Fraser and Hutchinson (2017) correlated $\delta^{13}C_{org}$ results from the Canol Formation to the global $\delta^{13}C_{carb}$ reference curve and associated Devonian global biotic crises. Eutrophication resulting in high biological productivity is commonly proposed as a cause of these Devonian global positive $\delta^{13}C$ excursions because of increased OM burial, producing depletion of ^{12}C in the marine C reservoir (e.g., Murphy et al., 2000; Pisarzowska and Racki, 2012). Moreover, for the N-09 and N-20 cores, Kabanov and Jiang (2020) observed $\delta^{13}C_{org}$ peaks in horizons of the Canol Formation that they also interpreted as Devonian global ocean anoxic events. The ultimate cause of eutrophication is debated, but high nutrient supply and elevated biological productivity is a widely accepted explanation for Devonian pulses of expanded marine anoxia (e.g., Algeo and Scheckler, 1998; Averbuch et al., 2005; Kaiho et al., 2021). To further investigate the possibility of $\delta^{13}C_{org}$ trends in the Horn River Group reflecting global patterns, correlation of Horn River

Group results with results from other age-equivalent organic-rich mudstone units is required in the future.

5.4 Depositional conditions

A prevalence of diazotrophs during deposition of the Horn River Group has implications for local marine conditions at the time. High N_2 fixation in modern oceans was initially thought to be associated mostly with oligotrophic areas (e.g., Carpenter et al., 1997; Kashiyama et al., 2008; Wada et al., 1990) because obtaining N by fixing atmospheric N_2 requires more energy than assimilating DIN from surface waters. Moreover, prolonged, abundant DIN depresses rates of N_2 fixation (Knapp, 2012 and references therein). Nonetheless, significant N_2 fixation has been observed in areas of coastal upwelling above OMZs characterized by denitrification (e.g., Fernandez et al., 2011) and several models predict highest N_2 fixation in areas downstream of upwelling zones (e.g., Deutsch et al., 2007; Wang et al., 2019). Experimental results from Knapp et al. (2012) suggest that higher abundances of NO_3^- can be counteracted by elevated PO_4^- abundance. Similarly, dissolved N:P ratios have been proposed as a major control on the global distribution of marine diazotrophs with higher N_2 fixation when N:P is lower (e.g., Deutsch et al., 2007; Fernandez et al., 2011; Ward et al., 2013). Several other factors have also been suggested as controls on N_2 fixation in the modern oceans including Fe abundance (Fe:N; e.g., Wang et al., 2019; Ward et al., 2013), dissolved oxygen (highest N2 fixation when dissolved oxygen is at a minimum; e.g., Fernandez et al., 2011; Luo et al., 2014), and temperature, with significant N_2 fixation limited to the tropics and subtropics (e.g., Luo et al., 2014).

Some of the proposed controls on modern diazotrophy, namely warm climates and limited dissolved oxygen in the water column, align with pre-existing interpretations of

depositional conditions for the Horn River Group of the NWT. The prevalence of diazotrophs and N sourced from N_2 fixation further suggests that dissolved N:P and N:Fe ratios were low in the vicinity of the N-09 and N-20 cores, likely a product of water-column denitrification and possibly from anoxic recycling of P in organic matter (e.g., Slomp et al., 2002).

In this Middle to Late Devonian example, relatively constant $\delta^{15}N_{bulk}$ values suggest that the dominant type of marine primary producers (diazotrophs) at this locality did not vary significantly as paleoredox conditions fluctuated (globally or locally). Rather, we propose that the biological productivity varied throughout deposition of the Canol Formation, likely on a global scale, as evidenced by trends in $\delta^{13}C_{org}$ that cannot be explained by variations in terrestrial OM input, thermal maturity, or microbial degradation. Studies synthesizing $^{15}N_{bulk}$, $\delta^{13}C_{org}$, and biomarker signatures from Middle to Late Devonian OM-rich mudstone successions worldwide would allow for the assessment of regional and global patterns in productivity and marine producers and their relationship to the series of global redox events and biotic crises that characterize these epochs.

2.6 Conclusions

A high-resolution dataset comprising $\delta^{13}C_{org}$ and $\delta^{15}N_{bulk}$ was collected from organic-rich mudstone samples of the Middle to Late Devonian Horn River at two locations in the Central Mackenzie Valley of the Northwest Territories, Canada. The following key conclusions are drawn from our results:

- The Horn River Group was deposited below a euxinic water column with oxygen only in the surface (wave-mixed) portion of the photic zone and periodic weak bottom water oxygenation. Through comparison to modern settings, periodic weak oxygenation is best

explained by downwards migration of the upper OMZ boundary, possibly associated with climatic periodicity comparable to El Nino Southern Oscillation (ENSO).

- $\delta^{13}C_{org}$ trends in the Canol Formation were produced by variations in biological productivity.
- $\delta^{15}N_{bulk}$ signatures in both cores suggest that diazotrophs (N_2 fixers) were dominant during deposition of the entire Horn River Group and basal Imperial Formation, despite variations in paleoredox conditions or biological productivity through time.
- A dominance of diazotrophs is suggestive of low N:P and N:Fe in ocean waters of the area at the time these cores were deposited.

2.7 Acknowledgments

We are grateful to the Northwest Territories Geological Survey and to the GSA (GSA Graduate Student Research Grant no. 13266-21) for funding of this work Additionally, we would like to thank Rizal Ignacio and Marcus Kehler for help with sample preparation.

2.8 References

Ader, M., Thomazo, C., Sansjofre, P., Busigny, V., Papineau, D., Laffont, R., Cartigny, P., Halverson, G.P., 2016. Interpretation of the nitrogen isotopic composition of Precambrian sedimentary rocks: Assumptions and perspectives. Chem. Geol. 429, 93–110. https://doi.org/10.1016/j.chemgeo.2016.02.010

Al-Aasm, I.S., Morad, S., Durocher, S., Muir, I., 1996. Sedimentology, C–S–Fe relationships and stable isotopic compositions in Devonian black mudrocks, Mackenzie Mountains,

Northwest Territories, Canada. Sediment. Geol. 106, 279–298. https://doi.org/10.1016/S0037-0738(96)00018-8

Algeo, T.J., Meyers, P.A., Robinson, R.S., Rowe, H., Jiang, G.Q., 2014. Icehouse–greenhouse variations in marine denitrification. Biogeosciences 11, 1273–1295. https://doi.org/10.5194/bg-11-1273-2014

Algeo, T.J., Scheckler, S.E., 1998. Terrestrial-marine teleconnections in the Devonian: links between the evolution of land plants, weathering processes, and marine anoxic events. Philos. Trans. R. Soc. Lond. B. Biol. Sci. 353, 113–130. https://doi.org/10.1098/rstb.1998.0195

Altabet, M.A., Pilskaln, C., Thunell, R., Pride, C., Sigman, D., Chavez, F., Francois, R., 1999. The nitrogen isotope biogeochemistry of sinking particles from the margin of the Eastern North Pacific. Deep Sea Res. Part Oceanogr. Res. Pap. 46, 655–679. https://doi.org/10.1016/S0967-0637(98)00084-3

Astor, Y., Muller-Karger, F., Scranton, M.I., 2003. Seasonal and interannual variation in the hydrography of the Cariaco Basin: implications for basin ventilation. Cont. Shelf Res. 23, 125–144. https://doi.org/10.1016/S0278-4343(02)00130-9

Averbuch, O., Tribovillard, N., Devleeschouwer, X., Riquier, L., Mistiaen, B., Van Vliet-Lanoe, B., 2005. Mountain building-enhanced continental weathering and organic carbon burial as major causes for climatic cooling at the Frasnian–Famennian boundary (c. 376 Ma)? Terra Nova 17, 25–34. https://doi.org/10.1111/j.1365-3121.2004.00580.x

Bauersachs, T., Schouten, S., Compaoré, J., Wollenzien, U., Stal, L.J., Sinninghe Damsteé, J.S., 2009. Nitrogen isotopic fractionation associated with growth on dinitrogen gas and nitrate

by cyanobacteria. Limnol. Oceanogr. 54, 1403–1411. https://doi.org/10.4319/lo.2009.54.4.1403

Becker, R.T., Marshall, J.E.A., Da Silva, A.-C., Agterberg, F.P., Gradstein, F.M., Ogg, J.G., 2020. Chapter 22 - The Devonian Period, in: Gradstein, Felix M., Ogg, James G., Schmitz, M.D., Ogg, G.M. (Eds.), Geologic Time Scale 2020. Elsevier, pp. 733–810. https://doi.org/10.1016/B978-0-12-824360-2.00022-X

Benner, R., Fogel, M.L., Sprague, E.K., Hodson, R.E., 1987. Depletion of 13C in lignin and its implications for stable carbon isotope studies. Nature 329, 708–710. https://doi.org/10.1038/329708a0

Beranek, L.P., Mortensen, J.K., Lane, L.S., Allen, T.L., Fraser, T.A., Hadlari, T., Zantvoort, W.G., 2010. Detrital zircon geochronology of the western Ellesmerian clastic wedge, northwestern Canada: Insights on Arctic tectonics and the evolution of the northern Cordilleran miogeocline. GSA Bull. 122, 1899–1911. https://doi.org/10.1130/B30120.1

Biddle, S.K., LaGrange, M.T., Harris, B.S., Fiess, K., Terlaky, V., Gingras, M.K., 2021. A fine detail physico-chemical depositional model for Devonian organic-rich mudstones: A petrographic study of the Hare Indian and Canol Formations, Central Mackenzie Valley, Northwest Territories. Sediment. Geol. 414, 105838. https://doi.org/10.1016/j.sedgeo.2020.105838

Bottcher, M.E., Oelschlager, B., Hopner, T., Brumsack, H.-J., Rullkotter, J., 1998. Sulfate reduction related to the early diagenetic degradation of organic matter and "black spot'' formation in tidal sandflats of the German Wadden Sea (southern North Sea): stable isotope (13C, 34S, 18O) and other geochemical results. Org Geochem 29, 1517–1530.

Boudou, J.-P., Schimmelmann, A., Ader, M., Mastalerz, M., Sebilo, M., Gengembre, L., 2008. Organic nitrogen chemistry during low-grade metamorphism. Geochim. Cosmochim. Acta 72, 1199–1221. https://doi.org/10.1016/j.gca.2007.12.004

Brandes, J.A., Devol, A.H., 2002. A global marine-fixed nitrogen isotopic budget: Implications for Holocene nitrogen cycling. Glob. Biogeochem. Cycles 16, 67-1-67–14. https://doi.org/10.1029/2001GB001856

Brandes, J.A., Devol, A.H., Yoshinari, T., Jayakumar, D.A., Naqvi, S.W.A., 1998. Isotopic composition of nitrate in the central Arabian Sea and eastern tropical North Pacific: A tracer for mixing and nitrogen cycles. Limnol. Oceanogr. 43, 1680–1689. https://doi.org/10.4319/lo.1998.43.7.1680

Brown, T., Kenig, F., 2004. Water column structure during deposition of Middle Devonian–Lower Mississippian black and green/gray shales of the Illinois and Michigan Basins: a biomarker approach. Palaeogeogr. Palaeoclimatol. Palaeoecol. 215, 59–85. https://doi.org/10.1016/S0031-0182(04)00452-3

Burnham, A.K., Sweeney, J.J., 1989. A chemical kinetic model of vitrinite maturation and reflectance. Geochim. Cosmochim. Acta 53, 2649–2657. https://doi.org/10.1016/0016-7037(89)90136-1

Carmichael, S.K., Waters, J.A., Königshof, P., Suttner, T.J., Kido, E., 2019. Paleogeography and paleoenvironments of the Late Devonian Kellwasser event: A review of its sedimentological and geochemical expression. Glob. Planet. Change 183, 102984. https://doi.org/10.1016/j.gloplacha.2019.102984

Carpenter, E.J., Harvey, H.R., Fry, B., Capone, D.G., 1997. Biogeochemical tracers of the marine cyanobacterium Trichodesmium. Deep Sea Res. Part Oceanogr. Res. Pap. 44, 27–38. https://doi.org/10.1016/S0967-0637(96)00091-X

Chen, F., Zhang, L., Yang, Y., Zhang, D., 2008. Chemical and isotopic alteration of organic matter during early diagenesis: Evidence from the coastal area off-shore the Pearl River estuary, south China. J. Mar. Syst. 74, 372–380. https://doi.org/10.1016/j.jmarsys.2008.02.004

Cheung, S., Xia, X., Guo, C., Liu, H., 2016. Diazotroph community structure in the deep oxygen minimum zone of the Costa Rica Dome. J. Plankton Res. 38, 380–391. https://doi.org/10.1093/plankt/fbw003

Cline, J.D., Kaplan, I.R., 1975. Isotopic fractionation of dissolved nitrate during denitrification in the eastern tropical north pacific ocean. Mar. Chem. 3, 271–299. https://doi.org/10.1016/0304-4203(75)90009-2

Cocks, L.R.M., Torsvik, T.H., 2011. The Palaeozoic geography of Laurentia and western Laurussia: A stable craton with mobile margins. Earth-Sci. Rev. 106, 1–51. https://doi.org/10.1016/j.earscirev.2011.01.007

Degens, E.T., Gullard, R.R., Sackett, W.M., Hellebust, J.A., 1968. Metabolic fractionation of carbon isotopes in marine plankton: 1. Temperature and respiration experiments. Deep-Sea Res. 15, 1–9. https://doi.org/10.1016/0011-7471(68)90024-7

Deutsch, C., Sarmiento, J.L., Sigman, D.M., Gruber, N., Dunne, J.P., 2007. Spatial coupling of nitrogen inputs and losses in the ocean. Nature 445, 163–167. https://doi.org/10.1038/nature05392

Dewing, K., Hadlari, T., Pearson, D.G., Matthews, W., 2019. Early Ordovician to Early Devonian tectonic development of the northern margin of Laurentia, Canadian Arctic Islands. GSA Bull. 131, 1075–1094. https://doi.org/10.1130/B35017.1

Emeis, K.-C., Whelan, J.K., Tarafa, M., 1991. Sedimentary and geochemical expressions of oxic and anoxic conditions on the Peru Shelf. Geol. Soc. Lond. Spec. Publ. 58, 155–170. https://doi.org/10.1144/GSL.SP.1991.058.01.11

Emerson, S., Stump, C., Wilbur, D., Quay, P., 1999. Accurate measurement of O2, N2, and Ar gases in water and the solubility of N2. Mar. Chem. 64, 337–347. https://doi.org/10.1016/S0304-4203(98)00090-5

Falkowski, P.G., 1991. Species variability in the fractionation of 13C and 12C by marine phytoplankton. J. Phytoplankton Res. 13, 21–28.

Fernandez, C., Farías, L., Ulloa, O., 2011. Nitrogen Fixation in Denitrified Marine Waters. PLOS ONE 6, e20539. https://doi.org/10.1371/journal.pone.0020539

Fraser, T.A., Hutchison, M.P., 2017. Lithogeochemical characterization of the Middle–Upper Devonian Road River Group and Canol and Imperial formations on Trail River, east Richardson Mountains, Yukon: age constraints and a depositional model for fine-grained strata in the Lower Paleozoic Richardson trough. Can. J. Earth Sci. 54, 731–765. https://doi.org/10.1139/cjes-2016-0216

Freeman, K.H., 2001. Isotopic Biogeochemistry of Marine Organic Carbon. Rev. Mineral. Geochem. 43, 579–605. https://doi.org/10.2138/gsrmg.43.1.579

Freudenthal, T., Wagner, T., Wenzhöfer, F., Zabel, M., Wefer, G., 2001. Early diagenesis of organic matter from sediments of the eastern subtropical Atlantic: evidence from stable

nitrogen and carbon isotopes. Geochim. Cosmochim. Acta 65, 1795–1808. https://doi.org/10.1016/S0016-7037(01)00554-3

Fritz, W.H., Cecile, M.P., Norford, B.S., Morrow, D., Geldsetzer, H.H.J., 1991. Cambrian to Middle Devonian Assemblages, in: Geology of the Cordilleran Orogen in Canada. Geological Society of America. https://doi.org/10.1130/DNAG-GNA-G2.151

Fry, B., Sherr, E.B., 1984. δ13C measurements as indicators of carbon flow in marine and freshwater ecosystems. Contrib. Mar. Sci. 27, 13–47.

Gal, L.P., Pyle, L.J., Hadlari, T., Allen, T.L., 2009. Chapter 6: Lower to Upper Devonian strata, Arnica-Landry play, and Kee Scarp play, in: Pyle, L.J., Jones, A. (Eds.), Regional Geoscience Studies and Petroleum Potential, Peel Plateau and Plain, Northwest Territories and Yukon: Project Volume, Northwest Territories Geoscience Office and Yukon Geological Survey, NWT, Open File 2009-002 and Yukon Geological Survey Open File 2009-25.

Galimov, E.M., 2004. The pattern of δ13Corg versus HI/OI relation in recent sediments as an indicator of geochemical regime in marine basins: comparison of the Black Sea, Kara Sea, and Cariaco Trench. Chem. Geol. 204, 287–301. https://doi.org/10.1016/j.chemgeo.2003.11.014

Garzione, C.N., Patchett, P.J., Ross, G.M., Nelson, J., 1997. Provenance of Paleozoic sedimentary rocks in the Canadian Cordilleran miogeocline: a Nd isotopic study. Can. J. Earth Sci. 34, 1603–1618. https://doi.org/10.1139/e17-129

Gutiérrez, D., Enríquez, E., Purca, S., Quipúzcoa, L., Marquina, R., Flores, G., Graco, M., 2008. Oxygenation episodes on the continental shelf of central Peru: Remote forcing and

benthic ecosystem response. Prog. Oceanogr. 79, 177–189. https://doi.org/10.1016/j.pocean.2008.10.025

Hadlari, T., 2015. Oil migration driven by exhumation of the Canol Formation oil shale: A new conceptual model for the Norman Wells oil field, northwestern Canada. Mar. Pet. Geol. 65, 172–177. https://doi.org/10.1016/j.marpetgeo.2015.03.027

Hadlari, T., Davis, W.J., Dewing, K., 2014. A pericratonic model for the Pearya terrane as an extension of the Franklinian margin of Laurentia, Canadian Arctic. Geol. Soc. Am. Bull. 126, 182–200. https://doi.org/10.1130/B30843.1

Harrington, R.R., Kennedy, B.P., Chamberlain, C.P., Blum, J.D., Folt, C.L., 1998. 15N enrichment in agricultural catchments: field patterns and applications to tracking Atlantic salmon (Salmo salar). Chem. Geol. 147, 281–294. https://doi.org/10.1016/S0009-2541(98)00018-7

Harris, B.S., LaGrange, M.T., Biddle, S.K., Playter, T.L., Fiess, K.M., Gingras, M.K., 2021. Chemostratigraphy as a tool for sequence stratigraphy in the Devonian Hare Indian Formation in the Mackenzie Mountains and Central Mackenzie Valley, Northwest Territories, Canada. Can. J. Earth Sci. 99, 1–17. https://doi.org/10.1139/cjes-2020-0198

Harris, N.B. (Ed.), 2005. Deposition of Organic-Carbon-Rich Sediments: Models. SEPM (Society for Sedimentary Geology). https://doi.org/10.2110/pec.05.82

Hills, L.V., Sangster, E.V., Suneby, L.B. (Eds.), 1981. Lexicon of Canadian stratigraphy, Volume 2. Yukon Territory and District of Mackenzie. Canadian Society of Petroleum Geologists, Calgary.

Hoch, M.P., Fogel, M.L., Kirchman, D.L., 1994. Isotope fractionation during ammonium uptake by marine microbial assemblages. Geomicrobiol. J. 12, 113–127. https://doi.org/10.1080/01490459409377977

Issler, D.R., Grist, A.M., Stasiuk, L.D., 2005. Post-Early Devonian thermal constraints on hydrocarbon source rock maturation in the Keele Tectonic Zone, Tulita area, NWT, Canada, from multi-kinetic apatite fission track thermochronology, vitrinite reflectance and shale compaction. Bull. Can. Pet. Geol. 53, 405–431. https://doi.org/10.2113/53.4.405

Jeletzky, J.A., 1975. Jurassic and lower Cretaceous Paleogeography and depositional tectonics of Porcupine Plateau, adjacent areas of northern Yukon and those of Mackenzie District (Paper No. 74–16). Geological Survey of Canada. https://doi.org/10.4095/ 102549

Junium, C.K., Arthur, M.A., 2007. Nitrogen cycling during the Cretaceous, Cenomanian-Turonian Oceanic Anoxic Event II. Geochem. Geophys. Geosystems 8. https://doi.org/10.1029/2006GC001328

Kabanov, P., 2019. Devonian (c. 388–375 Ma) Horn River Group of Mackenzie Platform (NW Canada) is an open-shelf succession recording oceanic anoxic events. J. Geol. Soc. 176, 29–45. https://doi.org/10.1144/jgs2018-075

Kabanov, P., Deblonde, C., 2019. Geological and geochemical data from Mackenzie Corridor. Part VIII: Middle-Upper Devonian lithostratigraphy, formation tops, and isopach maps in NTS areas 96 and 106, Northwest Territories and Yukon (Geological Survey of Canada Open File Report No. 8552). https://doi.org/10.4095/314785

Kabanov, P., Gouwy, S., Lawrence, P.A., Weleschuk, D.J., Chan, W.C., 2016. Geological and geochemical data from Mackenzie Corridor. Part III: New data on lithofacies,

micropaleontology, lithogeochemistry, and Rock-EvalTM pyrolysis from the Devonian Horn River Group in the Mackenzie Plain and Norman Range, Northwest Territories (Geological Survey of Canada Open File Report No. 7951).

Kabanov, P., Gouwy, S.A., 2017. The Devonian Horn River Group and the basal Imperial Formation of the central Mackenzie Plain, N.W.T., Canada: multiproxy stratigraphic framework of a black shale basin. Can. J. Earth Sci. 54, 409–429. https://doi.org/10.1139/cjes-2016-0096

Kabanov, P., Jiang, C., 2020. Photic-zone euxinia and anoxic events in a Middle-Late Devonian shelfal sea of Panthalassan continental margin, NW Canada: Changing paradigm of Devonian ocean and sea level fluctuations. Glob. Planet. Change 188, 103153. https://doi.org/10.1016/j.gloplacha.2020.103153

Kabanov, P.B., 2015. Geological and geochemical data from the Mackenzie Corridor. Part I: Devonian cored sections and results for 2014 on geochemistry, d13C - d18O, and Rock-Eval 6 pyrolysis (Geological Survey of Canada Open File Report No. 7840). https://doi.org/10.4095/297403

Kaiho, K., Miura, M., Tezuka, M., Hayashi, N., Jones, D.S., Oikawa, K., Casier, J.-G., Fujibayashi, M., Chen, Z.-Q., 2021. Coronene, mercury, and biomarker data support a link between extinction magnitude and volcanic intensity in the Late Devonian. Glob. Planet. Change 199, 103452. https://doi.org/10.1016/j.gloplacha.2021.103452

Kashiyama, Y., Ogawa, N.O., Kuroda, J., Shiro, M., Nomoto, S., Tada, R., Kitazato, H., Ohkouchi, N., 2008. Diazotrophic cyanobacteria as the major photoautotrophs during mid-Cretaceous oceanic anoxic events: Nitrogen and carbon isotopic evidence from

sedimentary porphyrin. Org. Geochem. 39, 532–549. https://doi.org/10.1016/j.orggeochem.2007.11.010

Kessler, A.J., Bristow, L.A., Cardenas, M.B., Glud, R.N., Thamdrup, B., Cook, P.L.M., 2014. The isotope effect of denitrification in permeable sediments. Geochim. Cosmochim. Acta 133, 156–167. https://doi.org/10.1016/j.gca.2014.02.029

Klemme, H.D., Ulmishek, G.F., 1991. Effective Petroleum Source Rocks of the World: Stratigraphic Distribution and Controlling Depositional Factors. Am. Assoc. Pet. Geol. Bull. 75, 1809–1851. https://doi-org.login.ezproxy.library.ualberta.ca/10.1306/0C9B2A47-1710-11D7-8645000102C1865D

Knapp, A., 2012. The sensitivity of marine N2 fixation to dissolved inorganic nitrogen. Front. Microbiol., Article 374 3, 1–14. https://doi.org/10.3389/fmicb.2012.00374

Knapp, A., Dekaezemacker, J., Bonnet, S., Sohm, J., Capone, D., 2012. Sensitivity of Trichodesmium erythraeum and Crocosphaera watsonii abundance and N<sub>2 fixation rates to varying NO<sub>3<sup>− and PO<sub>4<sup>3− concentrations in batch cultures. Aquat. Microb. Ecol. 66, 223–236. https://doi.org/10.3354/ame01577

Konhauser, K., 2007. Introduction to Geomicrobiology. Blackwell Pub., Malden, MA.

LaGrange, M.T., Atienza, N.M.M., Biddle, S.K., Harris, B.S., Fiess, K.M., Terlaky, V., Konhauser, K.O., Gingras, M.K., 2022. The nature, origin, and predictors of porosity in the Middle to Late Devonian Horn River Group of the Central Mackenzie Valley, Northwest Territories, Canada. Mar. Pet. Geol. 142, 105738. https://doi.org/10.1016/j.marpetgeo.2022.105738

Lamb, A.L., Wilson, G.P., Leng, M.J., 2006. A review of coastal palaeoclimate and relative sea-level reconstructions using δ13C and C/N ratios in organic material. Earth-Sci. Rev. 75, 29–57. https://doi.org/10.1016/j.earscirev.2005.10.003

Lash, G.G., 2019. A global biogeochemical perturbation during the Middle Frasnian punctata Event: Evidence from muted carbon isotope signature in the Appalachian Basin, New York State (USA). Glob. Planet. Change 177, 239–254. https://doi.org/10.1016/j.gloplacha.2019.01.006

Lazar, O.R., Bohacs, K.M., Macquaker, J.H.S., Schieber, J., Demko, T.M., 2015. Capturing key attributes of fine-grained sedimentary rocks in outcrops, cores, and thin sections: nomenclature and description guidelines. J. Sediment. Res. 85, 230–246. https://doi.org/10.2110/jsr.2015.11

Lehmann, M.F., Bernasconi, S.M., Barbieri, A., McKenzie, J.A., 2002. Preservation of organic matter and alteration of its carbon and nitrogen isotope composition during simulated and in situ early sedimentary diagenesis. Geochim. Cosmochim. Acta 66, 3573–3584. https://doi.org/10.1016/S0016-7037(02)00968-7

Lenz, A.C., 1972. Ordovician to Devonian history of northern Yukon and adjacent district of Mackenzie. Bull. Can. Pet. Geol. 20, 321–361. https://doi.org/10.35767/gscpgbull.20.2.321

Lewan, M.D., 1983. Effects of thermal maturation on stable organic carbon isotopes as determined by hydrous pyrolysis of Woodford Shale. Geochim. Cosmochim. Acta 47, 1471–1479. https://doi.org/10.1016/0016-7037(83)90306-X

Li, L., Zheng, Y.-F., Cartigny, P., Li, J., 2014. Anomalous nitrogen isotopes in ultrahigh-pressure metamorphic rocks from the Sulu orogenic belt: Effect of abiotic nitrogen

reduction during fluid–rock interaction. Earth Planet. Sci. Lett. 403, 67–78. https://doi.org/10.1016/j.epsl.2014.06.029

Li, Y., Li, L., Wu, Z., 2021. First-principles calculations of equilibrium nitrogen isotope fractionations among aqueous ammonium, silicate minerals and salts. Geochim. Cosmochim. Acta 297, 220–232. https://doi.org/10.1016/j.gca.2021.01.019

Loescher, C.R., Großkopf, T., Desai, F.D., Gill, D., Schunck, H., Croot, P.L., Schlosser, C., Neulinger, S.C., Pinnow, N., Lavik, G., Kuypers, M.M.M., LaRoche, J., Schmitz, R.A., 2014. Facets of diazotrophy in the oxygen minimum zone waters off Peru. ISME J. 8, 2180–2192. https://doi.org/10.1038/ismej.2014.71

Lu, M., Lu, Y., Ikejiri, T., Sun, D., Carroll, R., Blair, E.H., Algeo, T.J., Sun, Y., 2021. Periodic oceanic euxinia and terrestrial fluxes linked to astronomical forcing during the Late Devonian Frasnian–Famennian mass extinction. Earth Planet. Sci. Lett. 562, 116839. https://doi.org/10.1016/j.epsl.2021.116839

Luo, Y.-W., Lima, I.D., Karl, D.M., Deutsch, C.A., Doney, S.C., 2014. Data-based assessment of environmental controls on global marine nitrogen fixation. Biogeosciences 11, 691–708. https://doi.org/10.5194/bg-11-691-2014

MacLean, B.C., 2011. Tectonic and stratigraphic evolution of the Cambrian basin of northern Northwest Territories. Bull. Can. Pet. Geol. 59, 172–194. https://doi.org/10.2113/gscpgbull.59.2.172

MacLean, B.C., Fallas, K.M., Hadlari, T., 2014. The multi-phase Keele Arch, central Mackenzie Corridor, Northwest Territories. Bull. Can. Pet. Geol. 62, 68–104. https://doi.org/10.2113/gscpgbull.62.2.68

Madigan, M.T., 1995. Microbiology of Nitrogen Fixation by Anoxygenic Photosynthetic Bacteria, in: Blankenship, R.E., Madigan, M.T., Bauer, C.E. (Eds.), Anoxygenic Photosynthetic Bacteria. Advances in Photosynthesis and Respiration. Springer, Dordrecht.

Mayer, B., Boyer, E.W., Goodale, C., Jaworski, N.A., Van Breemen, N., Howarth, R.W., Seitzinger, S., Billen, G., Lajtha, K., Nadelhoffer, K., Van Dam, D., Hetling, L.J., Nosal, M., Paustian, K., 2002. Sources of nitrate in rivers draining sixteen watersheds in the northeastern U.S.: Isotopic constraints, in: Boyer, E.W., Howarth, R.W. (Eds.), The Nitrogen Cycle at Regional to Global Scales. Springer Netherlands, Dordrecht, pp. 171–197. https://doi.org/10.1007/978-94-017-3405-9_5

Mazzotti, S., Hyndman, R.D., 2002. Yakutat collision and strain transfer across the northern Canadian Cordillera. Geology 30, 495–498. https://doi-org.login.ezproxy.library.ualberta.ca/10.1130/0091-7613(2002)030<0495:YCASTA>2.0.CO;2

McGhee, G.R., Clapham, M.E., Sheehan, P.M., Bottjer, D.J., Droser, M.L., 2013. A new ecological-severity ranking of major Phanerozoic biodiversity crises. Palaeogeogr. Palaeoclimatol. Palaeoecol. 370, 260–270. https://doi.org/10.1016/j.palaeo.2012.12.019

Meyers, P.A., 1994. Preservation of elemental and isotopic source identification of sedimentary organic matter. Chem. Geol. 114, 289–302. https://doi.org/10.1016/0009-2541(94)90059-0

Meyers, P.A., Eadie, B.J., 1993. Sources, degradation and recycling of organic matter associated with sinking particles in Lake Michigan. Org. Geochem. 20, 47–56. https://doi.org/10.1016/0146-6380(93)90080-U

Minagawa, M., Wada, E., 1986. Nitrogen isotope ratios of red tide organisms in the East China Sea: A characterization of biological nitrogen fixation. Mar. Chem. 19, 245–259. https://doi.org/10.1016/0304-4203(86)90026-5

Montoya, J.P., Carpenter, E.J., Capone, D.G., 2002. Nitrogen fixation and nitrogen isotope abundances in zooplankton of the oligotrophic North Atlantic. Limnol. Oceanogr. 47, 1617–1628. https://doi.org/10.4319/lo.2002.47.6.1617

Morrow, D.W., 2018. Devonian of the Northern Canadian Mainland Sedimentary Basin: A Review. Bull. Can. Pet. Geol. 66, 623–694.

Muir, I., Dixon, O.A., 1984. Facies analysis of a Middle Devonian sequence in the Mountain River-Gayna River, in: Brophy, J. (Ed.), Contributions to the Geology of the Northwest Territories. Department of Indian Affairs and Northern Development, Canada., pp. 55–62.

Muir, I., Wong, P., Wendte, J., 1985. Devonian Hare Indian-Ramparts (Kee Scarp) evolution, Mackenzie Mountains and subsurface Norman Wells, NWT: basin-fill and platform reef development, in: Longman, M.W., Shanley, K.W., Lindsay, R.F., Eby, D.E. (Eds.), Rocky Mountain Carbonate Reservoirs: A Core Workshop. SEPM (Society for Sedimentary Geology), pp. 311–341. https://doi.org/10.2110/cor.85.07

Murphy, A.E., Sageman, B.B., Hollander, D.J., 2000. Eutrophication by decoupling of the marine biogeochemical cycles of C, N, and P: A mechanism for the Late Devonian mass extinction. Geology 28 (5), 427–430. https://doi.org/10.1130/0091-7613(2000)28<427:EBDOTM>2.0.CO;2

Norris, A.W., 1985. Stratigraphy of Devonian outcrop belts in northern Yukon Territory and northwestern District of Mackenzie (Operation Porcupine area) (Memoir No. 410). Geological Survey of Canada. https://doi.org/10.4095/120309

O'Leary, M.H., 1981. Carbon isotope fractionation in plants. Phytochemistry 20, 553–567. https://doi.org/10.1016/0031-9422(81)85134-5

Ormiston, A.R., Oglesby, R.J., 1995. Effect of Late Devonian Paleoclimate on Source Rock Quality and Location, in: Huc, A.-Y. (Ed.), Paleogeography, Paleoclimate, and Source Rocks. American Association of Petroleum Geologists. https://doi.org/10.1306/St40595C5

Pennington, J.T., Mahoney, K.L., Kuwahara, V.S., Kolber, D.D., Calienes, R., Chavez, F.P., 2006. Primary production in the eastern tropical Pacific: A review. Prog. Oceanogr. 69, 285–317. https://doi.org/10.1016/j.pocean.2006.03.012

Pennock, J.R., Velinsky, D.J., Ludlam, J.M., Sharp, J.H., Fogel, M.L., 1996. Isotopic fractionation of ammonium and nitrate during uptake by Skeletonema costatum: Implications for δ15N dynamics under bloom conditions. Limnol. Oceanogr. 41, 451–459. https://doi.org/10.4319/lo.1996.41.3.0451

Peters, K.E., Sweeney, R.E., Kaplan, I.R., 1978. Correlation of carbon and nitrogen stable isotope ratios in sedimentary organic matter 1: C and N isotopes. Limnol. Oceanogr. 23, 598–604. https://doi.org/10.4319/lo.1978.23.4.0598

Pisarzowska, A., Racki, G., 2012. Isotopic chemostratigraphy across the Early–Middle Frasnian transition (Late Devonian) on the South Polish carbonate shelf: A reference for the global punctata Event. Chem. Geol. 334, 199–220. https://doi.org/10.1016/j.chemgeo.2012.10.034

Powell, J.W., Issler, D.R., Schneider, D.A., Fallas, K.M., Stockli, D.F., 2020. Thermal history of the Mackenzie Plain, Northwest Territories, Canada: Insights from low-temperature thermochronology of the Devonian Imperial Formation. GSA Bull. 132, 767–783. https://doi.org/10.1130/B35089.1

Prahl, F.G., De Lange, G.J., Scholten, S., Cowie, G.L., 1997. A case of post-depositional aerobic degradation of terrestrial organic matter in turbidite deposits from the Madeira Abyssal Plain. Organic Geochemistry, Organic Geochemistry of Paleoclimatic Markers: Production, Preservation and Modeling 27, 141–152. https://doi.org/10.1016/S0146-6380(97)00078-8

Pugh, D.C., 1983. Pre-Mesozoic geology in the subsurface of Peel River map area, Yukon Territory and district of Mackenzie (Memoir No. 401). Geological Survey of Canada. https://doi.org/10.4095/119498

Pyle, L.J., Gal, L.P., 2016. Reference Section for the Horn River Group and Definition of the Bell Creek Member, Hare Indian Formation in central Northwest Territories. Bull. Can. Pet. Geol. 64, 67–98. https://doi.org/10.2113/gscpgbull.64.1.67

Pyle, L.J., Gal, L.P., Hadlari, T., 2015. Thermal maturity trends for Devonian Horn River Group units and equivalent strata in the Mackenzie Corridor, Northwest Territories and Yukon (Geological Survey of Canada Open File Report No. 7850). https://doi.org/10.4095/296446

Racki, G., Rakociński, M., Marynowski, L., Wignall, P.B., 2018. Mercury enrichments and the Frasnian-Famennian biotic crisis: A volcanic trigger proved? Geology 46, 543–546. https://doi.org/10.1130/G40233.1

Rivera, K.T., Puckette, J., Quan, T.M., 2015. Evaluation of redox versus thermal maturity controls on δ 15 N in organic rich shales: A case study of the Woodford Shale, Anadarko Basin, Oklahoma, USA. Org. Geochem. 83–84, 127–139. https://doi.org/10.1016/j.orggeochem.2015.03.005

Robinson, R.S., Kienast, M., Albuquerque, A.L., Altabet, M., Contreras, S., Holz, R.D.P., Dubois, N., Francois, R., Galbraith, E., Hsu, T.-C., Ivanochko, T., Jaccard, S., Kao, S.-J., Kiefer, T., Kienast, S., Lehmann, M., Martinez, P., McCarthy, M., Möbius, J., Pedersen, T., Quan, T.M., Ryabenko, E., Schmittner, A., Schneider, R., Schneider-Mor, A., Shigemitsu, M., Sinclair, D., Somes, C., Studer, A., Thunell, R., Yang, J.-Y., 2012. A review of nitrogen isotopic alteration in marine sediments. Paleoceanography 27. https://doi.org/10.1029/2012PA002321

Sackett, W.M., 1989. The Marine Environment, A, in: Fritz, P., Fontes, J.C. (Eds.), Handbook of Environmental Isotope Geochemistry. Elsevier Scientific Pub. Co, Amsterdam, pp. 139–169.

Schelske, C.L., Hodell, D.A., 1995. Using carbon isotopes of bulk sedimentary organic matter to reconstruct the history of nutrient loading and eutrophication in Lake Erie. Limnol. Oceanogr. 40, 918–929. https://doi.org/10.4319/lo.1995.40.5.0918

Scholz, F., Hensen, C., Noffke, A., Rohde, A., Liebetrau, V., Wallmann, K., 2011. Early diagenesis of redox-sensitive trace metals in the Peru upwelling area – response to ENSO-related oxygen fluctuations in the water column. Geochim. Cosmochim. Acta 75, 7257–7276. https://doi.org/10.1016/j.gca.2011.08.007

Scholz, F., Siebert, C., Dale, A.W., Frank, M., 2017. Intense molybdenum accumulation in sediments underneath a nitrogenous water column and implications for the reconstruction

of paleo-redox conditions based on molybdenum isotopes. Geochim. Cosmochim. Acta 213, 400–417. https://doi.org/10.1016/j.gca.2017.06.048

Schunck, H., Lavik, G., Desai, D.K., Großkopf, T., Kalvelage, T., Löscher, C.R., Paulmier, A., Contreras, S., Siegel, H., Holtappels, M., Rosenstiel, P., Schilhabel, M.B., Graco, M., Schmitz, R.A., Kuypers, M.M.M., LaRoche, J., 2013. Giant Hydrogen Sulfide Plume in the Oxygen Minimum Zone off Peru Supports Chemolithoautotrophy. PLoS ONE 8, e68661. https://doi.org/10.1371/journal.pone.0068661

Scotese, C.R., McKerrow, W.S., 1990. Revised World maps and introduction. Geol. Soc. Lond. Mem. 12, 1–21. https://doi.org/10.1144/GSL.MEM.1990.012.01.01

Sigurdsson, H., Leckie, R.M., Acton, G.D., 1997. Proceedings of the Ocean Drilling Program, Initial Reports. Coll. Stn. TX Ocean Drill. Program 165. https://doi.org/doi:10.2973/odp.proc.ir.165.1997

Slomp, C.P., Thomson, J., de Lange, G.J., 2002. Enhanced regeneration of phosphorus during formation of the most recent eastern Mediterranean sapropel (S1). Geochim. Cosmochim. Acta 66, 1171–1184. https://doi.org/10.1016/S0016-7037(01)00848-1

Snowdon, L.R., Brooks, P.W., Williams, G.K., Goodarzi, F., 1987. Correlation of the Canol Formation source rock with oil from Norman Wells. Org. Geochem. 11, 529–548. https://doi.org/10.1016/0146-6380(87)90008-8

Somes, C.J., Schmittner, A., Galbraith, E.D., Lehmann, M.F., Altabet, M.A., Montoya, J.P., Letelier, R.M., Mix, A.C., Bourbonnais, A., Eby, M., 2010. Simulating the global distribution of nitrogen isotopes in the ocean. Glob. Biogeochem. Cycles 24. https://doi.org/10.1029/2009GB003767

Tang, Y., Huang, Y., Ellis, G.S., Wang, Y., Kralert, P.G., Gillaizeau, B., Ma, Q., Hwang, R., 2005. A kinetic model for thermally induced hydrogen and carbon isotope fractionation of individual n-alkanes in crude oil. Geochim. Cosmochim. Acta 69, 4505–4520. https://doi.org/10.1016/j.gca.2004.12.026

Tassonyi, E.J., 1969. Subsurface geology, lower Mackenzie River and Anderson River area, District of Mackenzie (Paper No. 68–25). Geological Survey of Canada.

Terlaky, V., Fiess, K.M., Rocheleau, J.M., 2020. Outcrop description, lithogeochemical, and source-rock characterisation of the Devonian Horn River Group at the Arctic Red River East and Flyaway Creek outcrops – NTS 106F and 106G, Northwest Territories (No. NWT Open Report 2019-004).

Thunell, R.C., Sigman, D.M., Muller-Karger, F., Astor, Y., Varela, R., 2004. Nitrogen isotope dynamics of the Cariaco Basin, Venezuela. Glob. Biogeochem. Cycles 18. https://doi.org/10.1029/2003GB002185

Tissot, B.P., Pelet, R., Ungerer, PH., 1987. Thermal History of Sedimentary Basins, Maturation Indices, and Kinetics of Oil and Gas Generation1. AAPG Bull. 71, 1445–1466. https://doi.org/10.1306/703C80E7-1707-11D7-8645000102C1865D

Tocqué, E., Behar, F., Budzinski, H., Lorant, F., 2005. Carbon isotopic balance of kerogen pyrolysis effluents in a closed system. Org. Geochem. 36, 893–905. https://doi.org/10.1016/j.orggeochem.2005.01.007

Voss, M., Deutsch, B., Elmgren, R., Humborg, C., Kuuppo, P., Pastuszak, M., Rolff, C., Schulte, U., 2006. Source identification of nitrate by means of isotopic tracers in the Baltic Sea catchments. Biogeosciences 3, 663–676. https://doi.org/10.5194/bg-3-663-2006

Wada, E., Kabaya, Y., Tsuru, K., Ishiwatari, R., 1990. 13C and 15N abundance of sedimentary organic matter in estuarine areas of Tokyo Bay, Japan. Mass Spectrosc. 38, 307–318.

Walliser, O.H., 1996. Global Events in the Devonian and Carboniferous, in: Walliser, O.H. (Ed.), Global Events and Event Stratigraphy in the Phanerozoic. Springer Berlin Heidelberg, pp. 225–250.

Wang, W.-L., Moore, J.K., Martiny, A.C., Primeau, F.W., 2019. Convergent estimates of marine nitrogen fixation. Nature 566, 205–211. https://doi.org/10.1038/s41586-019-0911-2

Ward, B.A., Dutkiewicz, S., Moore, C.M., Follows, M.J., 2013. Iron, phosphorus, and nitrogen supply ratios define the biogeography of nitrogen fixation. Limnol. Oceanogr. 58, 2059–2075. https://doi.org/10.4319/lo.2013.58.6.2059

Williams, L.B., Ferrell, R.E., Hutcheon, I., Bakel, A.J., Walsh, M.M., Krouse, H.R., 1995. Nitrogen isotope geochemistry of organic matter and minerals during diagenesis and hydrocarbon migration. Geochim. Cosmochim. Acta 59, 765–779. https://doi.org/10.1016/0016-7037(95)00005-K

Wilson, G.P., Lamb, A.L., Leng, M.J., Gonzalez, S., Huddart, D., 2005. Variability of organic δ13C and C/N in the Mersey Estuary, U.K. and its implications for sea-level reconstruction studies. Estuar. Coast. Shelf Sci. 64, 685–698. https://doi.org/10.1016/j.ecss.2005.04.003

Yose, L.A., Brown, S., Davis, T.L., Eiben, T., Kompanik, G.S., Maxwell, S.R., 2001. 3-D geologic model of a fractured carbonate reservoir, Norman Wells Field, NWT, Canada. Bull. Can. Pet. Geol. 49, 86–116. https://doi.org/10.2113/49.1.86

Zambito, J.J., Brett, C.E., Baird, G.C., 2012. The Late Middle Devonian (Givetian) Global Taghanic Biocrisis in Its Type Area (Northern Appalachian Basin): Geologically Rapid

Faunal Transitions Driven by Global and Local Environmental Changes, in: Talent, J.A. (Ed.), Earth and Life: Global Biodiversity, Extinction Intervals and Biogeographic Perturbations through Time. Springer Netherlands.

Zhang, J.-Z., Millero, F.J., 1993. The chemistry of anoxic waters in the Cariaco Trench. Deep Sea Res. Part Oceanogr. Res. Pap. 40, 1023–1041. https://doi.org/10.1016/0967-0637(93)90088-K

Zhang, X., Joachimski, M.M., Over, D.J., Ma, K., Huang, C., Gong, Y., 2019. Late Devonian carbon isotope chemostratigraphy: A new record from the offshore facies of South China. Glob. Planet. Change 182, 103024. https://doi.org/10.1016/j.gloplacha.2019.103024

Zhang, X., Sigman, D.M., Morel, F.M.M., Kraepiel, A.M.L., 2014. Nitrogen isotope fractionation by alternative nitrogenases and past ocean anoxia. Proc. Natl. Acad. Sci. 111, 4782–4787. https://doi.org/10.1073/pnas.1402976111

Chapter 3: Porosity types and controls[1]

3.1 Introduction

Over the past two decades, the exploration of organic-rich mudstone intervals as unconventional hydrocarbon reservoirs has become increasingly prevalent. Owing to their apparent homogeneity at the core scale, several recently developed approaches are being used to investigate the properties of these units, including microfacies analysis at optical microscope- or scanning electron microscope (SEM)-scale (e.g., Egenhoff and Fishman, 2013; Biddle et al., 2021) and the use of geochemical proxies in chemostratigraphy (e.g., Ver Straeten et al., 2011; Ratcliffe et al., 2012; El Attar and Pranter, 2016; Turner et al., 2016; Playter et al., 2018; Harris et al., 2022). These techniques have revealed that fine-grained successions are in fact characterized by significant lateral and vertical variation. As with the methods employed in the study of coarser-grained intervals, the quantification of bulk porosity in prospective and producing organic-rich successions is important for modeling hydrocarbon storage capacity (Milliken and Curtis, 2016). In addition to the measurement of bulk porosity, the characterization of pore type, distribution, and origin through the use of SEM shows potential as a valuable tool for shedding further light on hydrocarbon storage (Ross and Bustin, 2009; Ambrose et al., 2010; Wang et al., 2013), permeability and flow pathways (Loucks et al., 2012; Han et al., 2016), wettability (Aplin and Macquaker, 2011; Begum et al., 2019), wellbore stability (Curtis et al., 2012b), and is fundamental to the successful prediction of porosity in these units (Löhr et al., 2015; Milliken and Curtis, 2016).

[1] This chapter has been published as: LaGrange, M.T., Atienza, N.M.M., Biddle, S.K., Harris, B.S., Fiess, K.M., Terlaky, V., Konhauser, K.O. and Gingras, M.K., 2022. The nature, origin, and predictors of porosity in the Middle to Late Devonian Horn River Group of the Central Mackenzie Valley, Northwest Territories, Canada. Mar. Pet. Geol. 142, 105738. https://doi.org/10.1016/j.marpetgeo.2022.105738

In the central Northwest Territories (NWT) of Canada, the Middle to Late Devonian Horn River Group comprises the Hare Indian and Canol Formations, which are mudstones, and the Ramparts Formation, a carbonate interval (Fig. 3.1). With maximum thickness exceeding 300 m (e.g., Kabanov and Deblonde, 2019) and total organic carbon (TOC) values ranging from approximately 1 to 17 wt. % (e.g., Pyle et al., 2015), this group comprises a world-class hydrocarbon resource roughly contemporaneous to many prolific mudstone reservoirs across North America. Although similarly named and age equivalent, the Horn River Group of the central NWT and Yukon comprises different formations than its southern counterpart, which is located approximately 600 km to the south in northeastern British Columbia (c.f. Dong et al., 2015). The Horn River Group of the NWT is also laterally equivalent to the prolific Middle to Late Devonian interval in Alberta, with the Canol Formation as the stratigraphic equivalent of the Duvernay Formation (Kabanov, 2019). In both the Horn River Group of British Columbia and the Duvernay Formation, porosity type and distribution have been described in detail (e.g., Dong et al., 2015; Dong et al., 2019; Knapp et al., 2020). In contrast, many questions remain about the nature of porosity in the Horn River Group of the central NWT. Particularly, the pore size, distribution, and degree of pore connectivity have not yet been assessed. Outstanding questions also surround the pore types and their origins as well as the controls and predictors of porosity in the Horn River Group. Finally, we do not yet understand how porosity in the Horn River Group compares to other North American unconventional mudstone reservoirs. To fill these gaps in knowledge, we investigate the porosity of organic-rich mudstone units in the Husky Little Bear N-09 core (N-09 core) from the Central Mackenzie Valley of the NWT (Fig. 3.2), which include the Hare Indian and Canol Formations of the Horn River Group, along with the basal Imperial Formation (Fig. 3.1). With respect to the Horn River Group interval in the N-09

core, the aims of this paper are fourfold: (1) porosity characterization and quantification, (2) interpretation of the origins of porosity, (3) identification of controls and predictors of porosity within the unit, and (4) comparison of porosity to other North American mudstone reservoirs. This study is the first detailed porosity characterization of Middle to Late Devonian mudstone strata in the frontier Northern Canadian Mainland Sedimentary Basin. Moreover, this work will ultimately facilitate the evaluation of reservoir potential in the Horn River Group of the NWT by allowing for more accurate hydrocarbon storage capacity estimates and contributing to our understanding of hydrocarbon flow pathways and wettability.

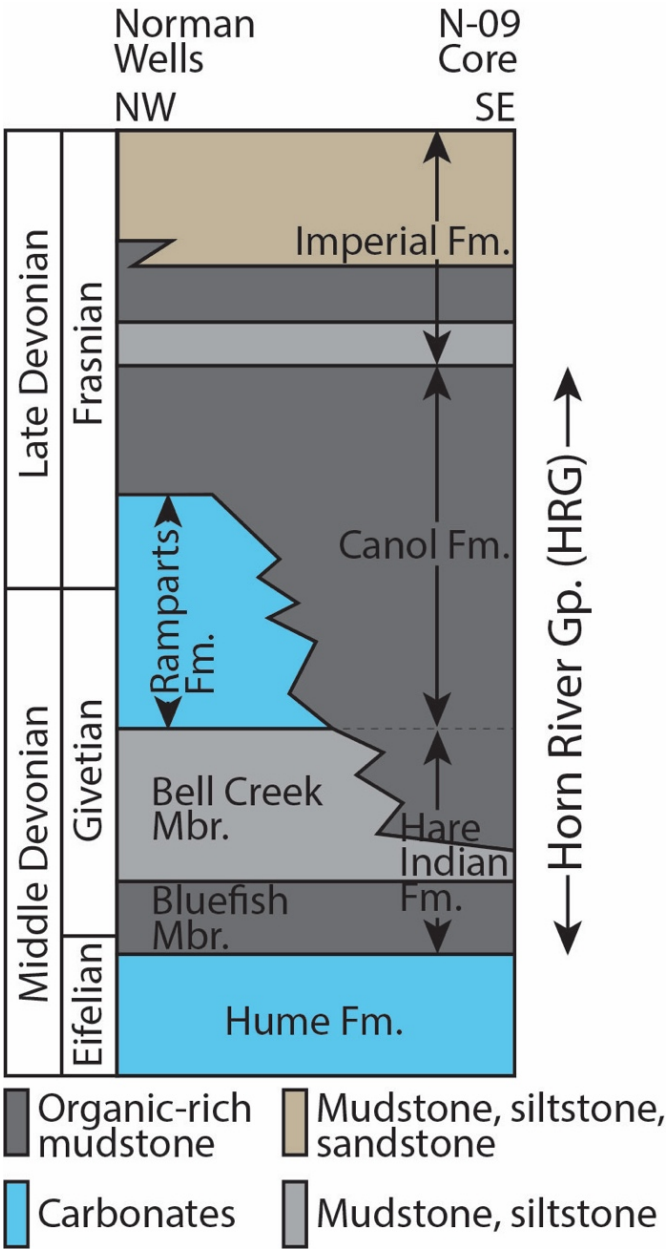

Figure 3.1 Stratigraphic column of the Horn River Group in the Central Mackenzie Valley, Northwest Territories. Modified from Kabanov and Gouwy (2017) and Pyle and Gal (2016). Abbreviations: Fm. – Formation, Mbr. – Member, and Gp. – Group.

Figure 3.2 Location map for the Husky Little Bear N-09 well in the Central Mackenzie Valley, Northwest Territories, Canada. Image modified from Google Earth Pro 7.1.8.3036 (2018). The study area is highlighted with a red box on the inset map and is shown in greater detail in the larger map. Central Mackenzie Valley and Mackenzie Mountains, Northwest Territories, Canada. 64º58'56.91" N, 127º49'26.08" W, Eye alt 323.9 km. Data SIO, NOAA, U.S. Navy, NGA, GEBCO. (Accessed October 4, 2019).

Many techniques used to measure porosity have limitations associated with the size range of resolvable pores (Milliken and Curtis, 2016; Katz and Arango, 2018). Nitrogen adsorption analysis is useful for studying mesopores (1–25 nm radius) and their distribution (Ross and Bustin, 2009; Mastalerz et al., 2013; Han et al., 2016), whereas He porosimetry resolves all pore sizes, including those smaller than 2 nm in diameter (micropores) (Mastalerz et al., 2013; Yang

et al., 2016). The lowest pore diameter detected by SEM is approximately 5–15 nm (e.g., Keller et al., 2011; Klaver et al., 2015; Löhr et al., 2015; Han et al., 2016), which can exclude a significant proportion of the porosity in fine-grained assemblages (Keller et al., 2011; Milliken and Curtis, 2016; Katz and Arango, 2018). Nonetheless, direct imaging through SEM is useful for pore characterization (Milliken and Curtis, 2016) and can be used to support and verify results produced with indirect measurement techniques such as He and N_2 porosimetry (Schieber, 2013). Thus, we assess porosity using a combination of He porosimetry, N_2 adsorption experiments, and scanning electron microscopy (SEM).

This paper follows the nomenclature and mudstone naming scheme of Lazar et al. (2015), with 'mudstone' used as the generic name for fine-grained sedimentary rocks with > 50% of grains smaller than 62.5 μm. Additionally, we use the pore type classification system of Loucks et al. (2012), which distinguishes three types of pores: (1) mineral matrix pores, which are subdivided into interparticle pores and intraparticle pores, (2) organic matter pores (intra-organic matter pores), (3) and fracture pores. The pore size distinctions put forth by the International Union of Pure and Applied Chemistry (e.g., Sing, 1982) are followed herein, classifying; (1) micropores (radius < 1 nm), (2) mesopores (radius 1–25 nm), and (3) macropores (radius > 25 nm).

3.2 Geological setting

The Middle to Late Devonian Horn River Group of the west-central NWT is a mixed mudstone-carbonate succession that includes the Hare Indian, Ramparts, and Canol Formations (Fig. 3.1; Pugh, 1983; Pyle and Gal, 2016; Kabanov and Gouwy, 2017). The Hare Indian Formation overlies the drowning unconformity at the top of the Hume Formation (Kabanov and Gouwy,

2017), and comprises the siliceous and organic-rich shales of the Bluefish Member, and the more argillaceous mudstones of the Bell Creek Member, both of which have variable carbonate content (Pyle and Gal, 2016). The overlying Ramparts Formation, a series of carbonate ramp, platform, and reef deposits (Muir et al., 1985), was deposited only in areas where the Hare Indian Formation is thickest and thus is locally absent in many cores in the Central Mackenzie Valley (Kabanov and Deblonde, 2019). The uppermost Horn River Group unit, the Canol Formation, is an organic-rich mudstone and the source of the conventional oil produced from the Norman Wells oil field, NWT, from the Kee Scarp Member of the Ramparts Formation (Snowdon et al., 1987). In the past two decades, interest has increased in the unconventional reservoir potential of the Canol Formation and the Bluefish Member of the underlying Hare Indian Formation. Preliminary estimates by the National Energy Board and the Northwest Territories Geological Survey reported 145 and 46 billion barrels of oil in place for the Canol Formation and Bluefish Member, respectively (NTGS and NEB, 2015).

It is worth noting that this paper follows the stratigraphic nomenclature of Pyle and Gal (2016) for the Horn River Group. In the framework of Pyle and Gal (2016), the Hare Indian Formation comprises the lower Bluefish Member and upper Bell Creek Member, and the Canol Formation is not subdivided at the member level (Fig. 3.1). Kabanov and Gouwy (2017) produced a more detailed stratigraphic framework for the Horn River Group, with the upper Hare Indian Formation assigned to three different members, and two members distinguished in the Canol Formation, which is useful for stratigraphic correlation. Nonetheless, given that the present study is not stratigraphical in nature, these authors opt to use the simpler framework of Pyle and Gal (2016). Moreover, herein, the Bell Creek Member Dark Facies (Pyle and Gal, 2016), which is lithologically similar to the lower Canol Formation (Kabanov and Gouwy, 2017)

and also termed the Prohibition Creek Member (Kabanov and Gouwy, 2017), is not distinguished from the Canol Formation.

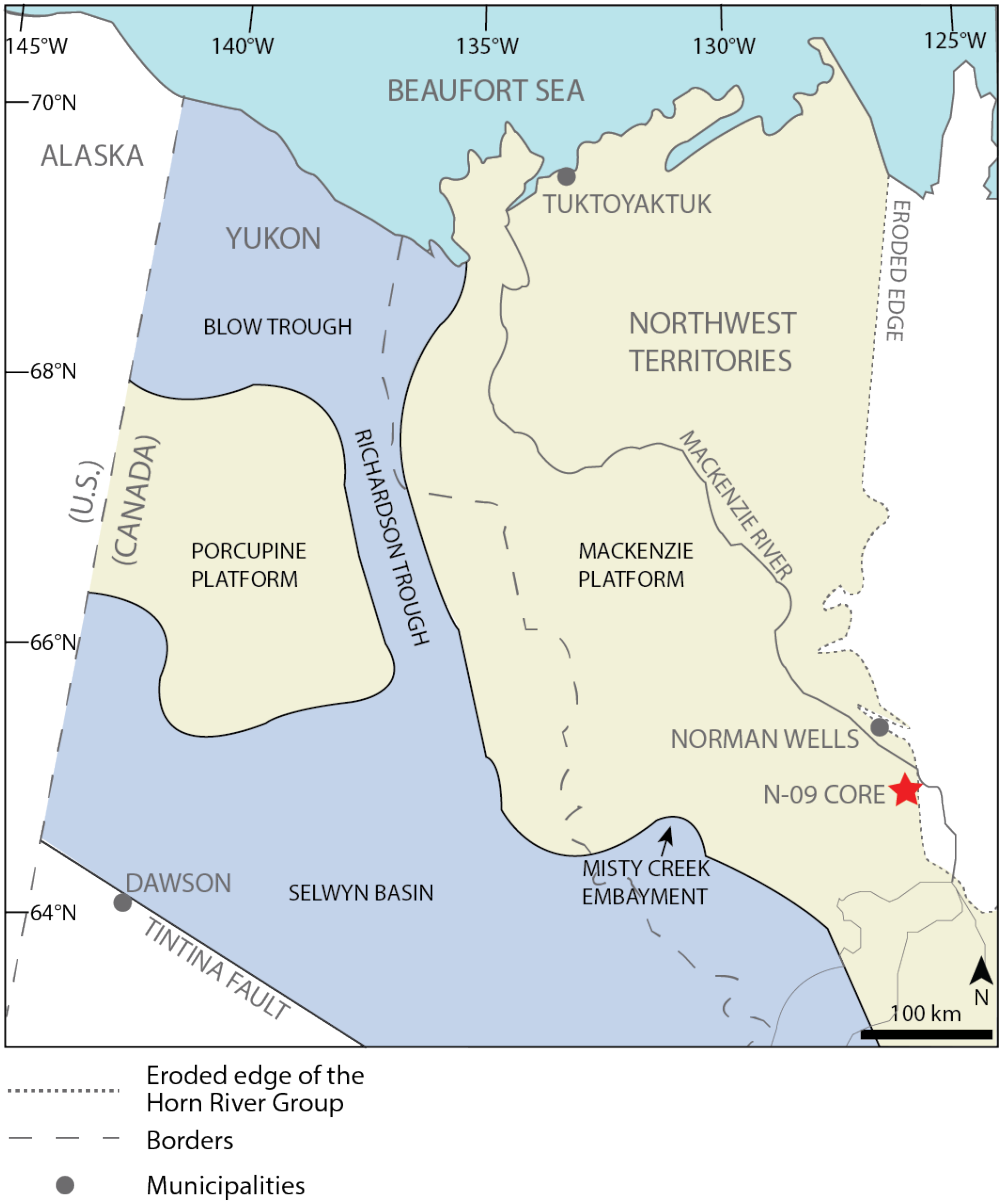

Figure 3.3 Structural features of the study area during the Middle to Late Devonian. Black lines and text represent modern-day geography, whereas grey lines and text indicate paleogeographic features during the Middle to Late Devonian. After Pugh (1983), Al-Aasm et al. (1996), and Morrow (2018).

This project focuses on the cored interval of the Horn River Group in the Husky Little Bear N-09 well, located at 64°58'55.2" N, 126°31'20.2" W in the Central Mackenzie Valley, NWT, Canada (Fig. 3.2), hereafter referred to as the N-09 core. In the Paleozoic, the present-day Central Mackenzie Valley was located along the northwestern margin of the Laurentian craton (Fraser and Hutchinson, 2017). Following Neoproterozoic supercontinent breakup, a passive margin developed along the western and northern fringes of Laurentia, with the northern (Franklinian) margin transitioning to a convergent margin in the early Paleozoic (Hadlari et al., 2014a; Dewing et al. 2019). In the study area, early to middle Cambrian extension, which produced a graben system (MacLean et al., 2011), was followed by a period of subsidence and carbonate platform development from the late Cambrian to Middle Devonian (Fritz et al., 1991; MacLean et al., 2014). Devonian sediment accumulation in the study area occurred along the Mackenzie Platform (Fig. 3.3; Lenz, 1972; Norris, 1985), which was separated from the Porcupine Platform to the west by the Richardson Trough (Fig. 3.3; Lenz, 1972; Jeletzky, 1975; Pugh, 1983).

Leading up to the Middle Devonian, shallow-water carbonate deposition occurred on the Mackenzie Platform, while organic-rich mudstones and carbonates accumulated in the Richardson Trough (Pugh, 1983). Deposition of the Horn River Group was initiated in the latest Eifelian with drowning of the Hume Formation carbonates, which were succeeded by the organic-rich mudstone of the Bluefish Member (Kabanov and Gouwy, 2017; Morrow, 2018). In areas where the Hare Indian Formation mudbank was thickest, deposition of the Ramparts Formation carbonates began (Kabanov, 2019; Fig. 3.1) and continued with the onset of another marine transgression (Muir et al., 1985; Morrow, 2018). Meanwhile, the organic-rich Canol Formation was deposited in off-bank areas (Kabanov and Gouwy, 2017). Ultimately, this

transgression led to drowning of the Ramparts carbonates and onlapping of the Canol Formation (Muir and Dixon, 1984; Muir et al., 1985; Yose et al., 2001). Horn River Group deposition concluded in the Late Devonian as the Ellesmerian Orogeny along the northern margin of Laurentia transformed the study area into a foreland basin and initiated deposition of the siliciclastic Imperial Formation, which overlies this group (Garzione et al., 1997; Beranek et al., 2010).

Peak thermal conditions during burial of the Horn River Group are interpreted to have taken place prior to the Cretaceous (Issler et al., 2005; Powell et al., 2020). Subsequent cooling and uplift produced a regional sub-Cretaceous unconformity, which was again followed by burial and erosion associated with the North American Cordillera foreland basin (Powell et al., 2020) produced by orogenesis in the Jurassic and Cretaceous (Hadlari et al., 2014b). Beginning in the Miocene, accretion of the Yakutat terrane to the North American craton in the Gulf of Alaska area caused ongoing crustal shortening in the study area (Mazzotti and Hyndman, 2002).

3.3 Data and methods

The slabbed, vertical core retrieved from the N-09 well is 167.8 m in length and includes the upper few metres of the Hume Formation, the entire Horn River Group (Hare Indian and Canol and Formations), and the lowermost Imperial Formation. Analytical methods consisted of sedimentological descriptions and the collection of samples to assess mineralogy, thermal maturity, and porosity.

3.3.1 Composition analysis

X-ray diffraction (XRD) analysis on 59 core samples was performed by Core Laboratories Canada. Samples were analyzed using a Philips automated powder diffractometer. Semi-quantitative determination of mineral abundance was performed using integrated peak areas and empirical reference intensity ratio factors. TOC measurements were collected for 55 samples with a LECO analyzer by Core Laboratories Canada. See Appendix 2 for extended methods.

3.3.2 Lithofacies

Detailed sedimentological observations of the N-09 core focused on lithology, bedding and laminae, fissility, fossils and trace fossils, and diagenetic features such as nodules. Core colour was described following the 2009 Munsell Geological Rock-Color Chart (Rock-Color Chart Committee, 2009). These observations were then synthesized to define lithofacies following the scheme outlined in Lazar et al. (2015), which names fine-grained sedimentary rocks according to grain size and then applies modifiers to describe bedding, composition, and other attributes (e.g., colour). To characterize the dominant composition of each lithofacies, the relative proportions of quartz, total clay, and carbonate (calcite and dolomite) were determined for each of the 59 samples analyzed by x-ray diffraction.

3.3.3 Thermal maturity

Vitrinite Reflectance (VRo) data for six samples were collected by Core Laboratories Canada using a Zeiss Axio Imager A2M microscope equipped with a CRAIC CoalPro Microspectrophotometer. Samples were first pulverized to 850 μm and then mixed with epoxy resin and hardener. Following hardening, these samples were ground and polished with a

Buehler AutoMet 250 instrument. Measurements from certain samples used vitrinite, whereas others were made on graptolite and converted following Bertrand (1990) or on bitumen and converted using the Jacob Formula (VRo = BRo x 0.618 + 0.4) where BRo is bitumen reflectance in oil. Several particles were measured for each sample and the reported VRo is the mean value. Please see the extended methods (Appendix 2) for further detail.

Source rock evaluation parameters (S1, S2, S3, and T_{max}) were measured by Core Laboratories Canada with a Rock-Eval 6 instrument. Sample preparation was the same as described for TOC measurements. Hydrogen Index (HI) was calculated using S2 and TOC values and Oxygen Index (OI) was calculated using S3 and TOC values (e.g., Tissot and Welte, 1984; Law et al., 1999).

3.3.4 Scanning electron microscope imaging

Samples from ten depths (Table 3.1) were investigated using SEM, comprising two representative samples from each of the five lithofacies. The selected samples are displayed in Table 3.1 along with lithofacies and lithostratigraphic information. Samples are named with their lithofacies number and either 'A' or 'B' (Table 3.1). Because of the fissile nature of Lithofacies 5, the sample from depth 1708.2 m (F5B), was analyzed parallel to bedding, whereas all other samples were analyzed perpendicular to bedding. Core pieces were polished through Broad Ion Beam (BIB) milling using Ar ions with a Fischione Model 1060 SEM Mill. Backscattered electron (BSE), secondary electron (SE), and InLens imagery of the carbon-coated core pieces were obtained using a Zeiss Sigma 300 VP scanning electron microscope with an accelerating voltage of 15 kV and an aperture of 30 μm. Energy-dispersive X-ray spectroscopy (EDS) with a

Bruker XFlash 6160 was used to characterize the elemental composition of components assessed using SEM.

Table 3.1 Samples characterized through N_2 porosimetry and SEM imaging from the N-09 core.

Depth (m)	Name	Lithofacies	Formation	Group
1670.28	F3A	3	Imperial	N/A (overlies Horn River)
1687.00	F5A	5	Imperial	N/A (overlies Horn River)
1708.20	F5B	5	Canol	Horn River
1715.25	F1A	1	Canol	Horn River
1727.05	F2A	2	Canol	Horn River
1751.00	F3B	3	Canol	Horn River
1799.35	F1B	1	Canol	Horn River
1810.00	F4A	4	Hare Indian (Bell Creek Member)	Horn River
1820.40	F4B	4	Hare Indian (Bell Creek Member)	Horn River
1825.00	F2B	2	Hare Indian (Bluefish Member)	Horn River

3.3.5 Porosimetry

Bulk porosity was measured by Core Laboratories Canada for 64 samples following the Gas Research Institute (GRI) methodology (e.g., Luffel and Guidry, 1993). Additionally, ten core

samples comprising two of each lithofacies were selected for low-pressure N_2 adsorption measurements (Table 3.1). Equivalent surface areas were determined using the Brunauer–Emmett–Teller (BET) method (Brunauer et al., 1938) and pore size distributions were calculated following Density Functional Theory (DFT; e.g., Olivier et al., 1994). See Appendix 2 for extended methods.

3.3.6 Multivariate statistical analysis

For this study, multivariate statistics were used to assess the covariance between several properties of the Horn River Group in the N-09 core including porosity, mineralogy, lithofacies, and TOC. Highly skewed variables were first log-transformed. The PCAmixdata package of R (https://cran.r-project.org/web/packages/PCAmixdata/PCAmixdata.pdf) was then used to perform analysis on a mixture of quantitative and categorical data, which involves a combination of two different methods: Principal Component Analysis (PCA) and Multiple Correspondence analysis (MCA; Chavent et al., 2015). PCA extracts the most important information from a data table composed of quantitative inter-related variables and from this produces principal components (dimensions), which comprise statistically independent linear combinations of the variables. From this, the relationships between different variables can be displayed (Abdi and Williams, 2010). In contrast, MCA allows for the analysis of relationships between categorical variables (Abdi and Valentin, 2007). PCAmix provides a means to illustrate covariance in a multivariate dataset comprised of both quantitative and qualitative properties (Chavent et al., 2015).

3.4 Results

Figure 3.4 gives the TOC, porosity, lithofacies, and mineralogy with depth in the N-09 core for each depth that a GRI bulk porosity measurement was taken.

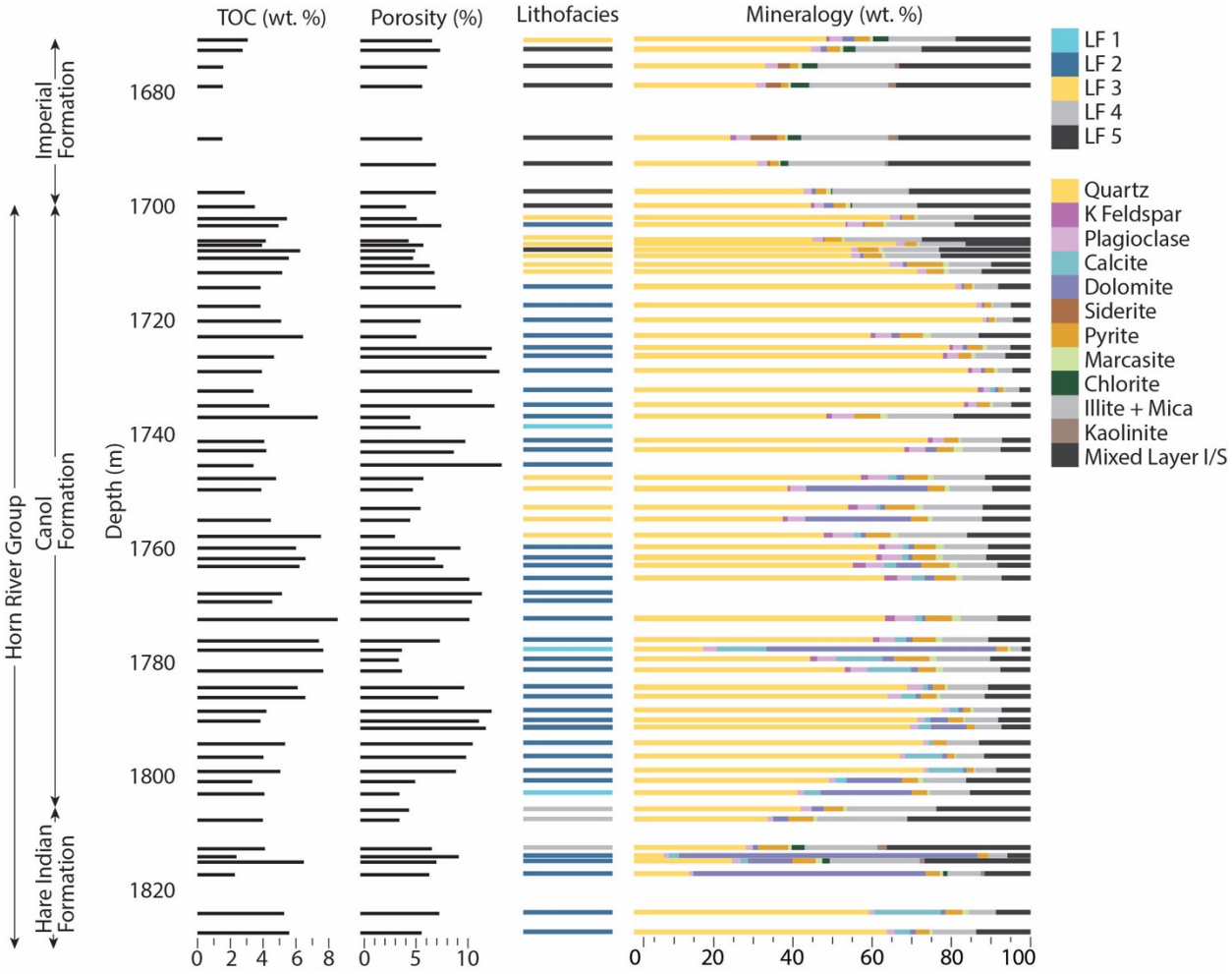

Figure 3.4 TOC, porosity, mineralogy, and lithofacies with depth in the N-09 core. Porosity values are bulk porosity measurements using the Gas Research Institute (GRI) method. Acronyms: LF– lithofacies, mixed layer I/S–mixed-layer illite-smectite, and TOC–total organic carbon.

3.4.1 Lithofacies

Five lithofacies are identified in the N-09 core. The characteristics of each lithofacies are summarized in Table 3.2 and illustrated in Figure 3.5. Figure 3.4 displays the lithofacies observed at each depth associated with a GRI porosity reading.

Table 3.2 Summary of the sedimentological, paleontological, and ichnological characteristics of each observed lithofacies.

Description	Sedimentology and Accessories	Fossils and Bioturbation
F1: Medium grey planar parallel-laminated siliceous calcareous to calcareous mudstone	• Planar parallel laminae, more commonly continuous but sometimes discontinuous • Non-fissile	• No fossils observed • Bioturbation not observed at this scale
F2: Brownish black continuous planar parallel-laminated siliceous mudstone with common calcareous laminae and centimetre-scale carbonate beds	• Planar parallel laminae common, most often continuous • May also appear homogeneous • Common calcareous/dolomitic laminae or cm-scale limestone/dolostone beds • Common calcite/dolomite and pyrite nodules (often have both carbonate and pyrite in the same nodule) • Pyrite streaks sometimes present • Low–moderate fissility	• Rarely, pyritized Tentaculitids are observed on bedding planes • Bioturbation not observed at this scale

F3: Brownish black continuous planar parallel-laminated siliceous mudstone	• Continuous planar parallel laminae are common but sometimes also appears homogeneous • Pyrite nodules common • Rare limestone/dolostone nodules • Abundant pyrite streaks • Low–moderate fissility	• No fossils observed • Bioturbation not observed at this scale
F4: Medium dark grey homogeneous-appearing fissile argillaceous mudstone	• Homogenous appearing • Occasional calcareous and dolomitic laminae or cm-scale beds • Occasional pyrite nodules • Moderate–high fissility	• None observed • Bioturbation not observed at this scale
F5: Medium grey homogeneous appearing highly fissile argillaceous mudstone with common fossil fragments	• Often appears homogeneous but planar parallel laminae also present in some intervals • Pyrite nodules common • High fissility	• Organic fragments and fossil fragments (including *Spathiocaris*) common on bedding planes • Bioturbation not observed at this scale

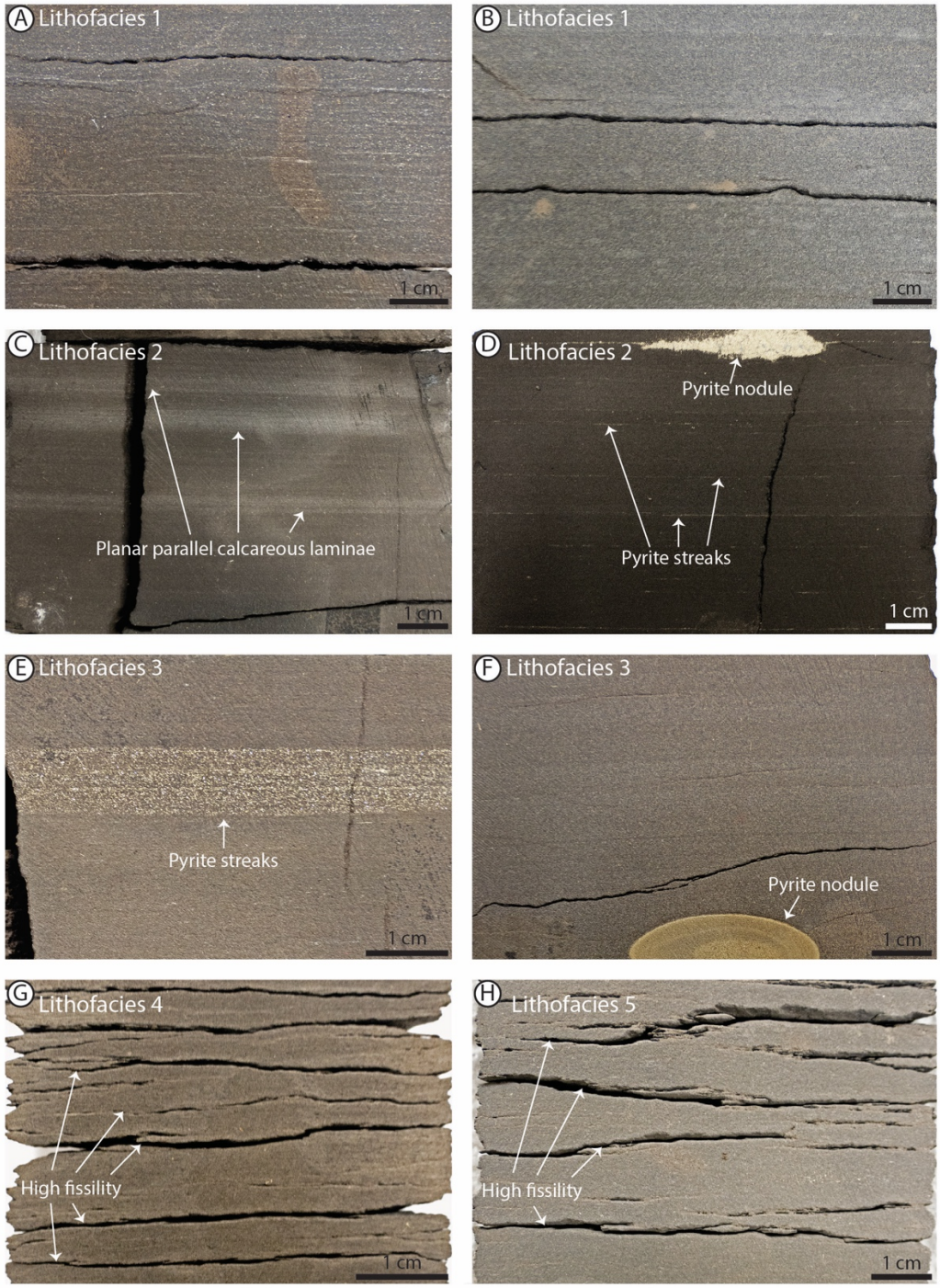

Figure 3.5 Representative core photographs illustrating the five different lithofacies present in the N-09 core. (A) Lithofacies 1 at 1777.3 m, (B) Lithofacies 1 at 1709.45 m, (C) Lithofacies 2 at 1765.4 m, (D) Lithofacies 2 at 1745.5 m, (E) Lithofacies 3 at 1704.45 m, (F) Lithofacies 3 at 1753.05 m, (G) Lithofacies 4 at 1810.15 m, (H) Lithofacies 5 at 1696.3 m.

3.4.2 Composition

Figure 3.4 shows mineralogy and TOC with depth in the N-09 core, with TOC values ranging from 1.54 wt. % to 8.63 wt. %. For the purposes of this discussion, we use low (0–30 %), moderate (30–60 %), and high (60–100 %) to describe mineral abundance. The mineralogical dataset shows that the Horn River Group in the N-09 core is composed primarily of siliceous mudstone, with certain intervals dominated by argillaceous or calcareous mudstone (Fig. 3.4). Lithofacies 1 has moderate to high carbonate content (Fig. 3.6). Most samples from Lithofacies 2 have high quartz and low carbonate content, although a few are characterized by a high proportion of carbonate, likely because of the common calcareous/dolomitic laminae and centimetre-scale beds associated with this lithofacies (Fig. 3.6). Lithofacies 3 is siliceous with low carbonate and a moderate to low abundance of clay, whereas Lithofacies 4 and 5 are argillaceous with moderate quartz content (Fig. 3.6).

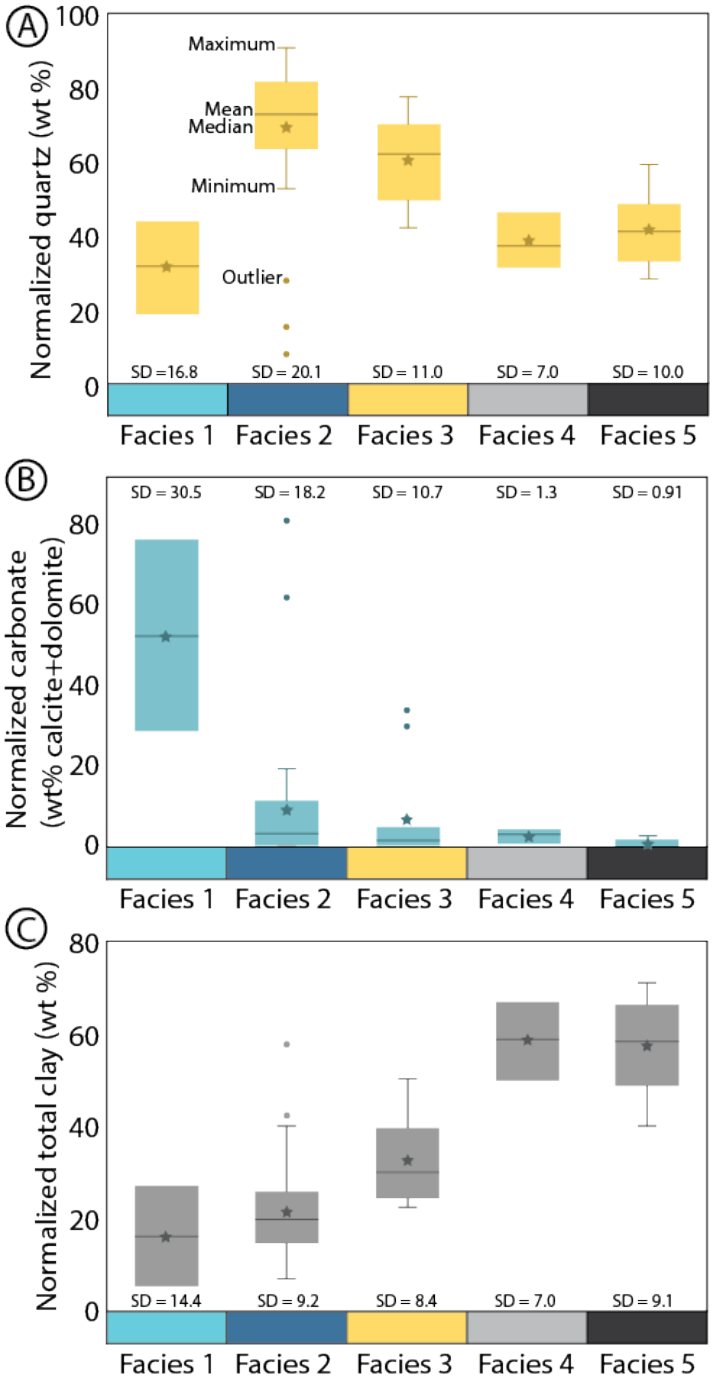

Figure 3.6 Mineralogy per lithofacies. Quartz, clay, and carbonate (calcite+ dolomite) were normalized to 100%. The upper bar represents the maximum, the lower bar is the minimum, the horizontal line denotes the median, and the star highlights the mean. Outliers are shown with points. Acronyms: SD–standard deviation.

3.4.3 Thermal maturity

Source rock evaluation parameters are displayed in Table 3.3. On a pseudo-Van Krevelen diagram (Fig. 3.7), these samples plot near the origin of the graph, typically indicating maturity (Law, 1999) and making it difficult to interpret the original kerogen type. Nonetheless, petrographic analyses of Bluefish Member and Canol Formation samples from 16 locations in the Central Mackenzie Valley by Snowdon et al. (1987) showed that organic matter in both those units is primarily Type II. Herein, vitrinite reflectance values range from 1.02–1.29 %, which places these samples in the late oil window (Tissot and Welte, 1984; Dembicki, 2009). The T_{max} values show an overall increasing trend with depth and range from 458–472 ºC (Table 3.3), characteristic of the late oil window to early gas window (Espitalié et al., 1985).

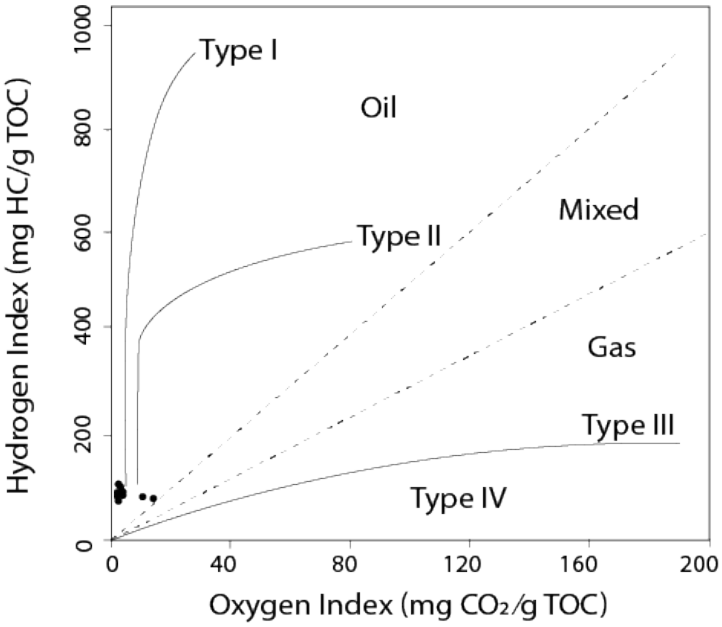

Figure 3.7 A pseudo-Van Krevelen diagram for the Horn River Group in the N-09 core. Fields on the plot (kerogen type trends and dashed lines denoting oil, mixed, and gas zones) are following Dembicki (2009). Acronyms: HC–Hydrocarbon, TOC–Total Organic Carbon.

Table 3.3 Source rock evaluation and TOC results. Acronyms: HI–Hydrogen Index, OI–Oxygen Index, TOC–Total Organic Carbon. HI is calculated as follows: S2 x 100/TOC. OI is calculated as follows: S3 x 100/TOC.

Depth (m)	Leco TOC (wt. %)	Rock-Eval S1 (mg HC/g)	Rock-Eval S2 (mg HC/g)	Rock-Eval S3 (mg CO2/g)	Tmax (°C)	HI	OI
1,692.58	2.22	0.53	1.54	0.17	458	69	8
1,710.08	7.94	0.19	3.32	0.10	464	42	1
1,724.50	4.31	0.27	1.63	0.06	461	38	1
1,738.45	2.24	0.14	0.81	0.19	470	36	8
1,752.53	6.94	0.88	3.80	0.12	466	55	2
1,765.07	5.95	0.16	3.07	0.10	466	52	2
1,779.04	8.89	0.26	4.55	0.12	468	51	1
1,791.31	3.38	0.13	1.07	0.13	467	32	4
1,805.38	6.17	0.47	4.02	0.08	472	65	1
1,820.00	4.55	0.82	2.81	0.13	472	62	3

3.4.4 GRI porosity

Porosity readings for the 64 samples analyzed with the GRI method are displayed in Figure 3.4. The porosity of the Horn River Group and lower Imperial Formation in the N-09 core ranges from 3.2% to 13.1%. Mean porosity is highest in Lithofacies 2, although this lithofacies displays a wide range of porosities (Fig. 3.8 A). The lowest mean porosity is observed in Lithofacies 1 (Fig. 3.8A). In the Canol Formation, mean porosity is 7.7%, with the highest standard deviation

of the lithostratigraphic units considered (Fig. 3.8 B). The Bell Creek Member of the Hare Indian Formation displays a mean porosity of 5.2%, whereas the Bluefish Member of this same formation has an average porosity of 7.1% (Fig. 3.8 B).

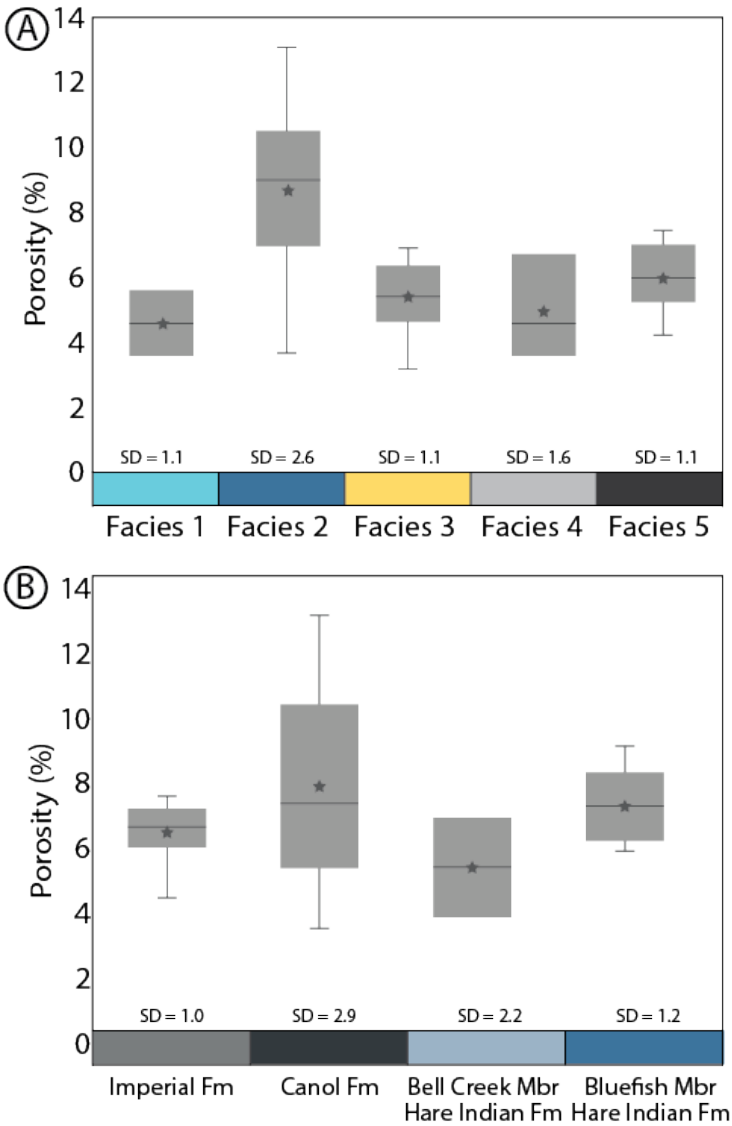

Figure 3.8 Gas Research Institute (GRI) method bulk porosity per (A) lithofacies and (B) lithostratigraphic unit in the N-09 core. The upper bar represents the maximum, the lower bar is the minimum, the horizontal line denotes the median, and the star highlights the mean. Outliers are shown with points. Acronyms: SD – standard deviation.

3.4.5 Pore types observed with scanning electron microscopy

The following section uses the pore type classification of Loucks et al. (2012), which classifies pores as (1) mineral matrix pores, subdivided into interparticle pores and intraparticle pores, (2) organic matter pores (intra-organic matter pores), (3) and fracture pores. For all samples, the mineral matrix comprises mainly quartz and clay minerals (Fig. 3.9 A–I), aside from sample F1B, which contains a high proportion of dolomite (Fig. 3.9 J). In varying proportions, pyrite, carbonates (primarily dolomite), and calcareous or pyritized microfossils (e.g., Tentaculitids in sample F4B; Fig. 3.9 D) are also present in the observed samples (Fig. 3.9). At SEM scale, the sedimentary fabric in both samples from Lithofacies 2 (F2A and F2B) and sample F3A consists of planar laminae defined by pyrite (Fig. 3.9 E, G, H). No clear fabric is observed at SEM scale in the Lithofacies 1 samples (F1A and F1B), the second Lithofacies 3 sample (F3B), the Lithofacies 4 samples (F4A, and F4B), or either Lithofacies 5 sample (F5A, F5B).

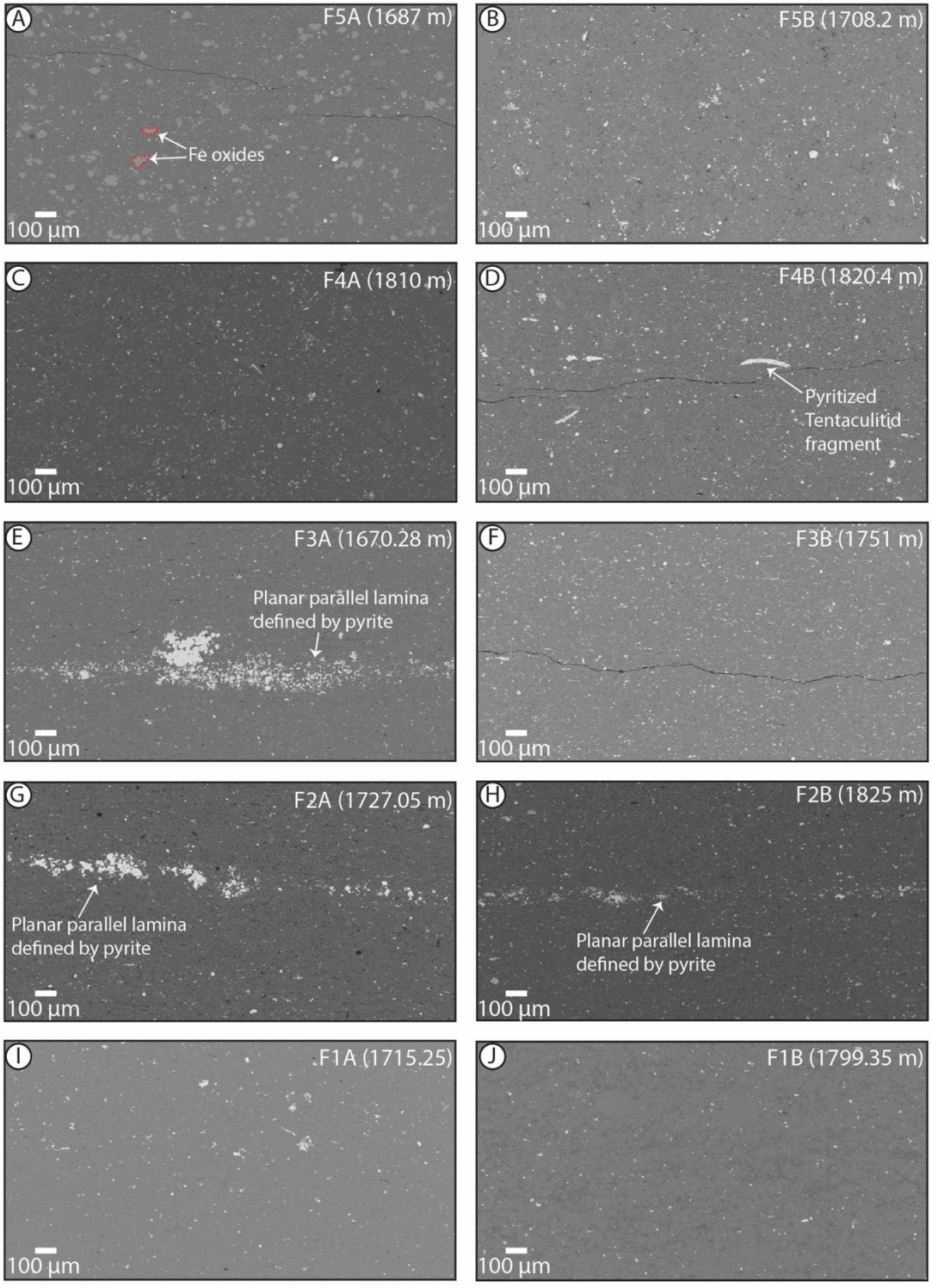

Figure 3.9 Overview of the sedimentary fabrics observed in ten samples from the N-09 core through scanning electron microscope (SEM) imaging. All images are captured with the backscattered-electron detector.

Loucks and Reed (2014) presented several criteria to distinguish migrated organic matter from original depositional organic matter. Criteria associated with migrated organic matter (solid bitumen or pyrobitumen) include (1) organic matter present where cementation has already occurred, (2) organic matter filling intraparticle pores, (3) spongy texture, (4) abundant connected organic matter-filled pores, (5) pores within organic matter that are not aligned, (6) devolatilization cracks in organic matter, and (7) anomalously large bubbles, which are formed when oil or gas is trapped in migrated organic matter (Loucks and Reed, 2014). All samples of the Horn River Group in this study appear to contain migrated organic matter. This interpretation stems from the presence of organic matter within pores that contain authigenic mineral growth (criterion 1, Fig. 3.10 A and B), organic matter infilling intraparticle pores (criterion 2, Fig. 3.10 C), pores within organic matter that are irregularly distributed and lack alignment (criterion 5, Fig. 3.10 D, E, and F) and the common presence of crack-like pores in organic matter (criterion 6, Fig. 3.10 E–H).

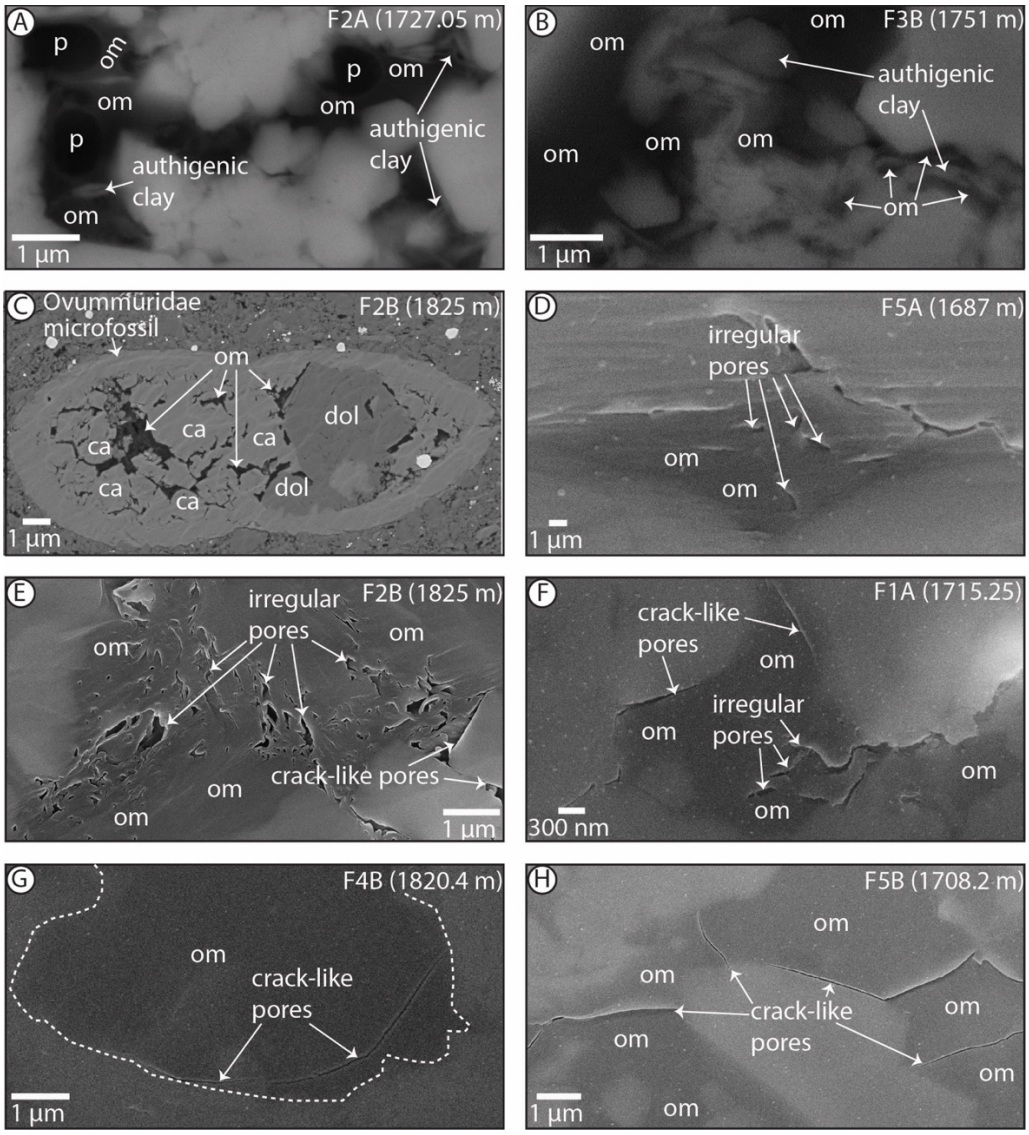

Figure 3.10 Organic matter in the observed samples from the N-09 core captured with a scanning electron microscope (SEM). (A) and (B) show organic matter in interparticle pores along with authigenic clay minerals. (C) displays organic matter filling intraparticle pores within a microfossil (possibly Ovummuridae). (E) displays irregular organic matter pores while (E) and (F) display primarily irregular organic matter pores with a few crack-like pores. Crack-like organic matter pores are shown in (G) and (H). Images (A)–(C) were captured with the backscattered electron detector, whereas images (F)–(H) used the InLens detector. Abbreviations: ca – calcite, dol – dolomite, om – organic matter, and p – pore.

In addition to organic matter pores (Fig. 3.10), SEM analysis also revealed the presence of mineral matrix pores (interparticle and intraparticle) in the observed samples (Fig. 3.11 and 3.12). Many interparticle pores are partially filled by authigenic minerals such as pyrite, clay, or dolomite and migrated organic matter (e.g., Fig. 3.11). Intraparticle pores are observed within clay platelets (e.g., Fig. 3.12 A and B), dolomite crystals (e.g., Fig. 3.12 C), pyritized microfossil fragments (e.g., Fig. 3.12 D), and in pyrite framboids (e.g., Fig. 3.12 E and F). Pyritized microfossil fragments may comprise hyalosponge spicules, which have been observed in the Horn River Group (Kabanov and Jiang, 2020), tentaculitids, which are common in the Bluefish Member of the Hare Indian Formation (Muir and Dixon, 1984; Pyle and Gal, 2016), or Ovummuridea, which are documented in Late Devonian strata of the southern Northwest Territories (MacNeil and Jones, 2006). In two dimensions, the observed interparticle, intraparticle, and organic matter pores are either irregular in shape or crack/slit-like (Fig. 3.10, 11, and 12). In SEM view, these pores are isolated and do not show connectivity to one another (Fig. 3.10, 3.11, and 3.12).

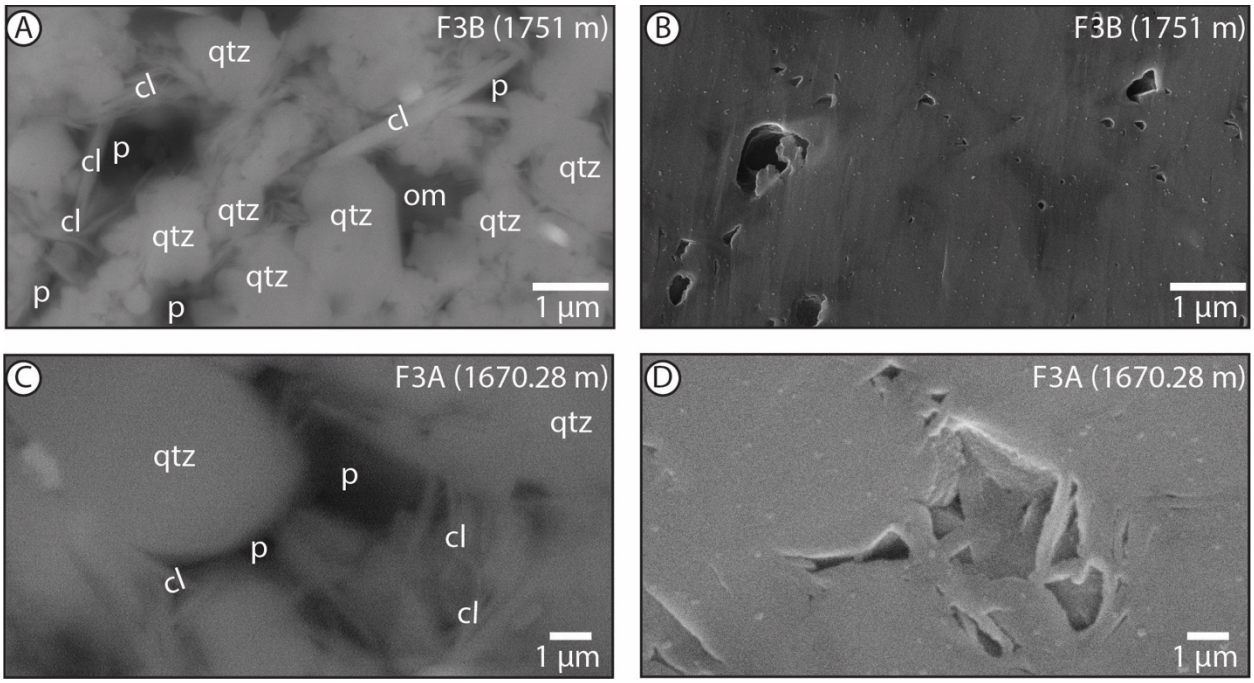

Figure 3.11 Interparticle pores observed in the N-09 core through scanning electron microscope (SEM) imaging. The top two images show interparticle pores containing authigenic clay minerals and organic matter from sample F3B with (A) the back-scattered electron detector and (B) the InLens detector. The bottom images are interparticle pores from Sample F3A with (C) the back-scattered electron detector and (D) the InLens detector. Abbreviations: cl – clay, om – organic matter, p – pore, and qtz – quartz.

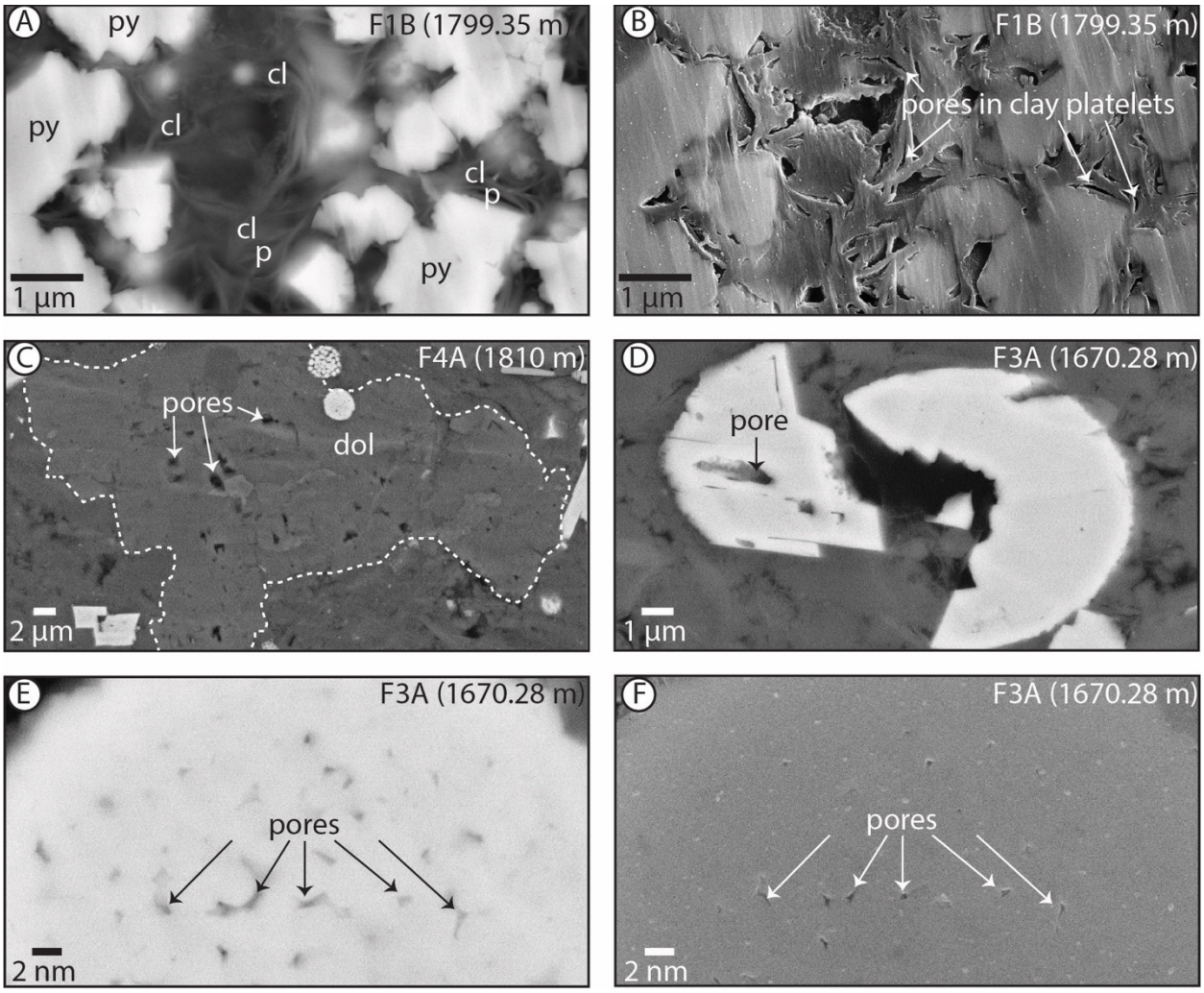

Figure 3.12 Scanning electron microscope (SEM) images of intraparticle pores in the studied samples. (A) shows intraparticle pores in clay platelets with the back-scattered electron detector and (B) is from the sample depth using the InLens detector. Intraparticle pores are also displayed in (C) a dolomite crystal (outlined with a white dashed line), (D) a microfossil, and (E) a pyrite framboid. The same area as shown in (E) with the back-scattered electron detector is displayed in (F) with the InLens detector. Abbreviations: cl – clay, dol – dolomite, and p – pore.

Fractures pores at the SEM-scale are present in samples F5A, F4B, and F3B (Figure 3.9 A, D, and F respectively) and EDS showed that they are filled only with epoxy and do not contain mineral cement. Additionally, open fractures are observed on a larger scale (centimetres to decimeters in length) at several depths throughout the N-09 core. Fractures are present in Lithofacies 1, 2, and 3, but are not observed in Lithofacies 4 and 5 (Fig. 3.13). Some of these fractures show connectivity in core, but others are isolated (Fig. 3.13). From previous outcrop and core observations, the Horn River Group of the study area is known to be naturally fractured, with both open and cemented fractures present (e.g., Irish and Kempthorne, 1987; Yose et al., 2001; Hadlari et al., 2015). These fractures were produced by exhumation from the compressional tectonic regime associated with the ongoing collision of the Yakutat terrane and the North American Plate (Hadlari et al., 2015). Thus, although it is possible that some of the fractures observed herein may be drilling-induced (or in the case of the SEM samples, caused by sample preparation), many of them are likely naturally occurring.

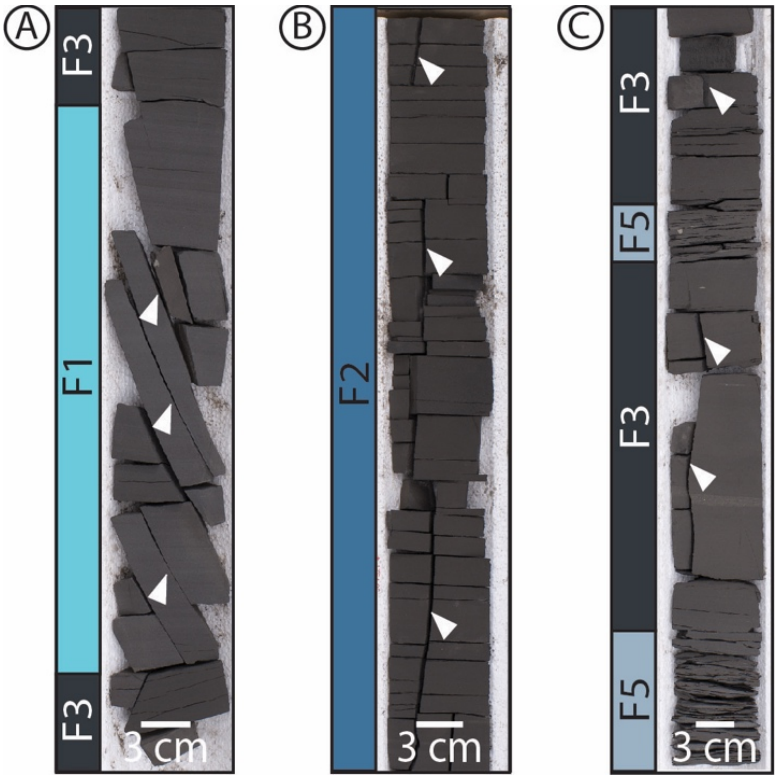

Figure 3.13 Macroscale fractures (white triangles) in the N-09 core (A) 1754.86 m – 1755.29 m, (B) 1763.59 m – 1765.47 m, (C) 1704.04 – 1704.65 m. Definitions: F1 – Lithofacies 1, F2 – Lithofacies 2, F3 – Lithofacies 3, F5 – Lithofacies 5.

3.4.6 N_2 Adsorption analysis

Figure 3.14 shows the mesopore volume of all ten samples analyzed with N_2 adsorption-desorption experiments. Both samples from Lithofacies 1 (F1A and F1B) show intermediate pore volume relative to the other samples. Pore volume from Lithofacies 2 is variable, with sample F2A plotting amongst the highest pore volume results and samples F2B showing one of the lowest pore volumes. Similarly, sample F3A from Lithofacies 3 has the highest pore volume, whereas the other Lithofacies 3 sample (F3B) shows low pore volume. Samples from Lithofacies 5 (F5A and F5B) plot near one another, exhibiting low total pore volume and the same pattern is

observed for samples from Lithofacies 4 (F4A and F4B). Mesopore size distribution results are presented in Figure 3.15. The highest mesopore volume is hosted by pores around 2 nm in all samples except for F4A and F2A, which both show slightly higher peaks near 2.5 nm.

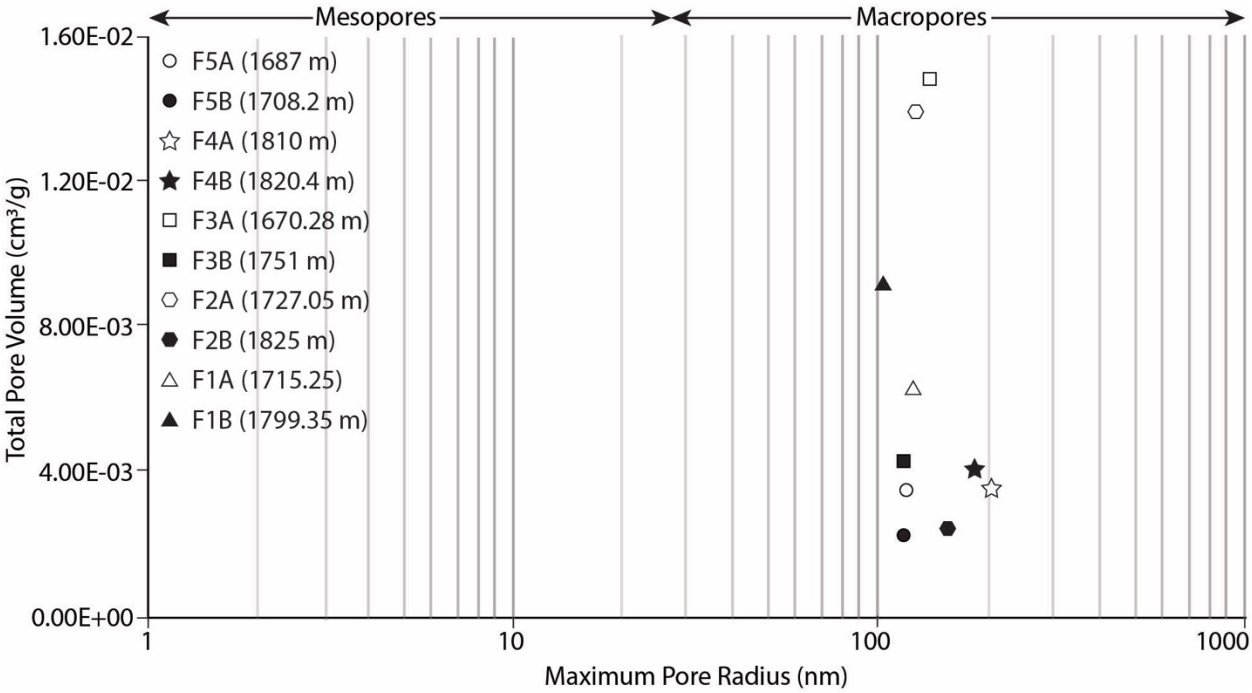

Figure 3.14 Mesopore volume results from N_2 adsorption and desorption experiments. Total pore volume includes pores smaller than the indicated maximum pore radius.

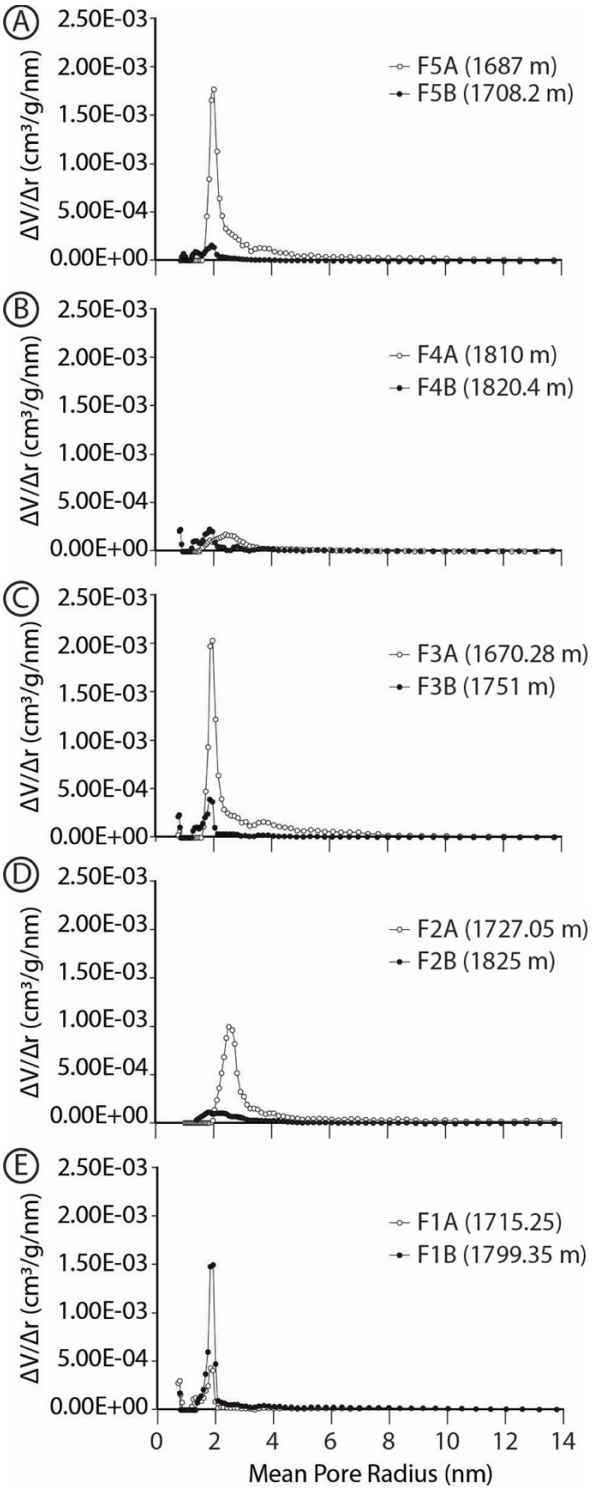

Figure 3.15 Mesopore size distribution by volume determined from N_2 adsorption and desorption experiments using Density Functional Theory (DFT; e.g., Olivier et al., 1994). Definitions: V – total pore volume, r – mean pore radius.

Adsorption hysteresis describes a deviation of the adsorption isotherm from the desorption isotherm (Sing, 1982). The N_2 adsorption and desorption isotherms for all samples analyzed are displayed in Figure 3.16. All isotherms show a similar shape to International Union of Pure and Applied Chemistry hysteresis loop type H3 (Appendix 2; SI Fig. 2.1), suggesting that the pores in these samples are slit-shaped. Many pores observed with SEM are also slit-shaped (e.g., Fig. 3.10 A, B, G, and H, some pores in Fig. 3.10 A and B, some pores in Fig. 3.11 C and D, and some pores in Fig. 3.12 A and B) although others are irregular (e.g., Fig. 3.10 E, Fig. 3.11 A and B, some pores in Fig. 3.11 C and D, Fig. 3.12 C, D, E, and F and some pores in Fig. 3.12 A and B). This difference in shape between pores observed with SEM compared to the interpreted pore shape from hysteresis loops is likely attributed to a difference in scale. Most of the pores observed with SEM are macropores and range from tens of nanometers to several micrometres in radius (e.g., Fig 3.10, Fig 3.11, Fig 3.12), whereas the N_2 adsorption technique characterized mesopores (1–25 nm), with the highest mesopore volume at approximately 2 nm.

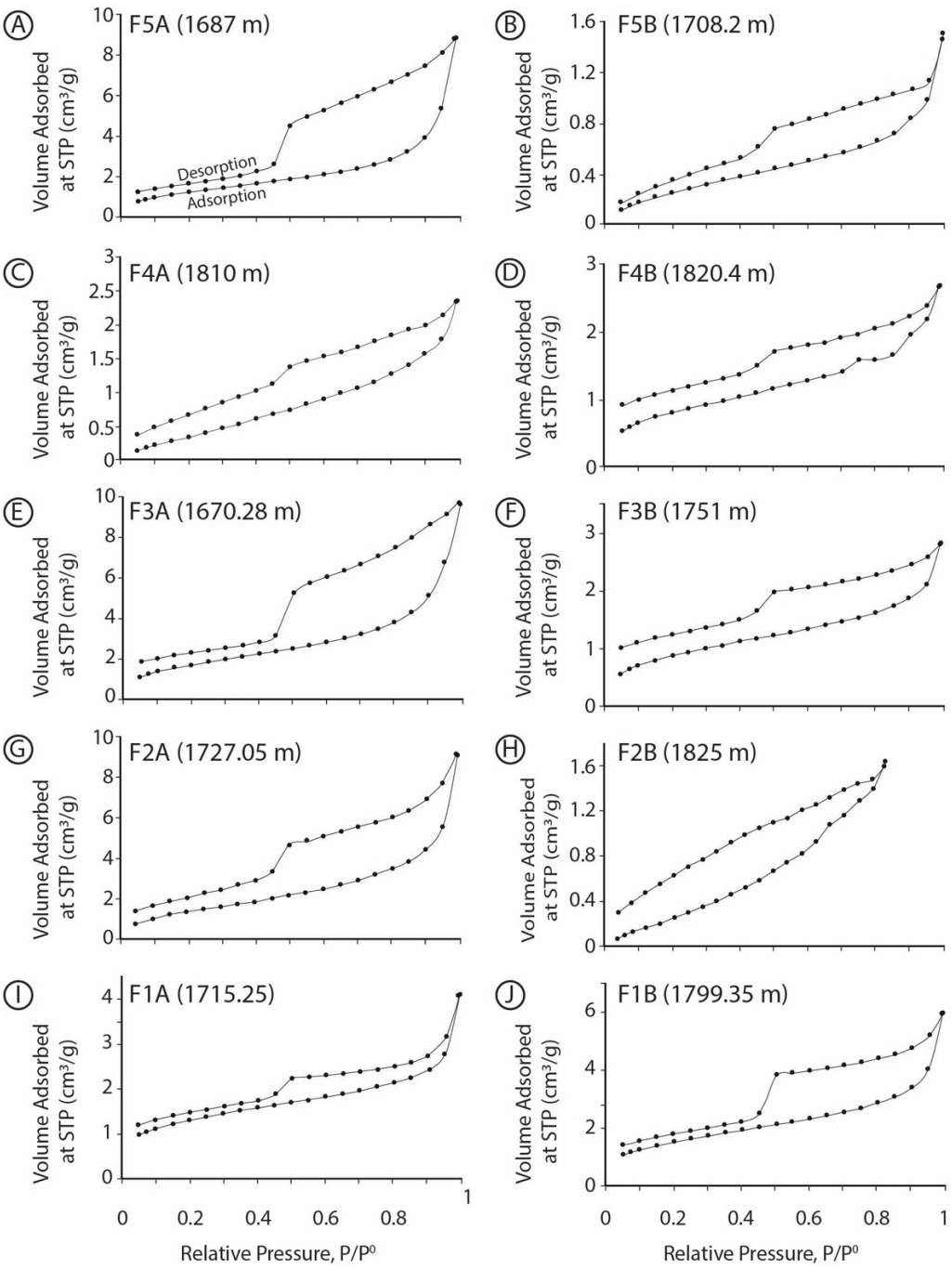

Figure 3.16 The relationship between the volume of N_2 adsorbed/desorbed and the N_2 equilibrium pressure for ten Horn River Group samples. Acronyms and definitions: STP – standard temperature and pressure, p^o – saturation pressure of N_2 at 77 K.

3.4.7 PCAmix

Figure 3.17 displays the relationships between qualitative variables (lithofacies) and quantitative variables (porosity, TOC, and mineralogy) from the Horn River Group of the N-09 core. Dimensions represent directions along which the dataset varies most (James et al., 2013). Herein, dimension 1 explains 23.27 % of the variance in the dataset, dimension 2 accounts for 20.45 %, and dimension 3 explains 12.79 %. Figure 3.17 A shows that porosity appears to be correlated most closely with the abundance of quartz and total clay. Similarly, Figure 3.17 B shows that porosity is closely related to the abundance of quartz. Further discussion of the relationships between variables shown in Figure 3.17 is beyond the scope of this study.

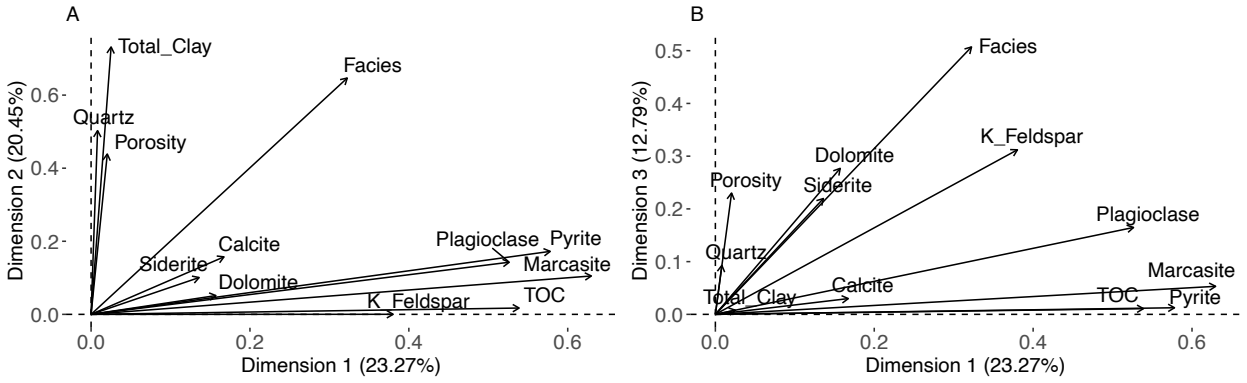

Figure 3.17 Results from multivariate statistical analysis (PCAmix) showing the covariance between porosity, mineralogy, TOC, and lithofacies (labelled 'facies') in relation to (A) dimension 1 and dimension 2, and (B) dimension 1 and dimension 3. Porosity values are bulk porosity measurements calculated with the Gas Research Institute (GRI) method.

3.5 Discussion

3.5.1 Porosity origins

In the Horn River Group, and particularly the Canol Formation, biogenic silica is often prevalent (Pyle and Gal, 2016) in the form of recrystallized radiolarian tests (e.g., Mackenzie, 1974; Kabanov, 2019; Biddle et al., 2021). Mudstone intervals rich in biogenic silica can undergo reduced compaction compared to more clay-rich units because of increased cementation and/or higher rigidity (Schieber, 2013; Dong et al., 2015; 2017; Milliken and Curtis, 2016; Liu et al., 2020; Knapp et al., 2020). Enhanced rigidity associated with abundant biogenic silica is a likely explanation for the prevalence of interparticle pores observed with SEM.

Pyrite framboids are a host of intraparticle porosity in the samples examined for this study (Fig. 3.12 E and F). Pyrite framboids can form either in the euxinic water column (syngenetic pyrite) or in sediment during diagenesis (Wignall and Newton, 1998; Suits and Wilkin, 1998; Roychoudhury et al., 2003). Previous interpretations of paleoredox conditions during deposition of the Horn River Group mudstone units suggested persistent euxinia, citing as evidence sedimentological attributes such as horizontal, apparently unbioturbated beds and laminae, and the prevalence of disseminated euhedral and framboidal pyrite (e.g., Tassonyi 1969; Al-Aasm et al.,1996); and geochemical evidence such as high TOC and high degree of pyritization values (Al-Aasm et al., 1996), high % S to % TOC ratios (Snowdon et al., 1987), and trace metal enrichment (e.g., Mo and U; Kabanov and Gouwy, 2017; Kabanov, 2019). These studies did not examine sedimentological or ichnological characteristics at the thin section scale. However, Biddle et al. (2021) presented an ichnological study of thin sections taken from several Horn River Group drill cores in the Central Mackenzie Valley, including the N-09 core discussed herein and observed the presence of microbioturbation in many of the mudstone intervals. They

concluded that at the time of deposition, dissolved oxygen levels in bottom waters likely ranged from 0.0–0.1 ml/l, corresponding to severe dysoxia to anoxia. Although other proxies suggest persistent euxinic conditions, this indicates that euxinia was likely intermittent at most with seasonal increases in sea floor oxygenation potentially associated with storms (Biddle et al., 2021). Similarly, based on the presence of benthic hyalosponge spicules in the Horn River Group, Kabanov and Jiang (2020) interpreted that the anoxic and/or euxinic conditions (suggested by geochemical and sedimentological proxies) were interrupted by periods of weak seafloor oxygenation. Thus, some of these pyrite framboids may have formed in the water column, whereas others originated in the sediment during diagenesis. The rigid nature of pyrite likely resulted in the preservation of intraparticle porosity within these framboids, despite compaction.

Intraparticle pores in this interval are also commonly observed in calcite and dolomite, with a noticeably higher abundance in samples F1B and F4A (e.g., Fig. 3.12 C). Organic acids, such as carboxylic acids, produced during thermal maturation of buried biomass, are a likely cause for the partial dissolution of carbonate grains (MacGowan and Surdam, 1990; Schieber et al., 2016; Li et al., 2018a). Clay platelets also host intraparticle pores in these samples, particularly in the authigenic clay minerals infilling interparticle porosity (e.g., Fig. 3.12 A and B), which are likely a result of smectite to illite transformations.

Organic matter pores can be primary in origin (present in original depositional kerogen) or secondary, which are produced later from thermal cracking (Milliken et al., 2013; Löhr et al., 2015; Katz and Arango, 2018). Primary organic matter porosity is believed to depend on kerogen maceral type (Curtis et al., 2012a), and it has been suggested that secondary organic matter porosity develops in response to thermal cracking of depositional kerogen or secondary thermal

cracking of migrated organic matter (Canter et al., 2016). The observed organic matter pores in the N-09 core are more likely to have been produced by thermal cracking because the host organic matter has characteristics suggestive of migration rather than original depositional kerogen. Crack-like pores found in organic matter or at the organic matter-mineral interface have been interpreted to form as devolatilization fractures during oil generation (e.g., Sondergeld et al., 2013), although several authors have also suggested that these crack-like pores are an artifact produced through desiccation or devolatilization during core retrieval and sample preparation (e.g., Fishman et al., 2012; Loucks et al., 2012; Loucks and Reed, 2014) or ion-milling (e.g., Schieber, 2013; Klaver et al., 2016).

Subvertical natural fractures are abundant in the Horn River Group of the Central Mackenzie Valley, with a primary orientation trending to the NE–SW and secondary NW–SE trend (Fig., 3.18; Irish and Kempthorne, 1987; Hadlari, 2015). In the N-09 core, these fractures are lithofacies-dependant (Fig. 3.13) and are more prevalent in the Canol Formation than in the underlying Hare Indian Formation. Natural fractures are thought to have formed during exhumation associated with thrust faulting that developed in response to the ongoing collision of the Yakutat terrane with the North American Plate, beginning in the Miocene (Hadlari, 2015).

In sum, the abundance and type of pores in the Horn River Group evolved as the sediment underwent compaction, burial diagenesis, and subsequent structural deformation. First, terrigenous sediment was deposited along with varying proportions of radiolarian tests, siliceous hyalosponge spicules, carbonate microfossils (e.g., tentaculitids), organic matter, and possibly pyrite framboids that formed in the water column during intermittent periods of euxinia. Early diagenesis of organic-rich mud commonly produces framboidal pyrite and carbonate precipitation (non-ferroan calcite and dolomite) through anaerobic microbial respiration

(Konhauser, 2007; Macquaker et al., 2014). The products of these reactions are observed in the Horn River Group, particularly framboidal pyrite and dolomite (e.g., Biddle et al., 2021). Compaction would have reduced interparticle porosity, with smaller pores more likely to be preserved than larger pores (Yang and Aplin, 2007; Emmanuel and Day-Stirrat, 2012). Starting at burial temperatures of approximately 20–60 ºC, biogenic opal-A transforms to Opal-CT and then eventually to quartz (Keller and Isaacs, 1985; Williams and Crerar, 1985). Abundant biogenic silica in this interval, particularly in the Canol Formation and Bluefish Member of the Hare Indian Formation (Pyle and Gal, 2016; Harris et al., 2022), may have reduced the degree of pore compaction through enhanced rigidity (Aplin and Macquaker, 2011; Schieber, 2013; Dong et al., 2015; 2017; Milliken and Curtis, 2016; Knapp et al., 2020). The rigidity of pyrite framboids also appears to have preserved some intraparticle porosity in these grains. During burial diagenesis, smectite to illite transformations occur between approximately 50–100 ºC, producing authigenic clay cement (Hower et al., 1976; Hover et al., 1996), and forming the intraparticle pores within authigenic clay platelets observed herein. Organic acids produced during catagenesis would have resulted in some degree of carbonate dissolution at burial temperatures of about 80–120 ºC (MacGowan and Surdam, 1990; Schieber et al., 2016; Li et al., 2018a), forming intraparticle pores, like those in Figure 3.12 C. Final developments in porosity would have included the development of devolatilization cracks in organic matter from oil migration, natural fracture development induced by terrane accretion beginning in the Miocene (Hadlari, 2015), and possibly desiccation cracks in organic matter following core retrieval.

3.5.2 Controls and predictors of porosity

Cross plots of porosity with quartz content, carbonate content, and total clay content suggest that of these factors, quartz content has the highest correlation with porosity, with an r^2 value of 0.3 (Fig. 3.18 A, C, and E). However, the relatively low r^2 values (0.3) observed for quartz–porosity suggests that other factors complicate this relationship. If samples with carbonate content exceeding 20 wt. % and total clay content exceeding 30 wt. % are excluded, the correlation coefficient between quartz and porosity increases and it is clear that clay and carbonate also influence porosity (Fig. 3.18 B). Negative covariation between clay and porosity is apparent for samples with clay content below 30 wt. % (r^2 of 0.5, excluding carbonate-rich samples; Fig. 3.18 F). Whereas for samples containing greater than 30 wt. % total clay, no obvious trend is present and all samples with total clay above 30 wt. %. are characterized by porosity between ~ 4–8 % (Fig. 3.18 F). A threshold may be present at approximately ~30 wt. % clay abundance, above which the degree of compaction was higher because of greater ductility associated with the clay minerals. Plots of illite and mica versus porosity and mixed layer illite/smectite versus porosity show similar patterns with a negative trend observed only in samples with a lower abundance of these clay minerals (Fig. 3.18 G and H). The carbonate–porosity cross plots display a low r^2 value (Fig. 3.18 C and D) likely reflecting a complex relationship between carbonate content and porosity, with the dissolution of carbonates by organic acids generating secondary intraparticle pores, but diagenetic precipitation of carbonates filling porosity. These interpretations are also supported by the PCAMix results, which show quartz and total clay plotting near porosity, indicating a higher correlation compared to dimensions that plot further away (Fig. 3.17).

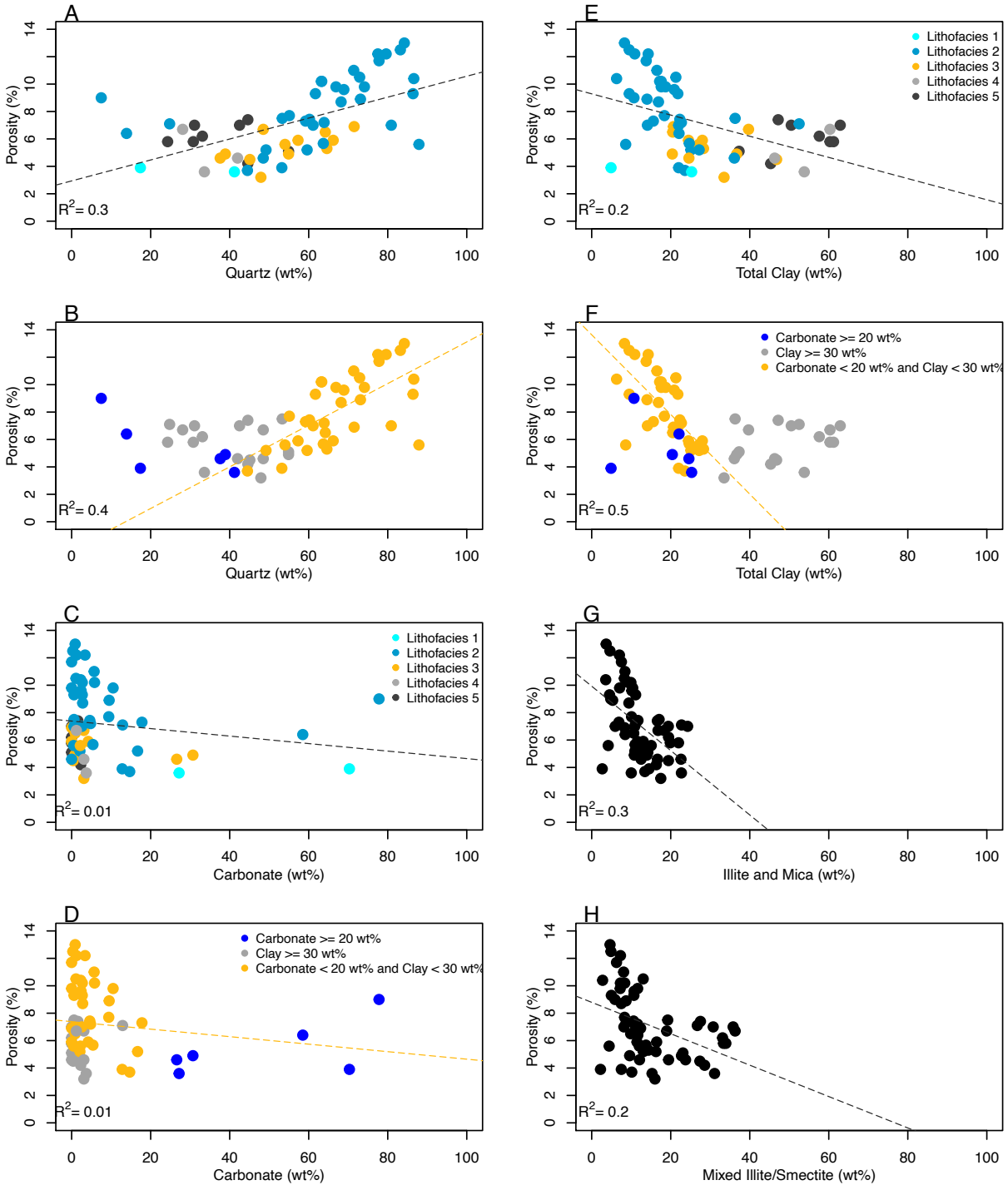

Figure 3.18 Cross-plots of mineralogy and depth with porosity. (A) quartz–porosity colour coded by lithofacies, (B) quartz–porosity colour-coded by mineralogy, (C) carbonate–porosity colour coded by lithofacies, (D) carbonate–porosity colour coded by mineralogy, (E) total clay–

porosity colour coded by lithofacies, (F) total clay– porosity colour coded by mineralogy, (G) illite and mica–porosity, and (H) mixed illite/smectite. The linear regressions in (B) and (F) exclude samples with carbonate content exceeding 20 wt. % and samples with clay content greater than 30 wt. %. Porosity values are bulk porosity measurements calculated with the Gas Research Institute (GRI) method. Abbreviations: wt% – weight percent.

Many previous studies of organic-rich mudstone units have also found that silica is a primary control on porosity. For example, Dong et al. (2015) interpreted that the positive correlation between silica and porosity in the Horn River Group of British Columbia arises either from covariance between TOC and biogenic silica, or from the presence of silica cement preventing the collapse of intraparticle pores between clay platelets. Similarly, Li et al. (2018b) explained differences in porosity and pore distribution between lithofacies by suggesting that although most matrix mineral pores (interparticle and intraparticle between clay platelets) collapse during compaction, interparticle pores between authigenic silica grains are more resistant to this process, leading to higher porosity in authigenic silica-rich lithofacies and lower porosity in units with a higher proportion of clay. Moreover, the findings of some authors have led them to suggest that higher silica content also leads to increased preservation of organic matter pores through greater resistance to mechanical compaction (e.g., Wang et al., 2013; Fishman et al., 2012). Specifically, Knapp et al. (2020) found that biogenic silica is associated with higher organic porosity and greater pore size in the Duvernay Formation and interpreted this to be the product of reduced compaction. Thus, the silica present in the Horn River Group likely influenced porosity by leading to greater preservation of both matrix mineral porosity and organic porosity during mechanical compaction. Conversely, the observed negative covariation

between clay mineral abundance and bulk porosity likely arises because of increased ductility and mineral matrix pore collapse in clay-rich intervals.

Unlike many other organic-rich mudstone resources worldwide, TOC is not a significant predictor of bulk porosity in the Horn River Group of the N-09 core ($r^2 = 0.02$ in Fig. 3.19 A; Fig. 3.17). For example, a relationship between TOC and bulk porosity is observed in the Marcellus Formation of Pennsylvania (e.g., Milliken et al., 2013), the Horn River Group of British Columbia (e.g., Dong et al., 2015), and the lower Cambrian to upper Ordovician strata of the Sichuan Basin, China (e.g., Wang et al., 2013; Yang et al., 2016; Li et al., 2018b). In all the above examples, organic matter pores comprised a dominant fraction of all pores (Milliken et al., 2013; Wang et al., 2013; Dong et al., 2015; Yang et al., 2016). Thus, a lack of TOC – bulk porosity relationship in the samples herein is suggestive of a lower relative abundance of organic matter pores in the N-09 core of the Horn River Group compared to the studied sections of the Marcellus Formation, the Horn River Group of British Columbia, and lower Cambrian to upper Ordovician strata of the Sichuan Basin.

There are a few possible explanations for a comparatively lower abundance of organic matter pores. First, a limited relative abundance of organic matter pores compared to other pore types was also observed in the Kimmeridge Clay Formation of the North Sea by Fishman et al. (2012), who suggested that a higher relative abundance of ductile components (e.g., kerogen and clay) compared to rigid components (e.g., silica or feldspar) may explain a lack of preservation of organic matter pores produced during hydrocarbon generation. Taking this a step further, Löhr et al. (2015) proposed that organic matter concentrated in laterally continuous laminae is more prone to loss of organic matter porosity due to greater ductile deformation. In the case of the Horn River Group in the N-09 core, the possibility of high plasticity resulting in greater

destruction of organic matter pores compared to other organic-rich intervals does not seem likely. The quartz content associated with the Horn River Group in the N-09 core is comparable to or higher than that of other such intervals for both the Bluefish Member and the Canol Formation (Fig. 3.20). Moreover, a significant proportion of this silica is thought to be biogenic in origin for both the Bluefish Member and the Canol Formation (e.g., Pyle and Gal, 2016; Kabanov and Gouwy, 2017), which is believed to enhance the preservation of organic porosity (Knapp et al., 2020). For these reasons, mineralogy and sedimentary fabric are not plausible explanations for a low abundance of organic matter pores and lack of TOC–porosity correlation.

A second potential reason for a low proportion of organic matter pores in the Horn River Group of the N-09 core could be the nature of the original organic matter associated with these samples. It has been proposed that the potential for development of organic porosity varies based on kerogen type (e.g., Curtis et al., 2012a; Loucks et al., 2012; Chen et al. 2015; Klaver et al., 2016; Li et al., 2018b) and previous work suggests that organic matter pores are more common in type II kerogen than type III kerogen (Loucks et al., 2012; Lu et al., 2015). Nonetheless, organic matter in this interval is interpreted as primarily type II (Snowdon et al., 1987). Hence, it is unlikely that the type of organic matter present in the Horn River Group of the N-09 core is responsible for the comparatively lower proportion of organic matter pores relative to other mudstone reservoirs.

Thirdly, Löhr et al. (2015) observed a lower relative abundance of organic matter pores in the oil-mature samples of the Woodford Formation of Oklahoma compared to those in the gas window. Upon further investigation, this is likely explained by the infilling of organic matter pores with migrated bitumen in oil-mature samples, making these pores difficult to discern with SEM imaging, and subsequent expulsion of this bitumen as thermal maturity increases (Löhr et

al., 2015). The N-09 core is within the geographic area interpreted as the oil window by Hadlari et al. (2015). Moreover, Rock-Eval Pyrolysis and vitrinite reflectance results from this study suggest that the N-09 core is in the late-oil to early-gas window, and thus, it is possible that bitumen has infilled organic pores and is masking their presence.

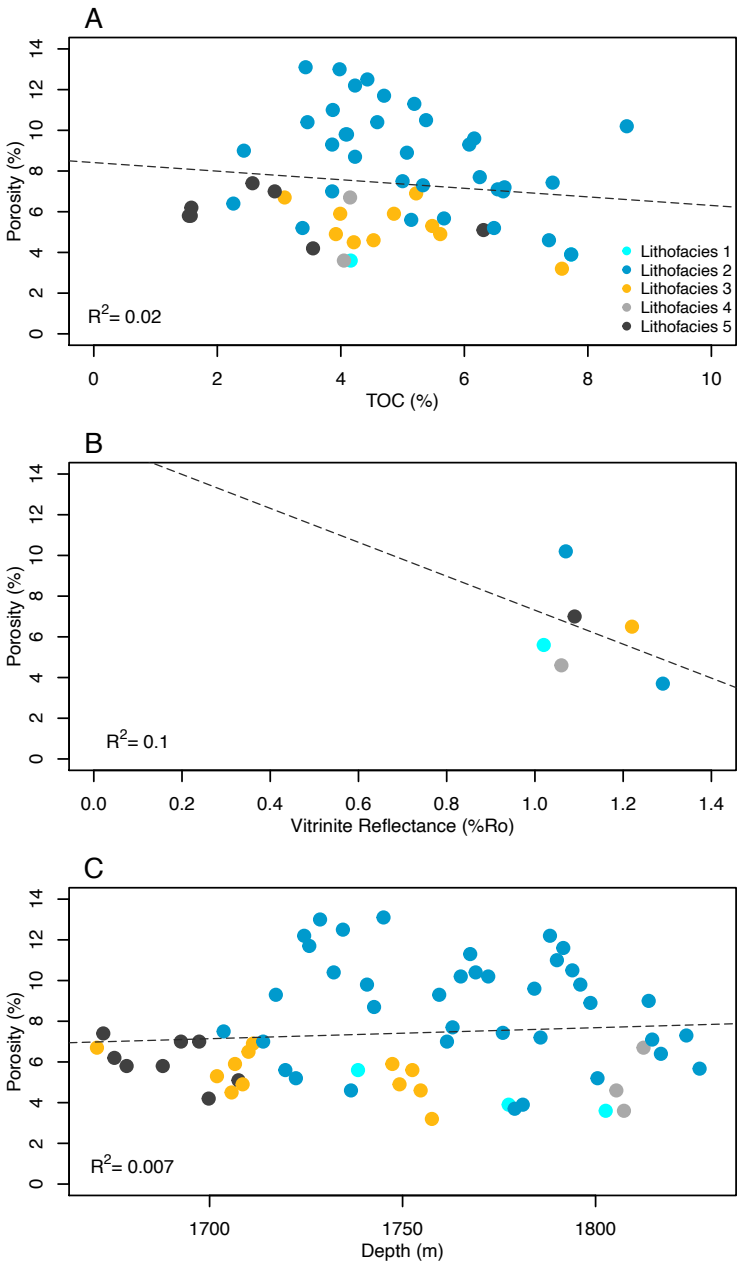

Figure 3.19 Crossplots of (A) TOC–porosity coloured by lithofacies, (B) vitrinite reflectance–porosity coloured by lithofacies, and (C) depth–porosity by lithofacies. Porosity values are bulk

porosity measurements calculated with the Gas Research Institute (GRI) method. Definitions: $\%R_o$ – percentage reflectance in oil immersion.

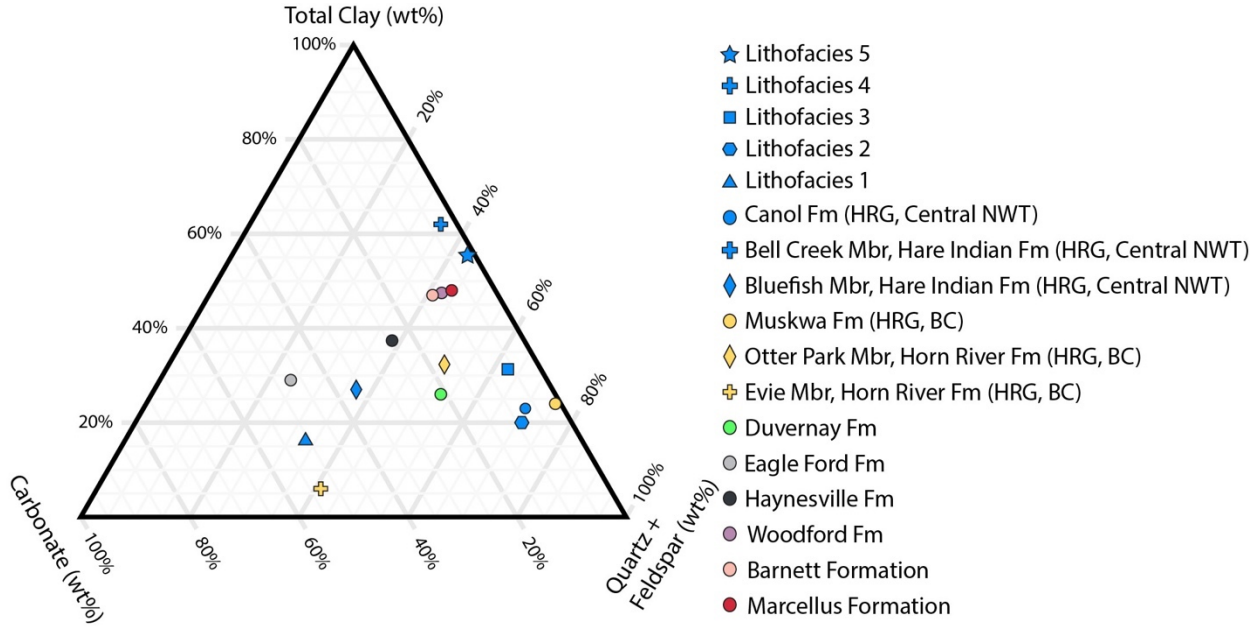

Figure 3.20 Ternary diagram illustrating the mineralogy of several fine-grained unconventional resource plays in North America relative to the units in the Horn River Group of the N-09 core (NWT). Total clay, quartz and feldspar, and carbonate (calcite and dolomite) abundance have been normalized to 100%. Horn River Group BC data from Dong et al. (2017), Duvernay data from Ghanizadeh et al. (2015), Yassin et al. (2017), and Yassin et al. (2018), Eagle Ford data from Jennings and Antia (2013), Barnett data from Loucks et al. (2009) and Chalmers et al. (2012), Marcellus data from Milliken et al. (2013) and Chalmers et al. (2012), Woodford data from Chalmers et al. (2012), and Haynesville data from Klaver et al. (2015) and Chalmers et al. (2012). The data points are all averages and the data points from Lithofacies 1–5, the Canol Formation and the Hare Indian Formation are averages of the data presented herein. The same symbol is used for Lithofacies 4 and the Bell Creek Member of the Hare Indian Formation

because the data points for both plot in the same area. Acronyms: BC – British Columbia, HRG – Horn River Group, NWT – Northwest Territories.

Thermal maturity has also been suggested as a controlling factor for organic porosity (e.g., Loucks et al., 2009; Curtis et al., 2012a; Mastalerz et al., 2013; Schieber, 2013; Klaver et al., 2016), although a clear relationship between thermal maturity and organic porosity has not typically been observed in organic-rich mudstone successions (see Katz and Arango, 2018 for an in-depth review of previous work surrounding thermal maturity and organic porosity). Nonetheless, in this case, there does appear to be some small degree of negative covariation between porosity and vitrinite reflectance (a proxy for thermal maturity), with an r^2 value of 0.1 (Fig. 3.19 B). Seeing as there is typically a linear relationship between depth and vitrinite reflectance (Carr, 2000; Dembicki, 2009), it is unusual that vitrinite reflectance shows some degree of correlation with porosity (Fig. 3.19 B), whereas the relationship between depth and porosity is significantly weaker (Fig. 3.19 C). This discrepancy may arise from changing levels of dissolved oxygen in bottom waters as the Horn River Group was deposited. Paleoredox conditions manifest control on vitrinite reflectance because dissolved oxygen availability affects the nature of early diagenetic biodegradation of vitrinite precursors (Fermont, 1988; Carr, 2000). The observed weak correlation between vitrinite reflectance and porosity may stem from the association of redox conditions and mineralogy, which are both at least in part related to the environmental conditions during deposition.

Related to both mineralogy and organic matter character or abundance is the influence of lithofacies on porosity. Recently, relationships between lithofacies and bulk porosity have been confirmed in certain fine-grained organic-rich successions, including the Horn River Group of

British Columbia, Canada (Dong et al., 2015) and the Wufeng and Longmaxi Formations of South China (Li et al., 2018b). For the Horn River Group of the N-09 core, there appears to be a relationship between lithofacies and porosity (Fig. 3.17), with the highest porosity samples belonging entirely to Lithofacies 2 (Fig. 3.18 A and E). N_2 adsorption total pore volume also shows trends by lithofacies, with low total pore volume in both samples from Lithofacies 4 and 5, intermediate pore volume in both Lithofacies 3 samples (Fig. 3.14). However, Lithofacies 2 and 3 display variable pore volume (Fig. 3.14). Compared to the mineralogical data (Fig. 3.6 A), it seems that the trends in porosity associated with each lithofacies (Fig. 3.8 A) can largely be explained by the respective proportions of quartz and clay. Additionally, macro-scale fractures in this interval are lithofacies-dependent, which is likely also controlled by the relative abundance of quartz, clay, and carbonate in each lithofacies, with fractures observed in the more quartz- or carbonate-rich Lithofacies 1–3, but an absence of fractures in Lithofacies 4 and 5 probably due to the higher clay content associated with these intervals.

3.5.3 Comparison to other fine-grained unconventional reservoirs

Mineralogically, the Canol Formation falls into the high end of quartz and feldspar content compared to other unconventional reservoirs and is most similar to the Devonian Muskwa Formation of the Horn River Group in British Columbia (Fig. 3.20). The Bluefish Member has levels of quartz and feldspar comparable to other fine-grained unconventional plays, with carbonate content more similar to the Eagle Ford of south Texas (Fig. 3.20). In contrast, the Bell Creek Member of the Hare Indian Formation has significantly higher clay content than the other organic-rich mudstone intervals considered (Fig. 3.20). Relative to the other units considered, Lithofacies 2 and 3 show high quartz and feldspar and plot near the average for the Canol

Formation (Fig. 3.20). Lithofacies 1 has higher carbonate content than the Bluefish Member average and plots close to the Eagle Ford Formation and the Evie Member of the Horn River Formation of British Columbia (Fig. 3.20). Lithofacies 4 and 5 are more clay-rich than all other units considered (Fig. 3.20).

Average bulk porosities of the Hare Indian and Canol Formations are similar to bulk porosities of other organic-rich mudstone plays from the literature, with the Canol Formation, Bluefish Member, and Lithofacies 2 plotting amongst the highest average porosities (Fig. 3.21A). Nonetheless, compared to the samples from the fine-grained intervals analyzed in Clarkson et al. (2013), all the N-09 core samples plot at the low end of N_2 pore volume (Fig. 3.21B). This may be explained by a lower proportion of mesopores in the N-09 core samples than the other fine-grained examples considered.

Pore type in the Horn River Group of the N-09 core differs from many other mudstone reservoirs. For example, intervals with a dominance of organic-hosted porosity include the Barnett Shale (Curtis et al., 2012b; Loucks et al., 2012), the Woodford Formation (Curtis et al., 2012b), the Marcellus Formation (Milliken et al., 2013), the Horn River Group of British Columbia (Dong et al., 2015), and the oil- and gas- window samples of the Duvernay Formation (Dong et al., 2019). Our results suggest that the pore network in the Horn River Group is more comparable to units that are not dominated by organic matter porosity. For example, the Bossier Formation displays dominantly intraparticle porosity (Loucks et al., 2012), intervals such as the Eagle Ford (Curtis et al., 2012b; Jennings and Antia, 2013) and the Kimmeridge Clay (Fishman et al., 2012) have mixed pore networks, and the Lower Cretaceous Pearsall Formation mudstone comprises primarily interparticle pores (Loucks et al., 2012).

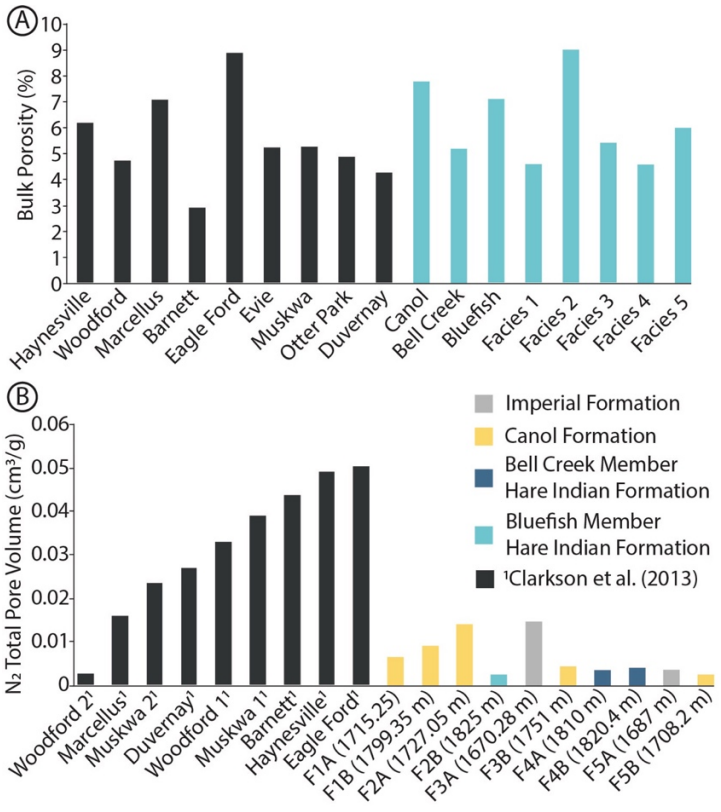

Figure 3.21 Comparison of porosity values for the Horn River Group and lower Imperial Formation of the N-09 core to those from other North American mudstone plays. (A) Comparison to bulk porosity data (Gas Research Institute method, from Hg intrusion and He pycnometry) from other fine-grained North American unconventional plays. The Evie, Muskwa, and Otter Park results are averages from Dong et al. (2017), the Duvernay results are an average of the data from Ghanizadeh et al. (2015), Yassin et al. (2017), and Yassin et al. (2018), the Eagle Ford results are an average of the data presented in Jennings and Antia (2013), the Barnett results are an average of the data presented in Loucks et al. (2009) and Chalmers et al. (2012), the Marcellus results are an average of the data presented in Milliken et al. (2013) and Chalmers et al. (2012), the Woodford results are from Chalmers et al. (2012), and the Haynesville results are from Chalmers et al. (2012). The data bars for Lithofacies 1–5, the Canol, the Bluefish, and the Bell Creek are averages of the dataset presented herein. (B) Nitrogen porosimetry pore

volumes from the Horn River Group relative to nitrogen porosimetry pore volumes from other unconventional reservoirs. Modified from Clarkson et al. (2013).

3.5.4 Significance to reservoir potential

Quartz increases brittleness in sedimentary rocks, with biogenic silica further increasing hardness because it produces an interconnected silica cement framework through recrystallization (Liu et al., 2020). Thus, the high quartz and biogenic silica content of the Bluefish Member and Canol Formation, and specifically Lithofacies 2 and 3, is favourable for hydraulic fracture propagation. Natural fractures may enhance production (e.g., the Eagle Ford Formation; Aguilera and Ramirez Vargas, 2016) by serving as pathways for hydrocarbon movement to mechanical fractures or to the wellbore (Gale et al., 2007; Löhr et al., 2015). This may prove to be the case for Horn River Group Lithofacies 1, 2, and 3. For intervals with pervasive and interconnected organic matter pores, it has been suggested, although not confirmed, that this network may also act as a hydrocarbon flow pathway to induced fractures (e.g., Loucks et al., 2009; Curtis et al., 2012b). This potential flow pathway through organic matter pores is not present in the Horn River Group of the N-09 core.

The prevalent pore type also has implications for wettability. It has been suggested that organic pores are hydrocarbon wet, whereas mineral matrix pores may be hydrophilic or mixed (e.g., Bennett et al., 2004; Aplin and Larter, 2005; Aplin and Macquaker, 2011; Curtis et al., 2012b). Recent work indicates that thermal maturity also influences this relationship, and results showed that organic matter wettability changes from water-wet at low thermal maturities to oil-wet at high thermal maturities (e.g., Hu et al., 2016; Yassin et al, 2017; Jagadisan and Heidari, 2019; Begum et al., 2019). Accordingly, based on the thermal maturity of the samples, the

organic matter pores in the N-09 core are likely somewhere in the middle of this spectrum (possibly mixed or oil-wet). However, a significantly greater proportion of interparticle pores compared to organic matter pores in the Horn River Group of the N-09 core could mean that overall, pores are primarily water-wet or mixed.

3.6 Conclusions

Porosity in the Devonian Horn River Group and lowermost Imperial Formation was assessed using a dataset comprising GRI porosity, TOC, XRD, vitrinite reflectance, Rock-Eval pyrolysis, SEM images, N_2 adsorption pore volume and pore size distribution, and lithofacies analysis from the Husky Little Bear N-09 core in the Central Mackenzie Valley of the NWT. The following key insights stem from our results:

(1) Interparticle pores, intraparticle pores and organic matter pores are all observed in the studied samples. Pores observed with SEM are irregular or slit-like, whereas the shape of hysteresis loops from N_2 porosimetry is suggestive of a slit-like shape. This difference is attributed to the difference in scale between the pores observed with SEM (mostly macropores) versus those included in N_2 results (mesopores). A lack of TOC-porosity correlation suggests that mineral matrix pores (interparticle and/or intraparticle) are dominant relative to organic matter pores.

(2) For all samples considered, the highest pore volume is hosted by mesopores with a radius of approximately 2 nm, which are interpreted to be mineral matrix pores because of the absence of a positive TOC-porosity relationship.

(3) Mineralogy (particularly quartz and total clay abundance) is the best predictor of porosity in this interval. Trends in porosity associated with the lithofacies are also apparent and

Lithofacies 2 is characterized by the highest mean porosity. The lithofacies-porosity trends are attributed to the differences in mineralogy between the lithofacies.

(4) Relative to other North American mudstone reservoirs, the Bluefish Member and Canol Formation, and particularly Lithofacies 2 and 3, plot amongst the units with the highest quartz+feldspar content and have comparable bulk porosity, although lower mesopore volume. In terms of primary pore type, the Horn River Group differs from organic matter pore-dominated units such as the Barnett Shale, Woodford Formation, Marcellus Formation, and Horn River Group of British Columbia.

(5) The Bluefish Member and Canol Formation are favourable prospects for hydraulic fracturing. Moreover, natural fractures may facilitate the movement of hydrocarbons to mechanical fractures. Nevertheless, these intervals appear to lack the interconnected network of organic matter pores that characterizes many other unconventional mudstone reservoirs. Although they lack this organic pore network, the Bluefish Member and the Canol Formation may be mixed-wet or water-wet compared to other such units.

These results further elucidate the character and distribution of prospective reservoir units in the Horn River Group of the NWT. Moreover, our findings will facilitate the prediction and modelling of hydrocarbon potential in the frontier Northern Canadian Mainland Sedimentary Basin. Finally, this work contributes to our understanding of porosity types, properties, and controls in highly siliceous mudstone lithologies, unique relative to most other fine-grained North American reservoirs.

3.7 Acknowledgements

We are grateful to Husky Energy and particularly Dave Herbers for providing us with this core and associated GRI porosity, TOC, XRD, vitrinite reflectance, and Rock-Eval pyrolysis datasets and to Dr. Nancy Zhang from the nanoFAB facility at the University of Alberta for training and guidance with N_2 porosimetry. We would also like to thank Carolyn Currie of Core Laboratories Canada Ltd. for providing guidance and clarification about methods, the Northwest Territories Geological Survey for generously funding this project, and Smriti Dhiman for her help with multivariate statistics. Finally, thank you to the editor, Dr. Bo Liu, for the handling of this manuscript and to the three anonymous reviewers for constructive feedback.

3.8 References

Abdi, H., Valenti, D., 2007. Multiple correspondence analysis, in: Salkind, N.J. (Ed.), Encyclopedia of Measurement and Statistics. Sage Publications, Thousand Oaks (CA, pp. 652–657. https://doi.org/10.4135/9781412952644

Abdi, H., Williams, L.J., 2010. Principal component analysis. Wiley Interdisciplinary Reviews: Comput. Stat. 2 (4), 433–459. https://doi.org/10.1002/wics.101

Aguilera, R., Ramirez Vargas, J.F., 2016. Factors controlling fluid migration and distribution in the Eagle Ford shale. SPE Reservoir Eval. Eng. 19 (3), 403–414. https://doi.org/10.2118/171626-PA

Al-Aasm, I.S., Morad, S., Durocher, S., Muir, I., 1996. Sedimentology, C–S–Fe relationships and stable isotopic compositions in Devonian black mudrocks, Mackenzie Mountains, Northwest Territories, Canada. Sediment. Geol. 106, 279–298. https://doi.org/10.1016/S0037-0738(96)00018-8.

Ambrose, R.J., Hartman, R.C., Diaz-Campos, M., Akkutlu, I.Y., Sondergeld, C.H., 2010. New pore-scale considerations for shale gas in place calculations: society of petroleum engineers unconventional gas conference. Pittsburgh, Pennsylvania. February 23–25, 2010, SPE Paper 131772, 17 pp. https://doi.org/10.2118/131772-MS

Aplin, A.C., Larter, S.R., 2005. Fluid flow, pore pressure, wettability, and leakage in mudstone cap rocks, in: Boult, P., Kaldi, J. (Eds.), Evaluating Fault and Cap Rock Seals. AAPG Hedberg Series 2, pp. 1–12.

Aplin, A.C., Macquaker, J.H.S., 2011. Mudstone diversity: origin and implications for source, seal, and reservoir properties in petroleum systems. AAPG (Am. Assoc. Pet. Geol.) Bull. 95, 2031–2059. https://doi.org/10.1306/03281110162

Begum, M., Yassin, M.R., Dehghanpour, H., 2019. Effect of kerogen maturity on organic shale wettability: a Duvernay case study. Mar. Petrol. Geol. 110, 483–496. https://doi.org/10.1016/j.marpetgeo.2019.07.012.

Bennett, B., Buckman, J.O., Bowler, B.F.J., Larter, S.R., 2004. Wettability alteration in petroleum systems: the role of polar nonhydrocarbons. Petrol. Geosci. 10, 271–277. https://doi.org/10.1144/1354-079303-606.

Beranek, L.P., Mortensen, J.K., Lane, L.S., Allen, T.L., Fraser, T.A., Hadlari, T., Zantvoort, W.G., 2010. Detrital zircon geochronology of the western Ellesmerian clastic wedge, northwestern Canada: insights on Arctic tectonics and the evolution of the northern Cordilleran miogeocline. GSA Bulletin 122 (11/12), 1899–1911, https://doi.org/10.1130/B30120.1

Bertrand, R., 1990. Correlations among the reflectances of vitrinite, chitinozoans, graptolites and scolecodonts. Org. Geochem. 15 (6), 565–574. https://doi.org/ 10.1016/0146-6380(90)90102-6.

Biddle, S.K., LaGrange, M.T., Harris, B.S., Fiess, K., Terlaky, V., Gingras, M.K., 2021. A fine detail physiochemical depositional model for Devonian organic-rich mudstones: a petrographic study of the Hare Indian and Canol formations, Central Mackenzie Valley, Northwest Territories. Sediment. Geol. 414, 105838. https://doi.org/10.1016/j. sedgeo.2020.105838

Brunauer, S., Emmett, P.H., Teller, E., 1938. Adsorption of gases in multimolecular layers. J. Am. Chem. Soc. 60 (2), 309–319. https://doi.org/10.1021/ja01269a023

Canter, L., Zhang, S., Sonnenfeld, M., Bugge, C., Guisinger, M., Jones, K., 2016. Primary and secondary organic matter habit in unconventional reservoirs, in: Olson, T. (Ed.), Imaging Unconventional Reservoir Pore Systems. AAPG Memoir 112, pp. 9–24. https://doi.org/10.1306/13592014M1123691

Carr, A.D., 2000. Suppression and retardation of vitrinite reflectance, part 1. Formation and significance for hydrocarbon generation. J. Petrol. Geol. 23 (3), 313–343. https://doi.org/10.1111/j.1747-5457.2000.tb01022.x

Chalmers, G.R., Bustin, R.M., Power, I.M., 2012. Characterization of gas shale pore systems by porosimetry, pycnometry, surface area, and field emission scanning electron microscopy/transmission electron microscopy image analyses: examples from the Barnett, Woodford, Haynesville, Marcellus, and Doig units. AAPG (Am. Assoc. Pet. Geol.) Bull. 96 (6), 1099–1119.

Chavent, M., Kuentz-Simonet, V., Labenne, A., Saracco, J., 2015. Multivariate Analysis of Mixed Data: the PCAmixdata R Package arXiv:1411.4911v3 [stat.CO] 4 Dec 2014.

Chen, Z., Wang, T., Liu, Q., Zhang, S., Zhang, L., 2015. Quantitative evaluation of potential organic-matter porosity and hydrocarbon generation and expulsion from mudstone in continental lake basins: a case study of Dongying sag, eastern China. Mar. Petrol. Geol. 66, 906–924. https://doi.org/10.1016/j.marpetgeo.2015.07.027

Clarkson, C.R., Solano, N., Bustin, R.M., Bustin, A.M.M., Chalmers, G.R.L., He, L., Melnichenko, Y.B., Radlinski, A.P., Blach, T.P., 2013. Pore structure characterization of North American shale gas reservoirs using USANS/SANS, gas adsorption, and mercury intrusion. Fuel 103, 606–616. https://doi.org/10.1016/j.fuel.2012.06.119.

Curtis, M.E., Cardott, B.J., Sondergeld, C.H., Rai, C.S., 2012a. Development of organic porosity in the Woodford Shale with increasing thermal maturity. Int. J. Coal Geol. 103, 26–31. https://doi.org/10.1016/j.coal.2012.08.004.

Curtis, M.E., Sondergeld, C.H., Ambrose, R.J., Rai, C.S., 2012b. Microstructural investigation of gas shales in two and three dimensions using nanometer-scale resolution imaging. AAPG (Am. Assoc. Pet. Geol.) Bull. 96 (4), 665–677. https://doi.org/10.1306/ 08151110188

Dembicki Jr., H., 2009. Three common source rock evaluation errors made by geologists during prospect or play appraisals. AAPG (Am. Assoc. Pet. Geol.) Bull. 93 (3), 341–356. https://doi.org/10.1306/10230808076

Dewing, K., Hadlari, T., Pearson, D.G., Matthews, W., 2019. Early ordovician to early devonian tectonic development of the northern margin of Laurentia, Canadian arctic islands. GSA Bulletin 131 (7/8), 1075–1094. https://doi.org/10.1130/B35017.1

Dong, T., Harris, N.B., Ayranci, K., Twemlow, C.E., Nassichuk, B.R., 2015. Porosity characteristics of the Devonian Horn River shale, Canada: insights from lithofacies classification and shale composition. Int. J. Coal Geol. 141–142, 74–90. https://doi.org/10.1016/j.coal.2015.03.001

Dong, T., Harris, N.B., Ayranci, K., Twemlow, C.E., Nassichuk, B.R., 2017. The impact of composition on pore throat size and permeability in high maturity shales: middle and Upper Devonian Horn River Group, northeastern British Columbia, Canada. Mar. Petrol. Geol. 81, 220–236. https://doi.org/10.1016/j.marpetgeo.2017.01.011

Dong, T., Harris, N.B., McMillan, J.M., Twemlow, C.E., Nassichuk, B.R., Bish, D.L., 2019. A model for porosity evolution in shale reservoirs: an example from the Upper Devonian Duvernay Formation. West. Canada Sediment. Basin: AAPG (Am. Assoc. Pet. Geol.) Bull. 103 (5), 1017–1044. https://doi.org/10.1306/10261817272

Egenhoff, S.O., Fishman, N.S., 2013. Traces in the dark—sedimentary processes and facies gradients in the upper shale member of the upper devonian–lower mississippian bakken formation, williston basin, North Dakota, USA. J. Sediment. Res. 83 (9), 803–824. https://doi.org/10.2110/jsr.2013.60

El Attar, A., Pranter, M.J., 2016. Regional stratigraphy, elemental chemostratigraphy, and organic richness of the Niobrara Member of the Mancos Shale. Piceance Basin, Colorado: AAPG (Am. Assoc. Pet. Geol.) Bull. 100 (3), 345–377. https://doi.org/10.1306/ 12071514127

Emmanuel, S., Day-Stirrat, R.J., 2012. A framework for quantifying size dependent deformation of nano-scale pores in mudrocks. J. Appl. Geophys. 86, 29–35. https://doi.org/10.1016/j.jappgeo.2012.07.011

Espitali´e, J., Deroo, G., Marquis, F., 1985. Rock-eval pyrolysis and its applications. Rev. Inst. Fr. Petrol 40 (5), 563–579. Fermont, W.J.J., 1988. Possible causes of abnormal vitrinite reflectance values in paralic deposits of the Carboniferous in the Achterhoek area. The Netherlanks: Org. Geochem. 12 (4), 401–411. https://doi.org/10.1016/0146-6380(88)90013-7

Fishman, N.S., Hackley, P.C., Lowers, H.A., Hill, R.J., Egenhoff, S.O., Eberl, D.E., Blum, A.E., 2012. The nature of porosity in organic-rich mudstones of the upper jurassic Kimmeridge Clay Formation, North Sea, offshore United Kingdom. Int. J. Coal Geol. 103, 32–50. https://doi.org/10.1016/j.coal.2012.07.012

Fraser, T.A., Hutchison, M.P., 2017. Lithogeochemical characterization of the middle–upper devonian road River Group and Canol and imperial formations on trail river, east Richardson Mountains, Yukon: age constraints and a depositional model for fine-grained strata in the lower paleozoic Richardson Trough. Can. J. Earth Sci. 54 (7), 731–765, https://doi.org/10.1139/cjes-2016-0216

Fritz, W.H., Cecile, M.P., Norford, B.S., Morrow, D., Geldsetzer, H.H.J., 1991. Cambrian to middle devonian assemblages, in: Gabrielse, H., Yorath, C.J. (Eds.), Geol. Cordilleran Orogen Canada: Geol. Surv. Canada, Geol. Canada 4, 151–218.

Gale, J.F., Reed, R.M., Holder, J., 2007. Natural fractures in the Barnett Shale and their importance for hydraulic fracture treatments. AAPG Bull. 91 (4), 603–622. https://doi.org/10.1306/ 11010606061

Garzione, C.N., Patchett, P.J., Ross, G.M., Nelson, J., 1997. Provenance of Paleozoic sedimentary rocks in the Canadian Cordilleran miogeocline: a Nd isotopic study. Can. J. Earth Sci. 34 (12), 1603–1618. https://doi.org/10.1139/e17-129

Ghanizadeh, A., Bhowmik, S., Haeri-Ardakani, O., Sanei, H., Clarkson, C.R., 2015. A comparison of shale permeability coefficients derived using multiple non-steady-state measurement techniques: examples from the Duvernay Formation, Alberta (Canada). Fuel 140, 371–387. https://doi.org/10.1016/j.fuel.2014.09.073

Hadlari, T., 2015. Oil migration driven by exhumation of the Canol Formation oil shale: a new conceptual model for the Norman Wells oil field, northwestern Canada. Mar. Petrol. Geol. 65, 172–177. https://doi.org/10.1016/j.marpetgeo.2015.03.027

Hadlari, T., Davis, W.J., Dewing, K., 2014a. A pericratonic model for the Pearya terrane as an extension of the Franklinian margin of Laurentia. Canadian Arctic: GSA Bulletin 126 (1/2), 182–200, https://doi.org/10.1130/B30843.1

Hadlari, T., MacLean, B.C., Galloway, J.M., Sweet, A.R., White, J.M., Thomson, D., Gabites, J., Schr¨oder-Adams, C.J., 2014b. The flexural margin, the foredeep, and the orogenic margin of a northern Cordilleran foreland basin: Cretaceous tectonostratigraphy and detrital zircon provenance, northwestern Canada. Mar. Petrol. Geol. 57, 173–186. https://doi.org/10.1016/j.marpetgeo.2014.05.019

Hadlari, T., MacLean, B.C., Pyle, L.J., Fallas, K.M., Durbano, A.M., 2015. A Combined Depth and Thermal Maturity Map of the Canol Formation, Northern Mackenzie Valley, Northwest Territories. Geological Survey of Canada. Open File 7865. https://doi.org/10.4095/296460

Han, C., Jiang, Z., Han, M., Wu, M., Lin, W., 2016. The lithofacies and reservoir characteristics of the upper ordovician and lower silurian black shale in the southern Sichuan Basin and its periphery, China. Mar. Petrol. Geol. 75, 181–191. https://doi. org/10.1016/j.marpetgeo.2016.04.014

Harris, B.S., LaGrange, M.T., Biddle, S.K., Playter, T.L., Fiess, K.M., Gingras, M.K., 2021. Chemostratigraphy as a tool for sequence stratigraphy in the Devonian Hare Indian Formation in the Mackenzie Mountains and Central Mackenzie Valley, Northwest Territories, Canada. Can. J. Earth Sci. 99, 1–17. https://doi.org/10.1139/cjes-2020-0198

Hover, V.C., Peacor, D.R., Walter, L.M., 1996. STEM/AEM evidence for preservation of burial diagenetic fabrics in Devonian shales; implications for fluid/rock interaction in cratonic basins (USA). J. Sediment. Res. 66 (3), 519–530. https://doi.org/10.1306/D4268397-2B26-11D7-8648000102C1865D

Hower, J., Eslinger, E.V., Hower, M.E., Perry, E.A., 1976. Mechanism of burial metamorphism of argillaceous sediment: 1. Mineralogical and chemical evidence. GSA Bulletin 87 (5), 725–737. https://doi.org/10.1130/0016-7606(1976)87<725:MOBMOA>2.0. CO;2

Hu, Y., Devegowda, D., Sigal, R., 2016. A microscopic characterization of wettability in shale kerogen with varying maturity levels. J. Nat. Gas Sci. Eng. 33, 1078–1086. https://doi.org/10.1016/j.jngse.2016.06.014.

Irish, J.P.R., Kempthorne, R.H., 1987. The study of natural fractures in a reef complex, Norman Wells Oilfield, Canada, in: Tillman, R.W., Weber, K.J. (Eds.), Res. Sedimentol.: Soc. Econ. Paleontol. Mineral. Spec. Publ. 40, 153–168. https://doi.org/10.2110/pec.87.40.0153

Issler, D.R., Grist, A.M., Stasiuk, L.D., 2005. Post-Early Devonian thermal constraints on hydrocarbon source rock maturation in the Keele Tectonic Zone, Tulita area, NWT, Canada, from multi-kinetic apatite fission track thermochronology, vitrinite reflectance and shale compaction. Bull. Can. Petrol. Geol. 53 (4), 405–431. https://doi.org/10.2113/53.4.405

Jagadisan, A., Heidari, Z., 2019. Experimental quantification of the effect of thermal maturity of kerogen on its wettability. SPE Reservoir Eval. Eng. 22 (4), 1323–1333. https://doi.org/10.2118/195684-PA.

James, G., Witten, D., Hastie, T., Tibshirani, R., 2013. An Introduction to Statistical Learning with Applications in R. Springer, New York, p. 426.

Jeletzky, J.A., 1975. Jurassic and Lower Cretaceous Paleogeography and Depositional Tectonics of Porcupine Plateau, Adjacent Areas of Northern Yukon and Those of Mackenzie District: Geological Survey of Canada. Paper 74-16, p. 52. https://doi.org/10.4095/102549

Jennings, D.S., Antia, J., 2013. Petrographic characterization of the Eagle Ford shale, south Texas: mineralogy, common constituents, and distribution of nanometer-scale pore types, in: Camp, W., Diaz, E., Wawak, B. (Eds.), Electron Microscopy of Shale Hydrocarbon Reservoirs: AAPG Memoir 102, pp. 101–113. https://doi.org/10.1306/13391708M1023586

Kabanov, P., 2019. Devonian (c. 388–375 Ma) Horn River Group of Mackenzie Platform (NW Canada) is an open-shelf succession recording oceanic anoxic events. J. Geol. Soc. 176 (1), 29–45. https://doi.org/10.1144/jgs2018-075

Kabanov, P., Deblonde, C., 2019. Geological and geochemical data from Mackenzie Corridor. Part VIII: middle-Upper Devonian lithostratigraphy, formation tops, and isopach maps in NTS areas 96 and 106, Northwest Territories and Yukon. Open File 8552 Geol. Surv. Canada 39. https://doi.org/10.4095/314785

Kabanov, P., Gouwy, S.A., 2017. The Devonian Horn River Group and the basal Imperial Formation of the central Mackenzie Plain, NWT, Canada: multiproxy stratigraphic

framework of a black shale basin. Can. J. Earth Sci. 54 (4), 409–429. https://doi.org/10.1139/cjes- 2016-0096

Kabanov, P., Jiang, C., 2020. Photic-zone euxinia and anoxic events in a Middle-Late Devonian shelfal sea of Panthalassan continental margin, NW Canada: changing paradigm of Devonian ocean and sea level fluctuations. Global Planet. Change 103153, 1–19. https://doi.org/10.1016/j.gloplacha.2020.103153

Katz, B.J., Arango, I., 2018. Organic porosity: a geochemist's view of the current state of understanding. Org. Geochem. 123, 1–16. https://doi.org/10.1016/j. orggeochem.2018.05.015

Keller, L.M., Holzer, L., Wepf, R., Gasser, P., Münch, B., Marschall, P., 2011. On the application of focused ion beam nanotomography in characterizing the 3D pore space geometry of Opalinus clay. Phys. Chem. Earth 36, 1539–1544. https://doi.org/ 10.1016/j.pce.2011.07.010. Parts A/B/C.

Keller, M.A., Isaacs, C.M., 1985. An evaluation of temperature scales for silica diagenesis in diatomaceous sequences including a new approach based on the Miocene Monterey Formation. California: Geo Mar. Lett. 5 (1), 31–35. https://doi.org/10.1007/BF02629794

Klaver, J., Desbois, G., Littke, R., Urai, J., 2015. BIB-SEM characterization of pore space morphology and distribution in postmature to overmature samples from the Haynesville and Bossier Shales. Mar. Petrol. Geol. 59, 451–466. https://doi.org/10.1016/j. marpetgeo.2014.09.020

Klaver, J., Desbois, G., Littke, R., Urai, J., 2016. BIB-SEM pore characterization of mature and post mature Posidonia Shale samples from the Hils area, Germany. Int. J. Coal Geol. 158, 78–89. https://doi.org/10.1016/j.coal.2016.03.003

Knapp, L.J., Ardakani, O.H., Uchida, S., Nanjo, T., Otomo, C., Hattori, T., 2020. The influence of rigid matrix minerals on organic porosity and pore size in shale reservoirs: upper Devonian Duvernay Formation, Alberta, Canada. Int. J. Coal Geol. 227, 103525. https://doi.org/10.1016/j.coal.2020.103525

Konhauser, K.O., 2007. Introduction to Geomicrobiology. Blackwell, Malden, Massachusetts.

Law, C.A., 1999. Evaluating source rocks, in: Beaumont, A.E., Foster, N.H. (Eds.), Treatise of Petroleum Geology/Handbook of Petroleum Geology: Exploring for Oil and Gas Traps. AAPG Special Bulletin, pp. 1–41 (Chapter 6).

Lazar, O.R., Bohacs, K.M., Macquaker, J.H.S., Schiber, J., Demko, T., 2015. Capturing key attributes of fine-grained sedimentary rocks in outcrops, cores, and thin sections: nomenclatures and description guidelines. J. Sediment. Res. 85, 230–246. https://doi.org/10.2110/ jsr.2015.11

Lenz, A.C., 1972. Ordovician to devonian history of northern Yukon and adjacent district of Mackenzie. Bull. Can. Petrol. Geol. 20 (2), 321–361. https://doi.org/10.35767/ gscpgbull.20.2.321

Li, J., Ma, Y., Huang, K., Zhang, Y., Wang, W., Liu, J., Li, Z., Lu, S., 2018a. Quantitative characterization of organic acid generation, decarboxylation, and dissolution in a shale reservoir and the corresponding applications—a case study of the Bohai Bay Basin. Fuel 214, 538–545. https://doi.org/10.1016/j.fuel.2017.11.034

Li, Y., Schieber, J., Fan, T., Wei, X., 2018b. Pore characterization and shale facies analysis of the Ordovician-Silurian transition of northern Guizhou, South China: the controls of shale facies on pore distribution. Mar. Petrol. Geol. 92, 697–718. https://doi.org/10.1016/j.marpetgeo.2017.12.001

Liu, B., Schieber, J., Mastalerz, M., Teng, J., 2020. Variability of rock mechanical properties in the sequence stratigraphic context of the upper devonian new albany shale, Illinois basin. Mar. Petrol. Geol. 112, 104068. https://doi.org/10.1016/j. marpetgeo.2019.104068

L¨ohr, S.C., Baruch, E.T., Hall, P.A., Kennedy, M.J., 2015. Is organic pore development in gas shales influenced by the primary porosity and structure of thermally immature organic matter. Org. Geochem. 87, 119–132. https://doi.org/10.1016/j. orggeochem.2015.07.010

Loucks, R.G., Reed, R.M., 2014. Scanning-Electron-Microscope petrographic evidence for distinguishing organic-matter pores associated with depositional organic matter versus migrated organic matter in mudrocks. Gulf Coast Ass. Geol. Soc. J. 3, 51–60.

Loucks, R.G., Reed, R.M., Ruppel, S.C., Hammes, U., 2012. Spectrum of pore types and networks in mudrocks and descriptive classification for matrix-related mudrock pores. AAPG (Am. Assoc. Pet. Geol.) Bull. 96 (6), 1071–1098. https://doi.org/10.1306/ 08171111061

Loucks, R.G., Reed, R.M., Ruppel, S.C., Jarvie, D.M., 2009. Morphology, genesis, and distribution of nanometer-scale pores in siliceous mudstones of the Mississippian Barnett Shale. J. Sediment. Res. 79, 848–861. https://doi.org/10.2110/jsr.2009.092

Lu, J., Ruppel, S.C., Rowe, H.D., 2015. Organic matter pores and oil generation in the Tuscaloosa marine shale. AAPG (Am. Assoc. Pet. Geol.) Bull. 99 (2), 333–357. https://doi.org/10.1306/08201414055

Luffel, D.L., Guidry, F.K., 1993. New core analysis methods for measuring reservoir rock properties of Devonian shale. J. Petrol. Technol. 44 (11), 1184–1190. https://doi.org/10.2118/ 20571-PA

MacGowan, D.B., Surdam, R.C., 1990. Carboxylic acid anions in formation waters, san joaquin basin and Louisiana Gulf coast, USA—implications for clastic diagenesis. Appl. Geochem. 5 (5–6), 687–701. https://doi.org/10.1016/0883-2927(90)90065-D

MacKenzie, W.S., 1974. Radiolaria from the Canol Formation, Northwest Territories. Geological Survey of Canada. Paper 74-1, Part A, 396 pp. https://doi.org/doi:10.4095/103272

MacLean, B.C., 2011. Tectonic and stratigraphic evolution of the Cambrian basin of northern Northwest Territories. Bull. Can. Petrol. Geol. 59 (2), 172–194. https://doi.org/10.2113/gscpgbull.59.2.172

MacLean, B.C., Fallas, K.M., Hadlari, T., 2014. The multi-phase keele arch, central Mackenzie corridor, Northwest Territories. Bull. Can. Petrol. Geol. 62 (2), 68–104. https://doi.org/10.2113/gscpgbull.62.2.68

MacNeil, A.J., Jones, B., 2006. Ovummuridae (calcareous microfossils) from a Late Devonian ramp: their distribution, preservation potential, and paleoecological significance. Can. J. Earth Sci. 43, 269–280. https://doi.org/10.1139/e05-105

Macquaker, J.H., Taylor, K.G., Keller, M., Polya, D., 2014. Compositional controls on early diagenetic pathways in fine-grained sedimentary rocks: implications for predicting unconventional reservoir attributes of mudstones. AAPG (Am. Assoc. Pet. Geol.) Bull. 98 (3), 587–603. https://doi.org/10.1306/08201311176

Mastalerz, M., Schimmelmann, A., Drobniack, A., Chen, Y., 2013. Porosity of Devonian and Mississippian New Albany Shale across a maturation gradient: insights from organic petrology, gas adsorption, and mercury intrusion. AAPG (Am. Assoc. Pet. Geol.) Bull. 97 (10), 1621–1643. https://doi.org/10.1306/04011312194

Mazzotti, S., Hyndman, R.D., 2002. Yakutat collision and strain transfer across the northern Canadian Cordillera. Geology 30 (6), 495–498. https://doi.org/10.1130/0091-7613(2002)030<0495:YCASTA>2.0.CO;2.

Milliken, K.L., Curtis, M.E., 2016. Imaging pores in sedimentary rocks: foundation of porosity prediction. Mar. Petrol. Geol. 73, 590–608. https://doi.org/10.1016/j.marpetgeo.2016.03.020.

Milliken, K.L., Rudnicki, M., Awwiller, D.N., Zhang, T., 2013. Organic matter-hosted pore system, in: Marcellus Formation (Devonian), vol. 97. AAPG Bulletin, Pennsylvania, pp. 177–200. https://doi.org/10.1306/07231212048

Morrow, D.W., 2018. Devonian of the northern Canadian mainland sedimentary basin: a review. Bull. Can. Petrol. Geol. 66 (3), 623–694.

Muir, I., Dixon, O.A., 1984. Facies analysis of a middle devonian sequence in the mountain river-gayna river, in: Brophy, J.A. (Ed.), Contributions to the Geology of the Northwest Territories, vol. 1, pp. 55–62.

Muir, I., Wong, P., Wendte, J., 1985. Devonian Hare Indian-Ramparts (Kee Scarp) Evolution, Mackenzie Mountains and Subsurface Norman Wells, NWT: Basin-Fill and Platform Reef Development: Society of Economic Paleontologists and Mineralogists (SEPM) Rocky Mountain Carbonate Reservoirs CW7, pp. 311–341.

Norris, A.W., 1985. Stratigraphy of Devonian Outcrop Belts in Northern Yukon Territory and Northwestern District of Mackenzie (Operation Porcupine Area). Memoir 410. Geological Survey of Canada, p. 81. https://doi.org/10.4095/120309

Northwest Territories Geological Survey (NTGS) and National Energy Board (NEB), 2015. An Assessment of the Unconventional Petroleum Resources of the Bluefish Shale and the

Canol Shale in the Northwest Territories - Energy Briefing Note. National Energy Board, Canada, p. 10.

Olivier, J.P., Conklin, W.B., Szombathely, M.v., 1994, in: Rouquerol, J., Rodriguez- Reinoso, F., Sing, K.S.W., Unger, K.K. (Eds.), Characterization of Porous Solids III, Studies in Surface Science and Catalysis, vol. 87, pp. 81–88.

Playter, T., Corlett, H., Konhauser, K., Robbins, L., Rohais, S., Crombez, V., Maccormack, K., Rokosh, D., Prenoslo, D., Furlong, C.M., Pawlowicz, J., Gingras, M., Lalonde, S., Lyster, S., Zonneveld, J.-P., 2018. Clinoform identification and correlation in fine-grained sediments: a case study using the Triassic Montney Formation. Sedimentology 65 (1), 263–302. https://doi.org/10.1111/sed.12403

Powell, J.W., Issler, D.R., Schneider, D.A., Fallas, K.M., Stockli, D.F., 2020. Thermal history of the Mackenzie plain, Northwest Territories, Canada: insights from low-temperature thermochronology of the devonian Imperial Formation. pp.3–4 GSA Bulletin v 132, 767–783. https://doi.org/10.1130/B35089.1

Pugh, D.C., 1983. Pre-Mesozoic geology in the subsurface of Peel River map area. Memoir 401, in: Yukon Territory and District of Mackenzie. Geological Survey of Canada, p. 56. https://doi.org/10.4095/119498

Pyle, L.J., Gal, L.P., Hadlari, T., 2015. Thermal Maturity Trends for Devonian Horn River Group Units and Equivalent Strata in the Mackenzie Corridor, Northwest Territories and Yukon: Geological Survey of Canada Open File Report No. 7850. https://doi.org/10.4095/ 296446.

Pyle, L.J., Gal, L.P., 2016. Reference section for the Horn River group and definition of the Bell Creek member, Hare Indian Formation in central Northwest Territories. Bull. Can. Petrol. Geol. 64 (1), 67–98. https://doi.org/10.2113/gscpgbull.64.1.67

Ratcliffe, K.T., Wright, A.M., Schmidt, K., 2012. Application of inorganic whole-rock geochemistry to shale resource plays: an example from the Eagle Ford Shale Formation. Texas: Sediment. Rec. 10 (2), 4–9. https://doi.org/10.2110/sedred.2012.2.4

Rock-Color Chart Committee, 2009. Geological Rock-Color Chart with Genuine Munsell Color Chips. Geological Society of America.

Ross, D.J.K., Bustin, M.R., 2009. The importance of shale composition and pore structure upon gas storage potential of shale gas reservoirs. Mar. Petrol. Geol. 26, 916–927. https://doi.org/10.1016/j.marpetgeo.2008.06.004

Roychoudhury, A.N., Kostka, J.E., Van Cappellen, P., 2003. Pyritization: a palaeoenvironmental and redox proxy reevaluated: Estuarine. Coast. Shelf Sci. 57, 1183–1193. https://doi.org/10.1016/S0272-7714(03)00058-1

Schieber, J., 2013. SEM observations on ion-milled samples of devonian black shales from Indiana and New York: the petrographic context of multiple pore types, in: Camp, W., Diaz, E., Wawak, B. (Eds.), Electron Microscopy of Shale Hydrocarbon Reservoirs: AAPG Memoir 102, pp. 153–171. https://doi.org/10.1306/13391711M1023589

Schieber, J., Lazar, R., Bohacs, K., Klimentidis, R., Dumitrescu, M., Ottman, J., 2016. An SEM study of porosity in the Eagle Ford Shale of Texas—pore types and porosity distribution in a depositional and sequence-stratigraphic context, in: Breyer, J.A. (Ed.), The Eagle Ford Shale: A Renaissance in U.S. Oil Production, AAPG Memoir 110, pp. 167–186. https://doi.org/10.1306/13541961M1103589

Sing, K.S.W., 1982. Reporting physisorption data for gas/solid systems with special reference to the determination of surface area and porosity. Pure Appl. Chem. 54 (11), 2201–2218. https://doi.org/10.1351/pac198254112201

Snowdon, L.R., Brooks, P.W., Williams, G.K., Goodarzi, F., 1987. Correlation of the Canol Formation source rock with oil from norman wells. Org. Geochem. 11 (6), 529–548. https://doi.org/10.1016/0146-6380(87)90008-8

Sondergeld, C.H., Rai, C.S., Curtis, M.E., 2013. Relationship between Organic Shale Microstructure and Hydrocarbon Generation. SPE Unconventional Resources Conference, The Woodlands, Texas, USA, p. 7. https://doi.org/10.2118/164540-MS

Suits, N.S., Wilkin, R.T., 1998. Pyrite formation in the water column and sediments of a meromictic lake. Geology 26 (12), 1099–1102. https://doi.org/10.1130/0091-7613(1998)026<1099:PFITWC>2.3.CO;2

Tassonyi, E.J., 1969. Subsurface geology, lower Mackenzie river and anderson river area, district of Mackenzie. paper 68–25 Geol. Surv. Canada 207, 10.4095/103335.

Tissot, B.P., Welte, D.H., 1984. Petroleum Formation and Occurrence. Springer-Verlag, Berlin, p. 699. https://doi.org/10.1007/978-3-642-87813-8

Turner, B.W., Treanton, J.A., Slatt, R.M., 2016. The use of chemostratigraphy to refine ambiguous sequence stratigraphic correlations in marine mudrocks. An example from the Woodford Shale. Oklahoma, USA: J. Geol. Soc. 173, 854–868. https://doi.org/10.1144/jgs2015-125

Ver Straeten, C.A., Brett, C.E., Sageman, B.B., 2011. Mudrock sequence stratigraphy: a multi-proxy (sedimentological, paleobiological and geochemical) approach. Devonian

Appalachian Basin: Palaeogeogr. Palaeoclimatol. Palaeoecol. 304 (1–2), 54–73. https://doi.org/10.1016/j.palaeo.2010.10.010

Wang, F., Guan, J., Feng, W., Bao, L., 2013. Evolution of Overmature Marine Shale Porosity and Implication to the Free Gas, vol. 40. Petroleum Exploration and Development, pp. 819–824. https://doi.org/10.1016/S1876-3804(13)60111-1

Wignall, P.B., Newton, R., 1998. Pyrite framboid diameter as a measure of oxygen deficiency in ancient mudrocks. Am. J. Sci. 298, 537–552. https://doi.org/10.2475/ajs.298.7.537

Williams, L.A., Crerar, D.A., 1985. Silica diagenesis; II, General mechanisms. J. Sediment. Res. 55 (3), 312–321. https://doi.org/10.1306/212F86B1-2B24-11D7-8648000102C1865D

Yang, Y., Aplin, A.C., 2007. Permeability and petrophysical properties of 30 natural mudstones. J. Geophys. Res. Solid Earth 112, 1–14. https://doi.org/10.1029/2005JB004243

Yang, R., He, S., Yi, J., Hu, Q., 2016. Nano-scale pore structure and fractal dimension of organic-rich Wufeng-Longmaxi shale from Jiaoshiba area, Sichuan Basin: investigations using FE-SEM, gas adsorption and helium pycnometry. Mar. Petrol. Geol. 70, 27–45. https://doi.org/10.1016/j.marpetgeo.2015.11.019

Yassin, M.R., Begum, M., Dehghanpour, H., 2017. Organic shale wettability and its relationship to other petrophysical properties: a Duvernay case study. Int. J. Coal Geol. 169, 74–91. https://doi.org/10.1016/j.coal.2016.11.015

Yassin, M.R., Dehghanpour, H., Begum, M., Dunn, L., 2018. Evaluation of imbibition oil recovery in the Duvernay Formation. Soc. Petrol. Eng. 21 (2), 257–272. https://doi.org/10.2118/185065-PA

Yose, L.A., Brown, S., Davis, T.L., Eiben, T., Kompanik, G.S., Maxwell, S.R., 2001. 3-D geologic model of a fractured carbonate reservoir, Norman Wells Field, NWT, Canada. Bull. Can. Petrol. Geol. 49 (1), 86–116. https://doi.org/10.2113/49.1.86

Chapter 4: A review of sequence stratigraphy in organic-rich, marine mudstone successions using chemostratigraphic datasets[2]

4.1 Introduction

Sequence stratigraphy was defined by Posamentier and Allen (1999) as "the analysis of cyclic sedimentation patterns that are present in stratigraphic successions, as they develop in response to variations in sediment supply and space available for sediment to accumulate" (p.1). In sequence stratigraphy, the unit deposited during one of these complete cycles is classified as a sequence (Catuneanu et al., 2009), and sequences are subdivided into systems tracts that consist of coeval depositional systems (Brown and Fisher, 1977). Systems tracts can be further subdivided into smaller scale sequence stratigraphic cycles (i.e., sequences), allostratigraphic cycles (i.e., parasequences), or sedimentological cycles (i.e., beds and bedsets) (Catuneanu, 2019a). Both sequences and systems tracts are bounded by sequence stratigraphic surfaces (Embry, 2002; Catuneanu, 2006; Catuneanu et al., 2009). Sequence stratigraphic units and bounding surfaces can be observed at different scales (i.e., hierarchical levels), depending on the purpose of study and/or the resolution of the data available (Catuneanu, 2019b).

The interpretations drawn from sequence stratigraphic analysis are used to gain insights into the evolution of sedimentary basins and predict facies distributions for hydrocarbon and mineral exploration (Embry, 2009; Catuneanu et al., 2011). Recently, the development of shale resource plays has resulted in an increased focus on understanding and predicting lateral and vertical lithological variations in organic-rich mudstone successions (e.g., Egenhoff and

[2] This chapter has been published as: LaGrange, M.T., Konhauser, K.O., Catuneanu, O., Harris, B.S., Playter, T.L. and Gingras, M.K., 2020. Sequence stratigraphy in organic-rich marine mudstone successions using chemostratigraphic datasets. Earth-Science Reviews, 203, 103137. https://doi.org/10.1016/j.earscirev.2020.103137

Fishman, 2013; Taylor and Macquaker, 2014; Wilson and Schieber, 2015; Birgenheier et al., 2017; Li and Schieber, 2019). As a result, establishing a sequence stratigraphic framework is a valuable tool for the evaluation of these successions because it allows for the delineation and subsurface correlation of higher quality reservoir intervals (Slatt and Rodriguez, 2012; Knapp et al., 2019).

However, making stratigraphic correlations in mudstone intervals presents unique challenges. These successions are characterized by more subtle macroscale sedimentological variations than those observed in coarser-grained clastic and carbonate successions, making lithological trends less feasible unless thin sections are available at a high resolution (Ratcliffe et al., 2012a; Borcovsky et al., 2017). Furthermore, the subtle compositional variability characteristic of fine-grained successions can be difficult to infer from petrophysical datasets (i.e., well logs), which are commonly used as a basis for stratigraphic correlations (Pearce et al., 2005; Turner et al., 2016; Knapp et al., 2019). In addition, as these mudstone intervals commonly represent sedimentation in distal areas of restricted basins, biostratigraphic datasets may be unavailable or of limited use (Raftcliffe et al., 2012a). Moreover, high-resolution biostratigraphic datasets are typically unavailable for Paleozoic or older mudstone intervals (Slatt and Rodriguez, 2012). The stratal geometries that allow researchers to make interpretations using seismic profiles are often absent (Pearce et al., 2005), seismic datasets may not exist, or the scale of the sequence stratigraphic analysis may be sub-seismic (Catuneanu, 2019b).

Given these challenges, it is becoming increasingly common for chemostratigraphic data to be integrated with other datasets in the study of mudstone successions (e.g., Pearce et al., 1999; Ratcliffe et al., 2010, 2012a, 2012b; Sano et al., 2013; Turner et al., 2015, 2016; El Attar and Pranter, 2016; Nyhuis et al., 2016; Pyle and Gal, 2016; Playter et al., 2018; DeReuil and

Birgenheier, 2019). This type of stratigraphy uses inorganic geochemical properties of whole-rock samples to characterize and correlate stratigraphic units (Pearce et al., 1999). More specifically, certain elements and elemental ratios are used as proxies for sediment provenance, paleoproductivity, paleoredox conditions in the water column and/or sediment pile, and other environmental conditions at the time of sediment deposition. Indeed, observed variations in these proxies with depth have been used to identify chemostratigraphic units with distinct geochemical characteristics (Pearce et al., 1999). As a result, chemostratigraphic units are now frequently applied as a means of subdivision and correlation (e.g., Pearce et al., 1999; Ratcliffe et al., 2010, 2012a; El Attar and Pranter, 2016; Pyle and Gal, 2016). Chemostratigraphic datasets have also been used to increase the resolution of sequence stratigraphic interpretations within mudstone intervals (e.g., Algeo et al., 2004; Ver Straeten et al., 2011; Hammes and Frebourg, 2012; Sano et al. 2013; Turner et al. 2015, 2016).

In this work, we review the elements and elemental ratios that can be used as chemostratigraphic proxies for sequence stratigraphic interpretation of organic-rich mudstone successions. Through this review, we aim to provide a systematic framework for the chemostratigraphic identification of sequence stratigraphic surfaces, systems tracts, and sequences in organic-rich mudstone intervals. This work follows the sequence stratigraphic terminology of Catuneanu (2019a) (Fig. 4.1). Herein, 'mudstone' is used as a general term referring to all fine-grained sedimentary rocks and is defined as a rock composed of greater than fifty percent silt and clay size grains following Lazar et al. (2015).

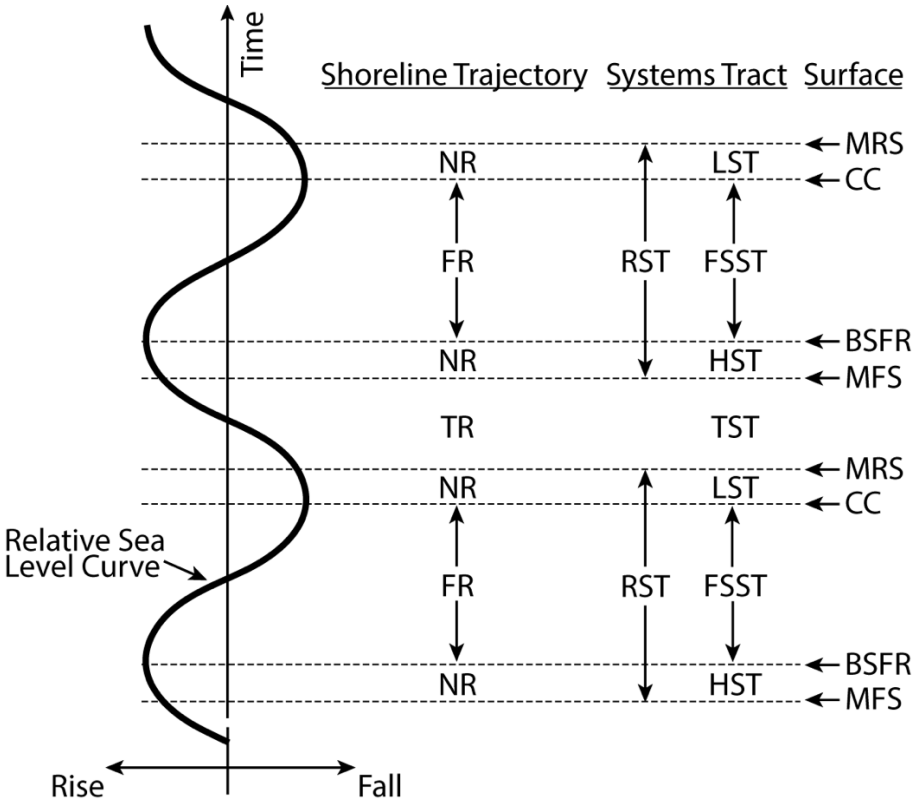

Figure 4.1 Sequence stratigraphic terminology used herein. Acronyms: NR–normal regression; FR–forced regression; TR–transgression; RST–regressive systems tract; LST–lowstand systems tract; FSST–falling-stage systems tract; HST–highstand systems tract; TST–transgressive systems tract; MRS–maximum regressive surface; CC–correlative conformity; BSFR–basal surface of forced regression; and MFS–maximum flooding surface. Modified from Catuneanu (2006).

4.2 Chemostratigraphic proxies

The following section reviews many of the elemental proxies useful to chemostratigraphy of mudstone intervals and how they are interpreted. Table 4.1 summarizes the main mineralogical controls on these elements, although there are other ways for these elements to become enriched in sediment (e.g., incorporation into nodules; adsorption onto mineral particles

in the water column; adsorption onto, or accumulation into, organic matter; diagenetic and metamorphic reactions, and interactions with secondary fluids). To confirm the primary controls on each element, many studies compare elemental composition data to mineralogical data obtained through x-ray diffraction analysis and perform statistical analyses such as Principal Component Analysis, Hierarchical Cluster Analysis, or Q-mode Factor Analysis to determine elemental associations (e.g., Pearce et al., 2005; Ver Straeten et al., 2011; Ratcliffe et al., 2012a; Sano et al., 2013; Turner et al., 2016; Playter et al., 2018). Table 4.2 summarizes the purpose of each elemental proxy discussed below. It is critical that elemental data are tied to mineralogical-data calibration points to ensure sound and accurate depositional and diagenetic interpretations of elemental data as they relate to mineralogical distribution.

Table 4.1. Primary mineralogical controls on elements commonly used as chemostratigraphic proxies in organic-rich mudstone successions.

Element	Typical Mineralogical Affinity	Reference
Al	Clay and feldspar.	(Ratcliffe et al., 2004; Brumsack, 2006; Tribovillard et al., 2006; Piper and Calvert, 2009)
Cr	Chromite, clay minerals, ferromagnesian minerals.	(Tribovillard et al. 2006)
K	Clay and feldspar.	(Ratcliffe et al., 2004; Turner et al., 2016)
Nb	Titanium oxides, silicates, or distinct mineral phase, clay minerals.	(Bonjour and Dabard, 1991; Dinelli *et al.,* 2007)
Rb	Clay and feldspar.	(Ratcliffe et al., 2004; Dinelli et al., 2007)
Th	Detrital. Associated with clay minerals, accessory minerals or adsorbed to mineral surfaces.	(Myers and Wignall, 1987; Rowe et al., 2017)
Ti	Titanium oxides, chlorite, illite/mica, biotite.	(Ratcliffe et al., 2004; Pearce et al., 2005; El Attar and Pranter, 2016)
U	Detrital or authigenic. Accessory minerals or adsorbed to mineral surfaces. Can also be adsorbed to organic matter or precipitated as uranium oxides.	(Myers and Wignall, 1987; Wignall and Twitchett, 1996; Tribovillard et al., 2006)
Y	Heavy minerals (zircon, garnet, monzanite, apatite, hornblende).	(Dinelli et al., 2007)
Zr	Zircon.	(Patchett et al., 1984; Ratcliffe et al., 2004; Mongelli et al., 2006; El Attar and Pranter, 2016)

Table 4.2 Elemental proxies useful for interpreting systems tracts, bounding surfaces, and sequences in marine organic-rich mudstone successions. Acronyms: TOC–total organic carbon.

Parameter	Potential Proxies	Details	Reference
Detrital Sediment	Elements predominantly associated with detrital sediment	Vary depending on the interval but commonly include Al, K, Zr, and Ti.	(e.g., Pearce et al., 2005; Ratcliffe et al., 2012b; Sano et al., 2013; Nyhius et al., 2016; Turner et al., 2016)
	Sums of detrital elements	For example, $Al_2O_3+TiO_2+Fe_2O_3+K_2O$ used by Ratcliffe et al. (2012b) or $Al_2O3+K_2O+TiO_2$ used by Sano et al. (2013).	(e.g., Ratcliffe et al., 2012b; Sano et al., 2013)
	Ti/Al	Higher Ti/Al as terrigenous input increases.	(Chen et al., 2013)
Grain Size	Si/Al	If silica is primarily detrital, can reflect changes in abundance of coarse sediment supply.	(e.g., Ratcliffe et al., 2004; Dinelli et al., 2007; Ratcliffe et al., 2012c)
	Zr/Al	May reflect changes in abundance of coarse sediment supply.	(e.g., Ratcliffe et al., 2004; Dinelli et al., 2007)
	Zr/Nb	May reflect changes in abundance of coarse sediment supply.	(e.g., Ratcliffe et al., 2006; Sano et al., 2013)
	Zr/Rb	May reflect changes in abundance of coarse sediment supply.	(e.g., Dinelli et al., 2007)
	Y/Al	Reflects changes in abundance of coarse sediment supply.	(e.g., Dinelli et al., 2007)
	Y/Rb	May reflect changes in abundance of coarse sediment supply.	(e.g., Dinelli et al., 2007)

Paleoredox	V	Can become enriched in anoxic to euxinic environments.	(Wanty and Goldhaber, 1992; Calvert and Pedersen, 1993; Tribovillard et al., 2006)
	Re	Can become enriched in anoxic to euxinic environments.	(Colodner et al., 1993; Crusius et al., 1996; Yamashita et al., 2007)
	Cr	Can become enriched in anoxic to euxinic environments.	(Calvert and Pedersen, 1993; Algeo and Maynard, 2004; Tribovillard et al., 2006)
	U	Can become enriched in anoxic to euxinic environments.	(Myers and Twitchett, 1987; Wignall and Twitchett, 1996; McManus et al., 2005; Tribovillard et al., 2006)
	Mo	Can become enriched in euxinic environments.	(Erickson and Helz, 2000)
	Ni	Can become enriched in euxinic environments	(Huerta-Diaz and Morse, 1992; Calvert and Pedersen, 1993; Tribovillard et al., 2006)
	Th/U	Th/U <2 reflects anoxic conditions, Th/U 2-7 suggests oxic environments, and Th/U >7 is indicative of sediment deposited under highly oxidizing conditions.	(Wignall and Twitchett, 1996)

Basin Restriction	Mo/TOC	Mo/TOC >35 x 10^{-4} in weakly restricted settings, ~15–35 x 10^{-4} in environments characterized by moderate restriction, and <15 x 10^{-4} in strongly restricted settings.	Algeo and Lyons (2006)
Excess Silica	Peaks in Si/Al	Al typically reflects clay abundance in mudstones (Sageman and Lyons, 2004; Rowe et al., 2017).	(Davis et al., 1999; Sageman and Lyons, 2003; Turner et al., 2015, 2016; Gambacorta et al., 2016; Zhang et al., 2019)
	Si-Al crossplot	See Figure 4.2.	(Tribovillard et al., 2006; Rowe et al., 2012; El Attar and Pranter, 2016)
	$Si_{excess} = Si_{sample}(Si/Al)_{average\ shale}$	Excess silica relative to average shale.	(Ross and Bustin, 2009; Shen et al., 2014; Arsairai et al., 2016)

4.2.1 Detrital sediment

The abundance of elements that are predominantly associated with detrital sediment can be used to make inferences about the abundance of terrigenous (i.e., continental) sediment input into the basin (Chen et al., 2013). These elements will vary depending on the interval but commonly include Al, K, Ti, and Zr (e.g., Pearce et al., 2005; Ratcliffe et al., 2012b; Sano et al., 2013; Nyhuis et al., 2016; Turner et al., 2016). In addition to single element patterns, summing a combination of the elements has also proven effective as a proxy for abundance of continental input (e.g., $Al_2O_3+TiO_2+Fe_2O_3+K_2O$) as was used by Ratcliffe et al. (2012b) to characterize chemostratigraphic units in the Horn River Formation (British Columbia, Canada). Similarly, Sano et al. (2013) used $Al_2O_3+K_2O+TiO_2$ in conjunction with other proxies to establish a

chronostratigraphic framework in the Haynesville Formation (Texas and Louisiana). Chen et al. (2013) suggested that because Ti is present in heavier minerals (e.g., rutile, ilmenite) that settle out sooner than Al-bearing minerals, the molar Ti/Al ratio can be used as a proxy for changes in proximity to detrital sediment sources and variation in relative sea level in intervals where sediment provenance remains constant. They observed similar trends in the reconstructed sea level profile based on benthic $\delta^{18}O$ profile and the Ti/Al profile of sediment cores from the South China Sea and Japan Sea, with lower Ti/Al in sediment deposited during interglacial periods and higher Ti/Al in sediments from glacial periods suggesting that increases in Ti/Al reflect increased continental sediment supply to the basin.

4.2.2 Grain size

Chemostratigraphic proxies can also be used to infer grain size variations. For instance, if the Si present in an interval is predominantly detrital, trends in Si/Al can reflect variations in the proportion of silt to clay size fraction (e.g., Ratcliffe et al., 2004; Dinelli et al., 2007; Ratcliffe et al., 2012c). Similarly, changes in Zr/Nb and Zr/Al can indicate changes in the abundance of coarse sediment supply if these ratios are primarily controlled by variations in the abundance of silt-size detrital zircon rather than variations in provenance (Ratcliffe et al., 2004, 2006; Dinelli et al., 2007; Sano et al., 2013). In this case, Ratcliffe et al. (2004) suggested that increasing Zr/Al results from an increased proportion of silt-size detrital zircon compared to clay minerals, whereas Ratcliffe et al. (2006) and Sano et al. (2013) observed that Zr/Nb followed grain size trends, with higher Zr/Nb in coarser grained intervals. Additionally, in a study of fine-grained Pleistocene and Holocene sediments, Dinelli et al. (2007) showed that ratios of Zr/Rb, Zr/Al, Y/Al, and Y/Rb correlated well to the coarse silt-size sediment fraction. Bloemsma et al. (2012)

assessed geochemical grain size proxies for three offshore fine-grained quaternary sediment cores. Two of these cores were retrieved from different locations off the coast of West Africa, whereas the third core was collected off the coast of Chile. In the two cores from West Africa, Si exhibited the strongest correlations with mean grain size, whereas Ti showed the strongest correlations with mean grain size for core collected offshore of Chile. Based on these results, Bloemsma et al. (2012) concluded that geochemical grain size proxies vary depending on the particular setting. The above studies suggest that geochemical grain size proxies should be determined for each interval on a case-by-case basis through comparison with grain size data.

4.2.3 Paleoredox

Variations in redox conditions change the solubility of many elements, with decreased oxygen levels at the sediment water interface resulting in the enrichment of certain metals in sediment; in this paper we focus on mudstone successions. When discussing paleoredox conditions, the terms oxic, suboxic, anoxic, and euxinic are used. The distinction between oxic, suboxic, and anoxic has commonly been used to distinguish the amount of dissolved oxygen available, with different authors using different concentrations (e.g., oxic, >4.5 uM; suboxic, 4.5 uM – 10 nM; anoxic, < 10 nM; Morrison et al., 1999; Revsbech et al., 2009; Tyson and Pearson, 1991). The terms are similarly used to refer to specific microbial metabolisms and the terminal electron acceptor (TEA) coupled to the oxidation of organic carbon (e.g., Froelich et al., 1979; Canfield and Thamdrup, 2009). Thus, oxic refers to aerobic respiration (where cells use O_2), suboxic refers to using nitrate (NO_3^-), while anoxic refers to using Mn(IV), Fe(III) or sulfate (SO_4^{2-}) (Konhauser, 2007). Additionally, the term euxinic will be used herein to describe anoxic conditions in which sulfate reduction results in the presence of hydrogen sulfide in the water column.

Trace element enrichment is commonly compared to an average shale with the enrichment factor for a given element (X) calculated as follows (Brumsack, 2006; Tribovillard et al., 2006):

$$EF_X = (X/Al)_{sample}/(X/Al)_{average\ shale} \quad \text{(Eq. 1)}$$

An element is considered to be enriched if this ratio exceeds 1 and depleted if the ratio is below 1 (Brumsack, 2006; Tribovillard et al., 2006). Alternatively, Brumsack (2006) argued that for intervals with low detrital input and, therefore low Al abundance, it is more suitable to evaluate enrichment of an element (X) by considering its non-detrital fraction, which can be calculated using the following formula:

$$X_{non\text{-}detrital} = X_{sample} - Al_{sample}\,(X/Al)_{average\ shale} \quad \text{(Eq. 2)}$$

Elemental concentrations from Average Shale (Wedepohl, 1971) or Post-Archean Average Australian Shale (Taylor and McLennan, 1985) are commonly used as comparators (e.g., Ross and Bustin, 2009; Rowe et al., 2009; Zhou and Jiang, 2009; Gambacorta et al. 2016).

Several trace elements, including V, Re, Cr, and U, may become enriched in anoxic to euxinic sediment. Vanadium is fixed in sediment under mildly anoxic conditions if the insoluble hydroxide $VO(OH)_2$ is formed once V(V) is reduced to V(IV) (Wanty and Goldhaber, 1992; Calvert and Pedersen, 1993). Under euxinic conditions, sedimentary V enrichment occurs through precipitation of V_2O_3 or $V(OH)_3$ upon reduction of V(IV) to V(III) (Wanty and Goldhaber, 1992; Calvert and Pedersen, 1993). Sedimentary enrichment of Re occurs under anoxic to euxinic conditions where Re(VII) is reduced to Re(IV) (Colodner et al., 1993; Crusius et al., 1996; Yamashita et al., 2007) and precipitated as sulfides or adsorbed to organic matter (Kendall et al., 2010). In anoxic settings, the conversion of Cr(VI) to Cr(III) leads to the latter being incorporated into organic compounds or Fe(III) and Mn(IV) oxyhydroxides (Calvert and

Pedersen, 1993; Algeo and Maynard, 2004). Chromium has been used to interpret paleoredox conditions in some studies (e.g., El Attar and Pranter, 2016), although the possibility of Cr loss from remineralization of organic matter in euxinic conditions (Algeo and Maynard, 2004) and the potential for Cr enrichment from an increased proportion of Cr in detrital sediment means that this proxy should be used with caution (Tribovillard et al., 2006).

Uranium is delivered to the oceans in detrital accessory minerals and in solution in the form of U(VI) (Myers and Wignall, 1987). Under oxic conditions, U(VI) binds with bicarbonate to form a soluble anion, while reducing conditions lead to the conversion of U(VI) to U(IV) and can lead to sedimentary enrichment of U in the form of uraninite, UO_2 (Myers and Wignall, 1987; Klinkhammer and Palmer, 1991; Wignall and Twitchett, 1996; McManus et al., 2005; Partin et al., 2013).

Molybdenum accumulates in sediment under euxinic conditions (Helz et al., 1996; Tribovillard et al., 2006; Scott and Lyons, 2012; Robbins et al., 2016). In seawater, Mo is present as molybdate (MoO_4^{2-}) and in the presence of H_2S reacts to form particle-reactive thiomolybdates (e.g., MoS_4^{2-}) (Helz et al., 1996), which is enriched in sediment through complexation with organic matter or reduced compounds (Helz et al., 1996; Erickson and Helz, 2000). Similarly, euxinic conditions result in enrichment of Ni through incorporation of NiS into sulfides (Huerta-Diaz and Morse, 1992; Calvert and Pedersen, 1993).

The Th/U ratio can be used as an indicator of paleoredox conditions (Myers and Wignall, 1987; Wignall and Twitchett, 1996; Kimura and Watanabe, 2001; Sano et al., 2013). As previously discussed, U can become enriched in sediment under anoxic conditions (Myers and Wignall, 1987; Wignall and Twitchett, 1996; Partin et al., 2013). In contrast, the abundance of Th in sediment is controlled by detrital input as it is insoluble in seawater, and consequently it

does not become authigenically enriched (Myers and Wignall, 1987; Wignall and Twitchett, 1996). Owing to their differing mobility, Th/U <2 is interpreted to reflect deposition under anoxic conditions, Th/U of 2-7 suggests oxic environments, and Th/U >7 are indicative of sediment deposited under highly oxidizing conditions (Wignall and Twitchett, 1996).

4.2.4 Basin restriction

In basins characterized by a degree of restriction from the global oceans, Algeo and Lyons (2006) proposed that Mo/total organic carbon (TOC) is an indicator of the extent of basin isolation. In that study, Mo–TOC relationships of sediment were demonstrated to vary as a function of deep-water dissolved Mo and deep-water renewal time in several restricted modern anoxic environments. Algeo and Lyons (2006) observed sedimentary Mo/TOC values of >35 x 10^{-4} in weakly restricted settings, ~15–35 x 10^{-4} in environments characterized by moderate restriction, and <15 x 10^{-4} in strongly restricted settings. This trend was interpreted to reflect a growing drawdown of the aqueous Mo reservoir in increasingly restricted settings caused by Mo removal to sediment outpacing Mo re-supply. These relationships have been used to interpret the level of basin isolation in several studies of organic-rich mudstone intervals including Harris et al. (2013), Turner and Slatt (2016), and Hines et al. (2019).

4.2.5 Biogenic sediment

Certain elements, elemental ratios, and cross-plots are used to estimate the proportion of biogenic silica (i.e., silica derived from organisms such as diatoms, radiolarians, or siliceous sponges) relative to other sources of silica. Understanding variations in the abundance of biogenic silica is important because these trends can be used to interpret variations in

productivity (Schieber et al., 2000; Harris et al., 2018) or variations in the degree of clastic dilution, with higher biogenic silica suggestive of condensed deposition (Bohacs, 1998; Gutierrez et al., 2017). Sources of Si in mudstone successions include detrital Si from fluvial or aeolian sources, precipitation of silica during clay diagenesis, and biogenic silica (Schieber, 1996; Taylor and Macquaker, 2014). Hydrothermal input can additionally serve as a potential source of silica in mudstone intervals (e.g., Adachi et al., 1986; Arsairai et al., 2016). Aluminium content typically reflects clay abundance in mudstone intervals (Sageman and Lyons, 2004; Rowe et al., 2017). Excess Si relative to Al is typically identified in the following three ways: (1) peaks in Si/Al (e.g. Dean and Arthur, 1998; Davis et al., 1999; Sageman and Lyons, 2004; Turner et al., 2016); (2) Si–Al crossplots (Fig. 4.2; Tribovillard et al., 2006; Rowe et al., 2012; El Attar and Pranter, 2016); and (3) calculating excess silica relative to the average shale using equation 3 (e.g., Ross and Bustin, 2009; Shen et al., 2014; Arsairai et al., 2016).

$$Si_{excess} = Si_{sample} - Al_{sample}\,(Si/Al)_{average\ shale} \quad \text{(Eq. 3)}$$

Where excess Si may be biogenic, aeolian, or hydrothermal in origin.

Al–Fe–Mn ternary diagrams can be used to distinguish non-hydrothermal silica from hydrothermal silica (see Adachi et al., 1986; Arsairai et al., 2016). Sageman and Lyons (2004) suggest that biogenic and aeolian silica can be distinguished by considering depositional environment, studying sedimentary textures, and by comparison with other elemental proxies. For example, the presence of biogenic silica is supported if the Zr/Al and Ti/Al profiles, which are interpreted to reflect the proportion of continental input, do not correspond to Si/Al peaks (Turner et al., 2015, 2016; Gambacorta et al., 2016). Similarly, Zhang et al. (2019) suggest that corresponding peaks in both Si/Al and Si/Ti indicate that excess silica is more likely biogenic than detrital. Petrographic analysis and scanning electron microscopy with associated imaging

techniques (e.g., cathodoluminescence or charge contrast imaging) can also be used to differentiate biogenic silica and detrital quartz (e.g., Schieber, 2000; Buckman et al., 2017).

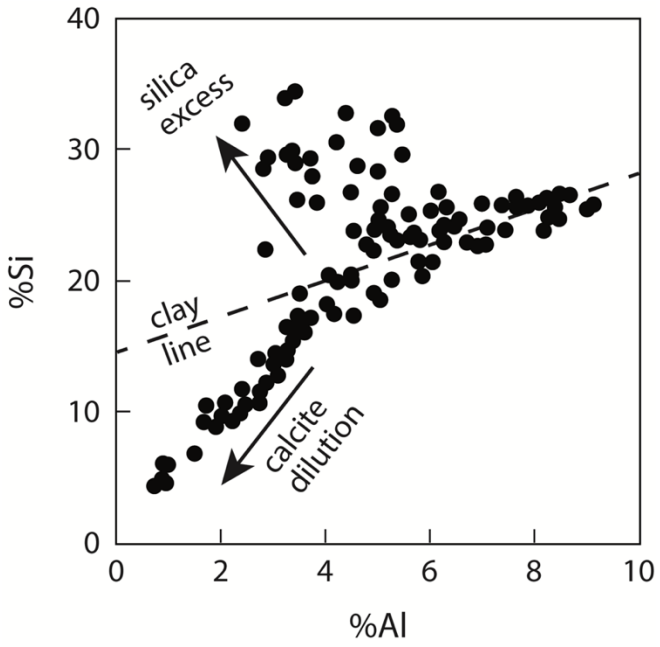

Figure 4.2 Example of a Si–Al cross-plot used to identify excess silica. Data is from the Barnett Shale in the 1-Blakely core in Wise County, Texas. Reproduced from Rowe et al. (2012) with permission.

Planktonic organisms can also have calcareous rather than siliceous skeletons (e.g., coccoliths, foraminifera). Several authors have proposed that lithological cycles observed in successions dominated by pelagic carbonates, marlstones, and mudstones are related to variations in relative sea level (e.g., Elder et al., 1994; Dean and Arthur, 1998; Hart et al., 2015). More specifically, Hart et al. (2015) proposed that pelagic carbonate content increases upwards through transgression to the maximum flooding surface and then decreases upwards during regression. $CaCO_3$ or calcite profiles have been used in conjunction with other datasets (e.g.,

sedimentological, petrophysical) to identify cycles in some of these studies (e.g., Dean and Arthur, 1998; Hart et al., 2015) suggesting that Ca could potentially be used as a proxy for pelagic carbonate if this relationship is first confirmed through comparison to XRD and sedimentological datasets.

4.2.6 Additional influences on composition

A number of factors can influence elemental distributions other than environmental conditions at the time of deposition (Pearce et al., 2005). These include provenance, bioturbation, post-depositional re-oxidation, diagenesis, oil generation and expulsion, and chemical weathering of outcrops. For example, although Th/U can be a paleoredox indicator (Myers and Wignall, 1987; Wignall and Twitchett, 1996; Kimura and Watanbe, 2001; Sano et al., 2013), it can also vary based on provenance and sedimentary recycling (McLennan et al., 1993). Similarly, trends in Zr/Nb can indicate grain size variations (e.g., Ratcliffe et al., 2006; Sano et al., 2013) or changes in sedimentary provenance, with higher Zr/Nb resulting from an increased proportion of zircon derived from a mature, recycled sedimentary provenance (Ratcliffe et al., 2006).

Bioturbation also affects trace element distribution. Using elemental maps obtained by synchrotron rapid scanning X-ray fluorescence, Harazim et al. (2015) observed partitioning of trace elements (e.g., Cr, V, and Zr) between burrows and burrow halos in Cretaceous continental mudstone samples, which was interpreted to have been caused by mechanical sorting of grains by the trace maker. In marine sedimentary rocks, elemental distributions have also been shown to be heavily impacted by the presence of bioturbation (e.g., Over, 1990). This highlights the importance of understanding the scale and distribution of bioturbation in the interval of interest and assessing geochemical heterogeneity caused by animal-sediment interactions where possible.

Many major and trace elements may be affected by diagenesis, and some elements are more prone to diagenetic remobilization than others (Pearce et al., 1999). For example, of elements often associated with detrital input (e.g., Al, Ti) are effectively immobile during diagenesis (e.g., Thomson et al., 1998; Brumsack, 2006; Tribovillard et al., 2006), although the observation of authigenic kaolinite in the Cretaceous Mancos Shale suggests that Si and Al can be mobile on at least a local scale (Taylor and Macquaker, 2014). Silica can be released during diagenesis through clay mineral transformations (e.g., smectite to illite or illite to muscovite) or through dissolution of silicate minerals or biogenic silica (Schieber, 1996; Taylor and Macquaker, 2014). The observation of early diagenetic quartz suggests that the low permeability and low diffusion coefficients of mudstone intervals prevents significant diagenetic mobility of silica (Taylor and Macquaker, 2014 and references therein). Similarly, K can be incorporated into clays during illitization, whereby a precursor smectite phase can be altered through pore-water enrichment in K^+. Two main mechanisms for smectite to illite transformation have been inferred, including the dissolution of the smectite lattice and growth of illite crystals due to the Ostwald ripening-like effect (Nadeau et al., 1985) and a biological role in which sedimentary microbes concentrated K^+ into their biomass which then becomes liberated during heterotrophic degradation (Aubineau et al., 2019).

Post-depositional diffusion of O_2 into bottom sediments, which can occur in situations such as glacial-interglacial transitions or deposition of turbidites in anoxic settings, leads to re-oxidation of reduced species which can, in turn, result in remobilization of certain elements (Morford et al., 2001; Tribovillard et al., 2006). This has been observed to potentially affect Cr, Mo, Ni, U, and V (e.g., Thomson et al., 1993, 1995; Rosenthal et al., 1995). Tribovillard et al. (2006) suggested that redox-sensitive trace metals associated with sulfides (e.g., Mo, Ni, Re)

should be immobile if post-depositional re-oxidation does not occur because sulfides are typically stable during diagenesis in sediments where organic supply is sufficient to support sulfate reduction, and hence sulfide generation.

The enrichment of Ni and V has been observed in oils derived from type II kerogens (Lewan and Maynard, 1982; Lewan, 1984). This may result in lower than expected enrichment of certain trace metals in organic-rich mudstone units that have undergone oil generation and expulsion (Harris et al., 2013). Chemical weathering also affects composition (Nesbitt and Young, 1982). For example, in a study of two organic-rich mudstone intervals from the Guizhou province in China, Liu et al. (2016) observed the loss of major elements, such as Na, Ca, Mg, Fe, and trace elements, including V and Ni, in outcrop samples compared to core samples. Weathering of organic matter in mudstone intervals has been observed to cause a pronounced breakdown of Ni and V metallo-organic complexes (Grosjean et al., 2004). In a study of the effects of weathering on proxies used for paleoenvironmental interpretation in mudstone successions, Marynowski et al. (2017) observed significant decreases in the concentrations of trace metals including, Mo, Ni, and U, which were attributed to degradation of organic matter and oxidation of pyrite. The depletion of Re from weathering of organic-rich mudstones has also been observed (e.g., Peucker-Ehrenbrink and Hannigan, 2000; Jaffe et al., 2002).

Due to complexities inherent in element and mineral distributions, good practice confirms element affinities using cross plots, comparisons, and statistical analyses. When possible, integrating chemostratigraphic interpretations with other datasets is also recommended (e.g., Algeo et al., 2004; Ver Straeten et al., 2011; Hammes and Frebourg, 2012).

4.2.7 Normalization to aluminium and the average shale

In many studies, elemental concentrations have been normalized to Al with the aim of accounting for dilution by other components and facilitating comparison between different locations and intervals (Pearce et al., 1999; Van der Weijden, 2002; Algeo et al., 2004; Algeo and Maynard, 2004; Harris et al., 2013). Moreover, elements are normalized to Al in order to compare with average shale values, which then provides an estimate of enrichment of those elements (Brumsack, 2006; Tribovillard et al., 2006). However, Van der Weijden (2002) demonstrated that normalization to Al can result in apparent correlations between unrelated variables or vice versa, especially if the coefficient of variation of Al is large compared to the coefficient of variation of the elements being normalized. Furthermore, Algeo and Lyons (2006) argued that given trace elements and TOC are both affected by dilution, trace metals should not be normalized to Al for comparison with trends in TOC. Finally, understanding the relative proportion and abundance of different elements or minerals is useful for sequence stratigraphy (e.g., identifying condensed sections) and normalizing to Al conflates the dataset. Consequently, normalization to Al should only be performed if the coefficient of variation of Al is similar to that of the element of interest and it is also recommended to consider both normalized profiles and raw profiles. Given its lower solubility, some trace element studies of ancient shales have instead relied on metal/Ti ratios as a proxy for authigenic enrichments (e.g., Reinhard et al., 2013; Fru et al., 2016).

4.3 Observed chemostratigraphic expression of surfaces

The geochemical expressions of sequence stratigraphic surfaces observed in fine-grained organic-rich intervals are summarized in Table 4.3.

Table 4.3 The observed chemostratigraphic expression of sequence stratigraphic surfaces in organic-rich mudstone units.

Sequence Stratigraphic Surface	Observed Chemostratigraphic Signature	Examples
Maximum Flooding Surface	Low abundance of terrigenous proxies	(Ratcliffe et al., 2012c; Turner et al., 2015, 2016; Harris et al., 2018)
	Minima in grain size proxies	(Ratcliffe et al., 2012c; Sano et al., 2013)
	Increase in proxies for biogenic silica	(Turner et al., 2015, 2016; Harris et al., 2018)
	Variable levels of redox proxies depending on paleohydrography	(Sano et al., 2013; Turner et al., 2015, 2016; Harris et al., 2018)
Maximum Regressive Surface	Peak in terrigenous proxies	(Ratcliffe et al., 2012c; Harris et al., 2018)
	Peak in grain size proxies	(Ratcliffe et al., 2012c; Sano et al., 2013)
	Minima in proxies for biogenic silica	(Harris et al., 2018)
	Variable levels of redox proxies depending on paleohydrography	(Sano et al., 2013; Harris et al., 2018)

4.3.1 Maximum flooding surface

The maximum flooding surface marks the switch from transgression to regression and the time of the maximum landward position of the shoreline (Posamentier and Allen, 1999). A few studies provide examples of the chemostratigraphic expression of this surface. Turner et al. (2016) produced a sequence stratigraphic framework for two outcrops and three cores in the

organic-rich Upper Devonian Woodford Shale of the Arkoma Basin, Oklahoma. The third-order maximum flooding surface identified in this interval is characterized by a maximum gamma ray response, relatively high Si/Al, local minimum concentration of terrigenous elements (Al, K, Ti, Zr). This surface also separates underlying strata with lower Mo and V abundance from overlying strata displaying higher Mo and V concentrations (Fig. 4.3). Higher-frequency surfaces that mark the shift from regression to transgression were recognized chemostratigraphically and are marked by local minima in terrigenous elements (e.g., Al, K, Ti, Zr) and commonly coincide with local maxima in Si/Al and Ca. Turner et al., (2016) refer to these as chemostratigraphic flooding surfaces, herein, these surfaces are interpreted as higher frequency maximum flooding surfaces. Ratcliffe et al. (2012c) and Sano et al. (2013) identified maximum flooding surfaces in the Upper Jurassic Haynesville Shale, an organic-rich mudstone deposited on the slope of a carbonate platform (Frebourg et al., 2013) in a restricted basin setting (Hammes et al., 2011). These studies placed maximum flooding surfaces in the Haynesville Shale at minimums in Zr/Nb, while chemostratigraphic data presented in Sano et al. (2013) also illustrates that maximum flooding surfaces in the Haynesville Shale are characterized by minimums in V abundance (Fig. 4.4). Data presented in Ratcliffe et al. (2012c) shows that maximum flooding surfaces in this interval typical fall at local lows in terrigenous content. Harris et al. (2018) presented geochemical data for cores from the Duvernay Formation — an organic-rich mudstone deposited in inter-reef settings during the Late Devonian in Alberta (Knapp et al., 2019) — that are included in a previously established sequence stratigraphic framework based on sedimentological and petrophysical attributes. Harris et al. (2018) use the formula for excess Si (Eqn. 3) and interpret all excess Si to be biogenic in origin, potentially because of the presence of siliceous radiolaria in several of the facies observed by Knapp et al. (2017). Maximum flooding

surfaces in cores from the West Shale Basin are often near lows in Al and typically correspond to highs in excess Si and Mo/Al. In the East Shale Basin, maximum flooding surfaces are typically near minima in Al, and separate intervals of lower Al with overlying intervals characterized by higher Al abundance. Patterns of excess Si enrichment and Mo/Al do not match those observed in the West Shale Basin, which Harris et al. (2018) attributed to higher carbonate dilution, lower productivity, and higher dissolved oxygen in the East compared to West Shale Basin.

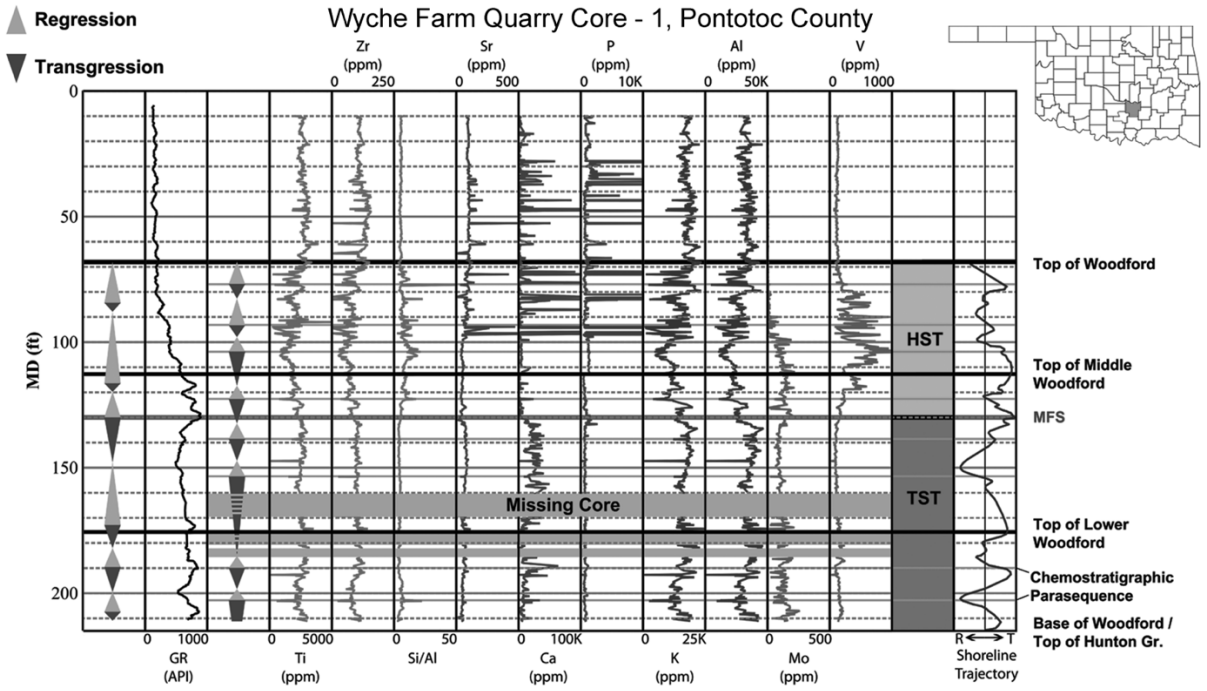

Figure 4.3 Chemostratigraphic profiles from the Woodford Formation in the Wyche Farm Quarry Core–1 in Pontotoc County, Oklahoma. Gamma ray log data and chemostratigraphic profiles are presented with the interpreted transgressive-regressive cycles shown to the left of each dataset. The shoreline trajectory shown presents the inferred local shoreline trajectory. The solid grey lines at the change from transgression to regression are herein interpreted as higher frequency maximum flooding surfaces. Acronyms: GR–gamma ray; HST–highstand systems

tract; MFS–maximum flooding surface; TST–transgressive systems tract. Reproduced with permission from Turner et al., (2016).

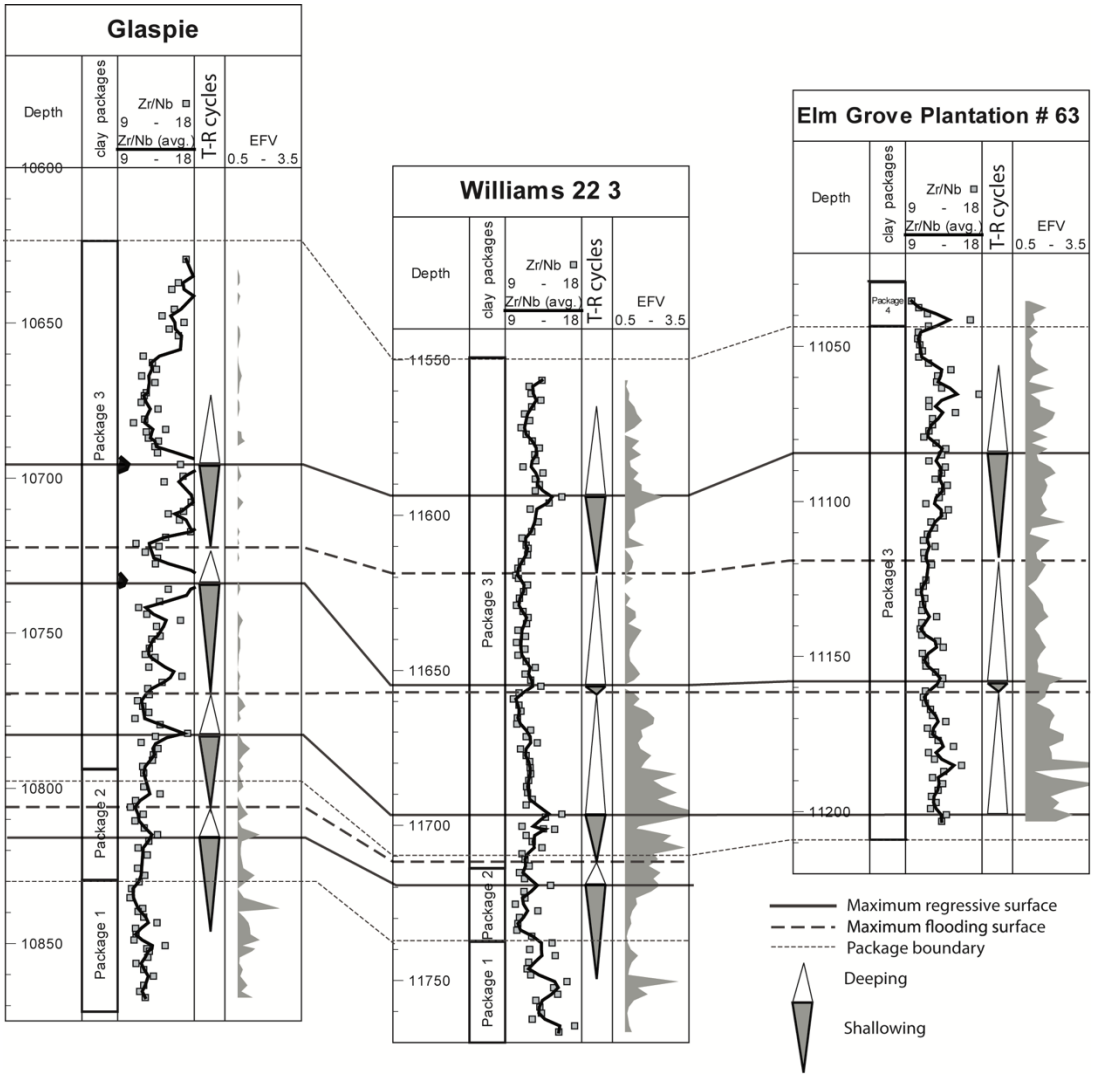

Figure 4.4 Chemostratigraphic profiles for the Upper Jurassic strata of three wells in eastern Louisiana and western Texas and associated sequence stratigraphic interpretation. Package 1 corresponds to the Smackover Formation, package 2 comprises the Gilmer Lime Formation, and package 3 and 4 are the Haynesville Formation. The solid Zr/Nb profile represents a moving average with n=2 and the associated squares are the raw data. Acronyms: T-R–transgressive-

regressive; EFV–enrichment factor of Vanadium. Reproduced from Sano et al. (2013). Copyright ©2013 by The American Association of Petroleum Geologists. Reprinted by permission of the AAPG whose permission is required for further use.

Results from these studies suggest that maximum flooding surfaces are typically characterized by relatively low levels of terrigenous elements (e.g., Al, K, Ti, Zr), minima in grain size proxies (e.g., Zr/Nb), and maxima in Si/Al (Table 4.3). The enrichment of redox-sensitive trace elements (e.g., Mo, V) at these surfaces appears to be variable. Seeing as maximum flooding surface records a time when continental sediment is stored in landward settings, which is accompanied by the formation of condensed sections in the marine environment (Loutit et al., 1988), a minimum abundance of detrital elements is expected (Turner et al., 2016). In shallow-marine systems, a maximum flooding surface also records the change from fining upwards to coarsening upwards (Embry, 2010). Peaks in Si/Al or excess Si observed by Turner et al. (2015, 2016) and Harris et al. (2018), respectively, were interpreted to reflect a higher proportion of biogenic silica. Both studies observed increases in biogenic silica proxies at maximum flooding surfaces, suggesting that higher biogenic silica content is associated with maximum flooding surfaces, which is also expected in condensed sections (e.g., Bohacs, 1998; Gutierrez et al., 2017). This has been interpreted as the result of increased primary productivity (e.g., Harris et al., 2018), decreased clastic dilution, or a combination thereof (Turner et al., 2016).

Differences in redox sensitive trace metal enrichment associated with maximum flooding surfaces from study to study likely occur because of differences in the paleohydrographic characteristics of the setting. As water depth at a point on the open shelf increases, dissolved oxygen at this location typically declines (Wilde et al., 1996). In modern oceans, consumption of

oxygen by degrading organic matter results in the decrease of dissolved oxygen from the surface to a minimum in the zone of lowest circulation (Wyrtki, 1962; Berry and Wilde, 1978). Below this depth, dissolved oxygen increases as a result of ventilation by cold, dense, oxygenated waters produced at high latitudes during the formation of sea ice (Wyrtki, 1962; Berry and Wilde, 1978). The depth of the oxygen minimum can intersect the seafloor from the shelf to the slope (Reichart et al., 1998; Helly and Levin, 2004). At depths near the oxygen minimum, transgression could result in a shift to more oxygenated conditions, whereas for positions well above the oxygen minimum, transgression should lead to a decline in dissolved oxygen. Additionally, transgression can result in rising wave base, causing decreased water column mixing and oxygenation, with the opposite occurring during falling relative sea level (Harris et al., 2013). This change in oxygen is reflected by the ichnofacies model (MacEachern et al., 2009a) with trace fossil assemblages transitioning to those made by organisms more tolerant of suboxic to anoxic conditions as water depth increases and mixing from waves becomes less common resulting in lower dissolved oxygen at the sediment-water interface (MacEachern et al., 2009b; Dashtgard and MacEachern, 2016).

In restricted basin settings, oxygen becomes depleted through decay of organic matter and is not replenished because these basins lack circulation and ventilation (Berry and Wilde, 1978; Schonfeld et al., 2015). If transgression results in increased connectivity to the open ocean, oxygenation can increase from input of ventilated water and improved circulation (Savrda and Bottjer, 1989; Bohacs, 1998). Additionally, Hines et al. (2019) attributed increased bottom water oxygenation during times of transgression to lower productivity, with higher productivity during regression resulting from an increased supply of terrigenous sediment and nutrients. For example, in a study of the Woodford Shale, Turner and Slatt (2016) used Mo/TOC relationships

and a decreasing upwards trend in redox-sensitive trace metal enrichment to interpret renewed circulation and decreased basin isolation resulting from transgression. Similarly, Sano et al., (2013) concluded that anoxic conditions during deposition of the Haynesville Shale, which occurred in a restricted intra-shelf basin, prevailed at the onset of transgression. This conclusion has also been made using other datasets. For example, by comparing trace fossil assemblages to organic-carbonate and carbonate content in the Upper Cretaceous Niobrara Formation (Colorado), Savrda and Bottjer (1989) interpreted intervals of increased oxygenation to reflect open marine circulation in the Western Interior Seaway during transgression. Because of differences in the effect of relative sea level on water column oxygenation depending on the setting, the relative enrichment of redox sensitive trace metals at maximum flooding surfaces depends on whether a shift from transgression to regression resulted in increased or decreased water column oxygenation.

4.3.2 Maximum regressive surface

The maximum regressive surface occurs at the change from regression to transgression and marks the maximum basinward shoreline position (Helland-Hansen and Martinsen, 1996). Chemostratigraphic examples of maximum regressive surfaces in the Haynesville Shale can be found in Ratcliffe et al. (2012c) and Sano et al. (2013) where they are identified by maxima in Zr/Nb. The terrigenous input profile (sum of Al, K, Na, Ti) plotted by Ratcliffe et al. (2012c) typically displays peaks at maximum regressive surfaces, while the V enrichment profile in Sano et al. (2013) shows that maximum regressive surfaces most often mark the shift from increasing V enrichment to decreasing V enrichment (Fig. 4.4). The chemostratigraphic data presented in Harris et al. (2018) shows that the maximum regressive surface identified in the Duvernay

Formation West Shale Basin by Knapp et al. (2019) is characterized by relatively high Al, minimum Mo/Al with values near 0, and low levels of biogenic Si.

In marine shelf environments, the maximum regressive surface typically records the shift from coarsening upwards to fining upwards (Catuneanu, 2002; Embry, 2010), which is reflected in these examples by peaks in grain size proxies or detrital elements. Results from Harris et al. (2018) suggest that maximum regressive surfaces are characterized by a low abundance of biogenic silica. As previously discussed, changes in relative sea level can have variable effects on water column oxygenation depending on the setting. The shift from increasing to decreasing V enrichment associated with maximum regressive surfaces in the Haynesville Shale is likely the product of highest levels of basin isolation at this time. Harris et al. (2018) interpreted that times of higher sea level during deposition of the Duvernay Formation were characterized by lower bottom water oxygenation because of reduced water column mixing, high productivity, and inflow of oxygen depleted bottom waters. This implies that minima in Mo/Al associated with the maximum regressive surface in the Duvernay Formation of the West Shale Basin can be explained by highest levels of mixing, lowest productivity, and minimum inflow of oxygen depleted bottom waters.

4.4 Observed geochemical expression of systems tracts

The geochemical expressions of systems tracts observed in fine-grained organic-rich intervals are summarized in Table 4.4.

Table 4.4 The observed chemostratigraphic expression of systems tracts in fine-grained organic-rich intervals. Abbreviations: TST–transgressive systems tract; HST–highstand systems tract; RST–regressive systems tracts.

Systems Tract	Observed Chemostratigraphic Signature	Examples
TST	Decreasing Al	(Hammes and Frebourg, 2011; Ver Straeten et al., 2011; Turner et al., 2015, 2016; Harris et al., 2018)
	Decreasing sums of terrigenous elements (e.g., Al+Ti+Na+K)	(Ratcliffe et al., 2012c)
	Variable trends in elements associated with heavy minerals (Ti and Zr):	
	Decreases	(Ver Straeten et al., 2011; Turner et al., 2016)
	Increases	(Hammes and Frebourg, 2011; Ver Straeten et al., 2011)
	Decreasing grain size proxies	(Ratcliffe et al., 2012c; Sano et al., 2013)
	Elevated proxies for biogenic silica	(Turner et al., 2015, 2016; Harris et al., 2018)
	Variable levels of redox proxies depending on paleohydrography	(Hammes and Frebourg, 2011; Ver Straeten et al., 2011; Sano et al., 013; Turner et al., 2015, 2016; Harris et al., 2018)
HST	Increasing Al	(Hammes and Frebourg, 2011; Turner et al., 2015, 2016; Harris et al., 2018)

	Variable trends in elements associated with heavy minerals (Ti and Zr):	
	Decreases	(Hammes and Frebourg, 2011)
	Increases	(Turner et al., 2015, 2016)
	Variable levels of biogenic silica proxies	(Harris et al., 2018)
	Variable levels of redox proxies depending on paleohydrography	(Turner et al., 2015, 2016; Harris et al., 2018)
	Increasing Al	(Turner et al., 2015, 2016; Ver Straeten et al., 2011)
	Variable trends in elements associated with heavy minerals (Ti and Zr):	
RST	Decreases	(Ver Straeten et al., 2011)
	Increases	(Turner et al., 2015, 2016; Ver Straeten et al., 2011)
	Increasing grain size proxies	(Ratcliffe et al., 2012c; Sano et al., 2013)

4.4.1 Transgressive systems tract

The transgressive systems tract comprises strata deposited when the rate of relative sea-level rise surpasses the rate of shoreline sediment supply (Posamentier and Allen, 1999). Examples of the chemostratigraphic expression of the transgressive systems tract include Turner et al. (2015, 2016), Sano et al. (2013), Ratcliffe et al. (2012c), Hammes and Frebourg (2011), Ver Straeten et al. (2011), and Harris et al. (2018). Turner et al. (2015) and (2016) interpret a third-order transgressive systems tract in the organic-rich Woodford Shale. In this example, the transgressive

systems tract is characterized by an overall decline in terrigenous elements (e.g., Ti, Zr, K, Al) and in redox sensitive elements (e.g., Mo, V) reflecting decreasing restriction, and often by increasing Si/Al that arises from an increasing proportion of biogenic silica (Fig. 4.3). However, in certain intervals, V is concentrated in phosphatic nodules, resulting in V abundance peaks that are not associated with reduced circulation (Turner et al., 2016). Turner et al. (2016) also identified fourth-order T-R cycles based on trends in Ti and Zr with trends of decreasing concentration characterizing transgression.

Other studies focus on the Upper Jurassic Haynesville Shale of Texas and Louisiana. Ratcliffe et al. (2012c) identified lower-frequency T-R cycles in the Haynesville Formation with higher-frequency T-R cycles superimposed on these trends. Higher-rank transgressive packages are characterized by a declining abundance of terrigenous content, which is the sum of Al_2O_3, TiO_2, Na_2O, and K_2O. Lower-rank transgressive intervals are characterized by declining Zr/Nb and SiO_2/Al_2O_3. Trends in Zr/Nb and SiO_2/Al_2O_3 follow one another, indicating that they are associated with the fraction of silt size sediment and that biogenic silica is proportionately less important in the Haynesville Formation (Ratcliffe et al., 2012c). This interpretation is supported by the clear positive trend between Zr and Si observed in the Si-Zr cross plot for the Haynesville Formation (Ratcliffe et al., 2012c). Sano et al. (2013) identified T-R sequences in the same three localities as Ratcliffe et al. 2012c (Fig. 4.4). In this case, V enrichment data is also presented, and those authors interpreted that anoxia decreases throughout transgression.

Hammes and Frebourg (2011) also studied the Haynesville Shale. In this dataset, the transgressive systems tract is expressed by lower Al concentration than the overlying highstand systems tract. In contrast, Si/Al, Ti/Al, and Zr/Al are elevated compared to the overlying highstand systems tract. The authors contended that an increased abundance of Ti and Zr

supports the interpretation that bottom waters were euxinic because they are redox sensitive elements. With that said, Ti and Zr are generally taken to reflect detrital input (Bhatia and Crook, 1986; Plank and Langmuir, 1998; Piper and Calvert, 2009), and have not been shown by previous studies to be redox sensitive. The opposite trends in the Al profile compared to the Si/Al, Ti/Al, and Zr/Al suggest decoupling between the sources of Al versus Si, Ti, and Zr, which could potentially occur if Si, Ti, and Zr are primarily associated with the wind-blown detrital fraction. Hammes and Frebourg (2011) did propose that the detrital fraction in the transgressive strata is likely primarily aeolian. The Mo enrichment profile is also elevated compared to the overlying highstand systems tract.

Ver Straeten et al. (2011) identified third-order transgressive systems tracts in the Middle Devonian Oatka Creek and Skaneateles formations deposited in the Appalachian Basin in western New York during the Middle Devonian. These formations are both included in the Hamilton Group and the Oatka Creek Formation is also a member of the Marcellus Subgroup (Arthur and Sageman, 2005). At this location, the Oatka Creek Formation dominantly comprises organic-rich shale with a few limestone interbeds and is interpreted to reflect deposition in primarily anoxic conditions (Ver Straeten et al. 2011). In this interval, the transgressive systems tract is characterized by a small decrease in Al and Ti/Al, and stable levels of Si/Al in the organic-rich mudstone intervals. This systems tract also shows markedly lower Mo abundance than the overlying regressive strata, suggesting a restricted depositional setting with increased connectivity to the open ocean in the transgressive systems tract. The Appalachian Basin was a restricted epicratonic basin (Rowe et al., 2008) and, therefore, increased oxygenation accompanying the transgressive systems tract is expected. The overlying Skaneateles Formation is composed primarily of interbedded mudstone and organic-rich mudstone and was deposited in

a dominantly suboxic environment (Ver Straeten et al., 2011). In this formation, the transgressive systems tract is expressed chemostratigraphically by overall low Mo, which is expected in a suboxic interval. Here the transgressive systems tract also shows a significant decrease in Al while Ti/Al and Si/Al show increasing trends that are opposite to trends in Al. Ver Straeten et al. (2011) suggested that increasing Ti/Al and Si/Al can be attributed to elevated levels of silica from aeolian or volcanic sources. Data presented by Harris et al. (2018) shows that transgressive systems tracts in the Devonian Duvernay Formation of the West Shale Basin in Alberta are characterized by decreasing Al_2O_3, rising excess Si, and elevated Mo/Al.

Together, the aforementioned studies suggest that the geochemical signature of a transgressive systems tract includes decreasing Al (Table 4.4). Other elements associated with detrital minerals (e.g., Ti, Zr) may also decrease (e.g., transgressive systems tract in the Oatka Creek Formation presented in Ver Straeten et al., 2011; Turner et al., 2016), and composite profiles of terrigenous elements may show declining trends (e.g., the terrigenous input profile of Ratcliffe et al. 2012c). Although in some instances, certain detrital elements (e.g., Ti, Zr) show increasing trends (e.g., transgressive systems tract in the Skaneateles Formation of Ver Straeten et al. (2011); Hammes and Frebourg, 2011). During a transgression, sediment trapping in fluvial and/or coastal environments while the shoreline moves landward results in a decrease in the abundance of fluvial detrital sediment that reaches the shelf and slope (Loutit et al., 1988; Mann and Stein, 1997; Catuneanu, 2006). This is likely the cause for the observed decreases in the abundance of Al and of other terrigenous elements where they occur. Turner et al. (2016) observed stronger declines in elements associated with heavy minerals (e.g., Ti and Zr) compared to elements associated with clay minerals (e.g., Al and K) and proposed that this is explained by terrestrial heavy minerals settling out sooner than clay minerals. Increases in Ti/Al

and Zr/Al observed in certain cases may be the product of increased aeolian or volcanic input as suggested by Ver Straeten et al. (2011). In marine shelf environments, transgressions are also typically characterized by fining-upwards grain size trends (Catuneanu et al., 2009; Embry, 2010), reflected by declining Zr/Nb and Si/Al in Haynesville Formation (e.g., Ratcliffe et al., 2012c; Sano et al., 2013).

These studies all display elevated proxies for excess silica during transgressive systems tracts. In certain cases, this was interpreted as biogenic silica (e.g., Turner et al., 2016; Harris et al., 2018). Condensed sections develop because of a decline in the abundance of terrigenous sediment input during transgression (Loutit et al., 1988; Galloway, 1989). The proportion of biogenic sediment increases in these intervals as dilution from detrital sediment declines (Arthur and Sageman, 2005; Ver Straeten et al. 2011). High levels of biogenic silica in transgressive systems tracts can also be interpreted as the product of increased biological productivity (e.g., Harris et al., 2018). Ver Straeten et al. (2011) interpreted that rising levels of Si/Al and Ti/Al in the transgressive systems tract of the Skaneateles Formation likely reflects higher aeolian or volcanic input.

Trends in redox sensitive trace metal enrichment through the transgressive systems tract are variable. Certain studies show decreasing paleoredox proxies (e.g., Sano et al., 2013; Ver Straeten et al., 2011; Turner et al., 2016), whereas others show increases (e.g., Hammes and Frebourg, 2011; Harris et al., 2018), likely because of differences between the paleohydrographic conditions of each depositional setting.

4.4.2 Highstand systems tract

Strata of the highstand systems tract are deposited when the rate of relative sea-level rise decreases such that the rate of sediment supply equals or exceeds the rate of accommodation generation at the shoreline (Posamentier and Allen, 1999). Examples of the geochemical expression of highstand systems tract deposits were presented by Turner et al. (2015, 2016) where they interpreted a third-order highstand systems tract at the top of the Woodford Shale characterized by increasing Ti, Zr, Al, and K, decreasing Si/Al, and relatively low Mo and V (Fig. 4.3). Similarly, Hammes and Frebourg (2011) suggested that the organic-rich Upper Jurassic Bossier Formation (Texas and Louisiana) records a second-order highstand systems tract, characterized by increasing Al upwards, and decreasing Si/Al, Ti/Al, and Zr/Al. Highstand systems tracts in the Duvernay Formation of the West Shale Basin show increasing Al. In this example, Mo/Al typically remains elevated moving from the maximum flooding surface until the mid-highstand systems tract, where it then begins to decline. The lowermost highstand systems tract exhibits decreasing biogenic Si, but subsequent highstand systems tract record continuing elevated levels of excess Si following transgressive systems tracts (Harris et al., 2018). It is important to note that the highstand systems tracts in all of the above examples were identified based on other datasets. At this point, criteria to identify the highstand systems tract chemostratigraphically are poorly constrained because no geochemical signature for the basal surface of forced regression has been defined. Nonetheless, in some cases it is possible to identify the highstand, falling-stage, and lowstand systems tracts in fine-grained unconventional plays using other datasets such as seismic (e.g., Dominguez and Catuneanu, 2017).

The highstand systems tracts described above are all characterized by increasing Al content, likely reflecting progradation associated with relative sea level highstand. Titanium and

Zr also increase in some instances and stable Ti/Al observed in one case likely reflects proportional increases in both Ti and Al. However, Zr/Al and Ti/Al decline throughout the highstand systems tracts in other studies, potentially due to falling aeolian or volcanic input. Decreasing Si/Al interpreted as declining biogenic silica moving upwards through highstand systems tracts is likely the product of higher dilution by detrital sediment or lower productivity. Conversely, increases in proxies for biogenic silica (e.g., Si/Al, excess Si) through the highstand systems tract can be interpreted as continuing elevated levels of biological productivity (e.g., Harris et al., 2018). The signature of redox proxies through the highstand systems tract depends on paleohydrographic conditions. For example, low levels of Mo and V observed by Turner et al. (2016) during a highstand systems tract in the Woodford Shale were interpreted as the product of greater oxygenation caused by a higher degree of connectivity between the Arkoma Basin and the Palaeotethys at this time. Harris et al., (2018) suggested that the Mo/Al patterns observed in highstand systems tracts of the Duvernay Formation in the West Shale Basin are attributed to higher input of anoxic nutrient-rich seawater from lower basin restriction leading to higher productivity and more reducing conditions during the upper transgressive systems tracts and lower highstand systems tracts.

4.4.3 Regressive systems tract

The regressive systems tract constitutes all strata deposited when the shoreline moves basinward (Embry, 2002; Embry and Johannssen, 1993). The regressive systems tract includes strata of the highstand, falling-stage, and lowstand systems tracts (Catuneanu, 2002). Turner et al. (2015) and (2016) interpreted fourth-order regressive systems tracts superimposed on third-order trends in the Woodford Shale based on Ti and Zr profiles, which displayed similar

signatures to trends in K and Al. These regressive intervals are typically characterized by increasing Ti, Zr, K, and Al (Fig. 4.3). Lower rank regressive systems tracts are interpreted in the Haynesville Shale by Ratcliffe et al. (2012c) and Sano et al. (2013). These regressive trends are characterized by increasing Zr/Nb and Si/Al in Ratcliffe et al. (2012c) and increasing Zr/Nb and V in Sano et al. (2013; Fig. 4.4). Ratcliffe et al. (2012c) interprets that Zr/Nb and Si/Al record grain size variations in the Haynesville Formation. Ver Straeten et al., (2011) presented geochemical profiles along with a previously established sequence stratigraphic interpretation for the Devonian Oatka Creek and Skaneateles formations. They use the term 'early highstand systems tract' for the highstand systems tract and the term 'late highstand systems tract' rather than 'falling-stage systems tract' for the interval deposited during relative sea level fall, following the Van Wagoner et al. (1988) model. In their interpretations, these are grouped together as the highstand systems tract rather than separated into the early highstand systems tract and late highstand systems tract. Ver Straeten et al. (2011) suggested that lowstand systems tracts are not present above these highstand systems tracts but are instead overlain by transgressive systems tracts. These highstand systems tracts are herein considered as regressive systems tracts as they may include both normal and forced regressive deposits. The third-order regressive systems tract in the Oatka Creek Formation is characterized by increasing Al, decreasing Si/Al, and Ti/Al, and a marked increase in Mo relative to the underlying transgressive systems tract. The regressive systems tract in the overlying Skaneateles Formation displays rising Al and Si/Al, with relatively stable Ti/Al. Molybdenum remains quite low through the entire interval.

These studies suggest that regressive systems tracts are typically characterized by an increasing abundance of detrital elements and grain size proxies reflecting ongoing progradation.

An exception to this is present in the regressive systems tract of the Oatka Creek Formation, where Si/Al and Ti/Al decline, which Ver Straeten et al. (2011) interpreted to have been caused by falling levels of aeolian input.

4.5 Discussion

To our knowledge, there are no existing examples of the chemostratigraphic expression of certain surfaces. These include the subaerial unconformity, correlative conformity, transgressive surface of erosion, regressive surface of marine erosion, and basal surface of forced regression. The subaerial unconformity is the unconformable portion of the surface that marks the end of forced regression and is typically developed in shelf or platform settings (Hunt and Tucker, 1992). This surface is defined by non-marine strata on top (Catuneanu, 2006; Shanmugam, 1988) and is not relevant to the marine mudstone successions discussed in this work. As the concept of integrating chemostratigraphic datasets for sequence stratigraphy is fairly recent, there are relatively few studies that have compared elemental proxies to previously established sequence stratigraphic frameworks or used chemostratigraphy to help identify surfaces. The recognition of sequence stratigraphic cyclicity within mudstone units is also relatively new (e.g., Bohacs and Schwalbach, 1992; Macquaker and Taylor, 1996; Bohacs, 1998; Schieber, 1998; Williams et al., 2001; Bohacs et al., 2005; Macquaker et al., 2007). For these reasons, it is not yet possible to define the chemostratigraphic expression of the correlative conformity and basal surface of forced regression. During a transgression, the transgressive surface of erosion forms from erosion by waves or tides (Swift, 1975; Catuneanu, 2002), and typically forms in coastal and upper shoreface settings (Catuneanu, 2002). Similarly, the regressive surface of marine erosion is cut by waves during forced regression (Plint and Nummedal, 2000) and this erosion takes place

on the inner shelf (Plint and Nummedal, 2000; Catuneanu, 2002). Until recently, fine-grained organic-rich successions were viewed as largely distal, deep-water deposits, which would suggest that the transgressive surface of erosion and regressive surface or marine erosion are not relevant to these units. However, many organic-rich mudstone successions are now being re-interpreted to reflect deposition in more proximal environments than originally thought (e.g., Schieber, 1994; Smith et al., 2019). This may lead to increased recognition of these surfaces and allow for future delineation of their chemostratigraphic characteristics.

Flooding surfaces and parasequences are not discussed in this work. A flooding surface (i.e., parasequence boundary) records an abrupt water deepening (Van Wagoner et al., 1988), which may or may not record a change in stratal stacking pattern (Catuneanu, 2019a); as such, it is a surface of allostratigraphy rather than sequence stratigraphy (Catuneanu, 2019a). Certain studies of mudstone intervals still make use of flooding surfaces and parasequences rather than lower rank sequence stratigraphic surfaces and sequences (e.g., Bohacs et al., 2014; Birgenheier et al., 2017; Borcovsky et al., 2017; Turner et al., 2015, 2016), even though the parasequence boundaries no longer comply with the original definition of a flooding surface. Therefore, following Catuneanu (2019a), this paper recommends that the use of scale-independent terminology (i.e., the recognition of higher-frequency sequence stratigraphic surfaces and systems tracts) provides a superior alternative for stratigraphic mapping and correlation than the delineation of parasequences (see Catuneanu, 2019a, for a full discussion).

The chemostratigraphic expression of lowstand systems tracts and falling-stage systems tracts have not yet been established, likely for similar reasons as discussed for the basal surface of forced regression and correlative conformity. Additionally, although all systems tracts may be present, higher frequency cycles identified using chemostratigraphic profiles in these units are

commonly limited to the identification of transgression and regression rather than parsing out normal from forced regressions (e.g., Ratcliffe et al., 2012c; Sano et al., 2013; Turner et al., 2015, 2016). As a result, only two systems tracts are commonly recognized: the transgressive systems tract and regressive systems tract. This is likely the case because in shelfal settings the regressive systems tract records ongoing progradation, making the basal surface of forced regression and correlative conformity cryptic in studies using log, core, or outcrop data (Catuneanu, 2006). This, therefore, leads to difficulty in distinguishing the highstand systems tract, lowstand systems tract, and falling-stage systems tract in these settings. It is also possible that certain systems tracts are not developed in particular depositional settings.

One disadvantage of using an undifferentiated regressive systems tract is that it amalgamates different genetic types of regressive strata, which lowers the resolution of the sequence stratigraphic study. Considering normal and forced regressive deposits together may also be disadvantageous if they have different characteristics related to their unconventional reservoir potential, for example variations in TOC have been recorded between forced vs. normal regressive systems tracts in unconventional plays (Dominguez et al., 2016; Dominguez and Catuneanu, 2017). These are limitations of using chemostratigraphic datasets to identify sequence stratigraphic cycles in fine-grained organic-rich units.

The geochemical characteristics of sequence stratigraphic surfaces and systems tracts in organic-rich mudstone intervals are expected to vary depending on the depositional setting. For example, based on comparison with coarser grained intervals, we expect that there are differences between the chemostratigraphic expression of certain surfaces in more proximal settings influenced by progradation compared to more distal settings beyond the influence of progradation where sediment-gravity deposition and pelagic sedimentation are dominant.

Examples of environments influenced by progradation are the continental shelf or a ramp setting under the influence of shoreline progradation. The slope or abyssal plain of a shelf-slope system or a ramp setting where sedimentation is dominated by sediment-gravity flows and pelagic fallout are examples of settings that are beyond the influence of shoreline progradation. Herein, environments experiencing progradation will be referred to as shallow-water settings, whereas settings beyond the influence of progradation where sedimentation is dominated by sediment-gravity flows and pelagic settling will be referred to as deep-water settings. During relative sea-level fall, the deep-water environment experiences maximum supply of detrital sediment, and the detrital sediment supplied to these settings is coarser than the sediment that accumulates during relative sea-level rise (Posamentier and Kolla, 2003). Unlike for prograding environments, deposition in deep-water is less predictable in terms of the locus of accumulation of depositional elements. However, general trends can still be established at the scale of composite profiles that integrate regional data (e.g., fig 36 in Catuneanu, 2019b). The main contrasts between the shallow- and deep-water settings are recorded by the grain-size changes associated with the correlative conformity and the maximum regressive surface. In shallow-water environments, the correlative conformity is more difficult to distinguish because it occurs within a prograding and coarsening upwards interval (Catuneanu, 2006), whereas the maximum regressive surface marks the change from coarsening to fining upwards grain size trends (Catuneanu, 2002; Embry, 2010). In coarser grained deep-water intervals dominated by sediment-gravity flows, the composite vertical profile coarsens upwards to the correlative conformity during relative sea-level fall, and then fines upwards through the lowstand systems tract to the maximum flooding surface (Catuneanu, 2006, 2019a). In this case, the maximum regressive surface is present within a fining upwards interval and is more difficult to distinguish (Catuneanu, 2019b). These trends

relate to the efficiency of transfer of fluvial sediment across the shelf to the deep-water setting, which is highest during forced regression (see full discussion in Catuneanu 2019a,b). We expect that this would affect the chemostratigraphic signatures of the correlative conformity and maximum regressive surface in organic-rich mudstone units depending on the setting, with the maximum regressive surface recording maxima in terrigenous proxies and grain size proxies in shallow-water settings, but the correlative conformity recording these maxima in deep-water settings, although this has not yet been confirmed. The examples discussed herein seem to correspond to the expected expression of the maximum regressive surface in settings influenced by progradation. Further work is required to provide examples of the chemostratigraphic expression of these surfaces and systems tracts in shallow- versus deep-water settings so that the chemostratigraphic expression can be confirmed.

In chemostratigraphic studies of mudstone successions, geochemical composition data is typically collected using either inductively coupled plasma (ICP) and inductively coupled plasma mass spectrometry (ICP-MS) or inductively coupled plasma optical emission spectrometry (ICP-OES) (e.g., Harris et al., 2013; 2018; Sano et al., 2013; Playter et al., 2017), or by portable energy-dispersive X-ray fluorescence (pXRF) (e.g., Hammes and Frebourg, 2012; Sano et al., 2013; Turner et al., 2015, 2016; El Attar and Pranter, 2016; Hines et al., 2019). Advantages of pXRF compared to ICP methods include time and cost efficiency as well as the non-destructive nature of the analysis, potentially allowing for the collection of higher-resolution datasets (Rowe et al., 2012; Rowe et al., 2017; Lemiere, 2018; Zhang et al., 2019). There are, however, some drawbacks associated with pXRF, including a more limited suite of elements that can be obtained compared to ICP analyses (Rowe et al., 2017), and for certain elements, poor accuracy relative to accepted values or concentrations obtained by other laboratory-based analyses (e.g.,

Rowe et al., 2012; Hines et al., 2019). The use of helium flow or high-performance detectors is now allowing for measurement of lighter elements (e.g., Al and Si), which were traditionally poorly detected by pXRF, although lower accuracy has been reported for Al compared to elements such as Si, Ti, and in some cases, Zr (Lemiere, 2018). Nonetheless, in a study specific to mudstone intervals, Rowe et al. (2012) observed high accuracy for Al and Si. Of the other elements discussed herein, Rowe et al. (2012) observed less reliable Cr pXRF measurements when concentrations were below 70 ppm, and unreliable U and Th results when pXRF data was compared to data collected using wavelength dispersive x-ray fluorescence. Uranium can be difficult to measure with XRF because of inter-element interference and low abundance in many samples (Rowe et al., 2017), and along with Zr, Cr, and Ni, U is one of the elements for which Hines et al. (2019) observed poor correlations between pXRF data and other laboratory-based measurements (fusion XRF and ICP-MS).

An additional drawback related to the integration of chemostratigraphic datasets for sequence stratigraphic interpretation is the requirement for fairly continuous measurements from core or outcrop intervals in order to identify surfaces (Pearce et al., 2010). For example, studies that identified sequence stratigraphic surfaces and systems tracts (e.g., Ver Straeten et al. 2011; Sano et al. 2013; Turner et al., 2016) sampled cores and outcrops at intervals ranging from 5-120 cm. These high-resolution sampling rates are not possible when relying on drill cuttings rather than core and outcrop samples because drill cuttings are typically taken at coarser intervals (Pearce et al., 1999). Given the limitations associated with the use of chemostratigraphic datasets, chemostratigraphy is more effective when used in conjunction with other datasets (e.g., sedimentological and petrophysical) to form robust sequence stratigraphic frameworks in organic-rich mudstone intervals (e.g., Ver Straeten et al. 2011; Hammes and Frebourg, 2012).

4.6 Conclusions

This review of documented elemental stratigraphic changes in marine mudstone successions and their interpretation allows for a preliminary delineation of the chemostratigraphic expression of certain sequence stratigraphic surfaces and systems tracts, namely the maximum flooding surface, maximum regressive surface, transgressive systems tract, and regressive systems tract. Chemostratigraphic characteristics of the highstand systems tract are presented, although this systems tract has been identified using criteria other than chemostratigraphic in all examples presented in this work, and presently cannot be distinguished from the regressive systems tract based on chemostratigraphic proxies alone. Available sequence stratigraphic interpretations of geochemical proxy datasets presented herein demonstrate that chemostratigraphic datasets are quite useful in interpreting transgressive-regressive cycles (regressive systems tracts and transgressive systems tracts separated by maximum regressive surfaces and maximum flooding surfaces, respectively). Also apparent is the need for integration with other datasets to further subdivide the regressive systems tract and confirm proxy signatures to produce robust sequence stratigraphic frameworks. To date, the utility of incorporating chemostratigraphic datasets for the study of sequence stratigraphic cyclicity in organic-rich mudstone successions has been demonstrated by a handful of studies. Nonetheless, the field remains quite new with limited published examples of the geochemical expression of surfaces and systems tracts. Furthermore, because of the lack of consensus and ongoing shift in our understanding of mudstone depositional systems, it is not yet possible to confirm many of the expected differences in the chemostratigraphic expression of surfaces and systems tracts depending on the depositional setting. The following are suggestions aimed at advancing the

field. First, the publication of studies comparing geochemical proxies to previously established sequence stratigraphic frameworks (based on other datasets) for fine-grained organic-rich intervals will enable further geochemical characterization of surfaces and systems tracts and allow chemostratigraphy to be better integrated with other datasets. Incorporating chemostratigraphic datasets while developing sequence stratigraphic interpretations in organic-rich intervals where these frameworks do not yet exist will serve a similar purpose. As our understanding of depositional systems for these units increases, characterizing the differences in chemostratigraphic expression of surfaces and systems tracts associated with variations in depositional setting will also further the utility of chemostratigraphic data to sequence stratigraphic studies of mudstone successions.

4.7 Acknowledgments

The authors would like to thank Kathryn Fiess, Viktor Terlaky, Dave Herbers, Carolyn Furlong, and Sara Biddle for their advice and guidance. Maya LaGrange, Brette Harris, and Murray Gingras acknowledge the Northwest Territories Geological Survey for generously providing funding of this work. Kurt Konhauser, Octavian Catuneanu, and Murray Gingras thank the Natural Sciences and Engineering Research Council of Canada (NSERC) for their financial support. We would also like to thank the editor Chris Fielding and reviewers Bruce Hart, Bryan Turner, and Lauren Birgenheier for providing feedback that greatly improved the quality of the manuscript.

4.8 References

Adachi, M., Yamamoto, K., Sugisaki, R., 1986. Hydrothermal chert and associated siliceous rocks from the northern Pacific their geological significance as indication of

ocean ridge activity. Sediment. Geol. 47 (1–2), 125–148. https://doi.org/10.1016/0037-0738(86)90075-8

Algeo, T.J., Lyons, T.W., 2006. Mo–total organic carbon covariation in modern anoxic marine environments: Implications for analysis of paleoredox and paleohydrographic conditions. Paleoceanography 21 (1), PA1016. https://doi.org/10.1029/2004PA001112

Algeo, T.J., Maynard, J.B., 2004. Trace-element behavior and redox facies in core shales of Upper Pennsylvanian Kansas-type cyclothems. Chem. Geol. 206 (3–4), 289–318. https://doi.org/10.1016/j.chemgeo.2003.12.009

Algeo, T.J., Schwark, L., Hower, J.C., 2004. High-resolution geochemistry and sequence stratigraphy of the Hushpuckney Shale (Swope Formation, eastern Kansas): implications for climato-environmental dynamics of the Late Pennsylvanian Midcontinent Seaway. Chem. Geol. 206 (3–4), 259–288. https://doi.org/10.1016/j.chemgeo.2003.12.028

Arsairai, B., Wannakomol, A., Feng, Q., Chonglakmani, C., 2016. Paleoproductivity and paleoredox condition of the Huai Hin Lat Formation in northeastern Thailand. J. Earth Sci. 27 (3), 350–364. https://doi.org/10.1007/s12583-016-0666-8

Arthur, M.A., Sageman, B.B., 2005. Sea-level control on source-rock development: perspectives from the Holocene Black Sea, the mid-Cretaceous Western Interior Basin, and the late Devonian Appalachian basin, in: Harris, N.B. (Ed.), The Deposition of Organic-Carbon-Rich Sediments: Models, Mechanisms, and Consequences: Society of Economic Paleontologists and Mineralogists Special Publication. 82. pp. 35–59.

Aubineau, J., El Abani, A., Bekker, A., Somogyi, A., Bankole, O.M., Macchiarelli, R., Meunier, A., Riboulleau, A., Reynaud, J.-Y., Konhauser, K.O., 2019. Microbially induced potassium enrichment in Paleoproterozoic shales and implications for reverse weathering

on early Earth. Nat. Commun. 10 (1), 1–9 2670. https://doi.org/10.1038/s41467-019-10620-3

Berry, W.B., Wilde, P., 1978. Progressive ventilation of the oceans; an explanation for the distribution of the lower Paleozoic black shales. Am. J. Sci. 278 (3), 257–275.

Bhatia, M.R., Crook, K.A., 1986. Trace element characteristics of graywackes and tectonic setting discrimination of sedimentary basins. Contrib. Mineral. Petrol. 92, 181–193. https://doi.org/10.1007/BF00375292

Birgenheier, L.P., Horton, B., McCauley, A.D., Johnson, C.L., Kennedy, A., 2017. A depositional model for offshore deposits of the lower Blue Gate Member, Mancos Shale, Uinta Basin, Utah, USA. Sedimentology 64 (5), 1402–1438. https://doi.org/10.1111/sed.12359

Bloemsma, M.R., Zabel, M., Stuut, J.B.W., Tjallingii, R., Collins, J.A., Weltje, G.J., 2012. Modelling the joint variability of grain size and chemical composition in sediments. Sediment. Geol. 280, 135–148. https://doi.org/10.1016/j.sedgeo.2012.04.009

Bohacs, K.M., 1998. Contrasting expressions of depositional sequences in mudrocks from marine to non-marine environs, in: Schieber, J., Zimmerle, W., Sethi, P.S. (Eds.), Shales and Mudstones: Volume I. E. Schweizerbart'sche Verlagsbuchhandlung (Nägele u. Obermiller), Stuttgart, pp. 33–78.

Bohacs, K.M., Schwalbach, J.R., 1992. Sequence stratigraphy of fine-grained rocks with special reference to the Monterey Formation, in: Schwalbach, J.R., Bohacs, K.M (Eds.), Sequence Stratigraphy in Fine-Grained Rocks: Examples from the Monterey Formation, pp. 7–19 Pacific Section, Society of Economic Paleontologists and Mineralogists, Book 70.

Bohacs, K.M., Grabowski Jr., G.J., Carroll, A.R., Mankiewicz, P.J., Miskell-Gerhardt, K.J., Schwalbach, J.R., Wegner, M.B., Simo, J.T., 2005. Production, destruction, and dilution—the many paths to source-rock development, in: Harris, N.B. (Ed.), The Deposition of Organic-Carbon-Rich Sediments: Models, Mechanisms, and Consequences: Society of Economic Paleontologists and Mineralogists Special Publication. 82. pp. 61–101.

Bohacs, K.M., Lazar, O.R., Demko, T.M., 2014. Parasequence types in shelfal mudstone strata—quantitative observations of lithofacies and stacking patterns, and conceptual link to modern depositional regimes. Geology 42 (2), 131–134.

Bonjour, J.L., Dabard, M.P., 1991. Ti/Nb ratios of clastic terrigenous sediments used as an indicator of provenance. Chem. Geol. 91 (3), 257–267.

Borcovsky, D., Egenhoff, S., Fishman, N., Maletz, J., Boehlke, A., Lowers, H., 2017. Sedimentology, facies architecture, and sequence stratigraphy of a Mississippian black mudstone succession—the upper member of the Bakken Formation, North Dakota, United States. Am. Assoc. Pet. Geol. Bull. 101 (10), 1625–1673. https://doi.org/10.1306/01111715183

Brown Jr., L.F., Fisher, W.L., 1977. Seismic stratigraphic interpretation of depositional systems: examples from Brazilian rift and pull apart basins, in: Payton, C.E. (Ed.), Seismic Stratigraphy—Applications to Hydrocarbon Exploration: American Association of Petroleum Geologists Memoir. 26. pp. 213–248.

Brumsack, H.J., 2006. The trace metal content of recent organic carbon-rich sediments: implications for Cretaceous black shale formation. Palaeogeogr. Palaeoclimatol. Palaeoecol. 232, 344–361. https://doi.org/10.1016/j.palaeo.2005.05.011

Buckman, J., Mahoney, C., März, C., Wagner, T., Blanco, V., 2017. Identifying biogenic silica: mudrock micro-fabric explored through charge contrast imaging. Am. Mineral. 102 (4), 833–844.

Calvert, S.E., Pedersen, T.F., 1993. Geochemistry of recent oxic and anoxic marine sediments: implications for the geological record. Mar. Geol. 113 (1–2), 67–88. https://doi.org/10.1016/0025-3227(93)90150-T

Canfield, D.E., Thamdrup, B., 2009. Towards a consistent classification scheme for geochemical environments, or, why we wish the term 'suboxic'would go away. Geobiology 7 (4), 385–392. https://doi.org/10.1111/j.1472-4669.2009.00214.x

Catuneanu, O., 2002. Sequence stratigraphy of clastic systems: concepts, merits, and pitfalls. J. Afr. Earth Sci. 35, 1–43.

Catuneanu, O., 2006. Principles of Sequence Stratigraphy. Elsevier, Amsterdam.

Catuneanu, O., 2019a. Model-independent sequence stratigraphy. Earth Sci. Rev. 188, 312–388. https://doi.org/10.1016/j.earscirev.2018.09.017

Catuneanu, O., 2019b. Scale in sequence stratigraphy. Mar. Pet. Geol. 106, 128–159. https://doi.org/10.1016/j.marpetgeo.2019.04.026

Catuneanu, O., Abreu, V., Bhattacharya, J.P., Blum, M.D., Dalrymple, R.W., Eriksson, P.G., Fielding, C.R., Fisher, W.L., Galloway, W.E., Gibling, M.R., Giles, K.A., Holbrook, J.M., Jordan, R., Kendall, C.G.S., Macurda, B., Martinsen, O.J., Miall, A.D., Neal, J.E., Nummedal, D., Pomar, L., Posamentier, H.W., Pratt, B.R., Sarg, J.F., Shanley, K.W., Steel, R.J., Strasser, A., Tucker, M.E., Winker, C., 2009. Towards the standardization of sequence stratigraphy. Earth Sci. Rev. 92, 1–33. https://doi.org/10.1016/j.earscirev.2008.10.003

Catuneanu, O., Galloway, W.E., Kendall, C.G.S., Miall, A.D., Posamentier, H.W., Strasser, A., Tucker, M.E., 2011. Sequence stratigraphy: methodology and nomenclature. Newsl. Stratigr. 44, 173–245.

Chen, H.-F., Yeh, P.-Y., Song, S.-R., Hsu, S.-C., Yang, T.-N., Wang, Y., Chi, Z., Lee, T.-Q., Chen, M.-T., Cheng, C.-L., Zou, J., Chang, Y.-P., 2013. The Ti/Al molar ratio as a new proxy for tracing sediment transportation processes and its application in aeolian events and sea level change in East Asia. J. Asian Earth Sci. 73, 31–38. Colodner, D., Sachs, J., Ravizza, G., Turekian, K., Edmond, J., Boyle, E., 1993. The geochemical cycle of rhenium: a reconnaissance. Earth Planet. Sci. Lett. 117 (1-2), 205–221. https://doi.org/10.1016/j.jseaes.2013.04.017

Crusius, J., Calvert, S., Pedersen, T., Sage, D., 1996. Rhenium and molybdenum enrichments in sediments as indicators of oxic, suboxic and sulfidic conditions of deposition. Earth Planet. Sci. Lett. 145 (1-4), 65–78. https://doi.org/10.1016/S0012-821X(96)00204-X

Dashtgard, S.E., MacEachern, J.A., 2016. Unburrowed mudstones may record only slightly lowered oxygen conditions in warm, shallow basins. Geology 44 (5), 371–374. https://doi.org/10.1130/G37648.1

Davis, C., Pratt, L., Sliter, W., Mompart, L., Mural, B., 1999. Factors influencing organic carbon and trace metal accumulation in the Upper Cretaceous La Luna Formation of the western Maracaibo Basin, Venezuela, in: Barrera, E., Johnson, C.C. (Eds.), Evolution of the Cretaceous Ocean-Climate System, Boulder, Colorado, Geological Society of America Special Paper 332. https://doi.org/10.1130/0-8137-2332-9.203

Dean, W.E., Arthur, M.A., 1998. Geochemical expressions of cyclicity in Cretaceous pelagic limestone sequences: Niobrara Formation, Western Interior Seaway, in: Dean, W.E.,

Arthur, M.A. (Eds.), Stratigraphy of Paleoenvironments of the Cretaceous Western Interior Seaway, USA, SEPM Concepts in Sedimentology and Paleontology No. 6. SEPM, Tulsa, OK, United States, pp. 227–255.

DeReuil, A.A., Birgenheier, L.P., 2019. Sediment dispersal and organic carbon preservation in a dynamic mudstone-dominated system, Juana Lopez Member, Mancos Shale. Sedimentology 66 (3), 1002–1041. https://doi.org/10.1111/sed.12532

Dinelli, E., Tateo, F., Summa, V., 2007. Geochemical and mineralogical proxies for grain size in mudstones and siltstones from the Pleistocene and Holocene of the Po River alluvial plain, Italy. Geol. Soc. Am. Spec. Pap. 420, 25–36.

Dominguez, R.F., Catuneanu, O., 2017. Regional stratigraphic framework of the Vaca Muerta – Quintuco system in the Neuquén Embayment, Argentina, in: Proceedings from: The 20th Geological Congress of Argentina, Tucuman, Argentina.

Dominguez, R.F., Continanzia, M.J., Mykietiuk, K., Ponce, C., Pérez, G., Guerello, R. Lanusse, N.I., Caneva, M., Di Benedetto, M., Catuneanu, O., Cristallini, E., 2016. Organic-rich stratigraphic units in the Vaca Muerta Formation, and their distribution and characterization in the Neuquén Basin (Argentina), in: Proceedings from: Unconventional Resources Technology Conference, San Antonio, Texas. https://doi.org/10.15530/URTEC-2016-2456851

Egenhoff, S.O., Fishman, N.S., 2013. Traces in the dark—Sedimentary processes and facies gradients in the upper shale member of the Upper Devonian–Lower Mississippian Bakken Formation, Williston Basin, North Dakota, USA. J. Sediment. Res. 83 (9), 803–824. https://doi.org/10.2110/jsr.2013.60

El Attar, A., Pranter, M.J., 2016. Regional stratigraphy, elemental chemostratigraphy, and organic richness of the Niobrara Member of the Mancos Shale, Piceance Basin, Colorado. Am. Assoc. Pet. Geol. Bull. 100 (3), 345–377. https://doi.org/10.1306/12071514127

Elder, W.P., Gustason, E.R., Sageman, B.B., 1994. Correlation of basinal carbonate cycles to nearshore parasequences in the Late Cretaceous Greenhorn seaway, Western Interior USA. Geol. Soc. Am. Bull. 106 (7), 892–902. https://doi.org/10.1130/0016-7606(1994)106<0892:COBCCT>2.3.CO;2

Embry, A.F., 2002. Transgressive-regressive (TR) sequence stratigraphy, in: Proceedings from: 22nd Annual Gulf Coast Section SEPM Foundation Bob F. Perkins Research Conference, Houston, Texas. https://doi.org/10.5724/gcs.02.22

Embry, A.F., 2009. Practical sequence stratigraphy. Can. Soc. Petrol. Geol. Reserv. 36, 1–6.

Embry, A.F., 2010. Correlation siliciclastic successions with sequence stratigraphy, in: Ratcliffe, K.T., Zaitlin, B.A. (Eds.), Application of Modern Stratigraphic Techniques: Theory and Case Histories, pp. 35–53 SEPM (Society for Sedimentary Geology) Special Publication, no. 94.

Embry, A.F., Johannessen, E.P., 1993. T–R sequence stratigraphy, facies analysis and reservoir distribution in the uppermost Triassic–Lower Jurassic succession, Western Sverdrup Basin, Arctic Canada. Norw. Petrol. Soc. Spec. Publ. 2, 121–146. https://doi.org/10.1016/B978-0-444-88943-0.50013-7

Erickson, B.E., Helz, G.R., 2000. Molybdenum (VI) speciation in sulfidic waters: stability and lability of thiomolybdates. Geochim. Cosmochim. Acta 64 (7), 1149–1158. https://doi.org/10.1016/S0016-7037(99)00423-8

Frébourg, G., Ruppel, S.C., Rowe, H., 2013. Sedimentology of the Haynesville (Upper Kimmeridgian) and Bossier (Tithonian) Formations, in the Western Haynesville Basin, Texas, U.S.A, in: Hammes, U., Gale, J. (Eds.), Geology of the Haynesville Gas Shale in East Texas and West Louisiana, U.S.A. pp. 47–67 America Association of Petroleum Geologists Memoir 105.

Froelich, P., Klinkhammer, G.P., Bender, M.L., Luedtke, N.A., Heath, G.R., Cullen, D., Dauphin, P., Hammond, D., Hartman, B., Maynard, V., 1979. Early oxidation of organic matter in pelagic sediments of the eastern equatorial Atlantic: suboxic diagenesis. Geochim. Cosmochim. Acta 43 (7), 1075–1090. https://doi.org/10.1016/0016-7037(79)90095-4

Fru, E.C., Rodríguez, N.P., Partin, C.A., Lalonde, S.V., Andersson, P., Weiss, D.J., El Albani, A., Rodushkin, I., Konhauser, K.O., 2016. Cu isotopes in marine black shales record the Great Oxidation Event. Proc. Natl. Acad. Sci. 113 (18), 4941–4946. https://doi.org/10.1073/pnas.1523544113

Galloway, W.E., 1989. Genetic stratigraphic sequences in basin analysis I: architecture and genesis of flooding-surface bounded depositional units. Am. Assoc. Pet. Geol. Bull. 73 (2), 125–142. https://doi.org/10.1306/703C9AF5-1707-11D7-8645000102C1865D

Gambacorta, G., Trincianti, E., Torricelli, S., 2016. Anoxia controlled by relative sea-level changes: an example from the Mississippian Barnett Shale Formation. Palaeogeogr. Palaeoclimatol. Palaeoecol. 459, 306–320. https://doi.org/10.1016/j.palaeo.2016.07.015

Grosjean, E., Adam, P., Connan, J., Albrecht, P., 2004. Effects of weathering on nickel and vanadyl porphyrins of a Lower Toarcian shale of the Paris basin. Geochim. Cosmochim. Acta 68 (4), 789–804. https://doi.org/10.1016/S0016-7037(03)00496-4

Gutierrez Parades, H.C., Catuneanu, O., Romano, U.H., 2017. Sequence stratigraphy of the Miocene section, southern Gulf of Mexico. Mar. Pet. Geol. 86, 711–732. https://doi.org/10.1016/j.marpetgeo.2017.06.022

Hammes, U., Frébourg, G., 2012. Haynesville and Bossier mudrocks: a facies and sequence stratigraphic investigation, East Texas and Louisiana, USA. Mar. Pet. Geol. 31 (1), 8–26. https://doi.org/10.1016/j.marpetgeo.2011.10.001

Hammes, U., Hamlin, H.S., Ewing, T.E., 2011. Geologic analysis of the Upper Jurassic Haynesville Shale in east Texas and west Louisiana. Am. Assoc. Pet. Geol. Bull. 95 (10), 1643–1666. https://doi.org/10.1306/02141110128

Harazim, D., McIlroy, D., Edwards, N.P., Wogelius, R.A., Manning, P.L., Poduska, K.M., Layne, G.D., Sokaras, D., Alonso-Mori, R., Bergmann, U., 2015. Bioturbating animals control the mobility of redox-sensitive trace elements in organic-rich mudstone. Geology 43 (11), 1007–1010. https://doi.org/10.1130/G37025.1

Harris, N.B., Mnich, C.A., Selby, D., Korn, D., 2013. Minor and trace element and Re–Os chemistry of the Upper Devonian Woodford Shale, Permian Basin, west Texas: insights into metal abundance and basin processes. Chem. Geol. 356, 76–93. https://doi.org/10.1016/j.chemgeo.2013.07.018

Harris, N.B., McMillan, J.M., Knapp, L.J., Mastalerz, M., 2018. Organic matter accumulation in the Upper Devonian Duvernay Formation, Western Canada Sedimentary Basin, from sequence stratigraphic analysis and geochemical proxies. Sediment. Geol. 376, 185–203. https://doi.org/10.1016/j.sedgeo.2018.09.004

Hart, B.S., 2015. The Greenhorn Cyclothem of the Cretaceous Western Interior Seaway: lithology trends, stacking patterns, log signatures, and, and application to the Eagle Ford of West Texas. Gulf Coast Assoc. Geol. Soc. Trans. 65, 155–174.

Helland-Hansen, W., Martinsen, O.J., 1996. Shoreline trajectories and sequences: description of variable depositional-dip scenarios. J. Sediment. Res. 66 (4), 670–688. https://doi.org/10.1306/D42683DD-2B26-11D7-8648000102C1865D

Helly, J.J., Levin, L.A., 2004. Global distribution of naturally occurring marine hypoxia on continental margins. Deep-Sea Res. I Oceanogr. Res. Pap. 51 (9), 1159–1168. https://doi.org/10.1016/j.dsr.2004.03.009

Helz, G.R., Miller, C.V., Charnock, J.M., Mosselmans, J.F.W., Pattrick, R.A.D., Garner, C.D., Vaughan, D.J., 1996. Mechanism of molybdenum removal from the sea and its concentration in black shales: EXAFS evidence. Geochim. Cosmochim. Acta 60 (19), 3631–3642. https://doi.org/10.1016/0016-7037(96)00195-0

Hines, B.R., Gazley, M.F., Collins, K.S., Bland, K.J., Crampton, J.S., Ventura, G.T., 2019. Chemostratigraphic resolution of widespread reducing conditions in the southwest Pacific Ocean during the Late Paleocene. Chem. Geol. 504, 236–252. https://doi.org/10.1016/j.chemgeo.2018.11.020

Huerta-Diaz, M.A., Morse, J.W., 1992. Pyritization of trace metals in anoxic marine sediments. Geochim. Cosmochim. Acta 56 (7), 2681–2702. https://doi.org/10.1016/0016-7037(92)90353-K

Hunt, D., Tucker, M.E., 1992. Stranded parasequences and the forced regressive wedge systems tract: deposition during base-level fall. Sediment. Geol. 81 (1–2), 1–9. https://doi.org/10.1016/0037-0738(92)90052-S

Jaffe, L.A., Peucker-Ehrenbrink, B., Petsch, S.T., 2002. Mobility of rhenium, platinum group elements and organic carbon during black shale weathering. Earth Planet. Sci. Lett. 198 (3–4), 339–353. https://doi.org/10.1016/S0012-821X(02)00526-5

Kendall, B., Reinhard, C.T., Lyons, T.W., Kaufman, A.J., Poulton, S.W., Anbar, A.D., 2010. Pervasive oxygenation along late Archaean ocean margins. Nat. Geosci. 3 (9), 647. https://doi.org/10.1038/ngeo942

Kimura, H., Watanabe, Y., 2001. Oceanic anoxia at the Precambrian-Cambrian boundary. Geology 29 (11), 995–998. https://doi.org/10.1130/0091-7613(2001)029<0995:OAATPC>2.0.CO;2

Klinkhammer, G.P., Palmer, M.R., 1991. Uranium in the oceans: where it goes and why. Geochim. Cosmochim. Acta 55 (7), 1799–1806. https://doi.org/10.1016/0016-7037(91)90024-Y

Knapp, L.J., McMillan, J.M., Harris, N.B., 2017. A depositional model for organic-rich Duvernay Formation mudstones. Sediment. Geol. 347, 160–182. https://doi.org/10.1016/j.sedgeo.2016.11.012

Knapp, L.J., Harris, N.B., McMillan, J.M., 2019. A sequence stratigraphic model for the organic-rich Upper Devonian Duvernay Formation, Alberta, Canada. Sediment. Geol. 387, 152–181. https://doi.org/10.1016/j.sedgeo.2019.04.008

Konhauser, K.O., 2007. Introduction to Geomicrobiology. Blackwell, Malden, Massachusetts.

Lazar, O.R., Bohacs, K.M., Macquaker, J.H., Schieber, J., Demko, T.M., 2015. Capturing key attributes of fine-grained sedimentary rocks in outcrops, cores, and thin sections: nomenclature and description guidelines. J. Sediment. Res. 85 (3), 230–246. https://doi.org/10.2110/ jsr.2015.11

Lemiere, B., 2018. A review of pXRF (field portable X-ray fluorescence) applications for applied geochemistry. J. Geochem. Explor. 188, 350–363. https://doi.org/10.2110/jsr.2015.11

Lewan, M.D., 1984. Factors controlling the proportionality of vanadium to nickel in crude oils. Geochim. Cosmochim. Acta 48 (11), 2231–2238. https://doi.org/10.1016/0016-7037(84)90219-9

Lewan, M.D., Maynard, J.B., 1982. Factors controlling enrichment of vanadium and nickel in the bitumen of organic sedimentary rocks. Geochim. Cosmochim. Acta 46 (12), 2547–2560. https://doi.org/10.1016/0016-7037(82)90377-5

Li, Z., Schieber, J., 2020. Application of sequence stratigraphic concepts to the Upper Cretaceous Tununk Shale Member of the Mancos Shale Formation, south-central Utah: parasequence styles in shelfal mudstone strata. Sedimentology 67 (1), 118–151. https://doi.org/10.1111/sed.12637

Liu, Y., Zhang, J., Tang, X., Yang, C., Tang, S., 2016. Weathering characteristics of the Lower Paleozoic black shale in northwestern Guizhou Province, south China. J. Earth Syst. Sci. 125 (5), 1061–1078. https://doi.org/10.1007/s12040-016-0718-6

Loutit, T.S., Hardenbol, J., Vail, P.R., Baum, G.R., 1988. Condensed sections: the key to age determination and correlation of continental margin sequences, in: Wilgus, C.K., Hastings, B.S., Kendall, C.G.S., Posamentier, H.W., Ross, C.A., Van Wagoner, J.C. (Eds.), Sea Level Changes – An Integrated Approach: Society of Economic Paleontologists and Geologists Special Publication. 42. pp. 183–213.

MacEachern, J.A., Bann, K.L., Pemberton, S.G., Gingras, M.K., 2009a. The ichnofacies paradigm: high-resolution paleoenvironmental interpretation of the rock record. SEPM Soc. Sediment. Geol. App. Ichnol. SC52, 27–64. https://doi.org/10.2110/pec.07.52.0027

MacEachern, J.A., Pemberton, S.G., Bann, K.L., Gingras, M.K., 2009b. Departures from the archetypal ichnofacies: effective recognition of physico-chemical stresses in the rock record. Soc. Sediment. Geol. Appl. Ichnol. SC52, 65–93. https://doi.org/10.2110/pec.07.52.0065

Macquaker, J.H., Taylor, K.G., 1996. A sequence stratigraphic interpretation of a mudstone-dominated succession: the Lower Jurassic Cleveland ironstone Formation, U.K. J. Geol. Soc. Lond. 153, 759–770. http://dx.doi.org/10.1144/gsjgs.153.5.0759

Macquaker, J.H., Taylor, K.G., Gawthorpe, R.L., 2007. High-resolution facies analyses of mudstones: implications for paleoenvironmental and sequence stratigraphic interpretations of offshore ancient mud-dominated successions. J. Sediment. Res. 77 (4), 324–339. https://doi.org/10.2110/jsr.2007.029

Mann, U., Stein, R., 1997. Organic facies variations, source rock potential, and sea level changes in Cretaceous black shales of the Quebrada Ocal, Upper Magdalena Valley, Colombia. Am. Assoc. Pet. Geol. Bull. 81 (4), 556–576. https://doi.org/10.1306/522B43CF-1727-11D7-8645000102C1865D

Marynowski, L., Pisarzowska, A., Derkowski, A., Rakociński, M., Szaniawski, R., Środoń, J., Cohen, A.S., 2017. Influence of palaeoweathering on trace metal concentrations and environmental proxies in black shales. Palaeogeogr. Palaeoclimatol. Palaeoecol. 472, 177–191. https://doi.org/10.1016/j.palaeo.2017.02.023

McLennan, S.M., Hemming, S., McDaniel, D.K., Hanson, G.N., 1993. Geochemical approaches to sedimentation, provenance, and tectonics. Geol. Soc. Am. Spec. Pap. 284, 21–40.

McManus, J., Berelson, W.M., Klinkhammer, G.P., Hammond, D.E., Holm, C., 2005. Authigenic uranium: relationship to oxygen penetration depth and organic carbon rain. Geochim. Cosmochim. Acta 69 (1), 95–108. https://doi.org/10.1016/j.gca.2004.06.023

Mongelli, G., Critelli, S., Perri, F., Sonnino, M., Perrone, V., 2006. Sedimentary recycling, provenance and paleoweathering from chemistry and mineralogy of Mesozoic continental redbed mudrocks, Peloritani Mountains, southern Italy. Geochem. J. 40 (20), 197–209. https://doi.org/10.2343/geochemj.40.197

Morford, J.L., Russell, A.D., Emerson, S., 2001. Trace metal evidence for changes in the redox environment associated with the transition from terrigenous clay to diatomaceous sediment, Saanich Inlet, BC. Mar. Geol. 174 (1–4), 355–369. https://doi.org/10.1016/S0025-3227(00)00160-2

Morrison, J.M., Codispoti, L.A., Smith, S.L., Wishner, K., Flagg, C., Gardner, W.D., Gaurin, S., Naqvi, S.W.A., Manghnani, V., Prosperie, L., Gundersen, J.S., 1999. The oxygen minimum zone in the Arabian Sea during 1995. Deep-Sea Res. II Top. Stud. Oceanogr. 46 (8–9), 1903–1931. https://doi.org/10.1016/S0967-0645(99)00048-X

Myers, K.J., Wignall, P.B., 1987. Understanding Jurassic organic-rich mudrocks—new concepts using gamma-ray spectrometry and palaeoecology: examples from the Kimmeridge Clay of Dorset and the Jet Rock of Yorkshire, in: Legget, J.K., Zuffa, G.G. (Eds.), Marine Clastic Sedimentology. Springer, Dordrecht, pp. 172–189. https://doi.org/10.1007/978-94-009-3241-8_9

Nadeau, P.H., Wilson, M.J., McHardy, W.J., Tait, J.M., 1985. The conversion of smectite to illite during diagenesis: evidence from some illitic clays from bentonites and sandstones. Mineral. Mag. 49 (352), 393–400. https://doi.org/10.1180/minmag.1985.049.352.10

Nesbitt, H.W., Young, G.M., 1982. Early Proterozoic climates and plate motions inferred from major element chemistry of lutites. Nature 299 (5885), 715–717. https://doi.org/10.1038/299715a0

Nyhuis, C.J., Riley, D., Kalasinska, A., 2016. Thin section petrography and chemostratigraphy: integrated evaluation of an upper Mississippian mudstone dominated succession from the southern Netherlands. Neth. J. Geosci. 95 (1), 3–22. https://doi.org/10.1017/njg.2015.25

Over, D.J., 1990. Trace metals in burrow walls and sediments, Georgia Bight, USA. Ichnos. Int. J. Plant Anim. 1 (1), 31–41. https://doi.org/10.1080/10420949009386329

Partin, C.A., Bekker, A., Planavsky, N.J., Scott, C.T., Gill, B.C., Li, C., Podkovyrov, V., Maslov, V., Konhauser, K.O., Lalonde, S.V., Love, G.D., Love, G.D., Poulton, S.W., Lyons, T.W., 2013. Large-scale fluctuations in Precambrian atmospheric and oceanic oxygen levels from the record of U in shales. Earth Planet. Sci. Lett. 369, 284–293. https://doi.org/10.1016/j.epsl.2013.03.031

Patchett, P.J., White, W.M., Feldmann, H., Kielinczuk, S., Hofmann, A.W., 1984. Hafnium/rare earth element fractionation in the sedimentary system and crustal recycling into the Earth's mantle. Earth Planet. Sci. Lett. 69 (2), 365–378. https://doi.org/10.1016/0012-821X(84)90195-X

Pearce, T.J., Besly, B.M., Wray, D.S., Wright, D.K., 1999. Chemostratigraphy: a method to improve interwell correlation in barren sequences—a case study using onshore

Duckmantian/Stephanian sequences (West Midlands, UK). Sediment. Geol. 124(1–4), 197–220. https://doi.org/10.1016/S0037-0738(98)00128-6

Pearce, T.J., Wray, D., Ratcliffe, K., Wright, D.K., Moscariello, A., 2005. Chemostratigraphy of the Upper Carboniferous Schooner Formation, southern North Sea, in: Collinson, J.D., Evans, D.J., Holliday, D.W. (Eds.), Carboniferous Hydrocarbon Resources: The Southern North Sea and Surrounding Onshore Areas: Occasional Publication Series of the Yorkshire Geological Society. 7. pp. 147–164.

Pearce, T.J., Martin, J.H., Cooper, D., Wray, D.S., 2010. Chemostratigraphy of upper carboniferous (Pennsylvanian) sequences from the Southern North Sea (United Kingdom), in: Application of Modern Stratigraphic Techniques: Theory and Case Histories: SEPM (Society for Sedimentary Geology) Special Publication, 94, pp. 109–127. http://dx.doi.org/10.2110/sepmsp.094.109

Peucker-Ehrenbrink, B., Hannigan, R.E., 2000. Effects of black shale weathering on the mobility of rhenium and platinum group elements. Geology 28 (5), 475–478. https://doi.org/10.1130/0091-7613(2000)28<475:EOBSWO>2.0.CO;2

Piper, D.Z., Calvert, S.E., 2009. A marine biogeochemical perspective on black shale deposition. Earth Sci. Rev. 95 (1–2), 63–96. https://doi.org/10.1016/j.earscirev.2009.03.001

Plank, T., Langmuir, C.H., 1998. The chemical composition of subducting sediment and its consequences for the crust and mantle. Chem. Geol. 145 (3), 325–394. https://doi.org/10.1016/S0009-2541(97)00150-2

Playter, T., Corlett, H., Konhauser, K., Robbins, L., Rohais, S., Crombez, V., Maccormack,K., Rokosh, D., Prenoslo, D., Furlong, C.M., Pawlowicz, J., Gingras, M., Lalonde, S., Lyster, S., Zonneveld, J.-P., 2018. Clinoform identification and correlation in fine-grained

sediments: a case study using the Triassic Montney Formation. Sedimentology 65 (1), 263–302. https://doi.org/10.1111/sed.12403

Plint, A.G., Nummedal, D., 2000. The falling stage systems tract: recognition and importance in sequence stratigraphic analysis. Geol. Soc. Lond., Spec. Publ. 172 (1), 1–17. http://dx.doi.org/10.1144/GSL.SP.2000.172.01.01

Posamentier, H.W., Allen, G.P., 1999. Siliciclastic sequence stratigraphy: concepts and applications. SEPM Soc. Sediment. Geol. Concepts Sedimentol. Paleontol. 7, 210.

Posamentier, H.W., Kolla, V., 2003. Seismic geomorphology and stratigraphy of depositional elements in deep-water settings. J. Sediment. Res. 73 (3), 367–388. https://doi.org/10.1306/111302730367

Pyle, L.J., Gal, L.P., 2016. Reference Section for the Horn River Group and Definition of the Bell Creek Member, Hare Indian Formation in central Northwest Territories. Bull. Can. Petrol. Geol. 64 (1), 67–98. https://doi.org/10.2113/gscpgbull.64.1.67

Ratcliffe, K.T., Wright, A.M., Hallsworth, C., Morton, A., Zaitlin, B.A., Potocki, D., Wray, D., 2004. An example of alternative correlation techniques in a low-accommodation setting, nonmarine hydrocarbon system: the (Lower Cretaceous) Mannville Basal Quartz succession of southern Alberta. Am. Assoc. Pet. Geol. Bull. 88 (10), 1419–1432. https://doi.org/10.1306/05100402035

Ratcliffe, K.T., Martin, J., Pearce, T.J., Hughes, A.D., Lawton, D.E., Wray, D.S., Bessa, F., 2006. A regional chemostratigraphically-defined correlation framework for the late Triassic TAG-I Formation in Blocks 402 and 405a, Algeria. Pet. Geosci. 12 (1), 3–12.

Ratcliffe, K., Wright, M., Montgomery, P., Palfrey, A., Vonk, A., Vermeulen, J., Barrett, M., 2010. Application of chemostratigraphy to the Mungaroo Formation, the Gorgon field,

offshore northwest Australia. APPEA J. 50 (1), 371–388. https://doi.org/10.1144/1354-079305-669

Ratcliffe, K.T., Wright, A.M., Schmidt, K., 2012a. Application of inorganic whole-rock geochemistry to shale resource plays: an example from the Eagle Ford Shale Formation, Texas. Sediment. Rec. 10 (2), 4–9. http://dx.doi.org/10.2110/sedred.2012.2.4

Ratcliffe, K.T., Woods, J., Rice, C., 2012b. Determining well-bore pathways during multilateral drilling campaigns in shale resource plays: an example using chemostratigraphy from the Horn River Formation, British Columbia, Canada, in: Proceedings from: Eastern Australasian Basin Symposium IV, Brisbane, Australia.

Ratcliffe, K.T., Wright, A.M., Spain, D.R., 2012 April/Mayc. Unconventional methods for unconventional plays: using elemental data to understand shale resource plays. Petrol. Explor. Soc. Aust. News Resour. 117, 50–54.

Reichart, G.J., Lourens, L.J., Zachariasse, W.J., 1998. Temporal variability in the northern Arabian Sea Oxygen Minimum Zone (OMZ) during the last 225,000 years. Paleoceanography 13 (6), 607–621. https://doi.org/10.1029/98PA02203

Reinhard, C.T., Planavsky, N.J., Robbins, L.J., Partin, C.A., Gill, B.C., Lalonde, S.V., Bekker, A., Konhauser, K.O., Lyons, T.W., 2013. Proterozoic ocean redox and biogeochemical stasis. Proc. Natl. Acad. Sci. 110 (14), 5357–5362. https://doi.org/10.1073/pnas.1208622110

Revsbech, N.P., Larsen, L.H., Gundersen, J., Dalsgaard, T., Ulloa, O., Thamdrup, B., 2009. Determination of ultra-low oxygen concentrations in oxygen minimum zones by the STOX sensor. Limnol. Oceanogr. Methods 7, 371–381. https://doi.org/10.4319/lom.2009.7.371

Robbins, L.J., Lalonde, S.V., Planavsky, N.J., Partin, C.A., Reinhard, C.T., Kendall, B., Scott, C., Hardisty, D.S., Gill, B.C., Alessi, D.S., Dupont, C.L., Saito, M.A., Crowe, S.A., Poulton, S.W., Bekker, A., Lyons, T.W., Konhauser, K.O., 2016. Trace elements at the intersection of marine biological and geochemical evolution. Earth Sci. Rev. 163, 323–348. https://doi.org/10.1016/j.earscirev.2016.10.013

Rosenthal, Y., Lam, P., Boyle, E.A., Thomson, J., 1995. Authigenic cadmium enrichmen in suboxic sediments: precipitation and postdepositional mobility. Earth Planet. Sci Lett. 132 (1–4), 99–111. https://doi.org/10.1016/0012-821X(95)00056-I

Ross, D.J., Bustin, R.M., 2009. Investigating the use of sedimentary geochemical proxies for paleoenvironment interpretation of thermally mature organic-rich strata: examples from the Devonian–Mississippian shales, Western Canadian Sedimentary Basin. Chem. Geol. 260 (1–2), 1–19. https://doi.org/10.1016/j.chemgeo.2008.10.027

Rowe, H., Hughes, N., Robinson, K., 2012. The quantification and application of handheld energy-dispersive x-ray fluorescence (ED-XRF) in mudrock chemostratigraphy and geochemistry. Chem. Geol. 324–325, 122–131. https://doi.org/10.1016/j.chemgeo.2011.12.023

Rowe, H.D., Loucks, R.G., Ruppel, S.C., Rimmer, S.M., 2008. Mississippian Barnett Formation, Fort Worth Basin, Texas: bulk geochemical inferences and Mo–TOC constraints on the severity of hydrographic restriction. Chem. Geol. 257 (1–2), 16–25. https://doi.org/10.1016/j.chemgeo.2008.08.006

Rowe, H., Ruppel, S., Rimmer, S., Loucks, R., 2009. Core-based chemostratigraphy of the Barnett Shale, Permian Basin, Texas. Gulf Coast Assoc. Geol. Soc. Trans. 59, 675–686.

Rowe, H., Wang, X., Fan, B., Zhang, T., Ruppel, S.C., Milliken, K.L., Loucks, R., Shen, Y., Zhang, J., Liang, Q., Sivil, E., 2017. Chemostratigraphic insights into fluvio-lacustrine deposition, Yanchang Formation, Upper Triassic, Ordos Basin, China. Interpretation 5 (2), SF149–SF165. https://doi.org/10.1190/INT-2016-0121.1

Sageman, B.B., Lyons, T.W., 2004. Geochemistry of fine-grained sediments and sedimentary rocks, in: Mackenzie, F.T. (Ed.), Sediments, Diagenesis, and Sedimentary Rocks: Treatise on Geochemistry, Second Edition, Volume 7. Elsevier Pergamon, Oxford, United Kingdom, pp. 116–148. https://doi.org/10.1016/B0-08-043751-6/07157-7

Sano, J.L., Ratcliffe, K.T., Spain, D.R., 2013. Chemostratigraphy of the Haynesville Shale, in: Hammes, U., Gales, J. (Eds.), Geology of the Hanyesville Gas Shale in East Texas and West Louisiana, U.S.A. pp. 137–154 American Association of Petroleum Geologists Memoir 105. http://dx.doi.org/10.1306/13441847M1053602

Savrda, C.E., Bottjer, D.J., 1989. Trace-fossil model for reconstructing oxygenation histories of ancient marine bottom waters: application to Upper Cretaceous Niobrara Formation, Colorado. Palaeogeogr. Palaeoclimatol. Palaeoecol. 74 (1–2), 49–74. https://doi.org/10.1016/0031-0182(89)90019-9

Schieber, J., 1994. Evidence for high-energy events and shallow-water deposition in the Chattanooga Shale, Devonian, central Tennessee, USA. Sediment. Geol. 93 (3-4), 193–208. https://doi.org/10.1016/0037-0738(94)90005-1

Schieber, J., 1996. Early diagenetic silica deposition in algal cysts and spores; a source of sand in black shales? J. Sediment. Res. 66 (1), 175–183. https://doi.org/10.1306/D42682ED-2B26-11D7-8648000102C1865D

Schieber, J., 1998. Developing a sequence stratigraphic framework for the Late Devonian Chattanooga Shale of the southeastern USA: relevance for the Bakken Shale, in: Christopher, J.E., Gilboy, C.F., Paterson, D.F., Bends, S.L. (Eds.), Eighth International Williston Basin Symposium, pp. 58–68 Saskatchewan Geological Society Special Publication No. 13.

Schieber, J., Krinsley, D., Riciputi, L., 2000. Diagenetic origin of quartz silt in mudstones and implications for silica cycling. Nature 406 (6799), 981. https://doi.org/10.1038/35023143

Schönfeld, J., Kuhnt, W., Erdem, Z., Flögel, S., Glock, N., Aquit, M., Frank, M., Holbourn, A., 2015. Records of past mid-depth ventilation: Cretaceous ocean anoxic event 2 vs. Recent oxygen minimum zones. Biogeosciences 12 (4), 1169–1189. https://doi.org/10.5194/bg-12-1169-2015

Scott, C., Lyons, T.W., 2012. Contrasting molybdenum cycling and isotopic properties in euxinic versus non-euxinic sediments and sedimentary rocks: refining the paleoproxies. Chem. Geol. 324–325, 19–27. https://doi.org/10.1016/j.chemgeo.2012.05.012

Shanmugam, G., 1988. Origin, recognition, and importance of erosional unconformities in sedimentary basins, in: New Perspectives in Basin Analysis. Springer, New York, NY, pp. 83–108. https://doi.org/10.1007/978-1-4612-3788-4_5

Shen, J., Zhou, L., Feng, Q., Zhang, M., Lei, Y., Zhang, N., Yu, J., Gu, S., 2014. Paleoproductivity evolution across the Permian-Triassic boundary and quantitative calculation of primary productivity of black rock series from the Dalong Formation, South China. Sci. China Earth Sci. 57 (7), 1583–1594. https://doi.org/10.1007/s11430-013-4780-5

Slatt, R.M., Rodriguez, N.D., 2012. Comparative sequence stratigraphy and organic geochemistry of gas shales: Commonality or coincidence? J. Nat. Gas Sci. Eng. 8, 68–84. https://doi.org/10.1016/j.jngse.2012.01.008

Smith, L.B., Schieber, J., Wilson, R.D., 2019. Shallow-water onlap model for the deposition of Devonian black shales in New York, USA. Geology 47 (3), 279–283. https://doi.org/10.1130/G45569.1

Swift, D.J., 1975. Barrier-island genesis: evidence from the central Atlantic shelf, eastern USA. Sediment. Geol. 14 (1), 1–43. https://doi.org/10.1016/0037-0738(75)90015-9

Taylor, K.G., Macquaker, J.H.S., 2014. Diagenetic alterations in a silt-and clay-rich mudstone succession: an example from the Upper Cretaceous Mancos Shale of Utah, USA. Clay Miner. 49 (2), 213–227. https://doi.org/10.1180/claymin.2014.049.2.05

Taylor, S.R., McLennan, S.M., 1985. The Continental Crust: Its Composition andEvolution. Blackwell, Malden, Massachusetts.

Thomson, J., Higgs, N.C., Croudace, I.W., Colley, S., Hydes, D.J., 1993. Redox zonation of elements at an oxic/post-oxic boundary in deep-sea sediments. Geochim. Cosmochim. Acta 57 (3), 579–595. http://dx.doi.org/10.1016/0016-7037(93)90369-8

Thomson, J., Higgs, N.C., Wilson, T.R.S., Croudace, I.W., De Lange, G.J., Van Santvoort, P.J.M., 1995. Redistribution and geochemical behaviour of redox-sensitive elements around S1, the most recent eastern Mediterranean sapropel. Geochim. Cosmochim. Acta 59 (17), 3487–3501. https://doi.org/10.1016/0016-7037(95)00232-O

Thomson, J., Jarvis, I., Green, D.R., Green, D., 1998. Oxidation fronts in Madeira Abyssal Plain turbidites: persistence of early diagenetic trace-element enrichments during burial, site

9501, in: Weaver, P.P.E., Schmincke, H.-U., Duffield, W. (Eds.), Proceedings of the Ocean Drilling Program, Scientific Results. Vol. 157. pp. 559–571.

Tribovillard, N., Algeo, T.J., Lyons, T., Riboulleau, A., 2006. Trace metals as paleoredox and paleoproductivity proxies: an update. Chem. Geol. 232 (1–2), 12–32. https://doi.org/10.1016/j.chemgeo.2006.02.012

Turner, B.W., Slatt, R.M., 2016. Assessing bottom water anoxia within the Late Devonian Woodford Shale in the Arkoma Basin, southern Oklahoma. Mar. Pet. Geol. 78, 536–546. https://doi.org/10.1016/j.marpetgeo.2016.10.009

Turner, B.W., Molinares-Blanco, C.E., Slatt, R.M., 2015. Chemostratigraphic, palynostratigraphic, and sequence stratigraphic analysis of the Woodford Shale, Wyche Farm Quarry, Pontotoc County, Oklahoma. Interpretation 3 (1), SH1–SH9. https://doi.org/10.1190/INT-2014-0089.1

Turner, B.W., Tréanton, J.A., Slatt, R.M., 2016. The use of chemostratigraphy to refine ambiguous sequence stratigraphic correlations in marine mudrocks. An example from the Woodford Shale, Oklahoma, USA. J. Geol. Soc. 173, 854–868. http://dx.doi.org/10.1144/jgs2015-125

Tyson, R.V., Pearson, T.H., 1991. Modern and ancient continental shelf anoxia: an overview. Geol. Soc. Lond., Spec. Publ. 58 (1), 1–24. http://dx.doi.org/10.1144/GSL.SP.1991.058.01.01

Van der Weijden, C.H., 2002. Pitfalls of normalization of marine geochemical data using a common divisor. Mar. Geol. 184 (3–4), 167–187. https://doi.org/10.1016/S0025-3227(01)00297-3

Van Wagoner, J.C., Posamentier, H.W., Mitchum, R.M.J., Vail, P.R., Sarg, J.F., Loutit, T.S., Hardenbol, J., 1988. An overview of the fundamentals of sequence stratigraphy and key definitions, in: Wilgus, C.K., Hastings, B.S., Kendall, C.G.S., Posamentier, H.W., Ross, C.A., Van Wagoner, J.C. (Eds.), Sea Level Changes–An Integrated Approach, pp. 39–45 SEPM (Society for Sedimentary Geology) Special Publication 42. https://doi.org/10.1016/S0025-3227(01)00297-3

Ver Straeten, C.A., Brett, C.E., Sageman, B.B., 2011. Mudrock sequence stratigraphy: a multi-proxy (sedimentological, paleobiological and geochemical) approach, Devonian Appalachian Basin. Palaeogeogr. Palaeoclimatol. Palaeoecol. 304 (1–2), 54–73. https://doi.org/10.1016/j.palaeo.2010.10.010

Wanty, R.B., Goldhaber, M.B., 1992. Thermodynamics and kinetics of reactions involving vanadium in natural systems: accumulation of vanadium in sedimentary rocks. Geochim. Cosmochim. Acta 56 (4), 1471–1483. https://doi.org/10.1016/0016-7037(92)90217-7

Wedepohl, K.H., 1971. Environmental influences on the chemical composition of shales and clays. Phys. Chem. Earth 8, 307–333. https://doi.org/10.1016/0079-1946(71)90020-6

Wignall, P.B., Twitchett, R.J., 1996. Oceanic anoxia and the end Permian mass extinction. Science 272 (5265), 1155–1158. https://doi.org/10.1126/science.272.5265.1155

Wilde, P., Quinby-Hunt, M.S., Erdtmann, B.D., 1996. The whole-rock cerium anomaly: a potential indicator of eustatic sea-level changes in shales of the anoxic facies. Sediment. Geol. 101 (1–2), 43–53. https://doi.org/10.1016/0037-0738(95)00020-8

Williams, C.J., Hesselbo, S.P., Jenkyns, H.C., Morgans-Bell, H.S., 2001. Quartz silt in mudrocks as a key to sequence stratigraphy (Kimmeridge Clay Formation, Late Jurassic, Wessex Basin, UK). Terra Nova 13, 449–455. https://doi.org/10.1046/j.1365-3121.2001.00378.x

Wilson, R.D., Schieber, J., 2015. Sedimentary facies and depositional environment of the Middle Devonian Geneseo Formation of New York, USA. J. Sediment. Res. 85 (11), 1393–1415. https://doi.org/10.2110/jsr.2015.88

Wyrtki, K., 1962. The oxygen minima in relation to ocean circulation. Deep-Sea Res. Oceanogr. Abstr. 9 (1-2), 11–23. https://doi.org/10.1016/0011-7471(62)90243-7

Yamashita, Y., Takahashi, Y., Haba, H., Enomoto, S., Shimizu, H., 2007. Comparison of reductive accumulation of Re and Os in seawater–sediment systems. Geochim. Cosmochim. Acta 71 (14), 3458–3475. https://doi.org/10.1016/j.gca.2007.05.003

Zhang, J., Zeng, Y., Slatt, R., 2019. XRF (X-ray fluorescence) applied to characterization of unconventional Woodford Shale (Devonian, USA) lateral well heterogeneity. Fuel 254, 115565. https://doi.org/10.1016/j.fuel.2019.05.148

Zhou, C., Jiang, S.Y., 2009. Palaeoceanographic redox environments for the lower Cambrian Hetang Formation in South China: evidence from pyrite framboids, redox sensitive trace elements, and sponge biota occurrence. Palaeogeogr. Palaeoclimatol. Palaeoecol. 271 (3–4), 279–286. https://doi.org/10.1016/j.palaeo.2008.10.024

Chapter 5: Sequence stratigraphy

5.1 Introduction

In studies of mudstone intervals, chemostratigraphic profiles are increasingly used to facilitate correlations and supplement traditional datasets for high-resolution sequence stratigraphic analyses (e.g., Harris et al., 2021; Li et al., 2021; Sano et al., 2013; Turner et al., 2016). The Middle to Late Devonian Horn River Group of the west central Northwest Territories (NWT), Canada, comprises mudstone units (Hare Indian and Canol Formations) with coeval platform and reef carbonate units of the Ramparts Formation (Fig. 5.1; Pugh, 1983). This group was deposited at an interesting time in Earth's history because of the widespread deposition of Middle to Late Devonian organic-rich mudstone units (e.g., Klemme and Ulmishek, 1991; Ormiston and Oglesby, 1995) and successive biotic crises in the Middle to Late Devonian (Becker et al., 2020; McGhee et al., 2013; e.g., Walliser, 1996). A chemostratigraphy-based sequence stratigraphic framework for the Hare Indian Formation (the lowermost unit of the Horn River Group) was presented by Harris et al. (2021). Moreover, the Horn River Group has been included in a broad-scale sequence stratigraphic framework for the Devonian of the entire Northern Canadian Mainland Sedimentary Basin, where the Horn River Group and surrounding formations are part of two transgressive-regressive (T-R) cycles (Morrow, 2018). In the 1980s, studies of the Horn River Group Kee Scarp Reef Member by Muir and co-authors also placed these reef strata in the context of two large-scale sequence stratigraphic cycles (e.g., Muir et al., 1985). Broadly, the two cycles of both Muir and Morrow are as follows: (1) Hume Formation – Hare Indian Formation or lower Ramparts Formation, (2) Hare Indian Formation or lower Ramparts Formation – Imperial Formation (Morrow, 2018; Muir et al., 1985), although specific details about the proposed boundaries between the transgressive and regressive portion of the cycles are

limited. At locations where the carbonate units are thick and the overlying Canol Formation is thin, higher-frequency cycles in the form of alternating transgressive systems tracts (TSTs) and highstand systems tracts (HSTs) and parasequences were identified in the Ramparts Formation (e.g., Muir et al., 1985; Muir and Dixon, 1984; Yose et al., 2001). To date for the west-central NWT, no high-resolution sequence stratigraphic analysis exists for the Canol Formation or the Horn River Group as a whole and detailed correlations have been lithostratigraphic in nature (e.g., Kabanov, 2019; Kabanov and Gouwy, 2020).

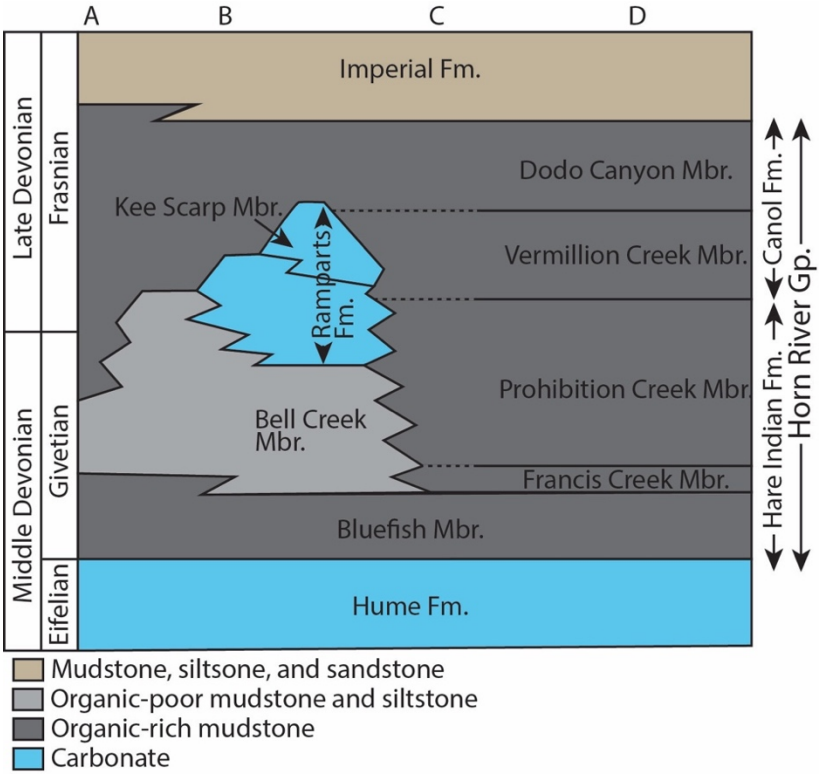

Figure 5.1 Schematic stratigraphic column for the Horn River Group in the Central Mackenzie Valley and Mackenzie Mountains of the Northwest Territories (NWT). The Francis Creek, Prohibition Creek, Vermillion Creek, and Dodo Canyon Members are defined for the Central Mackenzie Valley but have not been established in the Mackenzie Mountains. Locations A – D

marked at the top of the column denote the different stratigraphic profiles observed in different cores and outcrops of this study. Location A represents the stratigraphy at the Rumbly Creek outcrop in Mackenzie Mountains at the west of the study area. Location B reflects the stratigraphy at Powell Creek and Mountain River outcrops in the Mackenzie Mountains, located centrally in the study area. The stratigraphy of the Dodo Creek and Carcajou River outcrops in the eastern Mackenzie Mountains is shown by (C) whereas (D) shows the stratigraphy of the cores in the Central Mackenzie Valley. Acronyms and abbreviations: Fm. – formation, Gp. – group, Mbr. – member. Modified from Kabanov and Gouwy (2017).

In this study, we establish a high-resolution sequence stratigraphic framework for the Horn River Group of the Central Mackenzie Valley and Mackenzie Mountains of the NWT. We focus on locations where the reef units of the Horn River Group are absent and the mudstone intervals are thicker (i.e., locations A, B, C, and D in Figure 5.1 rather than the area between B and C, where the Kee Scarp Member is present). Our dataset from cores in the Central Mackenzie Valley includes lithological core descriptions, wireline gamma-ray logs, total organic carbon (TOC), mineralogical composition through X-ray diffraction (XRD) and geochemical composition from X-ray fluorescence. For outcrops in the Mackenzie Mountains, we collected a geochemical dataset through x-ray fluorescence and use chemostratigraphy as a means of sequence stratigraphic correlation between outcrops and cores. This work includes the previously published dataset from the Hare Indian Formation by Harris et al. (2021) combined with new results from the Ramparts, Canol, and Imperial Formations. Geochemical proxies for detrital sediment supply and biogenic silica form the basis of the sequence stratigraphic interpretation, with geochemical proxies for paleoredox considered alongside.

The Canol Formation is source rock for the hydrocarbons produced near the town of Norman Wells from the Kee Scarp Member (Snowdon et al., 1987) and beginning in the early 2000s, interested shifted to the unconventional reservoir potential of the Canol Formation and Bluefish Member of the Hare Indian Formation. This contribution will facilitate the mapping of higher reservoir quality intervals (i.e., those with higher silica and thus greater brittleness). The Horn River Group of the west central NWT also serves as a valuable record of local marine conditions during the Middle to Late Devonian, which can be considered along with other time-equivalent examples to build a more complete picture of the Middle to Late Devonian marine environment. Our framework provides insight about local fluctuations in the rate of sediment supply compared to the rate of relative sea-level rise and about variations in the proportions of detrital versus biogenic sediment. Finally, chemostratigraphic proxies illustrate the evolution of paleoredox conditions with time in this Middle to Late Devonian example and elucidate the relationship between paleoredox and the rates of relative sea-level change and sediment supply.

5.2 Geological background

5.2.1 Lithostratigraphy and depositional systems

The Horn River Group of the west central NWT is late Eifelian to Frasnian (Middle to Late Devonian) in age (Kabanov and Gouwy, 2017). This group comprises the Hare Indian, Ramparts, and Canol Formations with the Hume Formation below and the Imperial Formation above (Fig. 5.1). In areas where the Ramparts Formation is present, the Hare Indian Formation includes the Bluefish Member, an organic-rich mudstone unit (Pugh, 1983), and the Bell Creek Member, characterized by organic-poor mudstone with limestone and siltstone interbeds (Pyle

and Gal, 2016). Where the Ramparts Formation is absent in the Central Mackenzie Valley of the NWT (location D in Fig. 5.1), the Hare Indian Formation includes three Members: the Bluefish, Francis Creek (fissile, argillaceous mudstone), and Prohibition Creek (organic-rich mudstone) (Kabanov and Gouwy, 2017; Pugh, 1983) and the organic-rich mudstones of the Canol Formation are subdivided into the Vermillion Creek Member and the Dodo Canyon Member, distinguished because of a higher proportion of calcareous mudstone intervals in the Vermillion Creek (Kabanov and Gouwy, 2017). The Francis Creek, Prohibition Creek, Vermillion Creek, and Dodo Canyon Members of the Hare Indian and Canol Formations are not distinguished in the Mackenzie Mountains (locations A, B, and C in Fig. 5.1). Overall, the mudstone units of the Horn River Group are interpreted as a proximal to distal shelf depositional system (Biddle et al., 2021) with the Bell Creek Member possibly representing the distal portion of a delta (Biddle et al., 2021; Tassonyi, 1969). The Ramparts Formation is present where the Bell Creek Member is thickest and comprises limestone and calcareous mudstone ramp and platform deposits, with localized reef units of the Kee Scarp Member (Muir et al., 1985).

5.2.2 Tectonic Setting

In the Middle to Late Devonian, the study area was located along the northwestern margin of Ancestral North America at tropical latitudes near the paleoequator (e.g., Cocks and Torsvik, 2011; Scotese and McKerrow, 1990). Following supercontinent breakup in the Neoproterozoic, a passive margin developed along the present-day northwest of Ancestral North America with convergence to the north (Dewing et al., 2019; Hadlari et al., 2014). In the Late Devonian, the Ellesmerian orogeny along the northern margin of Ancestral North America produced a foreland basin in the study area, causing a shift from the organic-rich mudstones and carbonates of the

Horn River Group to deposition of the Imperial Formation siliciclastics (Beranek et al., 2010; Garzione et al., 1997). After the Late Devonian, a regional sub-Cretaceous unconformity was produced by uplift and cooling associated with basin inversion, which was followed by renewed burial and eventual exposure of the Horn River Group strata in the Mackenzie Mountains during development of the North American Cordillera Foreland Basin (Powell et al., 2020). The study area is currently experiencing compression produced by the accretion of the Yakutat terrane to the North American Craton in the Gulf of Alaska beginning in the Miocene (Mazzotti and Hyndman, 2002).

5.3 Samples and analytical methods

5.3.1 Cores and outcrops

This study focuses on four cores located in the Central Mackenzie Valley of the NWT and five outcrops situated in the adjacent Mackenzie Mountains (NWT). The core and outcrop locations are displayed in Figure 5.2 and summarized in Appendix 3 SI Table 3.1. The four cores are from (1) the MGM Shell East Mackay I-78 well (hereafter referred to as the I-78 core), (2) the Husky Little Bear N-09 well (hereafter referred to as the N-09 core), (3) the ConocoPhillips Mirror Lake N-20 (N-20 core), and (4) the ConocoPhillips Loon Creek O-06 well (O-06 core). The five outcrops are located along the banks of Carcajou River, Dodo Creek, Mountain River, Powell Creek, and Rumbly Creek, respectively and will be referred to according to those geographic names (Fig. 5.2).

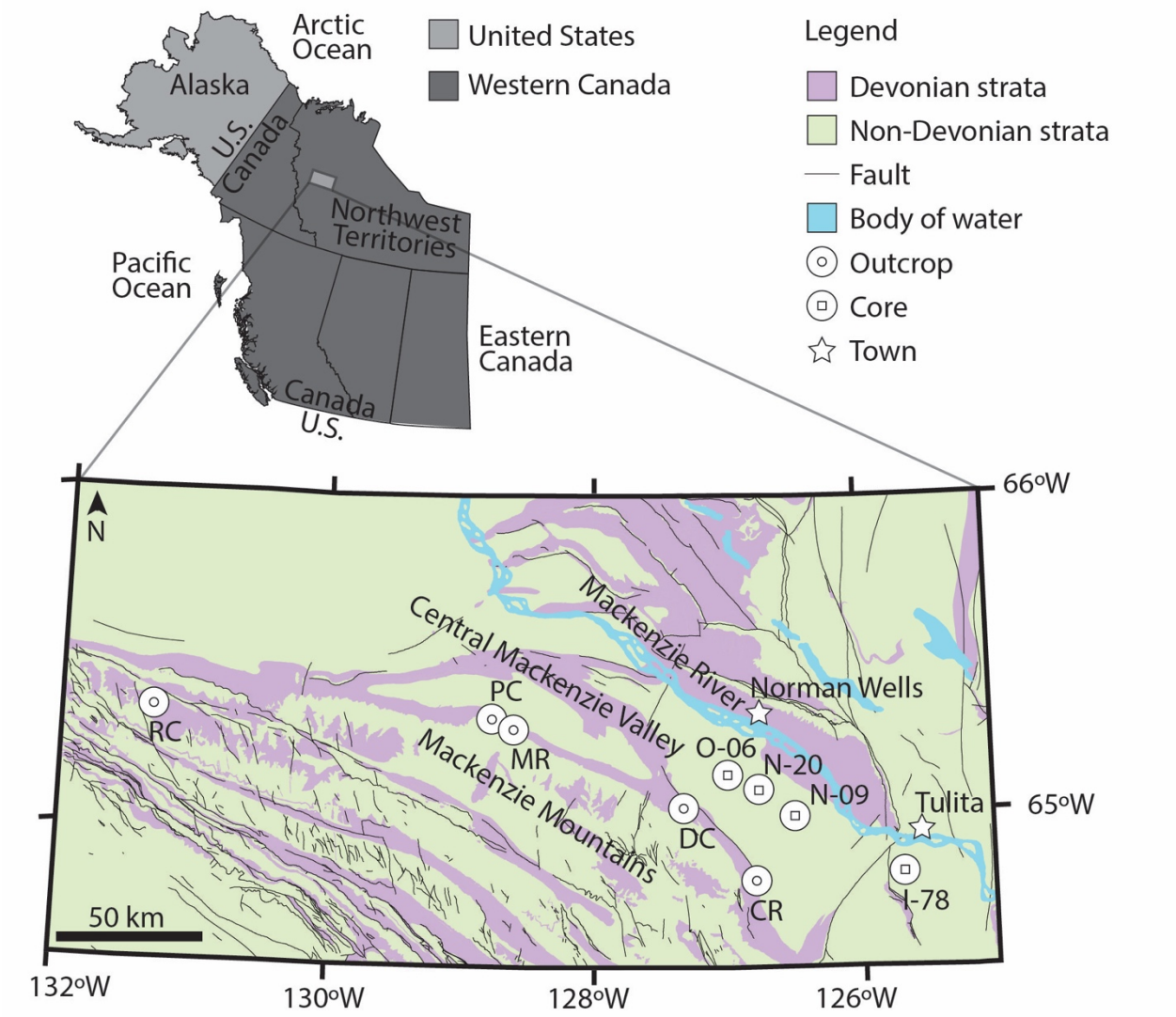

Figure 5.2 Geological map of the study area showing the locations of cores and outcrops in the Central Mackenzie Valley and Mackenzie Mountains of the Northwest Territories (NWT), Canada. Modified from Irwin (2020). Abbreviations: CR – Carcajou River, DC – Dodo Creek, MR – Mountain River, PC – Powell Creek, and RC – Rumbly Creek.

The I-78 core includes the uppermost Hume Formation, the Hare Indian Formation, and the Canol Formation. In the I-78 core, the interval of the Horn River Group from 1938 m to 1873.2 m (upper Hare Indian Formation and lower Canol Formation) was not cored and the

lithostratigraphic contacts in this interval were inferred based on thicknesses from the adjacent N-09 core. The N-09, N-20, and O-06 cores comprise the uppermost Hume Formation, the Hare Indian and Canol Formations in their entirety, and the lower portion of the Imperial Formation. At the Carcajou River outcrop, only the Canol Formation and Imperial Formation were accessible for sampling, and the lower Canol Formation contact with the underlying Hare Indian Formation could not be sampled. The Ramparts Formation is present at the Powell Creek outcrop and most of this formation was accessible to sample aside from the lowermost portion and contact with the underlying Hare Indian Formation. The Canol Formation and Imperial Formation were also accessible at Powell Creek except for a 20 m interval at the top of the Canol Formation and the base of the Imperial Formation, including the contact, which is inferred. The Canol Formation and Imperial Formation were sampled at Dodo Creek, but the basal contact of the Canol Formation and the underlying Hare Indian Formation were not accessible. The Ramparts Formation is also present at the Mountain River outcrop. The uppermost Hume Formation, the Ramparts and Canol Formations, and the lowermost Imperial Formation were sampled in their entirety at Mountain River. For the Hare Indian Formation, the Bluefish Member was accessible, however, a 15 m interval of the Bell Creek Member from 32.5 m to 47.5 m was covered and thus not accessible for sampling. Finally, at Rumbly Creek, only 30 m of the Canol Formation was accessible for sampling.

5.3.2 Sedimentology

The cores were described with observations focusing on lithology, bedding, sedimentary structures, fossils, trace fossils, fissility, and composition. Core colour was described following the Munsell Geological Rock-Color Chart. Core observations were then synthesized to produce

lithofacies. Lithofacies nomenclature follows the scheme presented in Lazar et al. (2015), which names fine-grained sedimentary rocks by grain size and then applies modifiers to describe characteristics such as bedding, composition, fossil or trace fossil content, and colour.

5.3.3 Composition

TOC data were collected with a LECO Analyzer by Weatherford Laboratories for the I-78 and N-20 cores and by Core Laboratories Canada for the N-09 core. The mineralogical composition of the four cores was assessed through XRD. The XRD datasets from the N-09, N-20, and O-06 cores were collected by Core Laboratories Canada while the XRD dataset from the I-78 core is from Weatherford Laboratories. Methods for XRD analysis comprised sample pulverization, packing into aluminum sample holders, and then analysis with a copper-source Philips automated powder diffractometer. Semi-quantitative mineral abundance was determined using integrated peak areas and empirical reference intensity ratio factors. Elemental distributions with depth were assessed through X-ray fluorescence (XRF). Outcrop samples were collected at an interval of 0.1 m to 2 m, with higher resolution in intervals of greater interest (e.g., the Hare Indian and Canol Formations compared to the Imperial Formation). These samples were then pulverized and placed into sample capsules with a polypropylene film base. XRF measurements from the cores were collected every 0.1 m and the core was washed in the areas of analysis. Outcrop and core samples were then analyzed with a Niton XL3t XL3t XRF Analyzer for 180 seconds in the mining code. The analyzer was purged with helium during analysis to increase the detection of light elements. The United States Geological Survey Brush Creek Shale (SBC-1) was used as a reference material to monitor accuracy and precision. For each element, the measured mean, the error reported as two standard deviations from the mean (2σ), and certified

values for SBC-1 are presented in Table 3.1. Enrichment factors for a given element (X) are calculated according to Equation 1 (e.g., Brumsack, 2006; Tribovillard et al., 2006). In this study, we calculated enrichment factors for Mo and V and used the Post-Archean Average Australian Shale (PAAS) for the average shale values, which gives an average of 84,000 ppm Al, 1 ppm Mo, and 140 ppm V (Taylor and McLennan, 1985).

$$EF_X = (X/Al)_{sample}/(X/Al)_{average\ shale} \quad \text{(Eqn. 1)}$$

Gamma-ray profiles for the cored intervals were collected by the respective companies when the wells were drilled.

Table 5.1 Accuracy and precision for the X-ray fluorescence (XRF) dataset by element based on the United States Geological Survey Brush Creek Shale (SBC-1). Precision is reported as 2σ (two standard deviations from the mean).

Element	Standard	Measured mean	Measured 2σ	Certified value	Certified 2σ
Si (wt. %)	SBC-1	25	3	22.3	0.17
Al (wt. %)	SBC-1	12	2	11.1	0.08
K (wt. %)	SBC-1	3	0.3	2.86	0.02
Ca (wt. %)	SBC-1	2	0.3	2.11	0.02
Ti (wt. %)	SBC-1	0.6	0.05	0.513	0.006
V (ppm)	SBC-1	383	41	220	2.8
Fe (wt. %)	SBC-1	7	0.4	6.79	0.04
Zr (ppm)	SBC-1	120	9	134	3.2
Mo (ppm)	SBC-1	0.2	1	2.4	0.1
Mn (wt. %)	SBC-1	0.1	0.01	0.12	0.002

5.3.4 Multivariate statistics methods

Principal Component Analysis (PCA) was used to assess the covariance between elements in the Horn River Group. Starting with a data matrix, this type of multivariate statistical analysis extracts the directions along which the dataset varies most, called principal components (James et al., 2013). Data points (observations) and variables can be viewed graphically in relation to the principal components, which illustrates their inter-relationships. In our study, highly skewed variables (Ca, Fe, Mo, V, Zr) were first log-transformed. Next, the prcomp() function of R was used for PCA of the dataset.

We considered nine elements as chemostratigraphic proxies: Al, Ca, Fe, K, Mo, Si, Ti, Zr, and V. In mudstone units, the elements often associated with detrital sediment include Al, Fe, K, Ti, and Zr (e.g., Ratcliffe et al., 2012a; Sano et al., 2013). Vanadium and molybdenum are redox-sensitive trace metals that become enriched under reducing conditions and their abundance is commonly used as a proxy for paleoredox conditions (e.g., Algeo and Liu, 2020; Tribovillard et al., 2006). Ca is included here as a proxy for carbonate mineral content and Si is considered as a proxy for quartz and aluminosilicate content. Multivariate statistical analysis (PCA) was used to illustrate the relationships between these nine elements. The PCA results were then used to select specific elements and ratios for sequence stratigraphic analysis.

5.3.5 Sequence stratigraphic nomenclature and framework

Sequence stratigraphic surfaces in this study are defined as described in Catuneanu (2019). Herein, we use transgressive-regressive (T-R) sequences, which comprise the transgressive systems tract (TST) and the regressive systems tract (RST) with the maximum regressive surface (MRS) as a sequence boundary (e.g., Embry and Johannessen, 1993). A review by LaGrange et

al. (2020) summarized the chemostratigraphic expressions of the maximum regressive surface (MRS), maximum flooding surface (MFS), regressive systems tract (RST), and transgressive systems tract (TST) in organic-rich marine mudstone intervals (Table 5.2). We used the criteria presented in Table 5.2 to establish a sequence stratigraphic framework for the Horn River Group and lower Imperial Formation in the study area.

Table 5.2 Chemostratigraphic characteristics of the maximum flooding surface (MFS), maximum regressive surface (MRS), regressive systems tract (RST), and transgressive systems tract (TST) in organic-rich, marine mudstone units. References listed after each bullet point are from publications containing examples of the described chemostratigraphic signatures. Modified from LaGrange et al. (2020).

Surface or Systems Tract	Chemostratigraphic Signature
MFS	• Terrigenous sediment proxies: lowest abundance (proxies associated with both aluminosilicates and heavy minerals) [1, 2, 3] • Biogenic silica proxies: peak[2, 3]
MRS	• Terrigenous sediment proxies: highest abundance (proxies associated with both aluminosilicates and heavy minerals)[1, 3] • Biogenic silica proxies: lowest abundance[3]
TST	• Terrigenous sediment proxies: decreasing proxies for aluminosilicates[1, 2, 3, 4, 5] • Terrigenous sediment proxies: variable trends in elements associated with heavy minerals depending on the interval[2, 5] • Biogenic silica proxies: high levels[2, 3]

	• Terrigenous sediment proxies: increasing proxies for aluminosilicates[2, 4]
RST	• Terrigenous sediment proxies: variable trends for elements associated with heavy minerals depending on the interval[2, 4]

[1] Ratcliffe et al. (2012)b
[2] Turner et al. (2016)
[3] Harris et al. (2018)
[4] Ver Straeten et al. (2011)
[5] Hammes and Frébourg (2012)

5.4 Results

5.4.1 Sedimentological results

We identified seven lithofacies in the Horn River Group and the lowermost Imperial Formation in our study area, which are summarized in Table 5.3. XRD data were used to characterize the mineralogy of each lithofacies, which is summarized in Table 5.3. Representative lithofacies photographs are shown in Figure 5.3.

Table 5.3 Characteristics of the seven lithofacies identified in the Horn River Group and lowermost Imperial Formation in the I-78, N-09, N-20, and O-06 cores. Quartz, total clay, and carbonate are normalized to 100 wt %.

Description	**Mineralogical Proportions**	**Sedimentology and Accessories**	**Fossils and Bioturbation**
F1: Intercalated planar parallel laminated light grey Tentaculitid grainstone and dark grey mudstone	• No data	• Tentaculitid grainstone intercalated with dark grey planar parallel laminated mudstone • Planar parallel laminae common • Low fissility	• Tentaculitids in limestone beds and laminae • Bioturbation not observed at this scale

F2: Medium grey parallel- and wavy laminated calcareous to calcareous siliceous mudstone with grading	• Quartz: 5 – 31 %, average of 14 % • Carbonate: 46 – 89 %, average of 74 % • Total clay: 6 – 23 %, average of 12 % • n = 3	• Grading is common, with an upwards decrease in the abundance of carbonate grains • Most often sharp based • Soft-sediment deformation structures (ball and pillow structures, load casts occasionally present at base) • Wavy discontinuous non-parallel laminae are present as well as continuous and discontinuous planar parallel laminae • Cone-in-cone structures may be present • Non-fissile	• Tentaculitids • Bioturbation not observed at this scale
F3: Medium grey planar parallel-laminated calcareous to siliceous calcareous mudstone	• Quartz: 19 – 44 %, average 31 % • Carbonate: 29 – 76 %, average of 52 % • Total clay: 5 – 16 %, average of 16 % • n = 2	• Planar parallel laminae common • Stylolites common on bedding planes • Non-fissile	• None observed • Bioturbation not observed at this scale
F4: Brownish black continuous planar parallel-laminated siliceous mudstone with common calcareous/dolomitic laminae and cm-scale carbonate beds	• Quartz: 8 – 93 %, average of 74 % • Carbonate: 6 – 58 %, average of 20 % • Total clay: 6 – 58 %, average of 20 % • n = 118	• Common calcareous/dolomitic laminae or cm-scale limestone/dolostone beds • Common calcite/dolomite and pyrite nodules (often have both carbonate and pyrite in same nodule) • Stylolites common on bedding planes • Planar parallel laminae common • May also appear homogeneous • Pyrite streaks sometimes present • Low-moderate fissility	• Pyritized Tentaculitids are rarely observed on bedding planes • Bioturbation not observed at this scale
F5: Brownish black continuous planar parallel-laminated siliceous mudstone	• Quartz: 30 – 91 %, average of 63 % • Carbonate: 0 – 57 %, average of 8 % • Total clay: 7 – 51 %, average of 29 % • n = 33	• Planar parallel laminae common but sometimes also appears homogeneous • Abundant pyrite streaks • Pyrite nodules common • Occasional calcareous or dolomitic laminae • Rare limestone/dolostone nodules • Low-moderate fissility	• None observed • Bioturbation not observed at this scale
F6: Medium dark grey planar parallel laminated fissile argillaceous to siliceous intraclast-rich mudstone	• Quartz: 1 – 67 %, average of 42 % • Carbonate: 0 – 17 %, average of 4 % • Total clay: 30 – 99 %, average of 54 % • n = 14	• Occasional pyrite nodules • Moderate-high fissility • Planar parallel laminae are common • Intraclasts often present along laminae • Rare calcareous laminae	• Rare *Spathiocaris* fossils on bedding planes • Bioturbation not observed at this scale

F7: Medium grey homogenous appearing fissile argillaceous to siliceous mudstone with common fossil fragments	• Quartz: 28 – 71 %, average of 48 % • Carbonate: 0 – 14 %, average of 1 % • Total clay: 27 – 72 %, average of 51 %	• Often appears homogeneous but planar parallel laminae also present • Pyrite nodules common • Occasional dolomitic laminae or cm-scale beds • High fissility	• Fossil fragments/organic fragments (including *Spathiocaris*) common on bedding planes • Bioturbation not observed at this scale

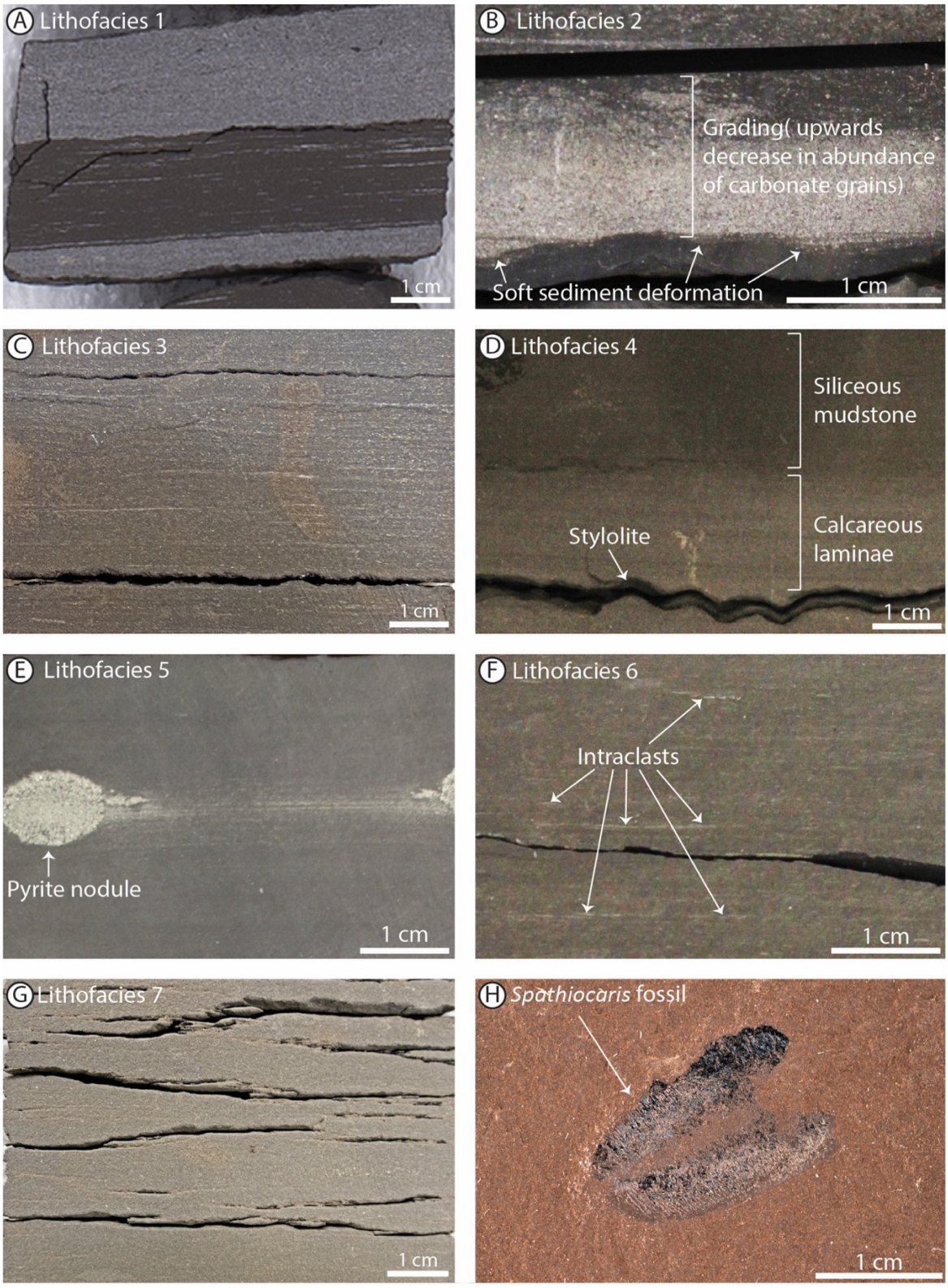

Figure 5.3 Photographs showing the seven lithofacies identified in the Horn River Group and overlying Imperial Formation of our studied cores: (A) Lithofacies 1 at a depth of 1823.3 m in

the Bluefish Member of the Hare Indian Formation in the N-09 core, (B) Lithofacies 2 in the O-06 core at 1787.1 m in the Francis Creek Member of the Hare Indian Formation, (C) Lithofacies 3 in the N-09 core at a depth of 1777.3 m in the Vermillion Creek Member of the Canol Formation, (D) Lithofacies 4 at 1749.2 m in the Vermillion Creek Member (Canol Formation) of the O-06 core, (E) Lithofacies 5 at 1677.7 m in the Dodo Canyon Member (Canol Formation) in the O-06 core, (F) Lithofacies 6 in the I-78 core at 1829.2 m in the Dodo Canyon Member of the Canol Formation, (F) Lithofacies 7 1696.3 m from the N-09 core in the Imperial Formation, (H) bedding image of Spathiocaris fossil at 1823.87 m in the I-78 core.

5.4.2 Multivariate statistics results

PCA results from the Horn River Group (Hare Indian, Canol, and Ramparts Formations) and the lowermost Imperial Formation are displayed in Figure 5.4. Principal component 1 (PC 1) explains 45.4 % of the variance in the Canol Formation dataset, 48.3 % of the variance in the Hare Indian Formation, 40 % in the Imperial Formation, and 75.2 % in the Ramparts Formation. Principal component 2 (PC 2) accounts for 27.4 %, 22.8 %, 26.8 %, and 9.8 % of the variance in the Canol, Hare Indian, Imperial, and Ramparts Formations datasets, respectively. In all four plots, Al, K, Ti, and Zr are clustered together (Fig. 5.4). In the Canol, Hare Indian, and Imperial Formations, Mo and V plot near one another, although in the Ramparts Formation, V plots with Al, K, Ti, and Zr rather than Mo (Fig. 5.4). Silicon is present in a similar zone to V and Mo in the Canol, Hare Indian, and Imperial Formations, but plots near Al, K, Ti, and Zr in the Ramparts Formation.

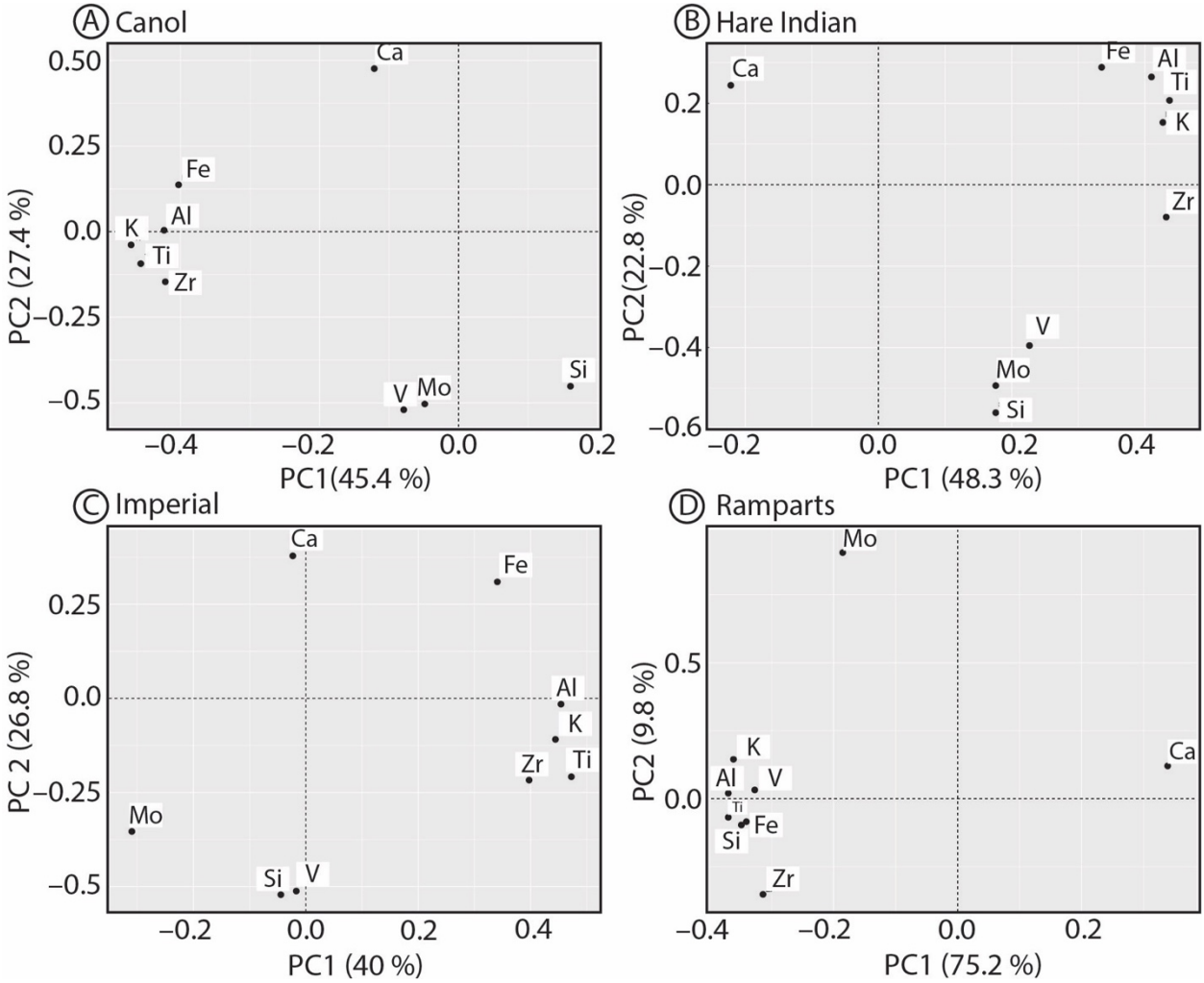

Figure 5.4 Principal Component Analysis results showing the covariance between elements from (A) the Canol Formation, (B) the Hare Indian Formation, (C) the Imperial Formation, and (D) the Ramparts Formation. Acronyms: PC – principal component.

5.4.3 Wireline, TOC, and chemostratigraphic results

The lithofacies distribution, gamma log (if available), TOC dataset (if available), and XRF results are presented for each outcrop and core in Figure 5.5 to 5.13. Only certain XRF chemostratigraphic proxies are presented in each figure because of spatial constraints. We include Al as a potential proxy for the abundance of aluminosilicate minerals (e.g., Piper and

Calvert, 2009). The ratio of Ti/Al is plotted to assess the relative abundance of heavy minerals compared to aluminosilicate minerals, which may vary with aeolian dust input (e.g., Wehausen and Brumsack, 1999) or changes in fluvial discharge (Sageman and Lyons, 2003). In Figure 5.4, K and Zr plot near Al and Ti, suggesting co-variance, and thus we do not display K and Zr because their general trends will match those of Al and Ti. The trends in Si are compared with those of Al to assess the presence of excess (non-aluminosilicate) Si, which is either aeolian, biogenic, or hydrothermal (e.g., Adachi et al., 1986; Sageman and Lyons, 2003). Finally, enrichment factors for Mo and V are displayed as proxies for paleoredox conditions (e.g., Algeo and Liu, 2020; Tribovillard et al., 2006).

Normalizing certain elements (e.g., Si, Ti, Mo, V) to Al can be useful for comparing their abundance to detrital aluminosilicate abundance. However, normalizing to Al can produce apparent correlations between unrelated elements, especially if the coefficient of variation (CV) for Al is large compared to that of the normalized elements (Van der Weijden, 2002). In our dataset, the CV of Al ranges from 25 % to 66 % depending on the core or outcrop, with an average of 47 % (Appendix 3 SI Table 3.2). This is similar to the CV for Ti (28 % to 74 %, average of 47 %) and lower than the CV for Mo (35 % to 174 %, average of 76 %) and V (37 % to 122 %, average of 66 %) and thus, these elements were normalized to Al for presentation in the results figures (Appendix 3 SI Table 3.2). Titanium was normalized directly to Al whereas Mo and V were normalized to Al and an average shale value (Equation 1). In contrast, the CV of Si ranges from 12 % to 54 %, with an average of 28 % (Appendix 3 SI Table 3.2) and thus, it was not normalized Al. Instead, we identify intervals of excess Si by comparing the trends in Si and Al.

In the cores of the Central Mackenzie Valley (Figures 5.5 to 5.8), trends in Si and Al are similar in the Hume Formation but opposite to one another in the Hare Indian, Canol, and Imperial Formations. The Ti/Al profile shows little variation in the cores aside from a spike at the top of the Hume Formation (Fig. 5.5 to 5.8). Vanadium and molybdenum enrichment factors (EFV and EF Mo) show similar patterns to each other, both with spikes in enrichment at or near the same depths (Fig. 5.5 to 5.8). TOC ranges from 0.1 wt. % to 9.2 wt. % in the I-78 core (Fig. 5.5), 1.5 wt. % to 8.6 wt. % in the N-09 core (Fig. 5.6), and 0.2 wt. % to 7.5 wt. % in the N-20 core (Fig. 5.7). Similarly to the cores, the outcrops from the Mackenzie Mountains are characterized by opposite trends in Si and Al for the Hare Indian, Canol, and Imperial Formations (Fig. 5.9 to 5.13). The Ramparts Formation is present at Mountain River and Powell Creek outcrops and this formation is characterized by variability in Si and Al, which show a similar overall pattern to one another (Fig. 5.11 and 5.12). Ti/Al shows very little change in the outcrop sections, aside for a spike in the lower Canol Formation at Powell Creek, which contains limestone turbidites, originating from the Kee Scarp Member reefs (Mackenzie, 1970) and sometimes referred to as the informal allochthonous limestone unit. The enrichment factors for V and Mo generally mirror one another in all outcrops (Fig. 5.9 to 5.13).

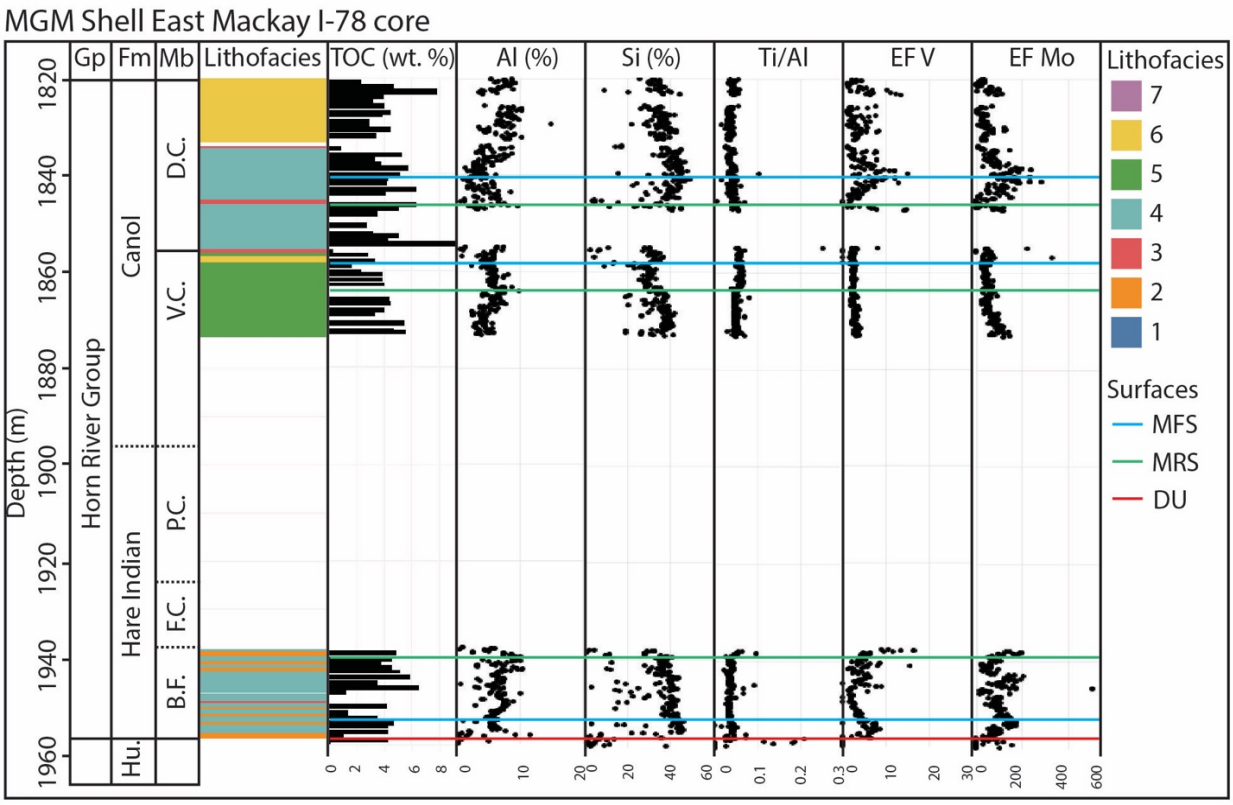

Figure 5.5 Lithofacies, total organic carbon (TOC), and x-ray fluorescence (XRF) geochemical results for the MGM Shell East Mackay I-78 core. Acronyms and abbreviations: D.C. – Dodo Canyon, DU – drowning unconformity, B.F. – Bluefish, EF V – V enrichment factor, EF Mo – Mo enrichment factor, F.C. – Francis Creek, Fm – Formation, Gp – group, Hu. – Hume, Mb – Member, MFS – maximum flooding surface, MRS – maximum regressive surface, P.C. – Powell Creek, TOC – total organic carbon, and V.C. – Vermillion Creek.

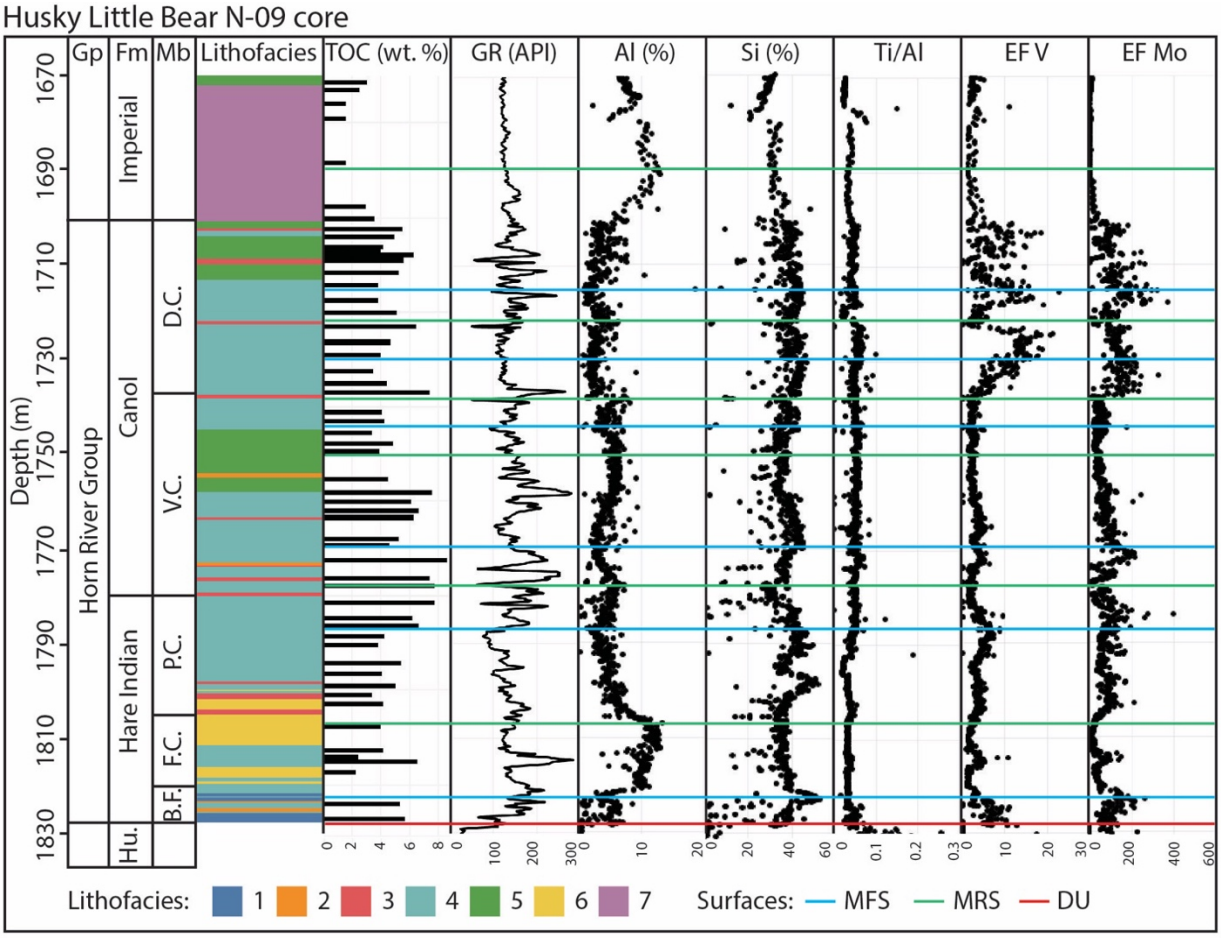

Figure 5.6 Lithofacies, total organic carbon (TOC), gamma-ray log, and x-ray fluorescence (XRF) results for the Husky Little Bear N-09 core. Acronyms and abbreviations: B.F. – Bluefish, D.C. – Dodo Canyon, DU – drowning unconformity, EF V – V enrichment factor, EF Mo – Mo enrichment factor, F.C. – Francis Creek, Fm – Formation, Gp – group, GR – gamma ray, Hu. – Hume, Mb – Member, MFS – maximum flooding surface, MRS – maximum regressive surface, P.C. – Powell Creek, TOC – total organic carbon, and V.C. – Vermillion Creek.

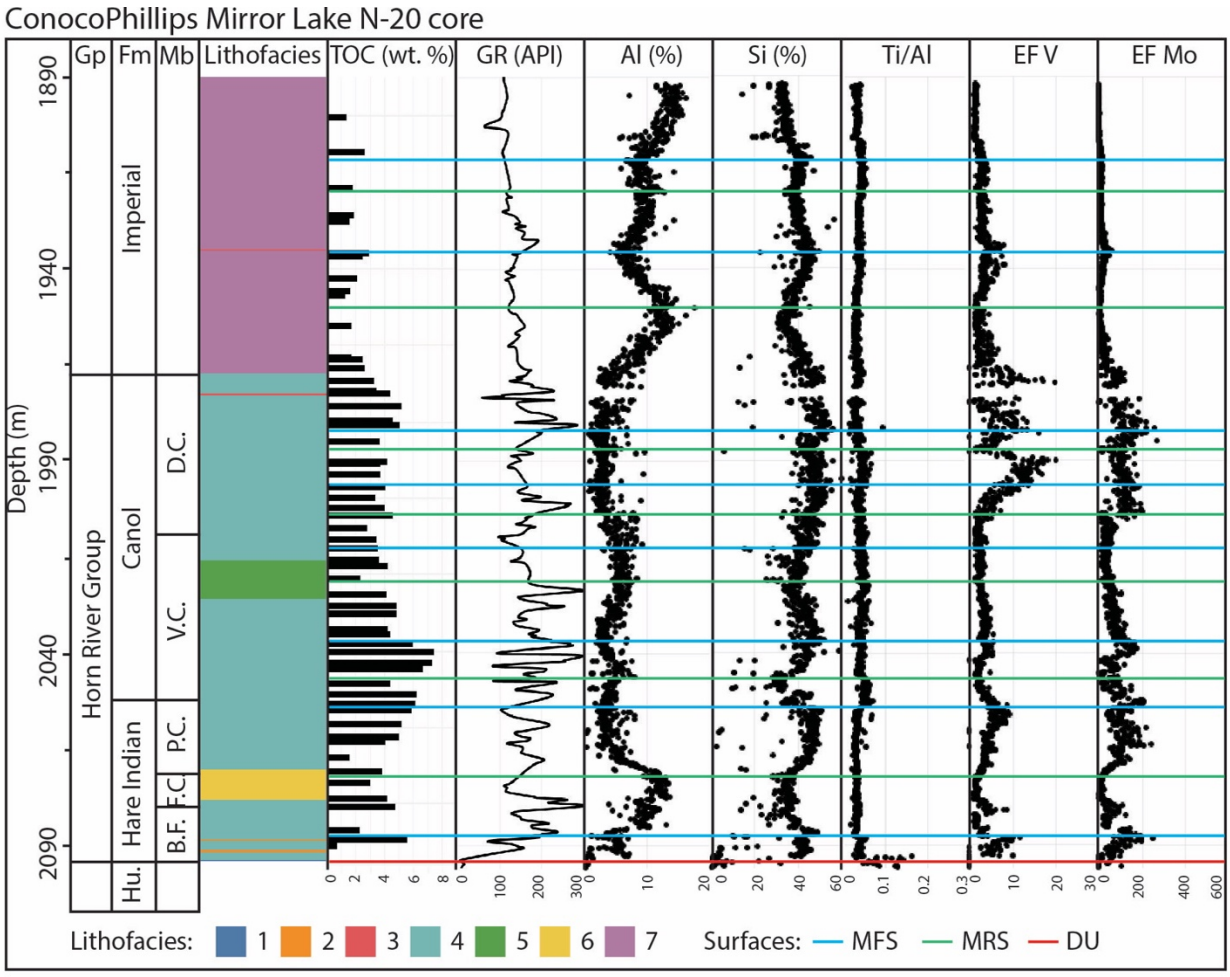

Figure 5.7 Lithofacies, total organic carbon (TOC), gamma ray log, and x-ray fluorescence (XRF) results for the ConocoPhillips Mirror Lake N-20 core. Acronyms and abbreviations: B.F. – Bluefish, D.C. – Dodo Canyon, DU – drowning unconformity, EF V – V enrichment factor, EF Mo – Mo enrichment factor, F.C. – Francis Creek, Fm – Formation, Gp – group, GR – gamma ray, Hu. – Hume, Mb – Member, MFS – maximum flooding surface, MRS – maximum regressive surface, P.C. – Powell Creek, TOC – total organic carbon, and V.C. – Vermillion Creek.

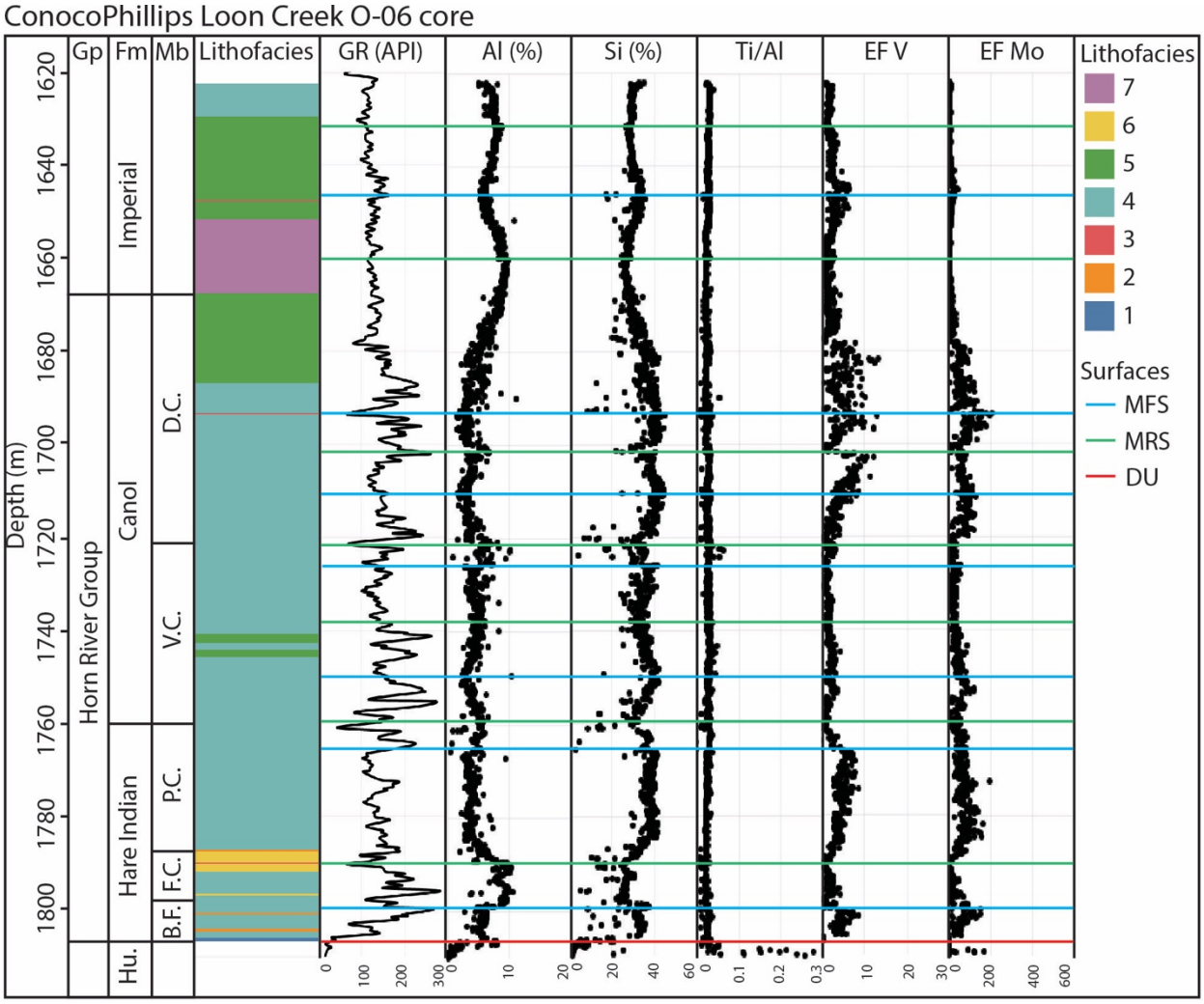

Figure 5.8 Lithofacies, gamma ray log, and x-ray fluorescence (XRF) results for the ConocoPhillips Loon Creek O-06 core. Acronyms and abbreviations: B.F. – Bluefish, D.C. – Dodo Canyon, DU – drowning unconformity, EF V – V enrichment factor, EF Mo – Mo enrichment factor, F.C. – Francis Creek, Fm – Formation, Gp – group, GR – gamma ray, Hu. – Hume, Mb – Member, MFS – maximum flooding surface, MRS – maximum regressive surface, P.C. – Powell Creek, and V.C. – Vermillion Creek.

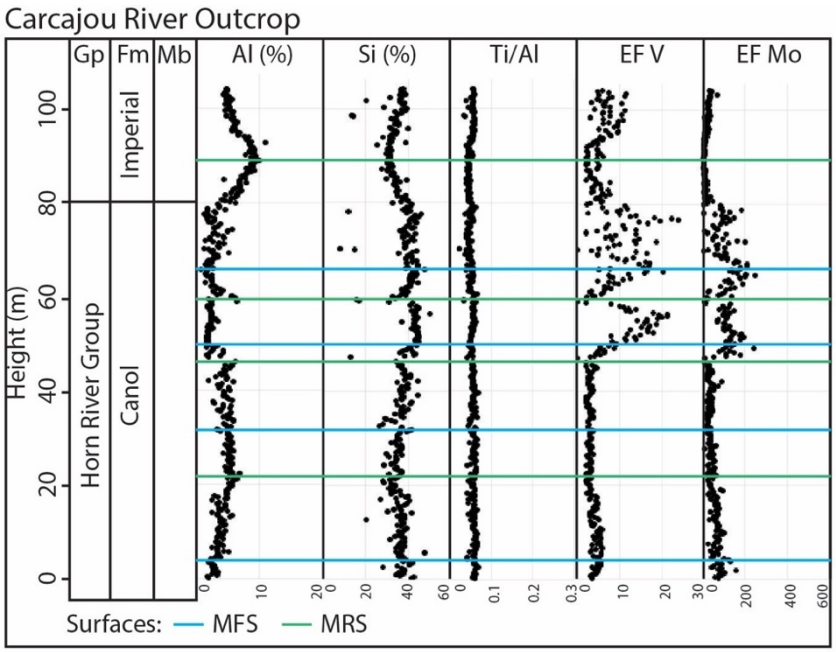

Figure 5.9 X-ray fluorescence (XRF) results from the Carcajou River outcrop. Acronyms and abbreviations: EF V – V enrichment factor, EF Mo – Mo enrichment factor, Fm – Formation, Gp – group, Mb – Member, MFS – maximum flooding surface, and MRS – maximum regressive surface.

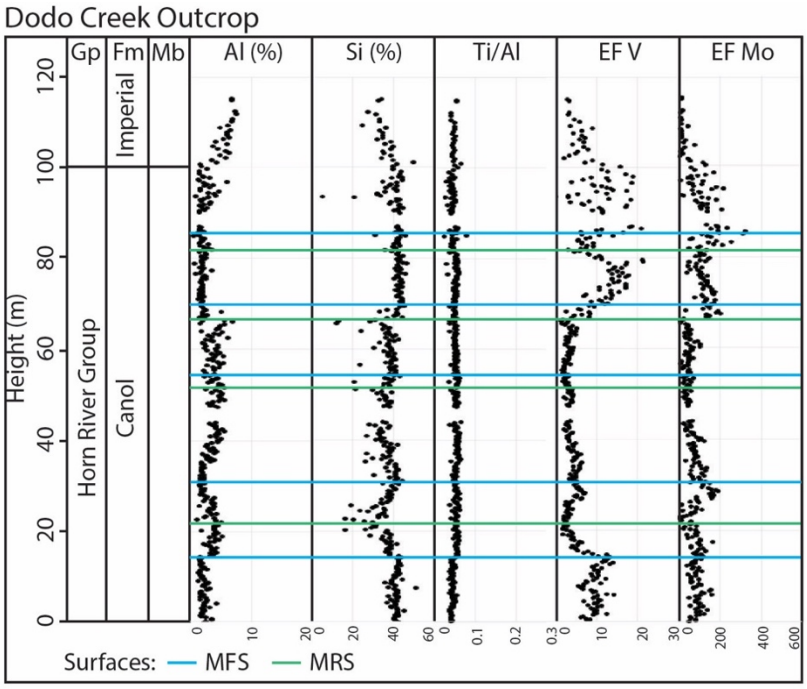

Figure 5.10 X-ray fluorescence (XRF) results from the Dodo Creek outcrop. Acronyms and abbreviations: EF V – V enrichment factor, EF Mo – Mo enrichment factor, Fm – Formation, Gp – group, Mb – Member, MFS – maximum flooding surface, and MRS – maximum regressive surface.

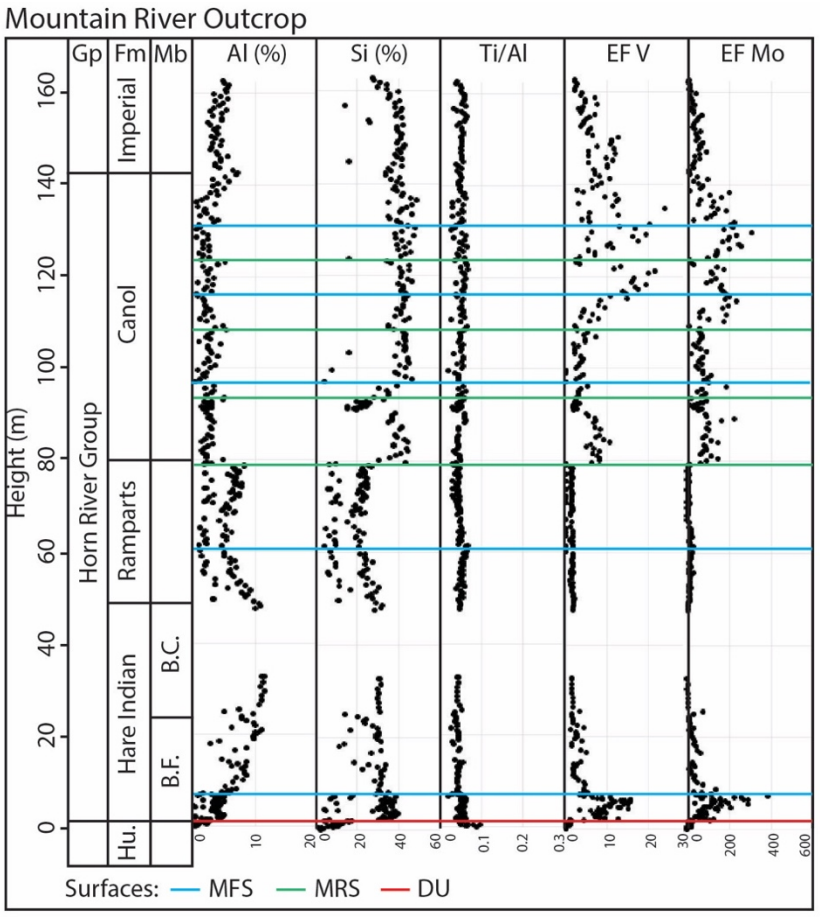

Figure 5.11 X-ray fluorescence (XRF) results from the Mountain River outcrop. Acronyms and abbreviations: B.C. – Bell Creek, B.F. – Bluefish, DU – drowning unconformity, EF V – V enrichment factor, EF Mo – Mo enrichment factor, Fm – Formation, Gp – group, Hu. – Hume, Mb – Member, MFS – maximum flooding surface, and MRS – maximum regressive surface.

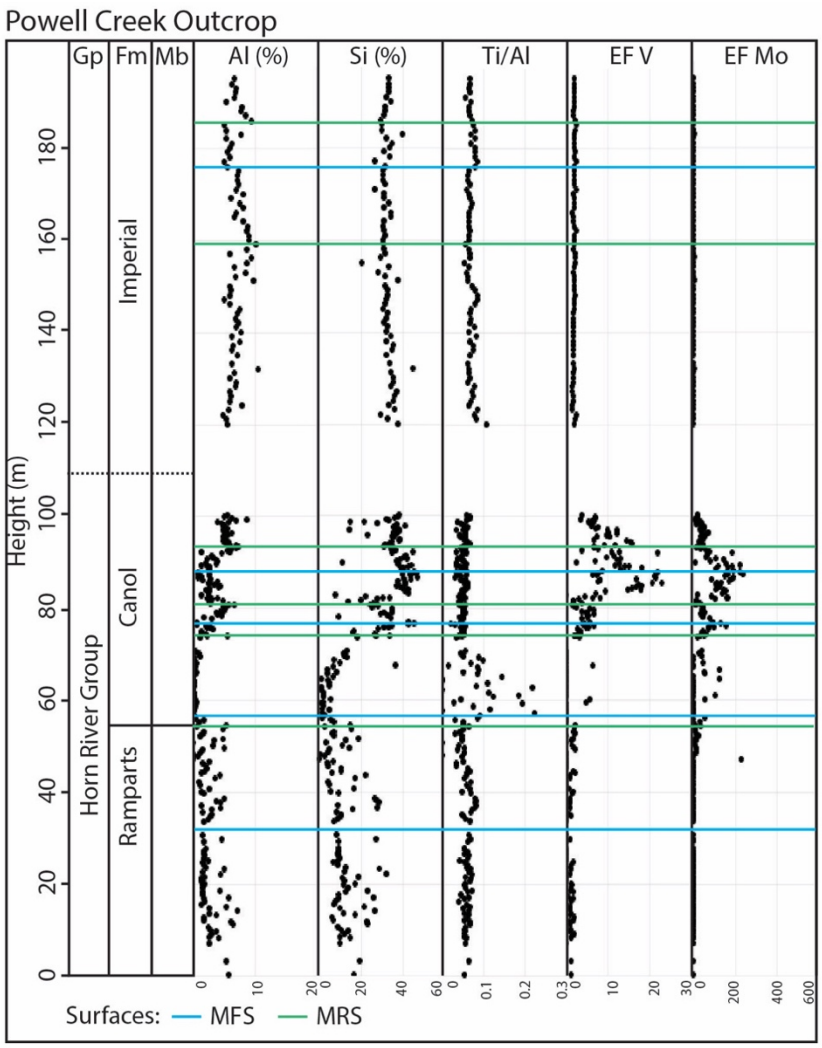

Figure 5.12 X-ray fluorescence (XRF) results from the Powell River outcrop. Acronyms and abbreviations: EF V – V enrichment factor, EF Mo – Mo enrichment factor, Fm – Formation, Gp – group, Mb – Member, MFS – maximum flooding surface, and MRS – maximum regressive surface.

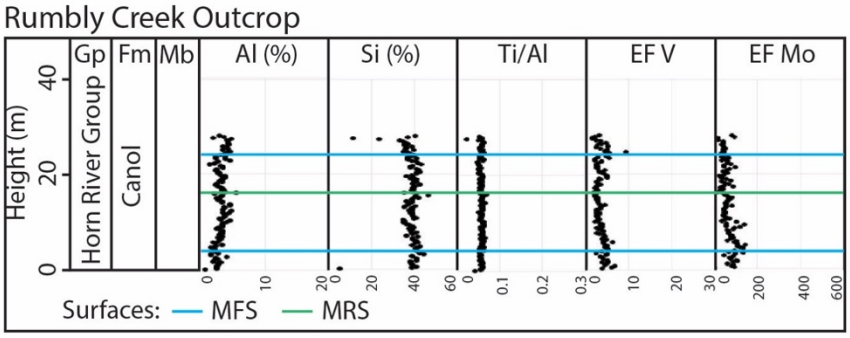

Figure 5.13 X-ray fluorescence (XRF) results from the Rumbly Creek outcrop. Acronyms and abbreviations: B.C. – Bell Creek, B.F. – Bluefish, EF V – V enrichment factor, EF Mo – Mo enrichment factor, Fm – Formation, Gp – group, Mb – Member, MFS – maximum flooding surface, and MRS – maximum regressive surface.

5.5 Discussion

5.5.1 Chemostratigraphic proxies

Aluminum is highest in lithofacies 7 and 8, which have the highest average clay mineral abundance of the seven lithofacies (Fig. 5.5 to 5.8; Table 5.3), lending support to the use of Al as a proxy for terrigenous sediment supply. The overall lack of variability in the Ti to Al ratio throughout the Horn River Group and Imperial Formation suggests that the abundance of Ti varies alongside the abundance of aluminosilicates, without instances of significantly increased or decreased heavy minerals compared to aluminosilicate supply. The Hare Indian, Canol, and Imperial Formations contain highs in Si that correspond to lows in Al, interpreted to contain 'excess silica' from: (1) aeolian, (2) hydrothermal, or (3) biogenic sources (e.g., Adachi et al., 1986; Sageman and Lyons, 2003). First, marine sediments that contain a higher windblown fraction can be characterized by higher ratios of Si/Al, Ti/Al, Zr/Al because quartz, rutile, and zircon are more resistant to weathering than clay minerals (Brumsack, 2006; Wehausen and

Brumsack, 1999). The excess Si peaks in the Horn River Group and Imperial Formation are not accompanied by peaks in Ti/Al and as such, we dismiss the possibility that this excess Si is derived from aeolian input. Secondly, excess silica may be hydrothermal in origin. Adachi et al. (1986) found that hydrothermal cherts could be distinguished from non-hydrothermal cherts and siliceous sediment through a Fe–Al–Mn ternary diagram. When all samples from the Hare Indian, Canol, and Imperial Formations are plotted onto this ternary diagram, most data falls in zone I (non-hydrothermal), with only a few data points falling into the zone II (hydrothermal), likely because these outlier samples contain a high proportion of sulphides (e.g., pyrite nodules). The excess silica in the Hare Indian, Canol, and Imperial Formations is thus best explained by the presence of biogenic silica derived from radiolarian tests, which are commonly observed in the Horn River Group (e.g., Biddle et al., 2021; Kabanov, 2019).

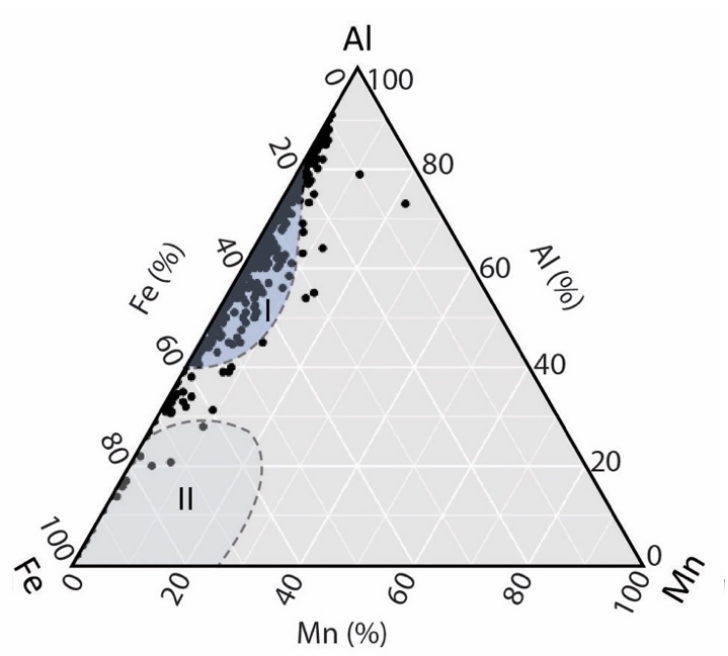

Figure 5.14 Fe – Al – Mn ternary diagram for all core and outcrop samples from the Hare Indian, Canol, and Imperial Formations. Field I represents non-hydrothermal cherts and siliceous rocks

whereas field II represents hydrothermal cherts and siliceous rocks. Modified from Adachi et al. (1986) and Arsairai et al. (2016).

5.5.2 Sequence stratigraphic interpretation

Maximum flooding surfaces and maximum regressive surfaces were interpreted using the criteria presented in Table 5.2. In the Hare Indian, Canol, and Imperial Formations, peaks in Si that do not correspond to peaks in Al are interpreted to represent intervals with a high proportion of excess (biogenic) Si, typically associated with maximum flooding surfaces. In the Ramparts Formation, trends in Si typically match those of Al (Fig. 5.4, 5.11, and 5.12) and the Si profile is interpreted the same way as the Al profile, as a proxy for terrigenous sediment. Sequence stratigraphic surfaces are marked on Figures 5.5 to 5.13 for each core and outcrop. Following previous authors (e.g., Kabanov, 2019; Morrow, 2018; Muir and Dixon, 1984), the transition from the Hume Formation to the Hare Indian Formation is interpreted as a drowning unconformity produced by relative sea-level rise and/or the spread of anoxic waters across the Hume carbonate platform. Figure 5.15 shows the correlation between outcrops and cores, moving approximately from northwest to southeast. Regressive systems tracts and transgressive systems tracts are interpreted following Table 5.2 and six complete transgressive-regressive (T-R) sequences are interpreted between the base of the Hare Indian Formation and the lowermost Imperial Formation (Fig. 5.15).

The T-R sequences range in thickness from approximately 10 m to 65 m with lateral thickness variations (Fig. 5.15). In most T-R cycles (with the exception of T-R cycle 2), the regressive portion of the T-R cycle (RST) is thicker than the transgressive portion (TST). Thickness variations within the same systems tract are attributed to differences in depositional

system. RST 1 is thickest at Mountain River outcrop, suggesting higher rates of sediment accumulation compared to the other sections, which is unsurprising given that at this location, RST 1 comprises the Bell Creek Member (distal deltaic mud banks), which is absent in the westward studied cores and outcrops (e.g., Kabanov and Deblonde, 2019; Pyle and Gal, 2016), probably because of lower proximity to the clastic sediment source. TST and RST 2 are also thickest at Powell Creek, where there is a thick succession of the Ramparts Formation carbonates, which likely experienced higher rates of sediment accumulation than in the off-bank areas where the other sections were deposited.

The lowermost portion of our sequence stratigraphic interpretation aligns with the previous framework for the Hare Indian Formation by Harris et al. (2021), with one complete T-R sequence identified in the basal Hare Indian Formation. Morrow (2018) interpreted Devonian T-R cycles on a basin-wide scale for the Northern Canadian Mainland Sedimentary Basin (north of 60 º and westward of the Canadian shield). T-R Cycle B of Morrow (2018) extends from the base of the Hume Formation to the top of the Hare Indian Formation, whereas T-R Cycle C extends from the top of the Hare Indian Formation into the Imperial Formation, with a maximum flooding surface in the Canol Formation (Morrow, 2018). Our results suggest that in our study area, higher-frequency T-R sequences are superimposed on the larger-scale basin-wide T-R sequences of Morrow (2018).

Visually, in the Hare Indian, Canol, and Imperial Formations, there are general patterns in the enrichment factors for V and Mo relative to sequence stratigraphic surfaces and systems tracts (Figs. 5 to 13). Maximum flooding surfaces are most often present at or just below peaks in EF V and EF Mo. Above the maximum flooding surfaces, EF V and EF Mo in RSTs typically display either a decreasing pattern or a peak followed by a decrease. Maximum regressive

surfaces often occur just below an increase in EF V and EF Mo with the TSTs above them characterized by increasing EF V and EF Mo moving upwards. Vanadium and molybdenum become more enriched in sediment under increasingly reducing conditions (Scott et al., 2017; e.g., Scott and Lyons, 2012). It follows that these trends in EF Mo and EF V are suggestive of most reducing sediment and/or bottom water conditions at or just after maximum flooding surfaces, followed by progressively less reducing conditions throughout the RST, and then a shift to more reducing conditions again after the maximum regressive surface in the TST. The observed pattern in redox conditions is also characteristic of an oceanographically open rather than restricted depositional setting (LaGrange et al., 2020), lending further support to the interpretation that the Middle to Late Devonian system of the study area was deposited in an unrestricted marine setting (e.g., Kabanov, 2019; Morrow, 2018). These observations also suggest that for the Hare Indian, Canol, and lower Imperial Formation depositional settings, paleoredox conditions varied alongside changes in the balance between relative sea level rise and sediment supply. The Ramparts Formation is not characterized by the same trends as those observed in the other formations of the Horn River Group or the Imperial Formation. Instead, very little enrichment of V and Mo is observed, without any clear changes in EF V or EF Mo alongside surfaces or systems tracts. The lack of V and Mo enrichment or trends may be explained by less reducing depositional conditions relative to the other formations, possibly from shallower water depths and/or oxygenated water entrained with material shed from the Kee Scarp Member reefs.

The balance between the rate of sedimentation and the rate of relative sea-level change determines whether a TST or RST will develop, with a higher rate of relative sea-level rise than sedimentation producing a TST. Regression (RST) may be produced either by relative sea-level

fall (forced regression) or sedimentation rate outpacing the rate of relative sea-level rise (normal regression). No evidence of subaerial exposure was observed in the platform and reef carbonates that comprise the Ramparts Formation of the Mackenzie Mountains (Muir, 1988) and Yose et al. (2001) interpreted a series of alternating TSTs and HSTs in the Ramparts Formation of the Norman Wells area in the Central Mackenzie Valley. Based on conodont biostratigraphy, the upper Hare Indian Formation and lower Canol Formation are time-equivalent to the Ramparts Formation (Kabanov and Gouwy, 2017, 2020), suggesting that at least in these portions of the Hare Indian and Canol Formations, the RSTs are likely HSTs. Unfortunately, because of limited age data throughout the Horn River Group, interpretation of the factors that controlled the balance between the rate of relative sea-level change and sedimentation (e.g., eustatic cycles or cycles in compressional tectonics along the northern margin of Ancestral North America) is not currently feasible.

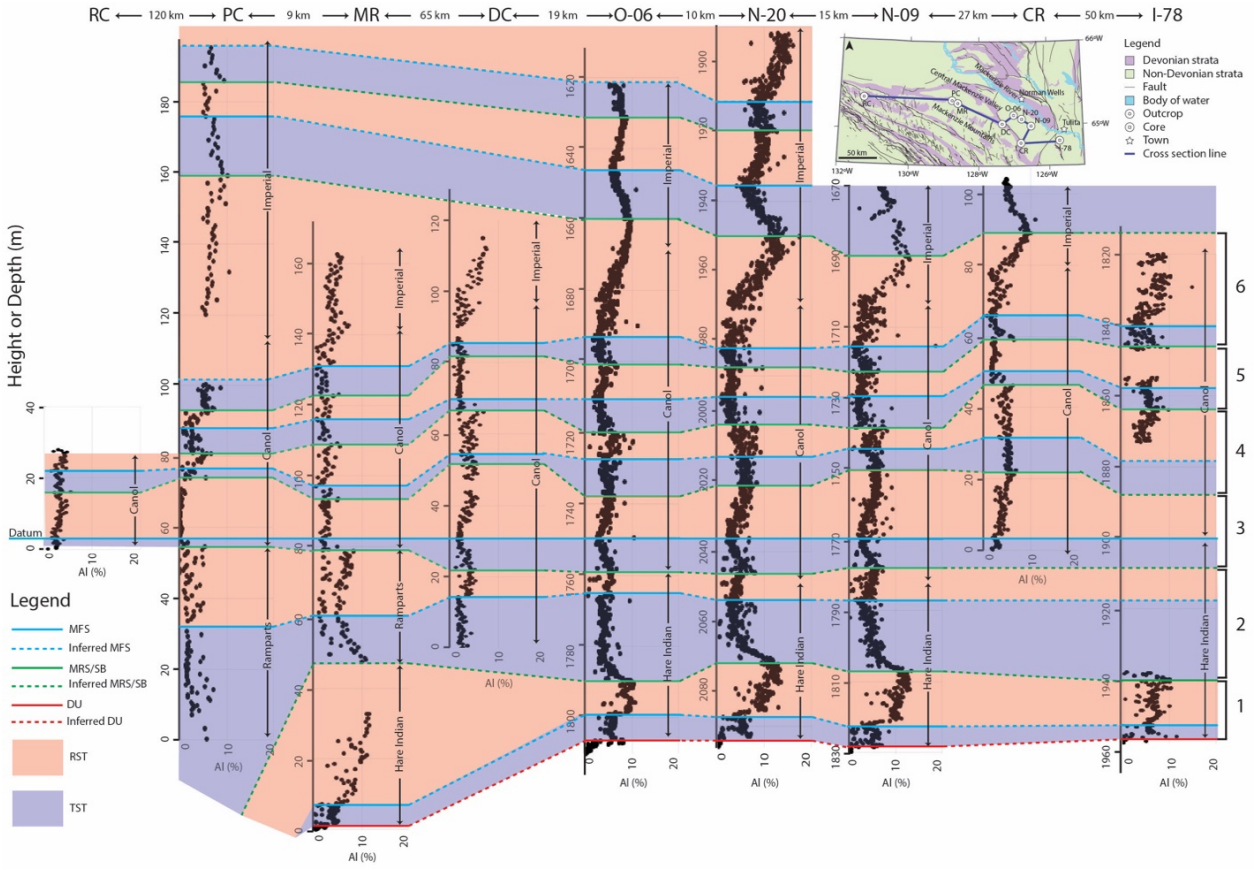

Figure 5.15 Sequence stratigraphic correlation of the Horn River Group (Hare Indian, Canol, and Ramparts Formations) and lower Imperial Formation from outcrops in the Mackenzie Mountains and cores from the Central Mackenzie Valley showing Al profiles in wt. %. Transgressive-regressive (T-R) sequences are numbered on the right side of the figure. Outcrop abbreviations: CR – Carcajou River, DC – Dodo Creek, MR – Mountain River, PC – Powell Creek, and RC – Rumbly Creek. Other acronyms and abbreviations: DU – drowning unconformity, MFS – maximum flooding surface, MRS – maximum regressive surface, RST.

5.5.3 Pitfalls

At the core-scale, the mudstone lithofacies observed are of limited use for the interpretation of shifts in depositional system because variations between lithofacies are generally minimal, with a

lack of diversity of in sedimentary structures and no clear grain size variations or bioturbation observed at this scale. In outcrops, weathering makes sedimentological variations in the mudstone units even more difficult to discern. Unfortunately, this means that the proximal versus distal shifts interpreted from chemostratigraphic terrigenous sediment proxies cannot be supported by lithofacies interpretations. A second pitfalls lies in the use of the RST, which amalgamates both normal and forced regressive strata. The RST is used in this work because chemostratigraphic criteria do not exist to identify the basal surface of forced regression or correlative conformity (LaGrange et al., 2022). In coarser-grained clastic successions or mixed clastic-carbonate intervals deposited in shelf settings, subtle lithological changes characterize these two surfaces (e.g., Catuneanu, 2019), however, the overall lithological homogeneity of the Horn River Group mudstone succession at the core and outcrop scale does not allow for the identification of these surfaces. Use of the RST means that periods of relative sea-level fall cannot be distinguished from times when sediment supply outpaced relative sea-level rise. Finally, the Rumbly Creek section is located 120 km west of the nearest outcrop (Powell Creek) and only the lowermost 30 m of the Canol Formation was accessible for sampling, making correlation with the other sections difficult. The chemostratigraphic profiles paired with the lithostratigraphic interpretation suggest that this section was deposited as part of sequences 3 and 4, however, we are less confident in this interpretation compared to other outcrops and cores because of the highly incomplete nature of the section and the distance to the nearest outcrop.

5.6 Conclusions

Chemostratigraphic proxies were used to establish a high-resolution sequence stratigraphic framework for the Horn River Group of the west central NWT spanning four cores in the Central

Mackenzie Valley and five outcrops in the Mackenzie Mountains. This framework shows that six T-R sequences are present from the base of the Hare Indian Formation to the lowermost Imperial Formation. Moreover, enrichment factors for V and Mo show patterns relative to proxies for terrigenous sediment and biogenic silica, interpreted to reflect most reducing sediment and/or bottom water conditions at or just after maximum flooding surfaces and suggesting a link between fluctuations in paleoredox and the balance between sediment supply and relative-sea level change. Through this framework, we also facilitate the prediction and mapping of higher quality reservoir intervals (associated with biogenic silica-rich maximum flooding surfaces) in the Bluefish Member and Canol Formation between wells in the Central Mackenzie Valley and provide the first non-lithostratigraphic correlation between the Horn River Group in the subsurface and in outcrop. Finally, this study serves as an example of the application of chemostratigraphy to sequence stratigraphic analyses in fine-grained sedimentary intervals. Future work involves integration of these results with the thin-section based depositional model of Biddle et al. (2021) for the Horn River Group mudstones to support and verify interpreted stacking patterns and systems tracts. Furthermore, conodont data suggests that the upper Hare Indian Formation and lower Canol Formation are time-equivalent to the Ramparts Formation (Kabanov and Gouwy, 2017), although correlations are at a low resolution. If in the future, a means of high-resolution correlation between the mudstones and the reef carbonates is established (possibly through stable C or Mo isotopes), subsequent work could consider whether T-R cycles in the upper Hare Indian and lower Canol Formation coincide with the previously interpreted cycles in the Kee Scarp Member of the Ramparts Formation.

5.7 Acknowledgments

We would like to thank John Duke for providing guidance related to X-ray fluorescence methods and for sharing with us the USGS Brush Creek (SBC-1) standard. These authors are also grateful to everyone who helped with the powdering of outcrop samples, including Skye Lybbert, Nicole Atienza, Rizal Ignacio, Marcus Kehler, Sheridan Sigstad, Adam Lariviere, and Daniel Baker. We also thank Devon Frayn for help with data collection and Dave Herbers for helpful discussions related to the Horn River Group and chemostratigraphy. Finally, we are appreciative of the project funding provided by the Northwest Territories Geological Survey.

5.8 References

Adachi, M., Yamamoto, K., Sugisaki, R., 1986. Hydrothermal chert and associated siliceous rocks from the northern Pacific their geological significance as indication of ocean ridge activity. Sediment. Geol. 47, 125–148. https://doi.org/10.1016/0037-0738(86)90075-8

Ader, M., Thomazo, C., Sansjofre, P., Busigny, V., Papineau, D., Laffont, R., Cartigny, P., Halverson, G.P., 2016. Interpretation of the nitrogen isotopic composition of Precambrian sedimentary rocks: Assumptions and perspectives. Chem. Geol. 429, 93–110. https://doi.org/10.1016/j.chemgeo.2016.02.010

Al-Aasm, I.S., Morad, S., Durocher, S., Muir, I., 1996. Sedimentology, C–S–Fe relationships and stable isotopic compositions in Devonian black mudrocks, Mackenzie Mountains, Northwest Territories, Canada. Sediment. Geol. 106, 279–298. https://doi.org/10.1016/S0037-0738(96)00018-8

Algeo, T.J., Liu, J., 2020. A re-assessment of elemental proxies for paleoredox analysis. Chem. Geol. 540, 119549. https://doi.org/10.1016/j.chemgeo.2020.119549

Algeo, T.J., Meyers, P.A., Robinson, R.S., Rowe, H., Jiang, G.Q., 2014. Icehouse–greenhouse variations in marine denitrification. Biogeosciences 11, 1273–1295. https://doi.org/10.5194/bg-11-1273-2014

Algeo, T.J., Scheckler, S.E., 1998. Terrestrial-marine teleconnections in the Devonian: links between the evolution of land plants, weathering processes, and marine anoxic events. Phil. Trans. R. Soc. Lond. B 353, 113–130. https://doi.org/10.1098/rstb.1998.0195

Altabet, M.A., Pilskaln, C., Thunell, R., Pride, C., Sigman, D., Chavez, F., Francois, R., 1999. The nitrogen isotope biogeochemistry of sinking particles from the margin of the Eastern North Pacific. Deep Sea Res. Part I: Oceanogr. Res. Pap. 46, 655–679. https://doi.org/10.1016/S0967-0637(98)00084-3

Arsairai, B., Wannakomol, A., Feng, Q., Chonglakmani, C., 2016. Paleoproductivity and paleoredox condition of the Huai Hin Lat Formation in northeastern Thailand. J. Earth Sci. 27, 350–364. https://doi.org/10.1007/s12583-016-0666-8

Astor, Y., Muller-Karger, F., Scranton, M.I., 2003. Seasonal and interannual variation in the hydrography of the Cariaco Basin: implications for basin ventilation. Cont. Shelf Res. 23, 125–144. https://doi.org/10.1016/S0278-4343(02)00130-9

Averbuch, O., Tribovillard, N., Devleeschouwer, X., Riquier, L., Mistiaen, B., Van Vliet-Lanoe, B., 2005. Mountain building-enhanced continental weathering and organic carbon burial as major causes for climatic cooling at the Frasnian–Famennian boundary (c. 376 Ma)? Terra Nova 17, 25–34. https://doi.org/10.1111/j.1365-3121.2004.00580.x

Bauersachs, T., Schouten, S., Compaoré, J., Wollenzien, U., Stal, L.J., Sinninghe Damsteé, J.S., 2009. Nitrogen isotopic fractionation associated with growth on dinitrogen gas and nitrate

by cyanobacteria. Limnol. Oceanogr. 54, 1403–1411. https://doi.org/10.4319/lo.2009.54.4.1403

Becker, R.T., Marshall, J.E.A., Da Silva, A.-C., Agterberg, F.P., Gradstein, F. M., Ogg, J. G., 2020. Chapter 22 - The Devonian Period, in: Gradstein, Felix M., Ogg, James G., Schmitz, M.D., Ogg, G.M. (Eds.), Geologic Time Scale 2020. Elsevier, pp. 733–810. https://doi.org/10.1016/B978-0-12-824360-2.00022-X

Benner, R., Fogel, M.L., Sprague, E.K., Hodson, R.E., 1987. Depletion of 13C in lignin and its implications for stable carbon isotope studies. Nature 329, 708–710. https://doi.org/10.1038/329708a0

Beranek, L.P., Mortensen, J.K., Lane, L.S., Allen, T.L., Fraser, T.A., Hadlari, T., Zantvoort, W.G., 2010. Detrital zircon geochronology of the western Ellesmerian clastic wedge, northwestern Canada: Insights on Arctic tectonics and the evolution of the northern Cordilleran miogeocline. GSA Bulletin 122, 1899–1911. https://doi.org/10.1130/B30120.1

Biddle, S., 2020. A Fine Detail Physicochemical Depositional Model for Devonian Organic-Rich Mudstones: A Petrographic Study of the Hare Indian and Canol Formations, Central Mackenzie Valley, Northwest Territories. University of Alberta (Canada). https://doi.org/10.7939/r3-jacj-jp38

Biddle, S.K., LaGrange, M.T., Harris, B.S., Fiess, K., Terlaky, V., Gingras, M.K., 2021. A fine detail physico-chemical depositional model for Devonian organic-rich mudstones: A petrographic study of the Hare Indian and Canol Formations, Central Mackenzie Valley, Northwest Territories. Sediment. Geol. 414, 105838. https://doi.org/10.1016/j.sedgeo.2020.105838

Bottcher, M.E., Oelschlager, B., Hopner, T., Brumsack, H.-J., Rullkotter, J., 1998. Sulfate reduction related to the early diagenetic degradation of organic matter and "black spot'' formation in tidal sandflats of the German Wadden Sea (southern North Sea): stable isotope (13C, 34S, 18O) and other geochemical results. Org. Geochem. 29, 1517–1530.

Boudou, J.-P., Schimmelmann, A., Ader, M., Mastalerz, M., Sebilo, M., Gengembre, L., 2008. Organic nitrogen chemistry during low-grade metamorphism. Geochim. Cosmochim. Acta 72, 1199–1221. https://doi.org/10.1016/j.gca.2007.12.004

Brandes, J.A., Devol, A.H., 2002. A global marine-fixed nitrogen isotopic budget: Implications for Holocene nitrogen cycling. Glob. Biogeochem. Cycles 16, 67-1-67–14. https://doi.org/10.1029/2001GB001856

Brandes, J.A., Devol, A.H., Yoshinari, T., Jayakumar, D.A., Naqvi, S.W.A., 1998. Isotopic composition of nitrate in the central Arabian Sea and eastern tropical North Pacific: A tracer for mixing and nitrogen cycles. Limnol. and Oceanogr. 43, 1680–1689. https://doi.org/10.4319/lo.1998.43.7.1680

Brown, T., Kenig, F., 2004. Water column structure during deposition of Middle Devonian–Lower Mississippian black and green/gray shales of the Illinois and Michigan Basins: a biomarker approach. Palaeogeogr., Palaeoclimatol., Palaeoecol. 215, 59–85. https://doi.org/10.1016/S0031-0182(04)00452-3

Brumsack, H.-J., 2006. The trace metal content of recent organic carbon-rich sediments: Implications for Cretaceous black shale formation. Palaeogeogr., Palaeoclimatol., Palaeoecol. 232, 344–361. https://doi.org/10.1016/j.palaeo.2005.05.011

Burnham, A.K., Sweeney, J.J., 1989. A chemical kinetic model of vitrinite maturation and reflectance. Geochim. Cosmochim. Acta 53, 2649–2657. https://doi.org/10.1016/0016-7037(89)90136-1

Carmichael, S.K., Waters, J.A., Königshof, P., Suttner, T.J., Kido, E., 2019. Paleogeography and paleoenvironments of the Late Devonian Kellwasser event: A review of its sedimentological and geochemical expression. Glob. and Planet. Change 183, 102984. https://doi.org/10.1016/j.gloplacha.2019.102984

Carpenter, E.J., Harvey, H.R., Fry, B., Capone, D.G., 1997. Biogeochemical tracers of the marine cyanobacterium Trichodesmium. Deep Sea Res. Part I: Oceanogr. Res. Pap. 44, 27–38. https://doi.org/10.1016/S0967-0637(96)00091-X

Catuneanu, O., 2019. Model-independent sequence stratigraphy. Earth-Sci. Rev. 188, 312–388. https://doi.org/10.1016/j.earscirev.2018.09.017

Chen, F., Zhang, L., Yang, Y., Zhang, D., 2008. Chemical and isotopic alteration of organic matter during early diagenesis: Evidence from the coastal area off-shore the Pearl River estuary, south China. J. Mar. Syst. 74, 372–380. https://doi.org/10.1016/j.jmarsys.2008.02.004

Cheung, S., Xia, X., Guo, C., Liu, H., 2016. Diazotroph community structure in the deep oxygen minimum zone of the Costa Rica Dome. J. Plankton Res. 38, 380–391. https://doi.org/10.1093/plankt/fbw003

Cline, J.D., Kaplan, I.R., 1975. Isotopic fractionation of dissolved nitrate during denitrification in the eastern tropical north pacific ocean. Mar. Chem. 3, 271–299. https://doi.org/10.1016/0304-4203(75)90009-2

Cocks, L.R.M., Torsvik, T.H., 2011. The Palaeozoic geography of Laurentia and western Laurussia: A stable craton with mobile margins. Earth-Sci. Rev. 106, 1–51. https://doi.org/10.1016/j.earscirev.2011.01.007

Degens, E.T., Gullard, R.R., Sackett, W.M., Hellebust, J.A., 1968. Metabolic fractionation of carbon isotopes in marine plankton: 1. Temperature and respiration experiments. Deep-Sea Res. 15, 1–9. https://doi.org/10.1016/0011-7471(68)90024-7

Deutsch, C., Sarmiento, J.L., Sigman, D.M., Gruber, N., Dunne, J.P., 2007. Spatial coupling of nitrogen inputs and losses in the ocean. Nature 445, 163–167. https://doi.org/10.1038/nature05392

Dewing, K., Hadlari, T., Pearson, D.G., Matthews, W., 2019. Early Ordovician to Early Devonian tectonic development of the northern margin of Laurentia, Canadian Arctic Islands. GSA Bulletin 131, 1075–1094. https://doi.org/10.1130/B35017.1

Embry, A.F., Johannessen, E.P., 1993. T–R sequence stratigraphy, facies analysis and reservoir distribution in the uppermost Triassic–Lower Jurassic succession, western Sverdrup Basin, Arctic Canada, in: Vorren, T.O., Bergsager, E., Dahl-Stamnes, Ø.A., Holter, E., Johansen, B., Lie, E., Lund, T.B. (Eds.), Norwegian Petroleum Society Special Publications. Elsevier, pp. 121–146. https://doi.org/10.1016/B978-0-444-88943-0.50013-7

Emeis, K.-C., Whelan, J.K., Tarafa, M., 1991. Sedimentary and geochemical expressions of oxic and anoxic conditions on the Peru Shelf. Geological Society, London, Special Publications 58, 155–170. https://doi.org/10.1144/GSL.SP.1991.058.01.11

Emerson, S., Stump, C., Wilbur, D., Quay, P., 1999. Accurate measurement of O2, N2, and Ar gases in water and the solubility of N2. Mar. Chem. 64, 337–347. https://doi.org/10.1016/S0304-4203(98)00090-5

Falkowski, P.G., 1991. Species variability in the fractionation of 13C and 12C by marine phytoplankton. J. Phytoplank. Res. 13, 21–28.

Fernandez, C., Farías, L., Ulloa, O., 2011. Nitrogen Fixation in Denitrified Marine Waters. PLOS ONE 6, e20539. https://doi.org/10.1371/journal.pone.0020539

Fraser, T.A., Hutchison, M.P., 2017. Lithogeochemical characterization of the Middle–Upper Devonian Road River Group and Canol and Imperial formations on Trail River, east Richardson Mountains, Yukon: age constraints and a depositional model for fine-grained strata in the Lower Paleozoic Richardson trough. Can. J. Earth Sci. 54, 731–765. https://doi.org/10.1139/cjes-2016-0216

Freeman, K.H., 2001. Isotopic Biogeochemistry of Marine Organic Carbon. Rev. Mineral. Geochem. 43, 579–605. https://doi.org/10.2138/gsrmg.43.1.579

Freudenthal, T., Wagner, T., Wenzhöfer, F., Zabel, M., Wefer, G., 2001. Early diagenesis of organic matter from sediments of the eastern subtropical Atlantic: evidence from stable nitrogen and carbon isotopes. Geochim. Cosmochim. Acta 65, 1795–1808. https://doi.org/10.1016/S0016-7037(01)00554-3

Fritz, W.H., Cecile, M.P., Norford, B.S., Morrow, D., Geldsetzer, H.H.J., 1991. Cambrian to Middle Devonian Assemblages, in: Geology of the Cordilleran Orogen in Canada. Geological Society of America. https://doi.org/10.1130/DNAG-GNA-G2.151

Fry, B., Sherr, E.B., 1984. δ13C measurements as indicators of carbon flow in marine and freshwater ecosystems. Contrib. Marine Science 27, 13–47.

Gal, L.P., Pyle, L.J., Hadlari, T., Allen, T.L., 2009. Chapter 6: Lower to Upper Devonian strata, Arnica-Landry play, and Kee Scarp play, in: Pyle, L.J., Jones, A. (Eds.), Regional Geoscience Studies and Petroleum Potential, Peel Plateau and Plain, Northwest Territories and Yukon: Project Volume, Northwest Territories Geoscience Office and Yukon Geological Survey, NWT, Open File 2009-002 and Yukon Geological Survey Open File 2009-25.

Galimov, E.M., 2004. The pattern of δ13Corg versus HI/OI relation in recent sediments as an indicator of geochemical regime in marine basins: comparison of the Black Sea, Kara Sea, and Cariaco Trench. Chem. Geol. 204, 287–301. https://doi.org/10.1016/j.chemgeo.2003.11.014

Garzione, C.N., Patchett, P.J., Ross, G.M., Nelson, J., 1997. Provenance of Paleozoic sedimentary rocks in the Canadian Cordilleran miogeocline: a Nd isotopic study. Can. J. Earth Sci. 34, 1603–1618. https://doi.org/10.1139/e17-129

Gutiérrez, D., Enríquez, E., Purca, S., Quipúzcoa, L., Marquina, R., Flores, G., Graco, M., 2008. Oxygenation episodes on the continental shelf of central Peru: Remote forcing and benthic ecosystem response. Prog. Oceanogr. 79, 177–189. https://doi.org/10.1016/j.pocean.2008.10.025

Hadlari, T., 2015. Oil migration driven by exhumation of the Canol Formation oil shale: A new conceptual model for the Norman Wells oil field, northwestern Canada. Mar. Pet. Geol. 65, 172–177. https://doi.org/10.1016/j.marpetgeo.2015.03.027

Hadlari, T., Davis, W.J., Dewing, K., 2014. A pericratonic model for the Pearya terrane as an extension of the Franklinian margin of Laurentia, Canadian Arctic. Geol. Soc. Am. Bull. 126, 182–200. https://doi.org/10.1130/B30843.1

Hadlari, T., MacLean, B.C., Pyle, L.J., Fallas, K.M., Durbano, A.M., 2015. A combined depth and thermal maturity map of the Canol Formation, northern Mackenzie Valley, Northwest Territories (No. Geological Survey of Canada, Open File 7865). https://doi.org/10.4095/296460

Hammes, U., Frébourg, G., 2012. Haynesville and Bossier mudrocks: A facies and sequence stratigraphic investigation, East Texas and Louisiana, USA. Mar. Pet. Geol., Insights into Shale Gas Exploration and Exploitation 31, 8–26. https://doi.org/10.1016/j.marpetgeo.2011.10.001

Harrington, R.R., Kennedy, B.P., Chamberlain, C.P., Blum, J.D., Folt, C.L., 1998. 15N enrichment in agricultural catchments: field patterns and applications to tracking Atlantic salmon (Salmo salar). Chem. Geol. 147, 281–294. https://doi.org/10.1016/S0009-2541(98)00018-7

Harris, B.S., LaGrange, M.T., Biddle, S.K., Playter, T.L., Fiess, K.M., Gingras, M.K., 2021. Chemostratigraphy as a tool for sequence stratigraphy in the Devonian Hare Indian Formation in the Mackenzie Mountains and Central Mackenzie Valley, Northwest Territories, Canada. Can. J. Earth Sci. 99, 1–17. https://doi.org/10.1139/cjes-2020-0198

Harris, N.B. (Ed.), 2005. Deposition of Organic-Carbon-Rich Sediments: Models. SEPM (Society for Sedimentary Geology). https://doi.org/10.2110/pec.05.82

Harris, N.B., McMillan, J.M., Knapp, L.J., Mastalerz, M., 2018. Organic matter accumulation in the Upper Devonian Duvernay Formation, Western Canada Sedimentary Basin, from sequence stratigraphic analysis and geochemical proxies. Sediment. Geol. 376, 185–203. https://doi.org/10.1016/j.sedgeo.2018.09.004

Hills, L.V., Sangster, E.V., Suneby, L.B. (Eds.), 1981. Lexicon of Canadian stratigraphy, Volume 2. Yukon Territory and District of Mackenzie. Canadian Society of Petroleum Geologists, Calgary.

Hoch, M.P., Fogel, M.L., Kirchman, D.L., 1994. Isotope fractionation during ammonium uptake by marine microbial assemblages. Geomicrobiol. J. 12, 113–127. https://doi.org/10.1080/01490459409377977

Irwin, D., 2020. Geology of the Northwest Territories. (No. NWT Open Report 2020-007.).

Issler, D.R., Grist, A.M., Stasiuk, L.D., 2005. Post-Early Devonian thermal constraints on hydrocarbon source rock maturation in the Keele Tectonic Zone, Tulita area, NWT, Canada, from multi-kinetic apatite fission track thermochronology, vitrinite reflectance and shale compaction. Bull. Can. Pet. Geol. 53, 405–431. https://doi.org/10.2113/53.4.405

James, G., Witten, D., Hastie, T., Tibshirani, R., 2013. An Introduction to Statistical Learning with Applications in R. Springer, New York.

Jeletzky, J.A., 1975. Jurassic and lower Cretaceous Paleogeography and depositional tectonics of Porcupine Plateau, adjacent areas of northern Yukon and those of Mackenzie District (Paper No. 74–16). Geological Survey of Canada. https://doi.org/10.4095/ 102549

Junium, C.K., Arthur, M.A., 2007. Nitrogen cycling during the Cretaceous, Cenomanian-Turonian Oceanic Anoxic Event II. Geochem., Geophys., Geosyst. 8. https://doi.org/10.1029/2006GC001328

Kabanov, P., 2019. Devonian (c. 388–375 Ma) Horn River Group of Mackenzie Platform (NW Canada) is an open-shelf succession recording oceanic anoxic events. J. Geol. Soc. 176, 29–45. https://doi.org/10.1144/jgs2018-075

Kabanov, P., Deblonde, C., 2019. Geological and geochemical data from Mackenzie Corridor. Part VIII: Middle-Upper Devonian lithostratigraphy, formation tops, and isopach maps in NTS areas 96 and 106, Northwest Territories and Yukon (Geological Survey of Canada Open File Report No. 8552). https://doi.org/10.4095/314785

Kabanov, P., Gouwy, S., Lawrence, P.A., Weleschuk, D.J., Chan, W.C., 2016. Geological and geochemical data from Mackenzie Corridor. Part III: New data on lithofacies, micropaleontology, lithogeochemistry, and Rock-EvalTM pyrolysis from the Devonian Horn River Group in the Mackenzie Plain and Norman Range, Northwest Territories (Geological Survey of Canada Open File Report No. 7951).

Kabanov, P., Gouwy, S.A., 2017. The Devonian Horn River Group and the basal Imperial Formation of the central Mackenzie Plain, N.W.T., Canada: multiproxy stratigraphic framework of a black shale basin. Can. J. Earth Sci. 54, 409–429. https://doi.org/10.1139/cjes-2016-0096

Kabanov, P., Jiang, C., 2020. Photic-zone euxinia and anoxic events in a Middle-Late Devonian shelfal sea of Panthalassan continental margin, NW Canada: Changing paradigm of Devonian ocean and sea level fluctuations. Glob. Planet. Change 188, 103153. https://doi.org/10.1016/j.gloplacha.2020.103153

Kabanov, P.B., 2015. Geological and geochemical data from the Mackenzie Corridor. Part I: Devonian cored sections and results for 2014 on geochemistry, d13C - d18O, and Rock-Eval 6 pyrolysis (Geological Survey of Canada Open File Report No. 7840). https://doi.org/10.4095/297403

Kabanov, P.B., Gouwy, S.A., 2020. The type section of the Canol Formation (Devonian black shale) at Powell Creek: Critical assessment and correlation in the northern Cordillera,

NWT, Canada. Bull. Can. Pet. Geol. 68, 123–140. https://doi.org/10.35767/gscpgbull.68.4.123

Kaiho, K., Miura, M., Tezuka, M., Hayashi, N., Jones, D.S., Oikawa, K., Casier, J.-G., Fujibayashi, M., Chen, Z.-Q., 2021. Coronene, mercury, and biomarker data support a link between extinction magnitude and volcanic intensity in the Late Devonian. Glob. Planet. Change 199, 103452. https://doi.org/10.1016/j.gloplacha.2021.103452

Kashiyama, Y., Ogawa, N.O., Kuroda, J., Shiro, M., Nomoto, S., Tada, R., Kitazato, H., Ohkouchi, N., 2008. Diazotrophic cyanobacteria as the major photoautotrophs during mid-Cretaceous oceanic anoxic events: Nitrogen and carbon isotopic evidence from sedimentary porphyrin. Org. Geochem. 39, 532–549. https://doi.org/10.1016/j.orggeochem.2007.11.010

Kessler, A.J., Bristow, L.A., Cardenas, M.B., Glud, R.N., Thamdrup, B., Cook, P.L.M., 2014. The isotope effect of denitrification in permeable sediments. Geochim. Cosmochim. Acta 133, 156–167. https://doi.org/10.1016/j.gca.2014.02.029

Klemme, H.D., Ulmishek, G.F., 1991. Effective Petroleum Source Rocks of the World: Stratigraphic Distribution and Controlling Depositional Factors. AAPG Bulletin 75, 1809–1851. https://doi-org.login.ezproxy.library.ualberta.ca/10.1306/0C9B2A47-1710-11D7-8645000102C1865D

Knapp, A., 2012. The sensitivity of marine N2 fixation to dissolved inorganic nitrogen. Front. Microbiol., Article 374 3, 1–14. https://doi.org/10.3389/fmicb.2012.00374

Knapp, A., Dekaezemacker, J., Bonnet, S., Sohm, J., Capone, D., 2012. Sensitivity of Trichodesmium erythraeum and Crocosphaera watsonii abundance and N<sub>2 fixation

rates to varying NO<sub>3<sup>− and PO<sub>4<sup>3− concentrations in batch cultures. Aquat. Microb. Ecol. 66, 223–236. https://doi.org/10.3354/ame01577

Konhauser, K., 2007. Introduction to Geomicrobiology. Blackwell Pub., Malden, MA.

LaGrange, M.T., Atienza, N.M.M., Biddle, S.K., Harris, B.S., Fiess, K.M., Terlaky, V., Konhauser, K.O., Gingras, M.K., 2022. The nature, origin, and predictors of porosity in the Middle to Late Devonian Horn River Group of the Central Mackenzie Valley, Northwest Territories, Canada. Mar. Pet. Geol. 142, 105738. https://doi.org/10.1016/j.marpetgeo.2022.105738

Lamb, A.L., Wilson, G.P., Leng, M.J., 2006. A review of coastal palaeoclimate and relative sea-level reconstructions using δ13C and C/N ratios in organic material. Earth-Sci. Rev. 75, 29–57. https://doi.org/10.1016/j.earscirev.2005.10.003

Lash, G.G., 2019. A global biogeochemical perturbation during the Middle Frasnian punctata Event: Evidence from muted carbon isotope signature in the Appalachian Basin, New York State (USA). Glob. Plan. Change 177, 239–254. https://doi.org/10.1016/j.gloplacha.2019.01.006

Lazar, O.R., Bohacs, K.M., Macquaker, J.H.S., Schieber, J., Demko, T.M., 2015. Capturing key attributes of fine-grained sedimentary rocks in outcrops, cores, and thin sections: nomenclature and description guidelines. J. Sediment. Res. 85, 230–246. https://doi.org/10.2110/jsr.2015.11

Lehmann, M.F., Bernasconi, S.M., Barbieri, A., McKenzie, J.A., 2002. Preservation of organic matter and alteration of its carbon and nitrogen isotope composition during simulated and in situ early sedimentary diagenesis. Geochim. Cosmochim. Acta 66, 3573–3584. https://doi.org/10.1016/S0016-7037(02)00968-7

Lenz, A.C., 1972. Ordovician to Devonian history of northern Yukon and adjacent district of Mackenzie. Bull. Can. Pet. Geol. 20, 321–361. https://doi.org/10.35767/gscpgbull.20.2.321

Lewan, M.D., 1983. Effects of thermal maturation on stable organic carbon isotopes as determined by hydrous pyrolysis of Woodford Shale. Geochim. Cosmochim. Acta 47, 1471–1479. https://doi.org/10.1016/0016-7037(83)90306-X

Li, C., Zhang, J., Li, W., Botting, J., Chen, Q., Fan, J., Zhang, Y., 2021. Multiple glacio-eustatic cycles and associated environmental changes through the Hirnantian (Late Ordovician) in South China. Glob. Planet. Change 207, 103668. https://doi.org/10.1016/j.gloplacha.2021.103668

Li, L., Zheng, Y.-F., Cartigny, P., Li, J., 2014. Anomalous nitrogen isotopes in ultrahigh-pressure metamorphic rocks from the Sulu orogenic belt: Effect of abiotic nitrogen reduction during fluid–rock interaction. Earth & Planet. Sci. Lett. 403, 67–78. https://doi.org/10.1016/j.epsl.2014.06.029

Li, Y., Li, L., Wu, Z., 2021. First-principles calculations of equilibrium nitrogen isotope fractionations among aqueous ammonium, silicate minerals and salts. Geochim. Cosmochim. Acta 297, 220–232. https://doi.org/10.1016/j.gca.2021.01.019

Loescher, C.R., Großkopf, T., Desai, F.D., Gill, D., Schunck, H., Croot, P.L., Schlosser, C., Neulinger, S.C., Pinnow, N., Lavik, G., Kuypers, M.M.M., LaRoche, J., Schmitz, R.A., 2014. Facets of diazotrophy in the oxygen minimum zone waters off Peru. ISME J 8, 2180–2192. https://doi.org/10.1038/ismej.2014.71

Lu, M., Lu, Y., Ikejiri, T., Sun, D., Carroll, R., Blair, E.H., Algeo, T.J., Sun, Y., 2021. Periodic oceanic euxinia and terrestrial fluxes linked to astronomical forcing during the Late

Devonian Frasnian–Famennian mass extinction. Earth Planet. Sci. Lett., 116839. https://doi.org/10.1016/j.epsl.2021.116839

Luo, Y.-W., Lima, I.D., Karl, D.M., Deutsch, C.A., Doney, S.C., 2014. Data-based assessment of environmental controls on global marine nitrogen fixation. Biogeosciences 11, 691–708. https://doi.org/10.5194/bg-11-691-2014

Mackenzie, W.S., 1970. Allochthonous Ree-Debris Limestone Turbidites Powell Creek, Northwest Territories. Bull. Can. Pet. Geol. 18, 474–492. https://doi.org/10.35767/gscpgbull.18.4.474

MacLean, B.C., 2011. Tectonic and stratigraphic evolution of the Cambrian basin of northern Northwest Territories. Bull. Can. Pet. Geol. 59, 172–194. https://doi.org/10.2113/gscpgbull.59.2.172

MacLean, B.C., Fallas, K.M., Hadlari, T., 2014. The multi-phase Keele Arch, central Mackenzie Corridor, Northwest Territories. Bull. Can. Pet. Geol. 62, 68–104. https://doi.org/10.2113/gscpgbull.62.2.68

Madigan, M.T., 1995. Microbiology of Nitrogen Fixation by Anoxygenic Photosynthetic Bacteria, in: Blankenship, R.E., Madigan, M.T., Bauer, C.E. (Eds.), Anoxygenic Photosynthetic Bacteria. Advances in Photosynthesis and Respiration. Springer, Dordrecht.

Mayer, B., Boyer, E.W., Goodale, C., Jaworski, N.A., Van Breemen, N., Howarth, R.W., Seitzinger, S., Billen, G., Lajtha, K., Nadelhoffer, K., Van Dam, D., Hetling, L.J., Nosal, M., Paustian, K., 2002. Sources of nitrate in rivers draining sixteen watersheds in the northeastern U.S.: Isotopic constraints, in: Boyer, E.W., Howarth, R.W. (Eds.), The

Nitrogen Cycle at Regional to Global Scales. Springer Netherlands, Dordrecht, pp. 171–197. https://doi.org/10.1007/978-94-017-3405-9_5

Mazzotti, S., Hyndman, R.D., 2002. Yakutat collision and strain transfer across the northern Canadian Cordillera. Geology 30, 495–498. https://doi-org.login.ezproxy.library.ualberta.ca/10.1130/0091-7613(2002)030<0495:YCASTA>2.0.CO;2

McGhee, G.R., Clapham, M.E., Sheehan, P.M., Bottjer, D.J., Droser, M.L., 2013. A new ecological-severity ranking of major Phanerozoic biodiversity crises. Palaeogeogr., Palaeoclimat., Palaeoecol. 370, 260–270. https://doi.org/10.1016/j.palaeo.2012.12.019

Meyers, P.A., 1994. Preservation of elemental and isotopic source identification of sedimentary organic matter. Chem. Geol. 114, 289–302. https://doi.org/10.1016/0009-2541(94)90059-0

Meyers, P.A., Eadie, B.J., 1993. Sources, degradation and recycling of organic matter associated with sinking particles in Lake Michigan. Org. Geochem. 20, 47–56. https://doi.org/10.1016/0146-6380(93)90080-U

Minagawa, M., Wada, E., 1986. Nitrogen isotope ratios of red tide organisms in the East China Sea: A characterization of biological nitrogen fixation. Mar. Chem. 19, 245–259. https://doi.org/10.1016/0304-4203(86)90026-5

Montoya, J.P., Carpenter, E.J., Capone, D.G., 2002. Nitrogen fixation and nitrogen isotope abundances in zooplankton of the oligotrophic North Atlantic. Limnol. Oceanogr. 47, 1617–1628. https://doi.org/10.4319/lo.2002.47.6.1617

Morrow, D.W., 2018. Devonian of the Northern Canadian Mainland Sedimentary Basin: A Review. Bull. Can. Pet. Geol. 66, 623–694.

Muir, I., Dixon, O.A., 1984. Facies analysis of a Middle Devonian sequence in the Mountain River-Gayna River, in: Brophy, J. (Ed.), Contributions to the Geology of the Northwest Territories. Department of Indian Affairs and Northern Development, Canada., pp. 55–62.

Muir, I., Wong, P., Wendte, J., 1985. Devonian Hare Indian-Ramparts (Kee Scarp) evolution, Mackenzie Mountains and subsurface Norman Wells, NWT: basin-fill and platform reef development, in: Longman, M.W., Shanley, K.W., Lindsay, R.F., Eby, D.E. (Eds.), Rocky Mountain Carbonate Reservoirs: A Core Workshop. SEPM (Society for Sedimentary Geology), pp. 311–341. https://doi.org/10.2110/cor.85.07

Muir, I.D., 1988. Devonian Hare Indian and Ramparts formations, MacKenzie Mountains, N.W.T. basin-fill, platform and reef development. (Thesis). University of Ottawa (Canada). https://doi.org/10.20381/ruor-10585

Murphy, A.E., Sageman, B.B., Hollander, D.J., 2000. Eutrophication by decoupling of the marine biogeochemical cycles of C, N, and P: A mechanism for the Late Devonian mass extinction. Geology 28 (5), 427–430. https://doi.org/10.1130/0091-7613(2000)28<427:EBDOTM>2.0.CO;2

Norris, A.W., 1985. Stratigraphy of Devonian outcrop belts in northern Yukon Territory and northwestern District of Mackenzie (Operation Porcupine area) (Memoir No. 410). Geological Survey of Canada. https://doi.org/10.4095/120309

O'Leary, M.H., 1981. Carbon isotope fractionation in plants. Phytochemistry 20, 553–567. https://doi.org/10.1016/0031-9422(81)85134-5

Ormiston, A.R., Oglesby, R.J., 1995. Effect of Late Devonian Paleoclimate on Source Rock Quality and Location, in: Huc, A.-Y. (Ed.), Paleogeography, Paleoclimate, and Source

Rocks. American Association of Petroleum Geologists. https://doi.org/10.1306/St40595C5

Pennington, J.T., Mahoney, K.L., Kuwahara, V.S., Kolber, D.D., Calienes, R., Chavez, F.P., 2006. Primary production in the eastern tropical Pacific: A review. Prog. Oceanogr. 69, 285–317. https://doi.org/10.1016/j.pocean.2006.03.012

Pennock, J.R., Velinsky, D.J., Ludlam, J.M., Sharp, J.H., Fogel, M.L., 1996. Isotopic fractionation of ammonium and nitrate during uptake by Skeletonema costatum: Implications for δ15N dynamics under bloom conditions. Limnol. Oceanogr. 41, 451–459. https://doi.org/10.4319/lo.1996.41.3.0451

Peters, K.E., Sweeney, R.E., Kaplan, I.R., 1978. Correlation of carbon and nitrogen stable isotope ratios in sedimentary organic matter 1: C and N isotopes. Limnol. Oceanogr. 23, 598–604. https://doi.org/10.4319/lo.1978.23.4.0598

Piper, D.Z., Calvert, S.E., 2009. A marine biogeochemical perspective on black shale deposition. Earth-Sci. Rev. 95, 63–96. https://doi.org/10.1016/j.earscirev.2009.03.001

Pisarzowska, A., Racki, G., 2012. Isotopic chemostratigraphy across the Early–Middle Frasnian transition (Late Devonian) on the South Polish carbonate shelf: A reference for the global punctata Event. Chem. Geol. 334, 199–220. https://doi.org/10.1016/j.chemgeo.2012.10.034

Powell, J.W., Issler, D.R., Schneider, D.A., Fallas, K.M., Stockli, D.F., 2020. Thermal history of the Mackenzie Plain, Northwest Territories, Canada: Insights from low-temperature thermochronology of the Devonian Imperial Formation. GSA Bulletin 132, 767–783. https://doi.org/10.1130/B35089.1

Prahl, F.G., De Lange, G.J., Scholten, S., Cowie, G.L., 1997. A case of post-depositional aerobic degradation of terrestrial organic matter in turbidite deposits from the Madeira Abyssal Plain. Organic Geochemistry, Organic Geochemistry of Paleoclimatic Markers: Production, Preservation and Modeling 27, 141–152. https://doi.org/10.1016/S0146-6380(97)00078-8

Pugh, D.C., 1983. Pre-Mesozoic geology in the subsurface of Peel River map area, Yukon Territory and district of Mackenzie (Memoir No. 401). Geological Survey of Canada. https://doi.org/10.4095/119498

Pyle, L.J., Gal, L.P., 2016. Reference Section for the Horn River Group and Definition of the Bell Creek Member, Hare Indian Formation in central Northwest Territories. Bull. Can. Pet. Geol. 64, 67–98. https://doi.org/10.2113/gscpgbull.64.1.67

Pyle, L.J., Gal, L.P., Hadlari, T., 2015. Thermal maturity trends for Devonian Horn River Group units and equivalent strata in the Mackenzie Corridor, Northwest Territories and Yukon (Geological Survey of Canada Open File Report No. 7850). https://doi.org/10.4095/296446

Racki, G., Rakociński, M., Marynowski, L., Wignall, P.B., 2018. Mercury enrichments and the Frasnian-Famennian biotic crisis: A volcanic trigger proved? Geology 46, 543–546. https://doi.org/10.1130/G40233.1

Ratcliffe, K. T., Woods, J., Rice, C., 2012a. Determining Well-Bore Pathways during Multilateral Drilling Campaigns in Shale Resource Plays: An Example Using Chemostratigraphy from the Horn River Formation, British Columbia, Canada.

Ratcliffe, K., Wright, M., Spain, D., 2012b. Unconventional Methods for Unconventional Plays: Using Elemental Data to Understand Shale Resource Plays. Petrol. Explor. Soc. Aust. News Resour. 117, 50–54.

Rivera, K.T., Puckette, J., Quan, T.M., 2015. Evaluation of redox versus thermal maturity controls on δ 15 N in organic rich shales: A case study of the Woodford Shale, Anadarko Basin, Oklahoma, USA. Org. Geochem. 83–84, 127–139. https://doi.org/10.1016/j.orggeochem.2015.03.005

Robinson, R.S., Kienast, M., Albuquerque, A.L., Altabet, M., Contreras, S., Holz, R.D.P., Dubois, N., Francois, R., Galbraith, E., Hsu, T.-C., Ivanochko, T., Jaccard, S., Kao, S.-J., Kiefer, T., Kienast, S., Lehmann, M., Martinez, P., McCarthy, M., Möbius, J., Pedersen, T., Quan, T.M., Ryabenko, E., Schmittner, A., Schneider, R., Schneider-Mor, A., Shigemitsu, M., Sinclair, D., Somes, C., Studer, A., Thunell, R., Yang, J.-Y., 2012. A review of nitrogen isotopic alteration in marine sediments. Paleoceanography 27. https://doi.org/10.1029/2012PA002321

Sackett, W.M., 1989. The Marine Environment, A, in: Fritz, P., Fontes, J.C. (Eds.), Handbook of Environmental Isotope Geochemistry. Elsevier Scientific Pub. Co, Amsterdam, pp. 139–169.

Sageman, B.B., Lyons, T.W., 2003. Geochemistry of Fine-grained Sediments and Sedimentary Rocks. Treatise on Geochemistry 7, 407. https://doi.org/10.1016/B0-08-043751-6/07157-7

Sano, J.L., Ratcliffe, K.T., Spain, D.R., 2013. Chapter 7: Chemostratigraphy of the Haynesville Shale 137–154, in: Hammes, U., Gales, J. (Eds.), Geology of the Hanyesville Gas Shale

in East Texas and West Louisiana, U.S.A. pp. 137–154 American Association of Petroleum Geologists Memoir 105. http://dx.doi.org/10.1306/13441847M1053602

Schelske, C.L., Hodell, D.A., 1995. Using carbon isotopes of bulk sedimentary organic matter to reconstruct the history of nutrient loading and eutrophication in Lake Erie. Limnol. Oceanogr. 40, 918–929. https://doi.org/10.4319/lo.1995.40.5.0918

Scholz, F., Hensen, C., Noffke, A., Rohde, A., Liebetrau, V., Wallmann, K., 2011. Early diagenesis of redox-sensitive trace metals in the Peru upwelling area – response to ENSO-related oxygen fluctuations in the water column. Geochim. Cosmochim. Acta 75, 7257–7276. https://doi.org/10.1016/j.gca.2011.08.007

Scholz, F., Siebert, C., Dale, A.W., Frank, M., 2017. Intense molybdenum accumulation in sediments underneath a nitrogenous water column and implications for the reconstruction of paleo-redox conditions based on molybdenum isotopes. Geochim. Cosmochim. Acta 213, 400–417. https://doi.org/10.1016/j.gca.2017.06.048

Schunck, H., Lavik, G., Desai, D.K., Großkopf, T., Kalvelage, T., Löscher, C.R., Paulmier, A., Contreras, S., Siegel, H., Holtappels, M., Rosenstiel, P., Schilhabel, M.B., Graco, M., Schmitz, R.A., Kuypers, M.M.M., LaRoche, J., 2013. Giant Hydrogen Sulfide Plume in the Oxygen Minimum Zone off Peru Supports Chemolithoautotrophy. PLoS ONE 8, e68661. https://doi.org/10.1371/journal.pone.0068661

Scotese, C.R., McKerrow, W.S., 1990. Revised World maps and introduction. Geol. Soc. Lond. Mem. 12, 1–21. https://doi.org/10.1144/GSL.MEM.1990.012.01.01

Scott, C., Lyons, T.W., 2012. Contrasting molybdenum cycling and isotopic properties in euxinic versus non-euxinic sediments and sedimentary rocks: Refining the paleoproxies. Chem. Geol., 324–325, 19–27. https://doi.org/10.1016/j.chemgeo.2012.05.012

Scott, C., Slack, J.F., Kelley, K.D., 2017. The hyper-enrichment of V and Zn in black shales of the Late Devonian-Early Mississippian Bakken Formation (USA). Chem. Geol. 452, 24–33. https://doi.org/10.1016/j.chemgeo.2017.01.026

Sigurdsson, H., Leckie, R.M., Acton, G.D., 1997. Proceedings of the Ocean Drilling Program, Initial Reports. College Station, TX (Ocean Drilling Program) 165. https://doi.org/doi:10.2973/odp.proc.ir.165.1997

Slomp, C.P., Thomson, J., de Lange, G.J., 2002. Enhanced regeneration of phosphorus during formation of the most recent eastern Mediterranean sapropel (S1). Geochim. Cosmochim. Acta 66, 1171–1184. https://doi.org/10.1016/S0016-7037(01)00848-1

Snowdon, L.R., Brooks, P.W., Williams, G.K., Goodarzi, F., 1987. Correlation of the Canol Formation source rock with oil from Norman Wells. Org. Geochem. 11, 529–548. https://doi.org/10.1016/0146-6380(87)90008-8

Somes, C.J., Schmittner, A., Galbraith, E.D., Lehmann, M.F., Altabet, M.A., Montoya, J.P., Letelier, R.M., Mix, A.C., Bourbonnais, A., Eby, M., 2010. Simulating the global distribution of nitrogen isotopes in the ocean. Global Biogeochemical Cycles 24. https://doi.org/10.1029/2009GB003767

Tang, Y., Huang, Y., Ellis, G.S., Wang, Y., Kralert, P.G., Gillaizeau, B., Ma, Q., Hwang, R., 2005. A kinetic model for thermally induced hydrogen and carbon isotope fractionation of individual n-alkanes in crude oil. Geochim. Cosmochim. Acta 69, 4505–4520. https://doi.org/10.1016/j.gca.2004.12.026

Tassonyi, E.J., 1969. Subsurface geology, lower Mackenzie River and Anderson River area, District of Mackenzie (Paper No. 68–25). Geological Survey of Canada.

Taylor, S.R., McLennan, S.M., 1985. The continental crust; its composition and evolution; an examination of the geochemical record preserved in sedimentary rocks. Blackwell, Oxford, United Kingdom.

Terlaky, V., Fiess, K.M., Rocheleau, J.M., 2020. Outcrop description, lithogeochemical, and source-rock characterisation of the Devonian Horn River Group at the Arctic Red River East and Flyaway Creek outcrops – NTS 106F and 106G, Northwest Territories (No. NWT Open Report 2019-004).

Thunell, R.C., Sigman, D.M., Muller-Karger, F., Astor, Y., Varela, R., 2004. Nitrogen isotope dynamics of the Cariaco Basin, Venezuela. Glob. Biogeochem. Cycles 18. https://doi.org/10.1029/2003GB002185

Tissot, B.P., Pelet, R., Ungerer, PH., 1987. Thermal History of Sedimentary Basins, Maturation Indices, and Kinetics of Oil and Gas Generation1. AAPG Bulletin 71, 1445–1466. https://doi.org/10.1306/703C80E7-1707-11D7-8645000102C1865D

Tocqué, E., Behar, F., Budzinski, H., Lorant, F., 2005. Carbon isotopic balance of kerogen pyrolysis effluents in a closed system. Org. Geochem. 36, 893–905. https://doi.org/10.1016/j.orggeochem.2005.01.007

Tribovillard, N., Algeo, T.J., Lyons, T., Riboulleau, A., 2006. Trace metals as paleoredox and paleoproductivity proxies: An update. Chem. Geol. 232, 12–32. https://doi.org/10.1016/j.chemgeo.2006.02.012

Turner, B.W., Tréanton, J.A., Slatt, R.M., 2016. The use of chemostratigraphy to refine ambiguous sequence stratigraphic correlations in marine mudrocks. An example from the Woodford Shale, Oklahoma, USA. J. Geol. Soc. 173, 854–868. https://doi.org/10.1144/jgs2015-125

Van der Weijden, C.H., 2002. Pitfalls of normalization of marine geochemical data using a common divisor. Mar. Geol. 184, 167–187. https://doi.org/10.1016/S0025-3227(01)00297-3

Ver Straeten, C.A., Brett, C.E., Sageman, B.B., 2011. Mudrock sequence stratigraphy: A multi-proxy (sedimentological, paleobiological and geochemical) approach, Devonian Appalachian Basin. Palaeogeogr. Palaeoclimat. Palaeoecol. 304 (1–2), 54–73. https://doi.org/10.1016/j.palaeo.2010.10.010

Voss, M., Deutsch, B., Elmgren, R., Humborg, C., Kuuppo, P., Pastuszak, M., Rolff, C., Schulte, U., 2006. Source identification of nitrate by means of isotopic tracers in the Baltic Sea catchments. Biogeosciences 3, 663–676. https://doi.org/10.5194/bg-3-663-2006

Wada, E., Kabaya, Y., Tsuru, K., Ishiwatari, R., 1990. 13C and 15N abundance of sedimentary organic matter in estuarine areas of Tokyo Bay, Japan. Mass Spectroscopy 38, 307–318.

Walliser, O.H., 1996. Global Events in the Devonian and Carboniferous, in: Walliser, O.H. (Ed.), Global Events and Event Stratigraphy in the Phanerozoic. Springer Berlin Heidelberg, pp. 225–250.

Wang, W.-L., Moore, J.K., Martiny, A.C., Primeau, F.W., 2019. Convergent estimates of marine nitrogen fixation. Nature 566, 205–211. https://doi.org/10.1038/s41586-019-0911-2

Ward, B.A., Dutkiewicz, S., Moore, C.M., Follows, M.J., 2013. Iron, phosphorus, and nitrogen supply ratios define the biogeography of nitrogen fixation. Limnol. Oceanogr. 58, 2059–2075. https://doi.org/10.4319/lo.2013.58.6.2059

Wehausen, R., Brumsack, H.-J., 1999. Cyclic variations in the chemical composition of eastern Mediterranean Pliocene sediments: a key for understanding sapropel formation. Mar. Geol. 153, 161–176. https://doi.org/10.1016/S0025-3227(98)00083-8

Williams, L.B., Ferrell, R.E., Hutcheon, I., Bakel, A.J., Walsh, M.M., Krouse, H.R., 1995. Nitrogen isotope geochemistry of organic matter and minerals during diagenesis and hydrocarbon migration. Geochim. Cosmochim. Acta 59, 765–779. https://doi.org/10.1016/0016-7037(95)00005-K

Wilson, G.P., Lamb, A.L., Leng, M.J., Gonzalez, S., Huddart, D., 2005. Variability of organic δ13C and C/N in the Mersey Estuary, U.K. and its implications for sea-level reconstruction studies. Estuar. Coast. and Shelf Sci. 64, 685–698. https://doi.org/10.1016/j.ecss.2005.04.003

Yose, L.A., Brown, S., Davis, T.L., Eiben, T., Kompanik, G.S., Maxwell, S.R., 2001. 3-D geologic model of a fractured carbonate reservoir, Norman Wells Field, NWT, Canada. Bull. Can. Pet. Geol. 49, 86–116. https://doi.org/10.2113/49.1.86

Zambito, J.J., Brett, C.E., Baird, G.C., 2012. The Late Middle Devonian (Givetian) Global Taghanic Biocrisis in Its Type Area (Northern Appalachian Basin): Geologically Rapid Faunal Transitions Driven by Global and Local Environmental Changes, in: Talent, J.A. (Ed.), Earth and Life: Global Biodiversity, Extinction Intervals and Biogeographic Perturbations through Time. Springer Netherlands.

Zhang, J.-Z., Millero, F.J., 1993. The chemistry of anoxic waters in the Cariaco Trench. Deep Sea Research Part I: Oceanographic Research Papers 40, 1023–1041. https://doi.org/10.1016/0967-0637(93)90088-K

Zhang, X., Joachimski, M.M., Over, D.J., Ma, K., Huang, C., Gong, Y., 2019. Late Devonian carbon isotope chemostratigraphy: A new record from the offshore facies of South China. Glob. Planet. Change 182, 103024. https://doi.org/10.1016/j.gloplacha.2019.103024

Zhang, X., Sigman, D.M., Morel, F.M.M., Kraepiel, A.M.L., 2014. Nitrogen isotope fractionation by alternative nitrogenases and past ocean anoxia. Proc Natl Acad Sci USA 111, 4782–4787. https://doi.org/10.1073/pnas.1402976111

Chapter 6: Conclusions

6.1 Conclusions

Within the past two-decades, organic-rich, marine mudstone successions have increasingly become the subject of research interest owing to their economic potential as unconventional reservoirs and because they often provide a valuable record of ocean history. This thesis focused specifically on the Canol Formation (Horn River Group), a Middle to Late Devonian, organic-rich mudstone deposited along the west coast of Ancestral North America, now the present-day Northwest Territories of Canada. In the west-central Northwest Territories, the Canol Formation has potential as an unconventional petroleum reservoir (e.g., Hadlari et al., 2015; Pyle et al., 2015). Moreover, this unit preserves a history of oceanographic conditions along the shelf of Ancestral North America in the Middle to Late Devonian, an important time in Earth's history characterized by successive biodiversity crises (e.g., Becker et al., 2020; McGhee et al., 2013; Walliser, 1996) and widespread organic-rich mudstone deposition (e.g., Klemme and Ulmishek, 1991; Ormiston and Oglesby, 1995).

The research presented in this thesis fills important gaps in our understanding of the depositional conditions and resource potential of the Canol Formation. In addition to providing a guide for the use of geochemical proxies in the sequence stratigraphic analysis of all marine organic-rich mudstones, it also serves as an example of the depositional conditions associated with organic matter burial. Chapter 2 examined stable C and N isotopic signatures, which are best explained by the dominance of diazotrophic primary producers throughout deposition of the Canol Formation and surrounding units with fluctuations in the rate of biological productivity through time as the Canol Formation accumulated. The second chapter also presented a succinct paleoredox model for the Horn River Group based on previous redox proxy results and proposed

that episodic downwards movement of the upper OMZ boundary, possibly associated with climatic periodicity, is a plausible mechanism for fluctuating paleoredox conditions in the depositional setting. Previous studies proposed that $\delta^{13}C_{org}$ trends in the Horn River Group may correspond to global-scale $\delta^{13}C$ trends and C cycles perturbations (e.g., Fraser and Hutchison, 2017; Kabanov and Jiang, 2020).

Chapter 3 evaluated porosity in the Canol Formation and the Horn River Group, which has previously been assessed in age-equivalent western Canadian mudstone resources (e.g., Dong et al., 2015; Dong et al., 2019; Knapp et al., 2020), but not for the Middle to Late Devonian succession of the frontier Northern Canadian Mainland Sedimentary Basin. Compared to many other North American mudstone reservoirs, this work showed that the Canol Formation and Bluefish Member (Hare Indian Formation) have comparable bulk porosity, lower mesopore volume, and are dominated by mineral matrix pores rather than organic matter pores. The presence of natural fractures may facilitate the movement of hydrocarbons to mechanical fractures. Mineralogy, and in particular high quartz and low clay abundance, are the best predictors of high porosity in the Horn River Group. In summary, the third chapter characterized the properties and distribution of prospective reservoir intervals in the Horn River Group and could contribute to more accurate modeling of resource potential in the future.

Establishing sequence stratigraphic correlations, which is important for understanding basin evolution and mapping economically significant horizons, can be challenging in organic-rich mudstone intervals using only traditional datasets (K.T. Ratcliffe et al., 2012; Turner et al., 2016). Chapter 4 reviewed the integration of geochemical datasets in sequence stratigraphic analyses of marine, organic-rich mudstone units. This chapter summarized the chemostratigraphic signature of the MFS, MRS, TST, RST and HST and serves a guide for the

interpretation of geochemical data in a sequence stratigraphic context for organic-rich, marine mudstones. Ultimately, this work concluded that chemostratigraphy is useful for identifying T-R cycles in organic-rich mudstones, but currently, no chemostratigraphic criteria exist to distinguish normal regression from forced regression in the RST.

In Chapter 5, a sequence stratigraphic framework for the Canol Formation was presented in the context of the entire Horn River Group, primarily based on high-resolution chemostratigraphic profiles. Six complete T-R cycles were identified from the base of the Horn River Group to the upper Imperial Formation. When compared to the sequence stratigraphic interpretation, redox-sensitive trace metal profiles (Mo and V) suggest that the most reducing conditions in the sediment and bottom waters occurred at or near the time of highest rates in relative sea-level rise. Chapter 4 showed that this type of pattern in Mo and V is characteristic of oceanographically open settings, lending further support to the interpretation that the Horn River Group was deposited in an unrestricted marine setting (e.g., Kabanov, 2019; Morrow, 2018). This chapter facilitates mapping of higher reservoir quality (more siliceous) maximum flooding surfaces in the Horn River Group and illustrates stratigraphic relationships across different lithologies. The sequence stratigraphic framework presented here also sheds light on changes in the balance between sedimentation and accommodation through time as the Horn River Group was deposited. Finally, Chapter 5 contributes an example to the growing body of research pertaining to the application of chemostratigraphy to mudstone sequence stratigraphy.

6.2 Future work

Correlation of $\delta^{13}C_{org}$ trends from the Canol Formation with $\delta^{13}C_{org}$ from age-equivalent organic-rich mudstone units worldwide is identified as a future research direction. This

comparison would contribute to our understanding of patterns in marine $\delta^{13}C$ throughout the Middle to Late Devonian and how they relate to paleoredox conditions and biodiversity crises. Additionally, a comparison to results from coeval mudstones units would allow for the assessment of regional or global scale patterns in primary producers throughout the Middle to Late Devonian in settings where organic-rich mudstones were deposited.

Two suggested directions of future research stemmed from the work in Chapter 4. First, further work is required to characterize sequence stratigraphic surfaces and systems tracts. This could be accomplished by the collection of geochemical datasets for comparison with previously established sequence stratigraphic frameworks and through projects that integrate chemostratigraphic proxies with other datasets to develop new sequence stratigraphic frameworks. Next, as we further our understanding of the depositional systems associated with fine-grained successions, characterizing the chemostratigraphic expression of surfaces and systems tracts in different settings will expand the utility of geochemical proxies in sequence stratigraphic analyses.

For Chapter 5, one future line of work is already planned: the sequence stratigraphic framework from this chapter will be integrated with the sedimentological and ichnological dataset collected from thin sections of the Horn River Group by Sara Biddle in her MSc thesis and subsequent publication (Biddle, 2020; Biddle et al., 2021). Integration of chemostratigraphic, sedimentological, and ichnological datasets will allow for verification of the shoreline shifts inferred through using chemostratigraphy and produce a more robust sequence stratigraphic framework. If in the future, a means of high-resolution correlation between the Kee Scarp Member reef units and the mudstone units of the Hare Indian and Canol Formations becomes

available, subsequent research could compare T-R cycles identified here to those previously identified in the Kee Scarp Member by Muir et al. (1985) and Yose et al. (2001).

6.3 References

Becker, R.T., Marshall, J.E.A., Da Silva, A.-C., Agterberg, F.P., Gradstein, F.M., Ogg, J.G., 2020. Chapter 22 - The Devonian Period, in: Gradstein, Felix M., Ogg, James G., Schmitz, M.D., Ogg, G.M. (Eds.), Geologic Time Scale 2020. Elsevier, pp. 733–810. https://doi.org/10.1016/B978-0-12-824360-2.00022-X

Biddle, S., 2020. A Fine Detail Physicochemical Depositional Model for Devonian Organic-Rich Mudstones: A Petrographic Study of the Hare Indian and Canol Formations, Central Mackenzie Valley, Northwest Territories. University of Alberta (Canada). https://doi.org/10.7939/r3-jacj-jp38

Biddle, S.K., LaGrange, M.T., Harris, B.S., Fiess, K., Terlaky, V., Gingras, M.K., 2021. A fine detail physico-chemical depositional model for Devonian organic-rich mudstones: A petrographic study of the Hare Indian and Canol Formations, Central Mackenzie Valley, Northwest Territories. Sedimentary Geology 414, 105838. https://doi.org/10.1016/j.sedgeo.2020.105838

Fraser, T.A., Hutchison, M.P., 2017. Lithogeochemical characterization of the Middle–Upper Devonian Road River Group and Canol and Imperial formations on Trail River, east Richardson Mountains, Yukon: age constraints and a depositional model for fine-grained strata in the Lower Paleozoic Richardson trough. Can. J. Earth Sci. 54, 731–765. https://doi.org/10.1139/cjes-2016-0216

Hadlari, T., MacLean, B.C., Pyle, L.J., Fallas, K.M., Durbano, A.M., 2015. A combined depth and thermal maturity map of the Canol Formation, northern Mackenzie Valley, Northwest Territories (No. Geological Survey of Canada, Open File 7865). https://doi.org/10.4095/296460

Kabanov, P., 2019. Devonian (c. 388–375 Ma) Horn River Group of Mackenzie Platform (NW Canada) is an open-shelf succession recording oceanic anoxic events. J. Geol. Soc. 176, 29–45. https://doi.org/10.1144/jgs2018-075

Kabanov, P., Jiang, C., 2020. Photic-zone euxinia and anoxic events in a Middle-Late Devonian shelfal sea of Panthalassan continental margin, NW Canada: Changing paradigm of Devonian ocean and sea level fluctuations. Glob. Plan. Change 188, 103153. https://doi.org/10.1016/j.gloplacha.2020.103153

Klemme, H.D., Ulmishek, G.F., 1991. Effective Petroleum Source Rocks of the World: Stratigraphic Distribution and Controlling Depositional Factors. AAPG Bulletin 75, 1809–1851. https://doi-org.login.ezproxy.library.ualberta.ca/10.1306/0C9B2A47-1710-11D7-8645000102C1865D

McGhee, G.R., Clapham, M.E., Sheehan, P.M., Bottjer, D.J., Droser, M.L., 2013. A new ecological-severity ranking of major Phanerozoic biodiversity crises. Palaeogeogr. Palaeoclimat. Palaeoecol. 370, 260–270. https://doi.org/10.1016/j.palaeo.2012.12.019

Morrow, D.W., 2018. Devonian of the Northern Canadian Mainland Sedimentary Basin: A Review. Bull. Can. Pet. Geol. 66, 623–694.

Muir, I., Wong, P., Wendte, J., 1985. Devonian Hare Indian-Ramparts (Kee Scarp) evolution, Mackenzie Mountains and subsurface Norman Wells, NWT: basin-fill and platform reef development, in: Longman, M.W., Shanley, K.W., Lindsay, R.F., Eby, D.E. (Eds.),

Rocky Mountain Carbonate Reservoirs: A Core Workshop. SEPM (Society for Sedimentary Geology), pp. 311–341. https://doi.org/10.2110/cor.85.07

Ormiston, A.R., Oglesby, R.J., 1995. Effect of Late Devonian Paleoclimate on Source Rock Quality and Location, in: Huc, A.-Y. (Ed.), Paleogeography, Paleoclimate, and Source Rocks. American Association of Petroleum Geologists. https://doi.org/10.1306/St40595C5

Pyle, L.J., Gal, L.P., Hadlari, T., 2015. Thermal maturity trends for Devonian Horn River Group units and equivalent strata in the Mackenzie Corridor, Northwest Territories and Yukon (Geological Survey of Canada Open File Report No. 7850). https://doi.org/10.4095/296446

Ratcliffe, K.T., Wright, A.M., Schmidt, K., 2012. Application of inorganic whole-rock geochemistry to shale resource plays: an example from the Eagle Ford Shale Formation, Texas. TSR 10, 4–9. https://doi.org/10.2110/sedred.2012.2.4

Turner, B.W., Tréanton, J.A., Slatt, R.M., 2016. The use of chemostratigraphy to refine ambiguous sequence stratigraphic correlations in marine mudrocks. An example from the Woodford Shale, Oklahoma, USA. J. Geol. Soc. 173, 854–868. https://doi.org/10.1144/jgs2015-125

Walliser, O.H., 1996. Global Events in the Devonian and Carboniferous, in: Walliser, O.H. (Ed.), Global Events and Event Stratigraphy in the Phanerozoic. Springer Berlin Heidelberg, pp. 225–250.

Yose, L.A., Brown, S., Davis, T.L., Eiben, T., Kompanik, G.S., Maxwell, S.R., 2001. 3-D geologic model of a fractured carbonate reservoir, Norman Wells Field, NWT, Canada. Bull. Can. Pet. Geol. 49, 86–116. https://doi.org/10.2113/49.1.86

Bibliography

Abdi, H., Valenti, D., 2007. Multiple correspondence analysis, in: Salkind, N.J. (Ed.), Encyclopedia of Measurement and Statistics. Sage Publications, Thousand Oaks (CA, pp. 652–657. https://doi.org/10.4135/9781412952644

Abdi, H., Williams, L.J., 2010. Principal component analysis. Wiley Interdisciplinary Reviews: Comput. Stat. 2 (4), 433–459. https://doi.org/10.1002/wics.101

Adachi, M., Yamamoto, K., Sugisaki, R., 1986. Hydrothermal chert and associated siliceous rocks from the northern Pacific their geological significance as indication of ocean ridge activity. Sediment. Geol. 47, 125–148. https://doi.org/10.1016/0037-0738(86)90075-8

Ader, M., Thomazo, C., Sansjofre, P., Busigny, V., Papineau, D., Laffont, R., Cartigny, P., Halverson, G.P., 2016. Interpretation of the nitrogen isotopic composition of Precambrian sedimentary rocks: Assumptions and perspectives. Chem. Geol. 429, 93–110. https://doi.org/10.1016/j.chemgeo.2016.02.010

Aguilera, R., Ramirez Vargas, J.F., 2016. Factors controlling fluid migration and distribution in the Eagle Ford shale. SPE Reservoir Eval. Eng. 19 (3), 403–414. https://doi.org/10.2118/171626-PA

Al-Aasm, I.S., Morad, S., Durocher, S., Muir, I., 1996. Sedimentology, C–S–Fe relationships and stable isotopic compositions in Devonian black mudrocks, Mackenzie Mountains, Northwest Territories, Canada. Sediment. Geol. 106, 279–298. https://doi.org/10.1016/S0037-0738(96)00018-8

Algeo, T.J., Liu, J., 2020. A re-assessment of elemental proxies for paleoredox analysis. Chem. Geol. 540, 119549. https://doi.org/10.1016/j.chemgeo.2020.119549

Algeo, T.J., Lyons, T.W., 2006. Mo–total organic carbon covariation in modern anoxic marine environments: Implications for analysis of paleoredox and paleohydrographic conditions. Paleoceanography 21 (1), PA1016. https://doi.org/10.1029/2004PA001112

Algeo, T.J., Maynard, J.B., 2004. Trace-element behavior and redox facies in core shales of Upper Pennsylvanian Kansas-type cyclothems. Chem. Geol. 206 (3–4), 289–318. https://doi.org/10.1016/j.chemgeo.2003.12.009

Algeo, T.J., Meyers, P.A., Robinson, R.S., Rowe, H., Jiang, G.Q., 2014. Icehouse–greenhouse variations in marine denitrification. Biogeosciences 11, 1273–1295. https://doi.org/10.5194/bg-11-1273-2014

Algeo, T.J., Scheckler, S.E., 1998. Terrestrial-marine teleconnections in the Devonian: links between the evolution of land plants, weathering processes, and marine anoxic events. Philos. Trans. R. Soc. Lond. B. Biol. Sci. 353, 113–130. https://doi.org/10.1098/rstb.1998.0195

Algeo, T.J., Schwark, L., Hower, J.C., 2004. High-resolution geochemistry and sequence stratigraphy of the Hushpuckney Shale (Swope Formation, eastern Kansas): implications for climato-environmental dynamics of the Late Pennsylvanian Midcontinent Seaway. Chem. Geol. 206 (3–4), 259–288. https://doi.org/10.1016/j.chemgeo.2003.12.028

Altabet, M.A., Pilskaln, C., Thunell, R., Pride, C., Sigman, D., Chavez, F., Francois, R., 1999. The nitrogen isotope biogeochemistry of sinking particles from the margin of the Eastern North Pacific. Deep Sea Res. Part Oceanogr. Res. Pap. 46, 655–679. https://doi.org/10.1016/S0967-0637(98)00084-3

Ambrose, R.J., Hartman, R.C., Diaz-Campos, M., Akkutlu, I.Y., Sondergeld, C.H., 2010. New pore-scale considerations for shale gas in place calculations: society of petroleum

engineers unconventional gas conference. Pittsburgh, Pennsylvania. February 23–25, 2010, SPE Paper 131772, 17 pp. https://doi.org/10.2118/131772-MS

Aplin, A.C., Larter, S.R., 2005. Fluid flow, pore pressure, wettability, and leakage in mudstone cap rocks, in: Boult, P., Kaldi, J. (Eds.), Evaluating Fault and Cap Rock Seals. AAPG Hedberg Series 2, pp. 1–12.

Aplin, A.C., Macquaker, J.H.S., 2011. Mudstone diversity: origin and implications for source, seal, and reservoir properties in petroleum systems. AAPG (Am. Assoc. Pet. Geol.) Bull. 95, 2031–2059. https://doi.org/10.1306/03281110162

Arsairai, B., Wannakomol, A., Feng, Q., Chonglakmani, C., 2016. Paleoproductivity and paleoredox condition of the Huai Hin Lat Formation in northeastern Thailand. J. Earth Sci. 27 (3), 350–364. https://doi.org/10.1007/s12583-016-0666-8

Arthur, M.A., Sageman, B.B., 2005. Sea-level control on source-rock development: perspectives from the Holocene Black Sea, the mid-Cretaceous Western Interior Basin, and the late Devonian Appalachian basin, in: Harris, N.B. (Ed.), The Deposition of Organic-Carbon-Rich Sediments: Models, Mechanisms, and Consequences: Society of Economic Paleontologists and Mineralogists Special Publication. 82. pp. 35–59.

Astor, Y., Muller-Karger, F., Scranton, M.I., 2003. Seasonal and interannual variation in the hydrography of the Cariaco Basin: implications for basin ventilation. Cont. Shelf Res. 23, 125–144. https://doi.org/10.1016/S0278-4343(02)00130-9

Aubineau, J., El Abani, A., Bekker, A., Somogyi, A., Bankole, O.M., Macchiarelli, R., Meunier, A., Riboulleau, A., Reynaud, J.-Y., Konhauser, K.O., 2019. Microbially induced potassium enrichment in Paleoproterozoic shales and implications for reverse weathering

on early Earth. Nat. Commun. 10 (1), 1–9 2670. https://doi.org/10.1038/s41467-019-10620-3

Averbuch, O., Tribovillard, N., Devleeschouwer, X., Riquier, L., Mistiaen, B., Van Vliet-Lanoe, B., 2005. Mountain building-enhanced continental weathering and organic carbon burial as major causes for climatic cooling at the Frasnian–Famennian boundary (c. 376 Ma)? Terra Nova 17, 25–34. https://doi.org/10.1111/j.1365-3121.2004.00580.x

Bassett, H.G., 1961. Devonian stratigraphy, central Mackenzie River region, Northwest Territories, Canada, in: G. Raasch (Ed.), Geology of the Arctic. Alberta Society of Petroleum Geologists and University of Toronto Press, pp. 481–498. https://doi.org/10.3138/9781487584979-043

Bauersachs, T., Schouten, S., Compaoré, J., Wollenzien, U., Stal, L.J., Sinninghe Damsteé, J.S., 2009. Nitrogen isotopic fractionation associated with growth on dinitrogen gas and nitrate by cyanobacteria. Limnol. Oceanogr. 54, 1403–1411. https://doi.org/10.4319/lo.2009.54.4.1403

Becker, R.T., Marshall, J.E.A., Da Silva, A.-C., Agterberg, F.P., Gradstein, F. M., Ogg, J. G., 2020. Chapter 22 - The Devonian Period, in: Gradstein, Felix M., Ogg, James G., Schmitz, M.D., Ogg, G.M. (Eds.), Geologic Time Scale 2020. Elsevier, pp. 733–810. https://doi.org/10.1016/B978-0-12-824360-2.00022-X

Becker, R.T., Marshall, J.E.A., Da Silva, A.C., Agterberg, F.P., Gradstein, F.M., Ogg, J.G., 2020. The Devonian Period, in: Geologic time scale 2020. Elsvier, pp. 733–810. https://doi.org/10.1016/B978-0-12-824360-2.00022-X

Begum, M., Yassin, M.R., Dehghanpour, H., 2019. Effect of kerogen maturity on organic shale wettability: a Duvernay case study. Mar. Petrol. Geol. 110, 483–496. https://doi.org/10.1016/j.marpetgeo.2019.07.012.

Benner, R., Fogel, M.L., Sprague, E.K., Hodson, R.E., 1987. Depletion of 13C in lignin and its implications for stable carbon isotope studies. Nature 329, 708–710. https://doi.org/10.1038/329708a0

Bennett, B., Buckman, J.O., Bowler, B.F.J., Larter, S.R., 2004. Wettability alteration in petroleum systems: the role of polar nonhydrocarbons. Petrol. Geosci. 10, 271–277. https://doi.org/10.1144/1354-079303-606.

Beranek, L.P., Mortensen, J.K., Lane, L.S., Allen, T.L., Fraser, T.A., Hadlari, T., Zantvoort, W.G., 2010. Detrital zircon geochronology of the western Ellesmerian clastic wedge, northwestern Canada: Insights on Arctic tectonics and the evolution of the northern Cordilleran miogeocline. GSA Bull. 122, 1899–1911. https://doi.org/10.1130/B30120.1

Berry, W.B., Wilde, P., 1978. Progressive ventilation of the oceans; an explanation for the distribution of the lower Paleozoic black shales. Am. J. Sci. 278 (3), 257–275.

Bertrand, R., 1990. Correlations among the reflectances of vitrinite, chitinozoans, graptolites and scolecodonts. Org. Geochem. 15 (6), 565–574. https://doi.org/ 10.1016/0146-6380(90)90102-6.

Bhatia, M.R., Crook, K.A., 1986. Trace element characteristics of graywackes and tectonic setting discrimination of sedimentary basins. Contrib. Mineral. Petrol. 92, 181–193. https://doi.org/10.1007/BF00375292

Biddle, S., 2020. A Fine Detail Physicochemical Depositional Model for Devonian Organic-Rich Mudstones: A Petrographic Study of the Hare Indian and Canol Formations, Central

Mackenzie Valley, Northwest Territories. University of Alberta (Canada). https://doi.org/10.7939/r3-jacj-jp38

Biddle, S.K., LaGrange, M.T., Harris, B.S., Fiess, K., Terlaky, V., Gingras, M.K., 2021. A fine detail physico-chemical depositional model for Devonian organic-rich mudstones: A petrographic study of the Hare Indian and Canol Formations, Central Mackenzie Valley, Northwest Territories. Sediment. Geol. 414, 105838. https://doi.org/10.1016/j.sedgeo.2020.105838

Birgenheier, L.P., Horton, B., McCauley, A.D., Johnson, C.L., Kennedy, A., 2017. A depositional model for offshore deposits of the lower Blue Gate Member, Mancos Shale, Uinta Basin, Utah, USA. Sedimentology 64 (5), 1402–1438. https://doi.org/10.1111/sed.12359

Bloemsma, M.R., Zabel, M., Stuut, J.B.W., Tjallingii, R., Collins, J.A., Weltje, G.J., 2012. Modelling the joint variability of grain size and chemical composition in sediments. Sediment. Geol. 280, 135–148. https://doi.org/10.1016/j.sedgeo.2012.04.009

Bohacs, K.M., 1998. Contrasting expressions of depositional sequences in mudrocks from marine to non-marine environs, in: Schieber, J., Zimmerle, W., Sethi, P.S. (Eds.), Shales and Mudstones: Volume I. E. Schweizerbart'sche Verlagsbuchhandlung (Nägele u. Obermiller), Stuttgart, pp. 33–78.

Bohacs, K.M., Grabowski Jr., G.J., Carroll, A.R., Mankiewicz, P.J., Miskell-Gerhardt, K.J., Schwalbach, J.R., Wegner, M.B., Simo, J.T., 2005. Production, destruction, and dilution—the many paths to source-rock development, in: Harris, N.B. (Ed.), The Deposition of Organic-Carbon-Rich Sediments: Models, Mechanisms, and

Consequences: Society of Economic Paleontologists and Mineralogists Special Publication. 82. pp. 61–101.

Bohacs, K.M., Lazar, O.R., Demko, T.M., 2014. Parasequence types in shelfal mudstone strata—quantitative observations of lithofacies and stacking patterns, and conceptual link to modern depositional regimes. Geology 42 (2), 131–134.

Bohacs, K.M., Schwalbach, J.R., 1992. Sequence stratigraphy of fine-grained rocks with special reference to the Monterey Formation, in: Schwalbach, J.R., Bohacs, K.M (Eds.), Sequence Stratigraphy in Fine-Grained Rocks: Examples from the Monterey Formation, pp. 7–19 Pacific Section, Society of Economic Paleontologists and Mineralogists, Book 70.

Bonjour, J.L., Dabard, M.P., 1991. Ti/Nb ratios of clastic terrigenous sediments used as an indicator of provenance. Chem. Geol. 91 (3), 257–267.

Borcovsky, D., Egenhoff, S., Fishman, N., Maletz, J., Boehlke, A., Lowers, H., 2017. Sedimentology, facies architecture, and sequence stratigraphy of a Mississippian black mudstone succession—the upper member of the Bakken Formation, North Dakota, United States. Am. Assoc. Pet. Geol. Bull. 101 (10), 1625–1673. https://doi.org/10.1306/01111715183

Bottcher, M.E., Oelschlager, B., Hopner, T., Brumsack, H.-J., Rullkotter, J., 1998. Sulfate reduction related to the early diagenetic degradation of organic matter and "black spot'' formation in tidal sandflats of the German Wadden Sea (southern North Sea): stable isotope (13C, 34S, 18O) and other geochemical results. Org Geochem 29, 1517–1530.

Boudou, J.-P., Schimmelmann, A., Ader, M., Mastalerz, M., Sebilo, M., Gengembre, L., 2008. Organic nitrogen chemistry during low-grade metamorphism. Geochim. Cosmochim. Acta 72, 1199–1221. https://doi.org/10.1016/j.gca.2007.12.004

Brandes, J.A., Devol, A.H., 2002. A global marine-fixed nitrogen isotopic budget: Implications for Holocene nitrogen cycling. Glob. Biogeochem. Cycles 16, 67-1-67–14. https://doi.org/10.1029/2001GB001856

Brandes, J.A., Devol, A.H., Yoshinari, T., Jayakumar, D.A., Naqvi, S.W.A., 1998. Isotopic composition of nitrate in the central Arabian Sea and eastern tropical North Pacific: A tracer for mixing and nitrogen cycles. Limnol. and Oceanogr. 43, 1680–1689. https://doi.org/10.4319/lo.1998.43.7.1680

Brown Jr., L.F., Fisher, W.L., 1977. Seismic stratigraphic interpretation of depositional systems: examples from Brazilian rift and pull apart basins, in: Payton, C.E. (Ed.), Seismic Stratigraphy—Applications to Hydrocarbon Exploration: American Association of Petroleum Geologists Memoir. 26. pp. 213–248.

Brown, T., Kenig, F., 2004. Water column structure during deposition of Middle Devonian–Lower Mississippian black and green/gray shales of the Illinois and Michigan Basins: a biomarker approach. Palaeogeogr. Palaeoclimatol. Palaeoecol. 215, 59–85. https://doi.org/10.1016/S0031-0182(04)00452-3

Brumsack, H.-J., 2006. The trace metal content of recent organic carbon-rich sediments: Implications for Cretaceous black shale formation. Palaeogeogr., Palaeoclimatol., Palaeoecol. 232, 344–361. https://doi.org/10.1016/j.palaeo.2005.05.011

Brunauer, S., Emmett, P.H., Teller, E., 1938. Adsorption of gases in multimolecular layers. J. Am. Chem. Soc. 60 (2), 309–319. https://doi.org/10.1021/ja01269a023

Buckman, J., Mahoney, C., März, C., Wagner, T., Blanco, V., 2017. Identifying biogenic silica: mudrock micro-fabric explored through charge contrast imaging. Am. Mineral. 102 (4), 833–844.

Burnham, A.K., Sweeney, J.J., 1989. A chemical kinetic model of vitrinite maturation and reflectance. Geochim. Cosmochim. Acta 53, 2649–2657. https://doi.org/10.1016/0016-7037(89)90136-1

Calvert, S.E., Pedersen, T.F., 1993. Geochemistry of recent oxic and anoxic marine sediments: implications for the geological record. Mar. Geol. 113 (1–2), 67–88. https://doi.org/10.1016/0025-3227(93)90150-T

Canfield, D.E., Thamdrup, B., 2009. Towards a consistent classification scheme for geochemical environments, or, why we wish the term 'suboxic'would go away. Geobiology 7 (4), 385–392. https://doi.org/10.1111/j.1472-4669.2009.00214.x

Canter, L., Zhang, S., Sonnenfeld, M., Bugge, C., Guisinger, M., Jones, K., 2016. Primary and secondary organic matter habit in unconventional reservoirs, in: Olson, T. (Ed.), Imaging Unconventional Reservoir Pore Systems. AAPG Memoir 112, pp. 9–24. https://doi.org/10.1306/13592014M1123691

Carmichael, S.K., Waters, J.A., Königshof, P., Suttner, T.J., Kido, E., 2019. Paleogeography and paleoenvironments of the Late Devonian Kellwasser event: A review of its sedimentological and geochemical expression. Glob. and Planet. Change 183, 102984. https://doi.org/10.1016/j.gloplacha.2019.102984

Carpenter, E.J., Harvey, H.R., Fry, B., Capone, D.G., 1997. Biogeochemical tracers of the marine cyanobacterium Trichodesmium. Deep Sea Res. Part Oceanogr. Res. Pap. 44, 27–38. https://doi.org/10.1016/S0967-0637(96)00091-X

Carr, A.D., 2000. Suppression and retardation of vitrinite reflectance, part 1. Formation and significance for hydrocarbon generation. J. Petrol. Geol. 23 (3), 313–343. https://doi.org/10.1111/j.1747-5457.2000.tb01022.x

Catuneanu, O., 2002. Sequence stratigraphy of clastic systems: concepts, merits, and pitfalls. J. Afr. Earth Sci. 35, 1–43.

Catuneanu, O., 2006. Principles of Sequence Stratigraphy. Elsevier, Amsterdam.

Catuneanu, O., 2019. Model-independent sequence stratigraphy. Earth-Sci. Rev. 188, 312–388. https://doi.org/10.1016/j.earscirev.2018.09.017

Catuneanu, O., 2019. Scale in sequence stratigraphy. Mar. Pet. Geol. 106, 128–159. https://doi.org/10.1016/j.marpetgeo.2019.04.026

Catuneanu, O., Abreu, V., Bhattacharya, J.P., Blum, M.D., Dalrymple, R.W., Eriksson, P.G., Fielding, C.R., Fisher, W.L., Galloway, W.E., Gibling, M.R., Giles, K.A., Holbrook, J.M., Jordan, R., Kendall, C.G.S., Macurda, B., Martinsen, O.J., Miall, A.D., Neal, J.E., Nummedal, D., Pomar, L., Posamentier, H.W., Pratt, B.R., Sarg, J.F., Shanley, K.W., Steel, R.J., Strasser, A., Tucker, M.E., Winker, C., 2009. Towards the standardization of sequence stratigraphy. Earth Sci. Rev. 92, 1–33. https://doi.org/10.1016/j.earscirev.2008.10.003

Catuneanu, O., Galloway, W.E., Kendall, C.G.S., Miall, A.D., Posamentier, H.W., Strasser, A., Tucker, M.E., 2011. Sequence stratigraphy: methodology and nomenclature. Newsl. Stratigr. 44, 173–245.

Chalmers, G.R., Bustin, R.M., Power, I.M., 2012. Characterization of gas shale pore systems by porosimetry, pycnometry, surface area, and field emission scanning electron microscopy/transmission electron microscopy image analyses: examples from the

Barnett, Woodford, Haynesville, Marcellus, and Doig units. AAPG (Am. Assoc. Pet. Geol.) Bull. 96 (6), 1099–1119.

Chavent, M., Kuentz-Simonet, V., Labenne, A., Saracco, J., 2015. Multivariate Analysis of Mixed Data: the PCAmixdata R Package arXiv:1411.4911v3 [stat.CO] 4 Dec 2014.

Chen, F., Zhang, L., Yang, Y., Zhang, D., 2008. Chemical and isotopic alteration of organic matter during early diagenesis: Evidence from the coastal area off-shore the Pearl River estuary, south China. J. Mar. Syst. 74, 372–380. https://doi.org/10.1016/j.jmarsys.2008.02.004

Chen, H.-F., Yeh, P.-Y., Song, S.-R., Hsu, S.-C., Yang, T.-N., Wang, Y., Chi, Z., Lee, T.-Q., Chen, M.-T., Cheng, C.-L., Zou, J., Chang, Y.-P., 2013. The Ti/Al molar ratio as a new proxy for tracing sediment transportation processes and its application in aeolian events and sea level change in East Asia. J. Asian Earth Sci. 73, 31–38. Colodner, D., Sachs, J., Ravizza, G., Turekian, K., Edmond, J., Boyle, E., 1993. The geochemical cycle of rhenium: a reconnaissance. Earth Planet. Sci. Lett. 117 (1-2), 205–221. https://doi.org/10.1016/j.jseaes.2013.04.017

Chen, Z., Wang, T., Liu, Q., Zhang, S., Zhang, L., 2015. Quantitative evaluation of potential organic-matter porosity and hydrocarbon generation and expulsion from mudstone in continental lake basins: a case study of Dongying sag, eastern China. Mar. Petrol. Geol. 66, 906–924. https://doi.org/10.1016/j.marpetgeo.2015.07.027

Cheung, S., Xia, X., Guo, C., Liu, H., 2016. Diazotroph community structure in the deep oxygen minimum zone of the Costa Rica Dome. J. Plankton Res. 38, 380–391. https://doi.org/10.1093/plankt/fbw003

Clarkson, C.R., Solano, N., Bustin, R.M., Bustin, A.M.M., Chalmers, G.R.L., He, L., Melnichenko, Y.B., Radlinski, A.P., Blach, T.P., 2013. Pore structure characterization of North American shale gas reservoirs using USANS/SANS, gas adsorption, and mercury intrusion. Fuel 103, 606–616. https://doi.org/10.1016/j.fuel.2012.06.119.

Cline, J.D., Kaplan, I.R., 1975. Isotopic fractionation of dissolved nitrate during denitrification in the eastern tropical north pacific ocean. Mar. Chem. 3, 271–299. https://doi.org/10.1016/0304-4203(75)90009-2

Cocks, L.R.M., Torsvik, T.H., 2011. The Palaeozoic geography of Laurentia and western Laurussia: A stable craton with mobile margins. Earth-Sci. Rev. 106, 1–51. https://doi.org/10.1016/j.earscirev.2011.01.007

Crusius, J., Calvert, S., Pedersen, T., Sage, D., 1996. Rhenium and molybdenum enrichments in sediments as indicators of oxic, suboxic and sulfidic conditions of deposition. Earth Planet. Sci. Lett. 145 (1-4), 65–78. https://doi.org/10.1016/S0012-821X(96)00204-X

Curtis, M.E., Cardott, B.J., Sondergeld, C.H., Rai, C.S., 2012. Development of organic porosity in the Woodford Shale with increasing thermal maturity. Int. J. Coal Geol. 103, 26–31. https://doi.org/10.1016/j.coal.2012.08.004.

Curtis, M.E., Sondergeld, C.H., Ambrose, R.J., Rai, C.S., 2012. Microstructural investigation of gas shales in two and three dimensions using nanometer-scale resolution imaging. AAPG (Am. Assoc. Pet. Geol.) Bull. 96 (4), 665–677. https://doi.org/10.1306/ 08151110188

Dashtgard, S.E., MacEachern, J.A., 2016. Unburrowed mudstones may record only slightly lowered oxygen conditions in warm, shallow basins. Geology 44 (5), 371–374. https://doi.org/10.1130/G37648.1

Davis, C., Pratt, L., Sliter, W., Mompart, L., Mural, B., 1999. Factors influencing organic carbon and trace metal accumulation in the Upper Cretaceous La Luna Formation of the western Maracaibo Basin, Venezuela, in: Barrera, E., Johnson, C.C. (Eds.), Evolution of the Cretaceous Ocean-Climate System, Boulder, Colorado, Geological Society of America Special Paper 332. https://doi.org/10.1130/0-8137-2332-9.203

Dean, W.E., Arthur, M.A., 1998. Geochemical expressions of cyclicity in Cretaceous pelagic limestone sequences: Niobrara Formation, Western Interior Seaway, in: Dean, W.E., Arthur, M.A. (Eds.), Stratigraphy of Paleoenvironments of the Cretaceous Western Interior Seaway, USA, SEPM Concepts in Sedimentology and Paleontology No. 6. SEPM, Tulsa, OK, United States, pp. 227–255.

Degens, E.T., Gullard, R.R., Sackett, W.M., Hellebust, J.A., 1968. Metabolic fractionation of carbon isotopes in marine plankton: 1. Temperature and respiration experiments. Deep-Sea Res. 15, 1–9. https://doi.org/10.1016/0011-7471(68)90024-7

Dembicki Jr., H., 2009. Three common source rock evaluation errors made by geologists during prospect or play appraisals. AAPG (Am. Assoc. Pet. Geol.) Bull. 93 (3), 341–356. https://doi.org/10.1306/10230808076

DeReuil, A.A., Birgenheier, L.P., 2019. Sediment dispersal and organic carbon preservation in a dynamic mudstone-dominated system, Juana Lopez Member, Mancos Shale. Sedimentology 66 (3), 1002–1041. https://doi.org/10.1111/sed.12532

Deutsch, C., Sarmiento, J.L., Sigman, D.M., Gruber, N., Dunne, J.P., 2007. Spatial coupling of nitrogen inputs and losses in the ocean. Nature 445, 163–167. https://doi.org/10.1038/nature05392

Dewing, K., Hadlari, T., Pearson, D.G., Matthews, W., 2019. Early Ordovician to Early Devonian tectonic development of the northern margin of Laurentia, Canadian Arctic Islands. GSA Bull. 131, 1075–1094. https://doi.org/10.1130/B35017.1

Dinelli, E., Tateo, F., Summa, V., 2007. Geochemical and mineralogical proxies for grain size in mudstones and siltstones from the Pleistocene and Holocene of the Po River alluvial plain, Italy. Geol. Soc. Am. Spec. Pap. 420, 25–36.

Dominguez, R.F., Catuneanu, O., 2017. Regional stratigraphic framework of the Vaca Muerta – Quintuco system in the Neuquén Embayment, Argentina, in: Proceedings from: The 20th Geological Congress of Argentina, Tucuman, Argentina.

Dominguez, R.F., Continanzia, M.J., Mykietiuk, K., Ponce, C., Pérez, G., Guerello, R. Lanusse, N.I., Caneva, M., Di Benedetto, M., Catuneanu, O., Cristallini, E., 2016. Organic-rich stratigraphic units in the Vaca Muerta Formation, and their distribution and characterization in the Neuquén Basin (Argentina), in: Proceedings from: Unconventional Resources Technology Conference, San Antonio, Texas. https://doi.org/10.15530/URTEC-2016-2456851

Dong, T., Harris, N.B., Ayranci, K., Twemlow, C.E., Nassichuk, B.R., 2015. Porosity characteristics of the Devonian Horn River shale, Canada: insights from lithofacies classification and shale composition. Int. J. Coal Geol. 141–142, 74–90. https://doi.org/10.1016/j.coal.2015.03.001

Dong, T., Harris, N.B., Ayranci, K., Twemlow, C.E., Nassichuk, B.R., 2017. The impact of composition on pore throat size and permeability in high maturity shales: middle and Upper Devonian Horn River Group, northeastern British Columbia, Canada. Mar. Petrol. Geol. 81, 220–236. https://doi.org/10.1016/j.marpetgeo.2017.01.011

Dong, T., Harris, N.B., McMillan, J.M., Twemlow, C.E., Nassichuk, B.R., Bish, D.L., 2019. A model for porosity evolution in shale reservoirs: an example from the Upper Devonian Duvernay Formation. West. Canada Sediment. Basin: AAPG (Am. Assoc. Pet. Geol.) Bull. 103 (5), 1017–1044. https://doi.org/10.1306/10261817272

Egenhoff, S.O., Fishman, N.S., 2013. Traces in the dark—Sedimentary processes and facies gradients in the upper shale member of the Upper Devonian–Lower Mississippian Bakken Formation, Williston Basin, North Dakota, USA. J. Sediment. Res. 83 (9), 803–824. https://doi.org/10.2110/jsr.2013.60

El Attar, A., Pranter, M.J., 2016. Regional stratigraphy, elemental chemostratigraphy, and organic richness of the Niobrara Member of the Mancos Shale, Piceance Basin, Colorado. Am. Assoc. Pet. Geol. Bull. 100 (3), 345–377. https://doi.org/10.1306/12071514127

Elder, W.P., Gustason, E.R., Sageman, B.B., 1994. Correlation of basinal carbonate cycles to nearshore parasequences in the Late Cretaceous Greenhorn seaway, Western Interior USA. Geol. Soc. Am. Bull. 106 (7), 892–902. https://doi.org/10.1130/0016-7606(1994)106<0892:COBCCT>2.3.CO;2

Embry, A.F., 2002. Transgressive-regressive (TR) sequence stratigraphy, in: Proceedings from: 22nd Annual Gulf Coast Section SEPM Foundation Bob F. Perkins Research Conference, Houston, Texas. https://doi.org/10.5724/gcs.02.22

Embry, A.F., 2009. Practical sequence stratigraphy. Can. Soc. Petrol. Geol. Reserv. 36, 1–6.

Embry, A.F., 2010. Correlation siliciclastic successions with sequence stratigraphy, in: Ratcliffe, K.T., Zaitlin, B.A. (Eds.), Application of Modern Stratigraphic Techniques: Theory and

Case Histories, pp. 35–53 SEPM (Society for Sedimentary Geology) Special Publication, no. 94.

Embry, A.F., Johannessen, E.P., 1993. T–R sequence stratigraphy, facies analysis and reservoir distribution in the uppermost Triassic–Lower Jurassic succession, western Sverdrup Basin, Arctic Canada, in: Vorren, T.O., Bergsager, E., Dahl-Stamnes, Ø.A., Holter, E., Johansen, B., Lie, E., Lund, T.B. (Eds.), Norwegian Petroleum Society Special Publications. Elsevier, pp. 121–146. https://doi.org/10.1016/B978-0-444-88943-0.50013-7

Emeis, K.-C., Whelan, J.K., Tarafa, M., 1991. Sedimentary and geochemical expressions of oxic and anoxic conditions on the Peru Shelf. Geol. Soc. Lond. Spec. Publ. 58, 155–170. https://doi.org/10.1144/GSL.SP.1991.058.01.11

Emerson, S., Stump, C., Wilbur, D., Quay, P., 1999. Accurate measurement of O2, N2, and Ar gases in water and the solubility of N2. Mar. Chem. 64, 337–347. https://doi.org/10.1016/S0304-4203(98)00090-5

Emmanuel, S., Day-Stirrat, R.J., 2012. A framework for quantifying size dependent deformation of nano-scale pores in mudrocks. J. Appl. Geophys. 86, 29–35. https://doi.org/10.1016/j.jappgeo.2012.07.011

Erickson, B.E., Helz, G.R., 2000. Molybdenum (VI) speciation in sulfidic waters: stability and lability of thiomolybdates. Geochim. Cosmochim. Acta 64 (7), 1149–1158. https://doi.org/10.1016/S0016-7037(99)00423-8

Espitali´e, J., Deroo, G., Marquis, F., 1985. Rock-eval pyrolysis and its applications. Rev. Inst. Fr. Petrol 40 (5), 563–579. Fermont, W.J.J., 1988. Possible causes of abnormal vitrinite reflectance values in paralic deposits of the Carboniferous in the Achterhoek area. The

Netherlanks: Org. Geochem. 12 (4), 401–411. https://doi.org/10.1016/0146-6380(88)90013-7

Falkowski, P.G., 1991. Species variability in the fractionation of 13C and 12C by marine phytoplankton. J. Phytoplank. Res. 13, 21–28.

Feinstein, S., Brooks, P.W., Fowler, M.G., Snowdon, L.R., Williams, G.K., 1988. Families of oils and source rocks in the central Mackenzie corridor: a geochemical oil-oil and oil-source rock correlation, in: James, D.P., Leckie, D.A. (Eds.), Sequences, Stratigraphy, Sedimentology: Surface and Subsurface. Canadian Society of Petroleum Geologists, Memoir 15, pp. 543–552.

Fernandez, C., Farías, L., Ulloa, O., 2011. Nitrogen Fixation in Denitrified Marine Waters. PLOS ONE 6, e20539. https://doi.org/10.1371/journal.pone.0020539

Fishman, N.S., Hackley, P.C., Lowers, H.A., Hill, R.J., Egenhoff, S.O., Eberl, D.E., Blum, A.E., 2012. The nature of porosity in organic-rich mudstones of the upper jurassic Kimmeridge Clay Formation, North Sea, offshore United Kingdom. Int. J. Coal Geol. 103, 32–50. https://doi.org/10.1016/j.coal.2012.07.012

Fraser, T.A., Hutchison, M.P., 2017. Lithogeochemical characterization of the Middle–Upper Devonian Road River Group and Canol and Imperial formations on Trail River, east Richardson Mountains, Yukon: age constraints and a depositional model for fine-grained strata in the Lower Paleozoic Richardson trough. Can. J. Earth Sci. 54, 731–765. https://doi.org/10.1139/cjes-2016-0216

Frébourg, G., Ruppel, S.C., Rowe, H., 2013. Sedimentology of the Haynesville (Upper Kimmeridgian) and Bossier (Tithonian) Formations, in the Western Haynesville Basin, Texas, U.S.A, in: Hammes, U., Gale, J. (Eds.), Geology of the Haynesville Gas Shale in

East Texas and West Louisiana, U.S.A. pp. 47–67 America Association of Petroleum Geologists Memoir 105.

Freeman, K.H., 2001. Isotopic Biogeochemistry of Marine Organic Carbon. Rev. Mineral. Geochem. 43, 579–605. https://doi.org/10.2138/gsrmg.43.1.579

Freudenthal, T., Wagner, T., Wenzhöfer, F., Zabel, M., Wefer, G., 2001. Early diagenesis of organic matter from sediments of the eastern subtropical Atlantic: evidence from stable nitrogen and carbon isotopes. Geochim. Cosmochim. Acta 65, 1795–1808. https://doi.org/10.1016/S0016-7037(01)00554-3

Fritz, W.H., Cecile, M.P., Norford, B.S., Morrow, D., Geldsetzer, H.H.J., 1991. Cambrian to middle devonian assemblages, in: Gabrielse, H., Yorath, C.J. (Eds.), Geol. Cordilleran Orogen Canada: Geol. Surv. Canada, Geol. Canada 4, 151–218.

Froelich, P., Klinkhammer, G.P., Bender, M.L., Luedtke, N.A., Heath, G.R., Cullen, D., Dauphin, P., Hammond, D., Hartman, B., Maynard, V., 1979. Early oxidation of organic matter in pelagic sediments of the eastern equatorial Atlantic: suboxic diagenesis. Geochim. Cosmochim. Acta 43 (7), 1075–1090. https://doi.org/10.1016/0016-7037(79)90095-4

Fru, E.C., Rodríguez, N.P., Partin, C.A., Lalonde, S.V., Andersson, P., Weiss, D.J., El Albani, A., Rodushkin, I., Konhauser, K.O., 2016. Cu isotopes in marine black shales record the Great Oxidation Event. Proc. Natl. Acad. Sci. 113 (18), 4941–4946. https://doi.org/10.1073/pnas.1523544113

Fry, B., Sherr, E.B., 1984. δ13C measurements as indicators of carbon flow in marine and freshwater ecosystems. Contrib. Mar. Sci. 27, 13–47.

Gal, L.P., Pyle, L.J., Hadlari, T., Allen, T.L., 2009. Chapter 6: Lower to Upper Devonian strata, Arnica-Landry play, and Kee Scarp play, in: Pyle, L.J., Jones, A. (Eds.), Regional Geoscience Studies and Petroleum Potential, Peel Plateau and Plain, Northwest Territories and Yukon: Project Volume, Northwest Territories Geoscience Office and Yukon Geological Survey, NWT, Open File 2009-002 and Yukon Geological Survey Open File 2009-25.

Gale, J.F., Reed, R.M., Holder, J., 2007. Natural fractures in the Barnett Shale and their importance for hydraulic fracture treatments. AAPG Bull. 91 (4), 603–622. https://doi.org/10.1306/ 11010606061

Galimov, E.M., 2004. The pattern of δ13Corg versus HI/OI relation in recent sediments as an indicator of geochemical regime in marine basins: comparison of the Black Sea, Kara Sea, and Cariaco Trench. Chem. Geol. 204, 287–301. https://doi.org/10.1016/j.chemgeo.2003.11.014

Galloway, W.E., 1989. Genetic stratigraphic sequences in basin analysis I: architecture and genesis of flooding-surface bounded depositional units. Am. Assoc. Pet. Geol. Bull. 73 (2), 125–142. https://doi.org/10.1306/703C9AF5-1707-11D7-8645000102C1865D

Gambacorta, G., Trincianti, E., Torricelli, S., 2016. Anoxia controlled by relative sea-level changes: an example from the Mississippian Barnett Shale Formation. Palaeogeogr. Palaeoclimatol. Palaeoecol. 459, 306–320. https://doi.org/10.1016/j.palaeo.2016.07.015

Garzione, C.N., Patchett, P.J., Ross, G.M., Nelson, J., 1997. Provenance of Paleozoic sedimentary rocks in the Canadian Cordilleran miogeocline: a Nd isotopic study. Can. J. Earth Sci. 34 (12), 1603–1618. https://doi.org/10.1139/e17-129

Ghanizadeh, A., Bhowmik, S., Haeri-Ardakani, O., Sanei, H., Clarkson, C.R., 2015. A comparison of shale permeability coefficients derived using multiple non-steady-state measurement techniques: examples from the Duvernay Formation, Alberta (Canada). Fuel 140, 371–387. https://doi.org/10.1016/j.fuel.2014.09.073

Grosjean, E., Adam, P., Connan, J., Albrecht, P., 2004. Effects of weathering on nickel and vanadyl porphyrins of a Lower Toarcian shale of the Paris basin. Geochim. Cosmochim. Acta 68 (4), 789–804. https://doi.org/10.1016/S0016-7037(03)00496-4

Gutierrez Parades, H.C., Catuneanu, O., Romano, U.H., 2017. Sequence stratigraphy of the Miocene section, southern Gulf of Mexico. Mar. Pet. Geol. 86, 711–732. https://doi.org/10.1016/j.marpetgeo.2017.06.022

Gutiérrez, D., Enríquez, E., Purca, S., Quipúzcoa, L., Marquina, R., Flores, G., Graco, M., 2008. Oxygenation episodes on the continental shelf of central Peru: Remote forcing and benthic ecosystem response. Prog. Oceanogr. 79, 177–189. https://doi.org/10.1016/j.pocean.2008.10.025

Hadlari, T., 2015. Oil migration driven by exhumation of the Canol Formation oil shale: A new conceptual model for the Norman Wells oil field, northwestern Canada. Mar. Pet. Geol. 65, 172–177. https://doi.org/10.1016/j.marpetgeo.2015.03.027

Hadlari, T., Davis, W.J., Dewing, K., 2014. A pericratonic model for the Pearya terrane as an extension of the Franklinian margin of Laurentia, Canadian Arctic. Geol. Soc. Am. Bull. 126, 182–200. https://doi.org/10.1130/B30843.1

Hadlari, T., MacLean B.C., Pyle L.J., Fallas K.M., and Durbano, A.M. 2015. A combined depth and thermal maturity map of the Canol Formation, northern Mackenzie Valley,

Northwest Territories. Geological Survey of Canada, Open File 7865, 1 .zip file. https://doi.org/10.4095/296460

Hadlari, T., MacLean, B.C., Galloway, J.M., Sweet, A.R., White, J.M., Thomson, D., Gabites, J., Schr¨oder-Adams, C.J., 2014b. The flexural margin, the foredeep, and the orogenic margin of a northern Cordilleran foreland basin: Cretaceous tectonostratigraphy and detrital zircon provenance, northwestern Canada. Mar. Petrol. Geol. 57, 173–186. https://doi.org/10.1016/j.marpetgeo.2014.05.019

Hammes, U., Frébourg, G., 2012. Haynesville and Bossier mudrocks: a facies and sequence stratigraphic investigation, East Texas and Louisiana, USA. Mar. Pet. Geol. 31 (1), 8–26. https://doi.org/10.1016/j.marpetgeo.2011.10.001

Hammes, U., Hamlin, H.S., Ewing, T.E., 2011. Geologic analysis of the Upper Jurassic Haynesville Shale in east Texas and west Louisiana. Am. Assoc. Pet. Geol. Bull. 95 (10), 1643–1666. https://doi.org/10.1306/02141110128

Han, C., Jiang, Z., Han, M., Wu, M., Lin, W., 2016. The lithofacies and reservoir characteristics of the upper ordovician and lower silurian black shale in the southern Sichuan Basin and its periphery, China. Mar. Petrol. Geol. 75, 181–191. https://doi. org/10.1016/j.marpetgeo.2016.04.014

Harazim, D., McIlroy, D., Edwards, N.P., Wogelius, R.A., Manning, P.L., Poduska, K.M., Layne, G.D., Sokaras, D., Alonso-Mori, R., Bergmann, U., 2015. Bioturbating animals control the mobility of redox-sensitive trace elements in organic-rich mudstone. Geology 43 (11), 1007–1010. https://doi.org/10.1130/G37025.1

Harrington, R.R., Kennedy, B.P., Chamberlain, C.P., Blum, J.D., Folt, C.L., 1998. 15N enrichment in agricultural catchments: field patterns and applications to tracking Atlantic

salmon (Salmo salar). Chem. Geol. 147, 281–294. https://doi.org/10.1016/S0009-2541(98)00018-7

Harris, B.S., LaGrange, M.T., Biddle, S.K., Playter, T.L., Fiess, K.M., Gingras, M.K., 2022. Chemostratigraphy as a tool for sequence stratigraphy in the Devonian Hare Indian Formation in the Mackenzie Mountains and Central Mackenzie Valley, Northwest Territories, Canada. Can. J. Earth Sci., 59(1), 29–45. https://doi.org/10.1139/cjes-2020-0198

Harris, N.B. (Ed.), 2005. Deposition of Organic-Carbon-Rich Sediments: Models. SEPM (Society for Sedimentary Geology). https://doi.org/10.2110/pec.05.82

Harris, N.B., McMillan, J.M., Knapp, L.J., Mastalerz, M., 2018. Organic matter accumulation in the Upper Devonian Duvernay Formation, Western Canada Sedimentary Basin, from sequence stratigraphic analysis and geochemical proxies. Sediment. Geol. 376, 185–203. https://doi.org/10.1016/j.sedgeo.2018.09.004

Harris, N.B., Mnich, C.A., Selby, D., Korn, D., 2013. Minor and trace element and Re–Os chemistry of the Upper Devonian Woodford Shale, Permian Basin, west Texas: insights into metal abundance and basin processes. Chem. Geol. 356, 76–93. https://doi.org/10.1016/j.chemgeo.2013.07.018

Hart, B.S., 2015. The Greenhorn Cyclothem of the Cretaceous Western Interior Seaway: lithology trends, stacking patterns, log signatures, and, and application to the Eagle Ford of West Texas. Gulf Coast Assoc. Geol. Soc. Trans. 65, 155–174.

Helland-Hansen, W., Martinsen, O.J., 1996. Shoreline trajectories and sequences: description of variable depositional-dip scenarios. J. Sediment. Res. 66 (4), 670–688. https://doi.org/10.1306/D42683DD-2B26-11D7-8648000102C1865D

Helly, J.J., Levin, L.A., 2004. Global distribution of naturally occurring marine hypoxia on continental margins. Deep-Sea Res. I Oceanogr. Res. Pap. 51 (9), 1159–1168. https://doi.org/10.1016/j.dsr.2004.03.009

Helz, G.R., Miller, C.V., Charnock, J.M., Mosselmans, J.F.W., Pattrick, R.A.D., Garner, C.D., Vaughan, D.J., 1996. Mechanism of molybdenum removal from the sea and its concentration in black shales: EXAFS evidence. Geochim. Cosmochim. Acta 60 (19), 3631–3642. https://doi.org/10.1016/0016-7037(96)00195-0

Hills, L.V., Sangster, E.V., Suneby, L.B. (Eds.), 1981. Lexicon of Canadian stratigraphy, Volume 2. Yukon Territory and District of Mackenzie. Canadian Society of Petroleum Geologists, Calgary.

Hines, B.R., Gazley, M.F., Collins, K.S., Bland, K.J., Crampton, J.S., Ventura, G.T., 2019. Chemostratigraphic resolution of widespread reducing conditions in the southwest Pacific Ocean during the Late Paleocene. Chem. Geol. 504, 236–252. https://doi.org/10.1016/j.chemgeo.2018.11.020

Hoch, M.P., Fogel, M.L., Kirchman, D.L., 1994. Isotope fractionation during ammonium uptake by marine microbial assemblages. Geomicrobiol. J. 12, 113–127. https://doi.org/10.1080/01490459409377977

Hover, V.C., Peacor, D.R., Walter, L.M., 1996. STEM/AEM evidence for preservation of burial diagenetic fabrics in Devonian shales; implications for fluid/rock interaction in cratonic basins (USA). J. Sediment. Res. 66 (3), 519–530. https://doi.org/10.1306/D4268397-2B26-11D7-8648000102C1865D

Hower, J., Eslinger, E.V., Hower, M.E., Perry, E.A., 1976. Mechanism of burial metamorphism of argillaceous sediment: 1. Mineralogical and chemical evidence. GSA Bulletin 87 (5), 725–737. https://doi.org/10.1130/0016-7606(1976)87<725:MOBMOA>2.0. CO;2

Hu, Y., Devegowda, D., Sigal, R., 2016. A microscopic characterization of wettability in shale kerogen with varying maturity levels. J. Nat. Gas Sci. Eng. 33, 1078–1086. https://doi.org/10.1016/j.jngse.2016.06.014.

Huerta-Diaz, M.A., Morse, J.W., 1992. Pyritization of trace metals in anoxic marine sediments. Geochim. Cosmochim. Acta 56 (7), 2681–2702. https://doi.org/10.1016/0016-7037(92)90353-K

Hume, G.C., 1922. Geology of the Norman Wells oil fields and a reconnaissance of a part of Liard River. Geological Survey of Canada, Summary Report Part B, Calgary, AB.

Hunt, D., Tucker, M.E., 1992. Stranded parasequences and the forced regressive wedge systems tract: deposition during base-level fall. Sediment. Geol. 81 (1–2), 1–9. https://doi.org/10.1016/0037-0738(92)90052-S

Irish, J.P.R., Kempthorne, R.H., 1987. The study of natural fractures in a reef complex, Norman Wells Oilfield, Canada, in: Tillman, R.W., Weber, K.J. (Eds.), Res. Sedimentol.: Soc. Econ. Paleontol. Mineral. Spec. Publ. 40, 153–168. https://doi.org/10.2110/pec.87.40.0153

Irwin, D., 2020. Geology of the Northwest Territories. (No. NWT Open Report 2020-007.).

Issler, D.R., Grist, A.M., Stasiuk, L.D., 2005. Post-Early Devonian thermal constraints on hydrocarbon source rock maturation in the Keele Tectonic Zone, Tulita area, NWT, Canada, from multi-kinetic apatite fission track thermochronology, vitrinite reflectance

and shale compaction. Bull. Can. Pet. Geol. 53, 405–431. https://doi.org/10.2113/53.4.405

Jaffe, L.A., Peucker-Ehrenbrink, B., Petsch, S.T., 2002. Mobility of rhenium, platinum group elements and organic carbon during black shale weathering. Earth Planet. Sci. Lett. 198 (3–4), 339–353. https://doi.org/10.1016/S0012-821X(02)00526-5

Jagadisan, A., Heidari, Z., 2019. Experimental quantification of the effect of thermal maturity of kerogen on its wettability. SPE Reservoir Eval. Eng. 22 (4), 1323–1333. https://doi.org/10.2118/195684-PA.

James, G., Witten, D., Hastie, T., Tibshirani, R., 2013. An Introduction to Statistical Learning with Applications in R. Springer, New York, p. 426.

Jeletzky, J.A., 1975. Jurassic and Lower Cretaceous Paleogeography and Depositional Tectonics of Porcupine Plateau, Adjacent Areas of Northern Yukon and Those of Mackenzie District: Geological Survey of Canada. Paper 74-16, p. 52. https://doi.org/10.4095/102549

Jennings, D.S., Antia, J., 2013. Petrographic characterization of the Eagle Ford shale, south Texas: mineralogy, common constituents, and distribution of nanometer-scale pore types, in: Camp, W., Diaz, E., Wawak, B. (Eds.), Electron Microscopy of Shale Hydrocarbon Reservoirs: AAPG Memoir 102, pp. 101–113. https://doi.org/10.1306/13391708M1023586

Junium, C.K., Arthur, M.A., 2007. Nitrogen cycling during the Cretaceous, Cenomanian-Turonian Oceanic Anoxic Event II. Geochem. Geophys. Geosystems 8. https://doi.org/10.1029/2006GC001328

Kabanov, P., 2019. Devonian (c. 388–375 Ma) Horn River Group of Mackenzie Platform (NW Canada) is an open-shelf succession recording oceanic anoxic events. J. Geol. Soc. 176 (1), 29–45. https://doi.org/10.1144/jgs2018-075

Kabanov, P., 2019. Devonian (c. 388–375 Ma) Horn River Group of Mackenzie Platform (NW Canada) is an open-shelf succession recording oceanic anoxic events. J. Geol. Soc. 176, 29–45. https://doi.org/10.1144/jgs2018-075

Kabanov, P., Deblonde, C., 2019. Geological and geochemical data from Mackenzie Corridor. Part VIII: Middle-Upper Devonian lithostratigraphy, formation tops, and isopach maps in NTS areas 96 and 106, Northwest Territories and Yukon (Geological Survey of Canada Open File Report No. 8552). https://doi.org/10.4095/314785

Kabanov, P., Gouwy, S., Lawrence, P.A., Weleschuk, D.J., Chan, W.C., 2016. Geological and geochemical data from Mackenzie Corridor. Part III: New data on lithofacies, micropaleontology, lithogeochemistry, and Rock-EvalTM pyrolysis from the Devonian Horn River Group in the Mackenzie Plain and Norman Range, Northwest Territories (Geological Survey of Canada Open File Report No. 7951).

Kabanov, P., Gouwy, S.A., 2017. The Devonian Horn River Group and the basal Imperial Formation of the central Mackenzie Plain, N.W.T., Canada: multiproxy stratigraphic framework of a black shale basin. Can. J. Earth Sci. 54, 409–429. https://doi.org/10.1139/cjes-2016-0096

Kabanov, P., Jiang, C., 2020. Photic-zone euxinia and anoxic events in a Middle-Late Devonian shelfal sea of Panthalassan continental margin, NW Canada: Changing paradigm of Devonian ocean and sea level fluctuations. Glob. Planet. Change 188, 103153. https://doi.org/10.1016/j.gloplacha.2020.103153

Kabanov, P.B., 2015. Geological and geochemical data from the Mackenzie Corridor. Part I: Devonian cored sections and results for 2014 on geochemistry, d13C - d18O, and Rock-Eval 6 pyrolysis (Geological Survey of Canada Open File Report No. 7840). https://doi.org/10.4095/297403

Kabanov, P.B., Gouwy, S.A., 2020. The type section of the Canol Formation (Devonian black shale) at Powell Creek: Critical assessment and correlation in the northern Cordillera, NWT, Canada. Bull. Can. Pet. Geol. 68, 123–140. https://doi.org/10.35767/gscpgbull.68.4.123

Kaiho, K., Miura, M., Tezuka, M., Hayashi, N., Jones, D.S., Oikawa, K., Casier, J.-G., Fujibayashi, M., Chen, Z.-Q., 2021. Coronene, mercury, and biomarker data support a link between extinction magnitude and volcanic intensity in the Late Devonian. Glob. Planet. Change 199, 103452. https://doi.org/10.1016/j.gloplacha.2021.103452

Kashiyama, Y., Ogawa, N.O., Kuroda, J., Shiro, M., Nomoto, S., Tada, R., Kitazato, H., Ohkouchi, N., 2008. Diazotrophic cyanobacteria as the major photoautotrophs during mid-Cretaceous oceanic anoxic events: Nitrogen and carbon isotopic evidence from sedimentary porphyrin. Org. Geochem. 39, 532–549. https://doi.org/10.1016/j.orggeochem.2007.11.010

Katz, B.J., Arango, I., 2018. Organic porosity: a geochemist's view of the current state of understanding. Org. Geochem. 123, 1–16. https://doi.org/10.1016/j.orggeochem.2018.05.015

Keller, L.M., Holzer, L., Wepf, R., Gasser, P., Münch, B., Marschall, P., 2011. On the application of focused ion beam nanotomography in characterizing the 3D pore space

geometry of Opalinus clay. Phys. Chem. Earth 36, 1539–1544. https://doi.org/10.1016/j.pce.2011.07.010. Parts A/B/C.

Keller, M.A., Isaacs, C.M., 1985. An evaluation of temperature scales for silica diagenesis in diatomaceous sequences including a new approach based on the Miocene Monterey Formation. California: Geo Mar. Lett. 5 (1), 31–35. https://doi.org/10.1007/BF02629794

Kendall, B., Reinhard, C.T., Lyons, T.W., Kaufman, A.J., Poulton, S.W., Anbar, A.D., 2010. Pervasive oxygenation along late Archaean ocean margins. Nat. Geosci. 3 (9), 647. https://doi.org/10.1038/ngeo942

Kessler, A.J., Bristow, L.A., Cardenas, M.B., Glud, R.N., Thamdrup, B., Cook, P.L.M., 2014. The isotope effect of denitrification in permeable sediments. Geochim. Cosmochim. Acta 133, 156–167. https://doi.org/10.1016/j.gca.2014.02.029

Kimura, H., Watanabe, Y., 2001. Oceanic anoxia at the Precambrian-Cambrian boundary. Geology 29 (11), 995–998. https://doi.org/10.1130/0091-7613(2001)029<0995:OAATPC>2.0.CO;2

Kindle, E.M., Bosworth, T.O., 1921. Oil bearing rocks of lower Mackenzie River Valley. Thomas Mulvey, Ottawa, Ontario.

Klaver, J., Desbois, G., Littke, R., Urai, J., 2015. BIB-SEM characterization of pore space morphology and distribution in postmature to overmature samples from the Haynesville and Bossier Shales. Mar. Petrol. Geol. 59, 451–466. https://doi.org/10.1016/j.marpetgeo.2014.09.020

Klaver, J., Desbois, G., Littke, R., Urai, J., 2016. BIB-SEM pore characterization of mature and post mature Posidonia Shale samples from the Hils area, Germany. Int. J. Coal Geol. 158, 78–89. https://doi.org/10.1016/j.coal.2016.03.003

Klemme, H.D., Ulmishek, G.F., 1991. Effective Petroleum Source Rocks of the World: Stratigraphic Distribution and Controlling Depositional Factors. Am. Assoc. Pet. Geol. Bull. 75, 1809–1851. https://doi.org/10.1306/0C9B2A47-1710-11D7-8645000102C1865D

Klinkhammer, G.P., Palmer, M.R., 1991. Uranium in the oceans: where it goes and why. Geochim. Cosmochim. Acta 55 (7), 1799–1806. https://doi.org/10.1016/0016-7037(91)90024-Y

Knapp, A., 2012. The sensitivity of marine N2 fixation to dissolved inorganic nitrogen. Front. Microbiol., Article 374 3, 1–14. https://doi.org/10.3389/fmicb.2012.00374

Knapp, A., Dekaezemacker, J., Bonnet, S., Sohm, J., Capone, D., 2012. Sensitivity of Trichodesmium erythraeum and Crocosphaera watsonii abundance and N<sub>2 fixation rates to varying NO<sub>3<sup>− and PO<sub>4<sup>3− concentrations in batch cultures. Aquat. Microb. Ecol. 66, 223–236. https://doi.org/10.3354/ame01577

Knapp, L.J., Ardakani, O.H., Uchida, S., Nanjo, T., Otomo, C., Hattori, T., 2020. The influence of rigid matrix minerals on organic porosity and pore size in shale reservoirs: upper Devonian Duvernay Formation, Alberta, Canada. Int. J. Coal Geol. 227, 103525. https://doi.org/10.1016/j.coal.2020.103525

Knapp, L.J., Harris, N.B., McMillan, J.M., 2019. A sequence stratigraphic model for the organic-rich Upper Devonian Duvernay Formation, Alberta, Canada. Sediment. Geol. 387, 152–181. https://doi.org/10.1016/j.sedgeo.2019.04.008

Knapp, L.J., McMillan, J.M., Harris, N.B., 2017. A depositional model for organic-rich Duvernay Formation mudstones. Sediment. Geol. 347, 160–182. https://doi.org/10.1016/j.sedgeo.2016.11.012

Konhauser, K.O., 2007. Introduction to Geomicrobiology. Blackwell, Malden, Massachusetts.

L¨ohr, S.C., Baruch, E.T., Hall, P.A., Kennedy, M.J., 2015. Is organic pore development in gas shales influenced by the primary porosity and structure of thermally immature organic matter. Org. Geochem. 87, 119–132. https://doi.org/10.1016/j. orggeochem.2015.07.010

LaGrange, M.T., Atienza, N.M.M., Biddle, S.K., Harris, B.S., Fiess, K.M., Terlaky, V., Konhauser, K.O., Gingras, M.K., 2022. The nature, origin, and predictors of porosity in the Middle to Late Devonian Horn River Group of the Central Mackenzie Valley, Northwest Territories, Canada. Mar. Pet. Geol. 142, 105738. https://doi.org/10.1016/j.marpetgeo.2022.105738

Lamb, A.L., Wilson, G.P., Leng, M.J., 2006. A review of coastal palaeoclimate and relative sea-level reconstructions using δ13C and C/N ratios in organic material. Earth-Sci. Rev. 75, 29–57. https://doi.org/10.1016/j.earscirev.2005.10.003

Lash, G.G., 2019. A global biogeochemical perturbation during the Middle Frasnian punctata Event: Evidence from muted carbon isotope signature in the Appalachian Basin, New York State (USA). Glob. Plan. Change 177, 239–254. https://doi.org/10.1016/j.gloplacha.2019.01.006

Law, C.A., 1999. Evaluating source rocks, in: Beaumont, A.E., Foster, N.H. (Eds.), Treatise of Petroleum Geology/Handbook of Petroleum Geology: Exploring for Oil and Gas Traps. AAPG Special Bulletin, pp. 1–41 (Chapter 6).

Lazar, O.R., Bohacs, K.M., Macquaker, J.H., Schieber, J., Demko, T.M., 2015. Capturing key attributes of fine-grained sedimentary rocks in outcrops, cores, and thin sections: nomenclature and description guidelines. J. Sediment. Res. 85 (3), 230–246.

Lazar, O.R., Bohacs, K.M., Macquaker, J.H.S., Schieber, J., Demko, T.M., 2015. Capturing key attributes of fine-grained sedimentary rocks in outcrops, cores, and thin sections: nomenclature and description guidelines. J. Sediment. Res. 85, 230–246. https://doi.org/10.2110/jsr.2015.11

Lehmann, M.F., Bernasconi, S.M., Barbieri, A., McKenzie, J.A., 2002. Preservation of organic matter and alteration of its carbon and nitrogen isotope composition during simulated and in situ early sedimentary diagenesis. Geochim. Cosmochim. Acta 66, 3573–3584. https://doi.org/10.1016/S0016-7037(02)00968-7

Lemiere, B., 2018. A review of pXRF (field portable X-ray fluorescence) applications for applied geochemistry. J. Geochem. Explor. 188, 350–363. https://doi.org/10.2110/jsr.2015.11

Lenz, A.C., 1972. Ordovician to Devonian history of northern Yukon and adjacent district of Mackenzie. Bull. Can. Pet. Geol. 20, 321–361. https://doi.org/10.35767/gscpgbull.20.2.321

Lewan, M.D., 1983. Effects of thermal maturation on stable organic carbon isotopes as determined by hydrous pyrolysis of Woodford Shale. Geochim. Cosmochim. Acta 47, 1471–1479. https://doi.org/10.1016/0016-7037(83)90306-X

Lewan, M.D., 1984. Factors controlling the proportionality of vanadium to nickel in crude oils. Geochim. Cosmochim. Acta 48 (11), 2231–2238. https://doi.org/10.1016/0016-7037(84)90219-9

Lewan, M.D., Maynard, J.B., 1982. Factors controlling enrichment of vanadium and nickel in the bitumen of organic sedimentary rocks. Geochim. Cosmochim. Acta 46 (12), 2547–2560. https://doi.org/10.1016/0016-7037(82)90377-5

Li, C., Zhang, J., Li, W., Botting, J., Chen, Q., Fan, J., Zhang, Y., 2021. Multiple glacio-eustatic cycles and associated environmental changes through the Hirnantian (Late Ordovician) in South China. Glob. Planet. Change 207, 103668. https://doi.org/10.1016/j.gloplacha.2021.103668

Li, J., Ma, Y., Huang, K., Zhang, Y., Wang, W., Liu, J., Li, Z., Lu, S., 2018. Quantitative characterization of organic acid generation, decarboxylation, and dissolution in a shale reservoir and the corresponding applications—a case study of the Bohai Bay Basin. Fuel 214, 538–545. https://doi.org/10.1016/j.fuel.2017.11.034

Li, L., Zheng, Y.-F., Cartigny, P., Li, J., 2014. Anomalous nitrogen isotopes in ultrahigh-pressure metamorphic rocks from the Sulu orogenic belt: Effect of abiotic nitrogen reduction during fluid–rock interaction. Earth & Planet. Sci. Lett. 403, 67–78. https://doi.org/10.1016/j.epsl.2014.06.029

Li, Y., Li, L., Wu, Z., 2021. First-principles calculations of equilibrium nitrogen isotope fractionations among aqueous ammonium, silicate minerals and salts. Geochim. Cosmochim. Acta 297, 220–232. https://doi.org/10.1016/j.gca.2021.01.019

Li, Y., Schieber, J., Fan, T., Wei, X., 2018. Pore characterization and shale facies analysis of the Ordovician-Silurian transition of northern Guizhou, South China: the controls of shale facies on pore distribution. Mar. Petrol. Geol. 92, 697–718. https://doi.org/10.1016/j.marpetgeo.2017.12.001

Li, Z., Schieber, J., 2020. Application of sequence stratigraphic concepts to the Upper Cretaceous Tununk Shale Member of the Mancos Shale Formation, south-central Utah: parasequence styles in shelfal mudstone strata. Sedimentology 67 (1), 118–151. https://doi.org/10.1111/sed.12637

Liu, B., Schieber, J., Mastalerz, M., Teng, J., 2020. Variability of rock mechanical properties in the sequence stratigraphic context of the upper devonian new albany shale, Illinois basin. Mar. Petrol. Geol. 112, 104068. https://doi.org/10.1016/j. marpetgeo.2019.104068

Liu, Y., Zhang, J., Tang, X., Yang, C., Tang, S., 2016. Weathering characteristics of the Lower Paleozoic black shale in northwestern Guizhou Province, south China. J. Earth Syst. Sci. 125 (5), 1061–1078. https://doi.org/10.1007/s12040-016-0718-6

Loescher, C.R., Großkopf, T., Desai, F.D., Gill, D., Schunck, H., Croot, P.L., Schlosser, C., Neulinger, S.C., Pinnow, N., Lavik, G., Kuypers, M.M.M., LaRoche, J., Schmitz, R.A., 2014. Facets of diazotrophy in the oxygen minimum zone waters off Peru. ISME J. 8, 2180–2192. https://doi.org/10.1038/ismej.2014.71

Loucks, R.G., Reed, R.M., 2014. Scanning-Electron-Microscope petrographic evidence for distinguishing organic-matter pores associated with depositional organic matter versus migrated organic matter in mudrocks. Gulf Coast Ass. Geol. Soc. J. 3, 51–60.

Loucks, R.G., Reed, R.M., Ruppel, S.C., Hammes, U., 2012. Spectrum of pore types and networks in mudrocks and descriptive classification for matrix-related mudrock pores. AAPG (Am. Assoc. Pet. Geol.) Bull. 96 (6), 1071–1098. https://doi.org/10.1306/ 08171111061

Loucks, R.G., Reed, R.M., Ruppel, S.C., Jarvie, D.M., 2009. Morphology, genesis, and distribution of nanometer-scale pores in siliceous mudstones of the Mississippian Barnett Shale. J. Sediment. Res. 79, 848–861. https://doi.org/10.2110/jsr.2009.092

Loutit, T.S., Hardenbol, J., Vail, P.R., Baum, G.R., 1988. Condensed sections: the key to age determination and correlation of continental margin sequences, in: Wilgus, C.K., Hastings, B.S., Kendall, C.G.S., Posamentier, H.W., Ross, C.A., Van Wagoner, J.C.

(Eds.), Sea Level Changes – An Integrated Approach: Society of Economic Paleontologists and Geologists Special Publication. 42. pp. 183–213.

Lu, J., Ruppel, S.C., Rowe, H.D., 2015. Organic matter pores and oil generation in the Tuscaloosa marine shale. AAPG (Am. Assoc. Pet. Geol.) Bull. 99 (2), 333–357. https://doi.org/10.1306/08201414055

Lu, M., Lu, Y., Ikejiri, T., Sun, D., Carroll, R., Blair, E.H., Algeo, T.J., Sun, Y., 2021. Periodic oceanic euxinia and terrestrial fluxes linked to astronomical forcing during the Late Devonian Frasnian–Famennian mass extinction. Earth Planet. Sci. Lett. 562, 116839. https://doi.org/10.1016/j.epsl.2021.116839

Luffel, D.L., Guidry, F.K., 1993. New core analysis methods for measuring reservoir rock properties of Devonian shale. J. Petrol. Technol. 44 (11), 1184–1190. https://doi.org/10.2118/ 20571-PA

Luo, Y.-W., Lima, I.D., Karl, D.M., Deutsch, C.A., Doney, S.C., 2014. Data-based assessment of environmental controls on global marine nitrogen fixation. Biogeosciences 11, 691–708. https://doi.org/10.5194/bg-11-691-2014

MacEachern, J.A., Bann, K.L., Pemberton, S.G., Gingras, M.K., 2009. The ichnofacies paradigm: high-resolution paleoenvironmental interpretation of the rock record. SEPM Soc. Sediment. Geol. App. Ichnol. SC52, 27–64. https://doi.org/10.2110/pec.07.52.0027

MacEachern, J.A., Pemberton, S.G., Bann, K.L., Gingras, M.K., 2009. Departures from the archetypal ichnofacies: effective recognition of physico-chemical stresses in the rock record. Soc. Sediment. Geol. Appl. Ichnol. SC52, 65–93. https://doi.org/10.2110/pec.07.52.0065

MacGowan, D.B., Surdam, R.C., 1990. Carboxylic acid anions in formation waters, san joaquin basin and Louisiana Gulf coast, USA—implications for clastic diagenesis. Appl. Geochem. 5 (5–6), 687–701. https://doi.org/10.1016/0883-2927(90)90065-D

Mackenzie, W.S., 1970. Allochthonous Ree-Debris Limestone Turbidites Powell Creek, Northwest Territories. Bull. Can. Pet. Geol. 18, 474–492. https://doi.org/10.35767/gscpgbull.18.4.474

MacKenzie, W.S., 1974. Radiolaria from the Canol Formation, Northwest Territories. Geological Survey of Canada. Paper 74-1, Part A, 396 pp. https://doi.org/doi:10.4095/103272

MacLean, B.C., 2011. Tectonic and stratigraphic evolution of the Cambrian basin of northern Northwest Territories. Bull. Can. Petrol. Geol. 59 (2), 172–194. https://doi.org/10.2113/gscpgbull.59.2.172

MacLean, B.C., Fallas, K.M., Hadlari, T., 2014. The multi-phase keele arch, central Mackenzie corridor, Northwest Territories. Bull. Can. Petrol. Geol. 62 (2), 68–104. https://doi.org/10.2113/gscpgbull.62.2.68

MacNeil, A.J., Jones, B., 2006. Ovummuridae (calcareous microfossils) from a Late Devonian ramp: their distribution, preservation potential, and paleoecological significance. Can. J. Earth Sci. 43, 269–280. https://doi.org/10.1139/e05-105

Macquaker, J.H., Bohacs, K.M., 2007. On the accumulation of mud. Science, 318(5857), 1734–1735. https://doi.org/10.1126/science.1151980

Macquaker, J.H., Taylor, K.G., 1996. A sequence stratigraphic interpretation of a mudstone-dominated succession: the Lower Jurassic Cleveland ironstone Formation, U.K. J. Geol. Soc. Lond. 153, 759–770. http://dx.doi.org/10.1144/gsjgs.153.5.0759

Macquaker, J.H., Taylor, K.G., Gawthorpe, R.L., 2007. High-resolution facies analyses of mudstones: implications for paleoenvironmental and sequence stratigraphic interpretations of offshore ancient mud-dominated successions. J. Sediment. Res. 77 (4), 324–339. https://doi.org/10.2110/jsr.2007.029

Macquaker, J.H., Taylor, K.G., Keller, M., Polya, D., 2014. Compositional controls on early diagenetic pathways in fine-grained sedimentary rocks: implications for predicting unconventional reservoir attributes of mudstones. AAPG (Am. Assoc. Pet. Geol.) Bull. 98 (3), 587–603. https://doi.org/10.1306/08201311176

Madigan, M.T., 1995. Microbiology of Nitrogen Fixation by Anoxygenic Photosynthetic Bacteria, in: Blankenship, R.E., Madigan, M.T., Bauer, C.E. (Eds.), Anoxygenic Photosynthetic Bacteria. Advances in Photosynthesis and Respiration. Springer, Dordrecht.

Mann, U., Stein, R., 1997. Organic facies variations, source rock potential, and sea level changes in Cretaceous black shales of the Quebrada Ocal, Upper Magdalena Valley, Colombia. Am. Assoc. Pet. Geol. Bull. 81 (4), 556–576. https://doi.org/10.1306/522B43CF-1727-11D7-8645000102C1865D

Marynowski, L., Pisarzowska, A., Derkowski, A., Rakociński, M., Szaniawski, R., Środoń, J., Cohen, A.S., 2017. Influence of palaeoweathering on trace metal concentrations and environmental proxies in black shales. Palaeogeogr. Palaeoclimatol. Palaeoecol. 472, 177–191. https://doi.org/10.1016/j.palaeo.2017.02.023

Mastalerz, M., Schimmelmann, A., Drobniack, A., Chen, Y., 2013. Porosity of Devonian and Mississippian New Albany Shale across a maturation gradient: insights from organic

petrology, gas adsorption, and mercury intrusion. AAPG (Am. Assoc. Pet. Geol.) Bull. 97 (10), 1621–1643. https://doi.org/10.1306/04011312194

Mayer, B., Boyer, E.W., Goodale, C., Jaworski, N.A., Van Breemen, N., Howarth, R.W., Seitzinger, S., Billen, G., Lajtha, K., Nadelhoffer, K., Van Dam, D., Hetling, L.J., Nosal, M., Paustian, K., 2002. Sources of nitrate in rivers draining sixteen watersheds in the northeastern U.S.: Isotopic constraints, in: Boyer, E.W., Howarth, R.W. (Eds.), The Nitrogen Cycle at Regional to Global Scales. Springer Netherlands, Dordrecht, pp. 171–197. https://doi.org/10.1007/978-94-017-3405-9_5

Mazzotti, S., Hyndman, R.D., 2002. Yakutat collision and strain transfer across the northern Canadian Cordillera. Geology 30 (6), 495–498. https://doi.org/10.1130/0091-7613(2002)030<0495:YCASTA>2.0.CO;2.

McGhee, G.R., Clapham, M.E., Sheehan, P.M., Bottjer, D.J., Droser, M.L., 2013. A new ecological-severity ranking of major Phanerozoic biodiversity crises. Palaeogeogr. Palaeoclimat. Palaeoecol. 370, 260–270. https://doi.org/10.1016/j.palaeo.2012.12.019

McLennan, S.M., Hemming, S., McDaniel, D.K., Hanson, G.N., 1993. Geochemical approaches to sedimentation, provenance, and tectonics. Geol. Soc. Am. Spec. Pap. 284, 21–40.

McManus, J., Berelson, W.M., Klinkhammer, G.P., Hammond, D.E., Holm, C., 2005. Authigenic uranium: relationship to oxygen penetration depth and organic carbon rain. Geochim. Cosmochim. Acta 69 (1), 95–108. https://doi.org/10.1016/j.gca.2004.06.023

Meyers, P.A., 1994. Preservation of elemental and isotopic source identification of sedimentary organic matter. Chem. Geol. 114, 289–302. https://doi.org/10.1016/0009-2541(94)90059-0

Meyers, P.A., 2006. Paleoceanographic and paleoclimatic similarities between Mediterranean sapropels and Cretaceous black shales. Palaeogeogr., Palaeoclimatol., Palaeoecol., 235(1-3), 305–320. https://doi.org/10.1016/j.palaeo.2005.10.025

Meyers, P.A., Eadie, B.J., 1993. Sources, degradation and recycling of organic matter associated with sinking particles in Lake Michigan. Org. Geochem. 20, 47–56. https://doi.org/10.1016/0146-6380(93)90080-U

Milliken, K.L., Curtis, M.E., 2016. Imaging pores in sedimentary rocks: foundation of porosity prediction. Mar. Petrol. Geol. 73, 590–608. https://doi.org/10.1016/j. marpetgeo.2016.03.020.

Milliken, K.L., Rudnicki, M., Awwiller, D.N., Zhang, T., 2013. Organic matter-hosted pore system, in: Marcellus Formation (Devonian), vol. 97. AAPG Bulletin, Pennsylvania, pp. 177–200. https://doi.org/10.1306/07231212048

Minagawa, M., Wada, E., 1986. Nitrogen isotope ratios of red tide organisms in the East China Sea: A characterization of biological nitrogen fixation. Mar. Chem. 19, 245–259. https://doi.org/10.1016/0304-4203(86)90026-5

Mongelli, G., Critelli, S., Perri, F., Sonnino, M., Perrone, V., 2006. Sedimentary recycling, provenance and paleoweathering from chemistry and mineralogy of Mesozoic continental redbed mudrocks, Peloritani Mountains, southern Italy. Geochem. J. 40 (20), 197–209. https://doi.org/10.2343/geochemj.40.197

Montoya, J.P., Carpenter, E.J., Capone, D.G., 2002. Nitrogen fixation and nitrogen isotope abundances in zooplankton of the oligotrophic North Atlantic. Limnol. Oceanogr. 47, 1617–1628. https://doi.org/10.4319/lo.2002.47.6.1617

Morford, J.L., Russell, A.D., Emerson, S., 2001. Trace metal evidence for changes in the redox environment associated with the transition from terrigenous clay to diatomaceous sediment, Saanich Inlet, BC. Mar. Geol. 174 (1–4), 355–369. https://doi.org/10.1016/S0025-3227(00)00160-2

Morrison, J.M., Codispoti, L.A., Smith, S.L., Wishner, K., Flagg, C., Gardner, W.D., Gaurin, S., Naqvi, S.W.A., Manghnani, V., Prosperie, L., Gundersen, J.S., 1999. The oxygen minimum zone in the Arabian Sea during 1995. Deep-Sea Res. II Top. Stud. Oceanogr. 46 (8–9), 1903–1931. https://doi.org/10.1016/S0967-0645(99)00048-X

Morrow, D.W., 2018. Devonian of the Northern Canadian Mainland Sedimentary Basin: A Review. Bull. Can. Pet. Geol. 66, 623–694.

Muir, I., Dixon, O.A., 1984. Facies analysis of a Middle Devonian sequence in the Mountain River-Gayna River, in: Brophy, J. (Ed.), Contributions to the Geology of the Northwest Territories. Department of Indian Affairs and Northern Development, Canada., pp. 55–62.

Muir, I., Wong, P., Wendte, J., 1985. Devonian Hare Indian-Ramparts (Kee Scarp) evolution, Mackenzie Mountains and subsurface Norman Wells, NWT: basin-fill and platform reef development, in: Longman, M.W., Shanley, K.W., Lindsay, R.F., Eby, D.E. (Eds.), Rocky Mountain Carbonate Reservoirs: A Core Workshop. SEPM (Society for Sedimentary Geology), pp. 311–341. https://doi.org/10.2110/cor.85.07

Muir, I.D., 1988. Devonian Hare Indian and Ramparts formations, MacKenzie Mountains, N.W.T. basin-fill, platform and reef development. (Thesis). University of Ottawa (Canada). https://doi.org/10.20381/ruor-10585

Murphy, A.E., Sageman, B.B., Hollander, D.J., 2000. Eutrophication by decoupling of the marine biogeochemical cycles of C, N, and P: A mechanism for the Late Devonian mass extinction. Geology 28 (5), 427–430. https://doi.org/10.1130/0091-7613(2000)28<427:EBDOTM>2.0.CO;2

Myers, K.J., Wignall, P.B., 1987. Understanding Jurassic organic-rich mudrocks—new concepts using gamma-ray spectrometry and palaeoecology: examples from the Kimmeridge Clay of Dorset and the Jet Rock of Yorkshire, in: Legget, J.K., Zuffa, G.G. (Eds.), Marine Clastic Sedimentology. Springer, Dordrecht, pp. 172–189. https://doi.org/10.1007/978-94-009-3241-8_9

Nadeau, P.H., Wilson, M.J., McHardy, W.J., Tait, J.M., 1985. The conversion of smectite to illite during diagenesis: evidence from some illitic clays from bentonites and sandstones. Mineral. Mag. 49 (352), 393–400. https://doi.org/10.1180/minmag.1985.049.352.10

Nesbitt, H.W., Young, G.M., 1982. Early Proterozoic climates and plate motions inferred from major element chemistry of lutites. Nature 299 (5885), 715–717. https://doi.org/10.1038/299715a0

Nichols, G., 2009. Sedimentology and Stratigraphy. John Wiley & Sons., Chichester, UK.

Norris, A.W., 1985. Stratigraphy of Devonian outcrop belts in northern Yukon Territory and northwestern District of Mackenzie (Operation Porcupine area) (Memoir No. 410). Geological Survey of Canada. https://doi.org/10.4095/120309

Northwest Territories Geological Survey (NTGS) and National Energy Board (NEB), 2015. An Assessment of the Unconventional Petroleum Resources of the Bluefish Shale and the Canol Shale in the Northwest Territories - Energy Briefing Note. National Energy Board, Canada, p. 10.

Nyhuis, C.J., Riley, D., Kalasinska, A., 2016. Thin section petrography and chemostratigraphy: integrated evaluation of an upper Mississippian mudstone dominated succession from the southern Netherlands. Neth. J. Geosci. 95 (1), 3–22. https://doi.org/10.1017/njg.2015.25

O'Leary, M.H., 1981. Carbon isotope fractionation in plants. Phytochemistry 20, 553–567. https://doi.org/10.1016/0031-9422(81)85134-5

Olivier, J.P., Conklin, W.B., Szombathely, M.v., 1994, in: Rouquerol, J., Rodriguez- Reinoso, F., Sing, K.S.W., Unger, K.K. (Eds.), Characterization of Porous Solids III, Studies in Surface Science and Catalysis, vol. 87, pp. 81–88.

Ormiston, A.R., Oglesby, R.J., 1995. Effect of Late Devonian Paleoclimate on Source Rock Quality and Location, in: Huc, A.-Y. (Ed.), Paleogeography, Paleoclimate, and Source Rocks. American Association of Petroleum Geologists. https://doi.org/10.1306/St40595C5

Over, D.J., 1990. Trace metals in burrow walls and sediments, Georgia Bight, USA. Ichnos. Int. J. Plant Anim. 1 (1), 31–41. https://doi.org/10.1080/10420949009386329

Partin, C.A., Bekker, A., Planavsky, N.J., Scott, C.T., Gill, B.C., Li, C., Podkovyrov, V., Maslov, V., Konhauser, K.O., Lalonde, S.V., Love, G.D., Love, G.D., Poulton, S.W., Lyons, T.W., 2013. Large-scale fluctuations in Precambrian atmospheric and oceanic oxygen levels from the record of U in shales. Earth Planet. Sci. Lett. 369, 284–293. https://doi.org/10.1016/j.epsl.2013.03.031

Patchett, P.J., White, W.M., Feldmann, H., Kielinczuk, S., Hofmann, A.W., 1984. Hafnium/rare earth element fractionation in the sedimentary system and crustal recycling into the Earth's mantle. Earth Planet. Sci. Lett. 69 (2), 365–378. https://doi.org/10.1016/0012-821X(84)90195-X

Pearce, T.J., Besly, B.M., Wray, D.S., Wright, D.K., 1999. Chemostratigraphy: a method to improve interwell correlation in barren sequences—a case study using onshore Duckmantian/Stephanian sequences (West Midlands, UK). Sediment. Geol. 124(1–4), 197–220. https://doi.org/10.1016/S0037-0738(98)00128-6

Pearce, T.J., Martin, J.H., Cooper, D., Wray, D.S., 2010. Chemostratigraphy of upper carboniferous (Pennsylvanian) sequences from the Southern North Sea (United Kingdom), in: Application of Modern Stratigraphic Techniques: Theory and Case Histories: SEPM (Society for Sedimentary Geology) Special Publication, 94, pp. 109–127. http://dx.doi.org/10.2110/sepmsp.094.109

Pearce, T.J., Wray, D., Ratcliffe, K., Wright, D.K., Moscariello, A., 2005. Chemostratigraphy of the Upper Carboniferous Schooner Formation, southern North Sea, in: Collinson, J.D., Evans, D.J., Holliday, D.W. (Eds.), Carboniferous Hydrocarbon Resources: The Southern North Sea and Surrounding Onshore Areas: Occasional Publication Series of the Yorkshire Geological Society. 7. pp. 147–164.

Pennington, J.T., Mahoney, K.L., Kuwahara, V.S., Kolber, D.D., Calienes, R., Chavez, F.P., 2006. Primary production in the eastern tropical Pacific: A review. Prog. Oceanogr. 69, 285–317. https://doi.org/10.1016/j.pocean.2006.03.012

Pennock, J.R., Velinsky, D.J., Ludlam, J.M., Sharp, J.H., Fogel, M.L., 1996. Isotopic fractionation of ammonium and nitrate during uptake by Skeletonema costatum: Implications for δ15N dynamics under bloom conditions. Limnol. Oceanogr. 41, 451–459. https://doi.org/10.4319/lo.1996.41.3.0451

Peters, K.E., Cassa, M.R., 1994. Applied source rock geochemistry, in: Magoon, L.B., Dow, W.G., (Eds.), The Petroleum System-from source to trap. AAPG Memoire 60, pp. 93–12.

Peters, K.E., Sweeney, R.E., Kaplan, I.R., 1978. Correlation of carbon and nitrogen stable isotope ratios in sedimentary organic matter 1: C and N isotopes. Limnol. Oceanogr. 23, 598–604. https://doi.org/10.4319/lo.1978.23.4.0598

Peucker-Ehrenbrink, B., Hannigan, R.E., 2000. Effects of black shale weathering on the mobility of rhenium and platinum group elements. Geology 28 (5), 475–478. https://doi.org/10.1130/0091-7613(2000)28<475:EOBSWO>2.0.CO;2

Piper, D.Z., Calvert, S.E., 2009. A marine biogeochemical perspective on black shale deposition. Earth Sci. Rev. 95 (1–2), 63–96. https://doi.org/10.1016/j.earscirev.2009.03.001

Pisarzowska, A., Racki, G., 2012. Isotopic chemostratigraphy across the Early–Middle Frasnian transition (Late Devonian) on the South Polish carbonate shelf: A reference for the global punctata Event. Chem. Geol. 334, 199–220. https://doi.org/10.1016/j.chemgeo.2012.10.034

Plank, T., Langmuir, C.H., 1998. The chemical composition of subducting sediment and its consequences for the crust and mantle. Chem. Geol. 145 (3), 325–394. https://doi.org/10.1016/S0009-2541(97)00150-2

Playter, T., Corlett, H., Konhauser, K., Robbins, L., Rohais, S., Crombez, V., Maccormack,K., Rokosh, D., Prenoslo, D., Furlong, C.M., Pawlowicz, J., Gingras, M., Lalonde, S., Lyster, S., Zonneveld, J.-P., 2018. Clinoform identification and correlation in fine-grained sediments: a case study using the Triassic Montney Formation. Sedimentology 65 (1), 263–302. https://doi.org/10.1111/sed.12403

Plint, A.G., Nummedal, D., 2000. The falling stage systems tract: recognition and importance in sequence stratigraphic analysis. Geol. Soc. Lond., Spec. Publ. 172 (1), 1–17. http://dx.doi.org/10.1144/GSL.SP.2000.172.01.01

Posamentier, H.W., Allen, G.P., 1999. Siliciclastic sequence stratigraphy: concepts and applications. SEPM Soc. Sediment. Geol. Concepts Sedimentol. Paleontol. 7, 210.

Posamentier, H.W., Kolla, V., 2003. Seismic geomorphology and stratigraphy of depositional elements in deep-water settings. J. Sediment. Res. 73 (3), 367–388. https://doi.org/10.1306/111302730367

Powell, J.W., Issler, D.R., Schneider, D.A., Fallas, K.M., Stockli, D.F., 2020. Thermal history of the Mackenzie Plain, Northwest Territories, Canada: Insights from low-temperature thermochronology of the Devonian Imperial Formation. GSA Bull. 132, 767–783. https://doi.org/10.1130/B35089.1

Prahl, F.G., De Lange, G.J., Scholten, S., Cowie, G.L., 1997. A case of post-depositional aerobic degradation of terrestrial organic matter in turbidite deposits from the Madeira Abyssal Plain. Organic Geochemistry, Organic Geochemistry of Paleoclimatic Markers: Production, Preservation and Modeling 27, 141–152. https://doi.org/10.1016/S0146-6380(97)00078-8

Pugh, D.C., 1983. Pre-Mesozoic geology in the subsurface of Peel River map area, Yukon Territory and district of Mackenzie (Memoir No. 401). Geological Survey of Canada. https://doi.org/10.4095/119498

Pyle, L.J., Fiess, K.M., Rocheleau, J., Terlaky, V., 2018. Source rock characterization data from the Devonian Horn River Group, Imperial Formation, and Cretaceous Slater River Formation outcrops - NTS 96D, 96E, and 106H, Northwest Territories. Northwest Territories Geological Survey, NWT Open Report 2016-013, 42 pages and appendices.

Pyle, L.J., Gal, L.P., 2016. Reference Section for the Horn River Group and Definition of the Bell Creek Member, Hare Indian Formation in central Northwest Territories. Bull. Can. Pet. Geol. 64, 67–98. https://doi.org/10.2113/gscpgbull.64.1.67

Pyle, L.J., Gal, L.P., Hadlari, T., 2015. Thermal maturity trends for Devonian Horn River Group units and equivalent strata in the Mackenzie Corridor, Northwest Territories and Yukon (Geological Survey of Canada Open File Report No. 7850). https://doi.org/10.4095/296446

Pyle, L.J., Gal, L.P., Hadlari, T., 2015. Thermal maturity trends for Devonian Horn River Group units and equivalent strata in the Mackenzie Corridor, Northwest Territories and Yukon (Geological Survey of Canada Open File Report No. 7850). https://doi.org/10.4095/296446

Racki, G., Rakociński, M., Marynowski, L., Wignall, P.B., 2018. Mercury enrichments and the Frasnian-Famennian biotic crisis: A volcanic trigger proved? Geology 46, 543–546. https://doi.org/10.1130/G40233.1

Ratcliffe, K.T., Martin, J., Pearce, T.J., Hughes, A.D., Lawton, D.E., Wray, D.S., Bessa, F., 2006. A regional chemostratigraphically-defined correlation framework for the late Triassic TAG-I Formation in Blocks 402 and 405a, Algeria. Pet. Geosci. 12 (1), 3–12. Ratcliffe, K., Wright, M., Montgomery, P., Palfrey, A., Vonk, A., Vermeulen, J., Barrett, M., 2010. Application of chemostratigraphy to the Mungaroo Formation, the Gorgon field, offshore northwest Australia. APPEA J. 50 (1), 371–388. https://doi.org/10.1144/1354-079305-669

Ratcliffe, K.T., Woods, J., Rice, C., 2012. Determining well-bore pathways during multilateral drilling campaigns in shale resource plays: an example using chemostratigraphy from the

Horn River Formation, British Columbia, Canada, in: Proceedings from: Eastern Australasian Basin Symposium IV, Brisbane, Australia.

Ratcliffe, K.T., Wright, A.M., Hallsworth, C., Morton, A., Zaitlin, B.A., Potocki, D., Wray, D., 2004. An example of alternative correlation techniques in a low-accommodation setting, nonmarine hydrocarbon system: the (Lower Cretaceous) Mannville Basal Quartz succession of southern Alberta. Am. Assoc. Pet. Geol. Bull. 88 (10), 1419–1432. https://doi.org/10.1306/05100402035

Ratcliffe, K., Wright, M., Montgomery, P., Palfrey, A., Vonk, A., Vermeulen, J., Barrett, M., 2010. Application of chemostratigraphy to the Mungaroo Formation, the Gorgon field, offshore northwest Australia. The APPEA Journal, 50(1), 371–388. https://doi.org/10.1071/AJ09022

Ratcliffe, K.T., Wright, A.M., Schmidt, K., 2012. Application of inorganic whole-rock geochemistry to shale resource plays: an example from the Eagle Ford Shale Formation, Texas. TSR 10, 4–9. https://doi.org/10.2110/sedred.2012.2.4

Ratcliffe, K.T., Wright, A.M., Spain, D.R., 2012. Unconventional methods for unconventional plays: using elemental data to understand shale resource plays. Petrol. Explor. Soc. Aust. News Resour. 117, 50–54.

Reichart, G.J., Lourens, L.J., Zachariasse, W.J., 1998. Temporal variability in the northern Arabian Sea Oxygen Minimum Zone (OMZ) during the last 225,000 years. Paleoceanography 13 (6), 607–621. https://doi.org/10.1029/98PA02203

Reinhard, C.T., Planavsky, N.J., Robbins, L.J., Partin, C.A., Gill, B.C., Lalonde, S.V., Bekker, A., Konhauser, K.O., Lyons, T.W., 2013. Proterozoic ocean redox and biogeochemical

stasis. Proc. Natl. Acad. Sci. 110 (14), 5357–5362. https://doi.org/10.1073/pnas.1208622110

Revsbech, N.P., Larsen, L.H., Gundersen, J., Dalsgaard, T., Ulloa, O., Thamdrup, B., 2009. Determination of ultra-low oxygen concentrations in oxygen minimum zones by the STOX sensor. Limnol. Oceanogr. Methods 7, 371–381. https://doi.org/10.4319/lom.2009.7.371

Rivera, K.T., Puckette, J., Quan, T.M., 2015. Evaluation of redox versus thermal maturity controls on δ 15 N in organic rich shales: A case study of the Woodford Shale, Anadarko Basin, Oklahoma, USA. Org. Geochem. 83–84, 127–139. https://doi.org/10.1016/j.orggeochem.2015.03.005

Robbins, L.J., Lalonde, S.V., Planavsky, N.J., Partin, C.A., Reinhard, C.T., Kendall, B., Scott, C., Hardisty, D.S., Gill, B.C., Alessi, D.S., Dupont, C.L., Saito, M.A., Crowe, S.A., Poulton, S.W., Bekker, A., Lyons, T.W., Konhauser, K.O., 2016. Trace elements at the intersection of marine biological and geochemical evolution. Earth Sci. Rev. 163, 323–348. https://doi.org/10.1016/j.earscirev.2016.10.013

Robinson, R.S., Kienast, M., Albuquerque, A.L., Altabet, M., Contreras, S., Holz, R.D.P., Dubois, N., Francois, R., Galbraith, E., Hsu, T.-C., Ivanochko, T., Jaccard, S., Kao, S.-J., Kiefer, T., Kienast, S., Lehmann, M., Martinez, P., McCarthy, M., Möbius, J., Pedersen, T., Quan, T.M., Ryabenko, E., Schmittner, A., Schneider, R., Schneider-Mor, A., Shigemitsu, M., Sinclair, D., Somes, C., Studer, A., Thunell, R., Yang, J.-Y., 2012. A review of nitrogen isotopic alteration in marine sediments. Paleoceanography 27. https://doi.org/10.1029/2012PA002321

Rock-Color Chart Committee, 2009. Geological Rock-Color Chart with Genuine Munsell Color Chips. Geological Society of America.

Rosenthal, Y., Lam, P., Boyle, E.A., Thomson, J., 1995. Authigenic cadmium enrichmen in suboxic sediments: precipitation and postdepositional mobility. Earth Planet. Sci Lett. 132 (1–4), 99–111. https://doi.org/10.1016/0012-821X(95)00056-I

Ross, D.J., Bustin, R.M., 2009. Investigating the use of sedimentary geochemical proxies for paleoenvironment interpretation of thermally mature organic-rich strata: examples from the Devonian–Mississippian shales, Western Canadian Sedimentary Basin. Chem. Geol. 260 (1–2), 1–19. https://doi.org/10.1016/j.chemgeo.2008.10.027

Ross, D.J.K., Bustin, M.R., 2009. The importance of shale composition and pore structure upon gas storage potential of shale gas reservoirs. Mar. Petrol. Geol. 26, 916–927. https://doi.org/10.1016/j.marpetgeo.2008.06.004

Rowe, H., Hughes, N., Robinson, K., 2012. The quantification and application of handheld energy-dispersive x-ray fluorescence (ED-XRF) in mudrock chemostratigraphy and geochemistry. Chem. Geol. 324–325, 122–131. https://doi.org/10.1016/j.chemgeo.2011.12.023

Rowe, H., Ruppel, S., Rimmer, S., Loucks, R., 2009. Core-based chemostratigraphy of the Barnett Shale, Permian Basin, Texas. Gulf Coast Assoc. Geol. Soc. Trans. 59, 675–686.

Rowe, H., Wang, X., Fan, B., Zhang, T., Ruppel, S.C., Milliken, K.L., Loucks, R., Shen, Y., Zhang, J., Liang, Q., Sivil, E., 2017. Chemostratigraphic insights into fluvio-lacustrine deposition, Yanchang Formation, Upper Triassic, Ordos Basin, China. Interpretation 5 (2), SF149–SF165. https://doi.org/10.1190/INT-2016-0121.1

Rowe, H.D., Loucks, R.G., Ruppel, S.C., Rimmer, S.M., 2008. Mississippian Barnett Formation, Fort Worth Basin, Texas: bulk geochemical inferences and Mo–TOC constraints on the severity of hydrographic restriction. Chem. Geol. 257 (1–2), 16–25. https://doi.org/10.1016/j.chemgeo.2008.08.006

Roychoudhury, A.N., Kostka, J.E., Van Cappellen, P., 2003. Pyritization: a palaeoenvironmental and redox proxy reevaluated: Estuarine. Coast. Shelf Sci. 57, 1183–1193. https://doi.org/10.1016/S0272-7714(03)00058-1

Sackett, W.M., 1989. The Marine Environment, A, in: Fritz, P., Fontes, J.C. (Eds.), Handbook of Environmental Isotope Geochemistry. Elsevier Scientific Pub. Co, Amsterdam, pp. 139–169.

Sageman, B.B., Lyons, T.W., 2003. Geochemistry of Fine-grained Sediments and Sedimentary Rocks. Treatise on Geochemistry 7, 407. https://doi.org/10.1016/B0-08-043751-6/07157-7

Sageman, B.B., Lyons, T.W., 2004. Geochemistry of fine-grained sediments and sedimentary rocks, in: Mackenzie, F.T. (Ed.), Sediments, Diagenesis, and Sedimentary Rocks: Treatise on Geochemistry, Second Edition, Volume 7. Elsevier Pergamon, Oxford, United Kingdom, pp. 116–148. https://doi.org/10.1016/B0-08-043751-6/07157-7

Sano, J.L., Ratcliffe, K.T., Spain, D.R., 2013. Chemostratigraphy of the Haynesville Shale, in: Hammes, U., Gales, J. (Eds.), Geology of the Hanyesville Gas Shale in East Texas and West Louisiana, U.S.A. pp. 137–154 American Association of Petroleum Geologists Memoir 105. http://dx.doi.org/10.1306/13441847M1053602

Savrda, C.E., Bottjer, D.J., 1989. Trace-fossil model for reconstructing oxygenation histories of ancient marine bottom waters: application to Upper Cretaceous Niobrara Formation,

Colorado. Palaeogeogr. Palaeoclimatol. Palaeoecol. 74 (1–2), 49–74. https://doi.org/10.1016/0031-0182(89)90019-9

Schelske, C.L., Hodell, D.A., 1995. Using carbon isotopes of bulk sedimentary organic matter to reconstruct the history of nutrient loading and eutrophication in Lake Erie. Limnol. Oceanogr. 40, 918–929. https://doi.org/10.4319/lo.1995.40.5.0918

Schieber, J., 1994. Evidence for high-energy events and shallow-water deposition in the Chattanooga Shale, Devonian, central Tennessee, USA. Sediment. Geol. 93 (3-4), 193–208. https://doi.org/10.1016/0037-0738(94)90005-1

Schieber, J., 1996. Early diagenetic silica deposition in algal cysts and spores; a source of sand in black shales? J. Sediment. Res. 66 (1), 175–183. https://doi.org/10.1306/D42682ED-2B26-11D7-8648000102C1865D

Schieber, J., 1998. Developing a sequence stratigraphic framework for the Late Devonian Chattanooga Shale of the southeastern USA: relevance for the Bakken Shale, in: Christopher, J.E., Gilboy, C.F., Paterson, D.F., Bends, S.L. (Eds.), Eighth International Williston Basin Symposium, pp. 58–68 Saskatchewan Geological Society Special Publication No. 13.

Schieber, J., 2003. Simple gifts and buried treasures–implications of finding bioturbation and erosion surfaces in black shales. The Sedimentary Record, 1(2), 4–8.

Schieber, J., 2013. SEM observations on ion-milled samples of devonian black shales from Indiana and New York: the petrographic context of multiple pore types, in: Camp, W., Diaz, E., Wawak, B. (Eds.), Electron Microscopy of Shale Hydrocarbon Reservoirs: AAPG Memoir 102, pp. 153–171. https://doi.org/10.1306/13391711M1023589

Schieber, J., Krinsley, D., Riciputi, L., 2000. Diagenetic origin of quartz silt in mudstones and implications for silica cycling. Nature 406 (6799), 981. https://doi.org/10.1038/35023143

Schieber, J., Lazar, R., Bohacs, K., Klimentidis, R., Dumitrescu, M., Ottman, J., 2016. An SEM study of porosity in the Eagle Ford Shale of Texas—pore types and porosity distribution in a depositional and sequence-stratigraphic context, in: Breyer, J.A. (Ed.), The Eagle Ford Shale: A Renaissance in U.S. Oil Production, AAPG Memoir 110, pp. 167–186. https://doi.org/10.1306/13541961M1103589

Scholz, F., Hensen, C., Noffke, A., Rohde, A., Liebetrau, V., Wallmann, K., 2011. Early diagenesis of redox-sensitive trace metals in the Peru upwelling area – response to ENSO-related oxygen fluctuations in the water column. Geochim. Cosmochim. Acta 75, 7257–7276. https://doi.org/10.1016/j.gca.2011.08.007

Scholz, F., Siebert, C., Dale, A.W., Frank, M., 2017. Intense molybdenum accumulation in sediments underneath a nitrogenous water column and implications for the reconstruction of paleo-redox conditions based on molybdenum isotopes. Geochim. Cosmochim. Acta 213, 400–417. https://doi.org/10.1016/j.gca.2017.06.048

Schönfeld, J., Kuhnt, W., Erdem, Z., Flögel, S., Glock, N., Aquit, M., Frank, M., Holbourn, A., 2015. Records of past mid-depth ventilation: Cretaceous ocean anoxic event 2 vs. Recent oxygen minimum zones. Biogeosciences 12 (4), 1169–1189. https://doi.org/10.5194/bg-12-1169-2015

Schunck, H., Lavik, G., Desai, D.K., Großkopf, T., Kalvelage, T., Löscher, C.R., Paulmier, A., Contreras, S., Siegel, H., Holtappels, M., Rosenstiel, P., Schilhabel, M.B., Graco, M., Schmitz, R.A., Kuypers, M.M.M., LaRoche, J., 2013. Giant Hydrogen Sulfide Plume in

the Oxygen Minimum Zone off Peru Supports Chemolithoautotrophy. PLoS ONE 8, e68661. https://doi.org/10.1371/journal.pone.0068661

Scotese, C.R., 2014. Atlas of Devonian Paleogeographic Maps, PALEOMAP Atlas for ArcGIS, volume 4, The Late Paleozoic, Maps 65-72, Molleweide Projection.

Scotese, C.R., McKerrow, W.S., 1990. Revised World maps and introduction. Geol. Soc. Lond. Mem. 12, 1–21. https://doi.org/10.1144/GSL.MEM.1990.012.01.01

Scott, C., Lyons, T.W., 2012. Contrasting molybdenum cycling and isotopic properties in euxinic versus non-euxinic sediments and sedimentary rocks: refining the paleoproxies. Chem. Geol. 324–325, 19–27. https://doi.org/10.1016/j.chemgeo.2012.05.012

Scott, C., Lyons, T.W., Bekker, A., Shen, Y.A., Poulton, S.W., Chu, X.L., & Anbar, A.D., 2008. Tracing the stepwise oxygenation of the Proterozoic ocean. Nature, 452(7186), 456–459. https://doi.org/10.1038/nature06811

Scott, C., Slack, J.F., Kelley, K.D., 2017. The hyper-enrichment of V and Zn in black shales of the Late Devonian-Early Mississippian Bakken Formation (USA). Chem. Geol. 452, 24–33. https://doi.org/10.1016/j.chemgeo.2017.01.026

Shanmugam, G., 1988. Origin, recognition, and importance of erosional unconformities in sedimentary basins, in: New Perspectives in Basin Analysis. Springer, New York, NY, pp. 83–108. https://doi.org/10.1007/978-1-4612-3788-4_5

Shen, J., Zhou, L., Feng, Q., Zhang, M., Lei, Y., Zhang, N., Yu, J., Gu, S., 2014. Paleoproductivity evolution across the Permian-Triassic boundary and quantitative calculation of primary productivity of black rock series from the Dalong Formation, South China. Sci. China Earth Sci. 57 (7), 1583–1594. https://doi.org/10.1007/s11430-013-4780-5

Sigurdsson, H., Leckie, R.M., Acton, G.D., 1997. Proceedings of the Ocean Drilling Program, Initial Reports. Coll. Stn. TX Ocean Drill. Program 165. https://doi.org/doi:10.2973/odp.proc.ir.165.1997

Sing, K.S.W., 1982. Reporting physisorption data for gas/solid systems with special reference to the determination of surface area and porosity. Pure Appl. Chem. 54 (11), 2201–2218. https://doi.org/10.1351/pac198254112201

Slatt, R.M., Rodriguez, N.D., 2012. Comparative sequence stratigraphy and organic geochemistry of gas shales: Commonality or coincidence? J. Nat. Gas Sci. Eng. 8, 68–84. https://doi.org/10.1016/j.jngse.2012.01.008

Slomp, C.P., Thomson, J., de Lange, G.J., 2002. Enhanced regeneration of phosphorus during formation of the most recent eastern Mediterranean sapropel (S1). Geochim. Cosmochim. Acta 66, 1171–1184. https://doi.org/10.1016/S0016-7037(01)00848-1

Smith, L.B., Schieber, J., Wilson, R.D., 2019. Shallow-water onlap model for the deposition of Devonian black shales in New York, USA. Geology 47 (3), 279–283. https://doi.org/10.1130/G45569.1

Snowdon, L.R., Brooks, P.W., Williams, G.K., Goodarzi, F., 1987. Correlation of the Canol Formation source rock with oil from norman wells. Org. Geochem. 11 (6), 529–548. https://doi.org/10.1016/0146-6380(87)90008-8

Somes, C.J., Schmittner, A., Galbraith, E.D., Lehmann, M.F., Altabet, M.A., Montoya, J.P., Letelier, R.M., Mix, A.C., Bourbonnais, A., Eby, M., 2010. Simulating the global distribution of nitrogen isotopes in the ocean. Glob. Biogeochem. Cycles 24. https://doi.org/10.1029/2009GB003767

Sondergeld, C.H., Rai, C.S., Curtis, M.E., 2013. Relationship between Organic Shale Microstructure and Hydrocarbon Generation. SPE Unconventional Resources Conference, The Woodlands, Texas, USA, p. 7. https://doi.org/10.2118/164540-MS

Stow, D.A.V., Reading, H.G., & Collinson J.D., 1996. Deep seas, in: Reading, H.G. (Ed.), Sedimentary Environments: Processes, Facies and Stratigraphy. Oxford: Blackwell Science, pp.395–453.

Suits, N.S., Wilkin, R.T., 1998. Pyrite formation in the water column and sediments of a meromictic lake. Geology 26 (12), 1099–1102. https://doi.org/10.1130/0091-7613(1998)026<1099:PFITWC>2.3.CO;2

Swift, D.J., 1975. Barrier-island genesis: evidence from the central Atlantic shelf, eastern USA. Sediment. Geol. 14 (1), 1–43. https://doi.org/10.1016/0037-0738(75)90015-9

Tang, Y., Huang, Y., Ellis, G.S., Wang, Y., Kralert, P.G., Gillaizeau, B., Ma, Q., Hwang, R., 2005. A kinetic model for thermally induced hydrogen and carbon isotope fractionation of individual n-alkanes in crude oil. Geochim. Cosmochim. Acta 69, 4505–4520. https://doi.org/10.1016/j.gca.2004.12.026

Tassonyi, E.J., 1969. Subsurface geology, lower Mackenzie River and Anderson River area, District of Mackenzie (Paper No. 68–25). Geological Survey of Canada.

Taylor, K.G., Macquaker, J.H.S., 2014. Diagenetic alterations in a silt-and clay-rich mudstone succession: an example from the Upper Cretaceous Mancos Shale of Utah, USA. Clay Miner. 49 (2), 213–227. https://doi.org/10.1180/claymin.2014.049.2.05

Taylor, S.R., McLennan, S.M., 1985. The continental crust; its composition and evolution; an examination of the geochemical record preserved in sedimentary rocks. Blackwell, Oxford, United Kingdom.

Terlaky, V., Fiess, K.M., and Rocheleau, J., 2020. Outcrop description, lithogeochemical, and source-rock characterisation of the Devonian Horn River Group at the Arctic Red River East and Flyaway Creek outcrops – NTS 106F and 106G, Northwest Territories; Northwest Territories Geological Survey, NWT Open Report 2019-004, 54 pages and appendices.

Terlaky, V., Fiess, K.M., Rocheleau, J.M., 2020. Outcrop description, lithogeochemical, and source-rock characterisation of the Devonian Horn River Group at the Arctic Red River East and Flyaway Creek outcrops – NTS 106F and 106G, Northwest Territories (No. NWT Open Report 2019-004).

Thomson, J., Higgs, N.C., Croudace, I.W., Colley, S., Hydes, D.J., 1993. Redox zonation of elements at an oxic/post-oxic boundary in deep-sea sediments. Geochim. Cosmochim. Acta 57 (3), 579–595. http://dx.doi.org/10.1016/0016-7037(93)90369-8

Thomson, J., Higgs, N.C., Wilson, T.R.S., Croudace, I.W., De Lange, G.J., Van Santvoort, P.J.M., 1995. Redistribution and geochemical behaviour of redox-sensitive elements around S1, the most recent eastern Mediterranean sapropel. Geochim. Cosmochim. Acta 59 (17), 3487–3501. https://doi.org/10.1016/0016-7037(95)00232-O

Thomson, J., Jarvis, I., Green, D.R., Green, D., 1998. Oxidation fronts in Madeira Abyssal Plain turbidites: persistence of early diagenetic trace-element enrichments during burial, site 9501, in: Weaver, P.P.E., Schmincke, H.-U., Duffield, W. (Eds.), Proceedings of the Ocean Drilling Program, Scientific Results. Vol. 157. pp. 559–571.

Thunell, R.C., Sigman, D.M., Muller-Karger, F., Astor, Y., Varela, R., 2004. Nitrogen isotope dynamics of the Cariaco Basin, Venezuela. Glob. Biogeochem. Cycles 18. https://doi.org/10.1029/2003GB002185

Tissot, B.P., Welte, D.H., 1984. Petroleum Formation and Occurrence. Springer-Verlag, Berlin, p. 699. https://doi.org/10.1007/978-3-642-87813-8

Tissot, B.P., Pelet, R., Ungerer, PH., 1987. Thermal History of Sedimentary Basins, Maturation Indices, and Kinetics of Oil and Gas Generation1. AAPG Bull. 71, 1445–1466. https://doi.org/10.1306/703C80E7-1707-11D7-8645000102C1865D

Tocqué, E., Behar, F., Budzinski, H., Lorant, F., 2005. Carbon isotopic balance of kerogen pyrolysis effluents in a closed system. Org. Geochem. 36, 893–905. https://doi.org/10.1016/j.orggeochem.2005.01.007

Tourtelot, H.A., 1979. Black shale—its deposition and diagenesis. Clays and Clay Miner., 27(5), 313–321. https://doi.org/10.1346/CCMN.1979.0270501

Tribovillard, N., Algeo, T.J., Lyons, T., Riboulleau, A., 2006. Trace metals as paleoredox and paleoproductivity proxies: an update. Chem. Geol. 232 (1–2), 12–32. https://doi.org/10.1016/j.chemgeo.2006.02.012

Turner, B.W., Molinares-Blanco, C.E., Slatt, R.M., 2015. Chemostratigraphic, palynostratigraphic, and sequence stratigraphic analysis of the Woodford Shale, Wyche Farm Quarry, Pontotoc County, Oklahoma. Interpretation 3 (1), SH1–SH9. https://doi.org/10.1190/INT-2014-0089.1

Turner, B.W., Slatt, R.M., 2016. Assessing bottom water anoxia within the Late Devonian Woodford Shale in the Arkoma Basin, southern Oklahoma. Mar. Pet. Geol. 78, 536–546. https://doi.org/10.1016/j.marpetgeo.2016.10.009

Turner, B.W., Tréanton, J.A., Slatt, R.M., 2016. The use of chemostratigraphy to refine ambiguous sequence stratigraphic correlations in marine mudrocks. An example from the

Woodford Shale, Oklahoma, USA. J. Geol. Soc. 173, 854–868. http://dx.doi.org/10.1144/jgs2015-125

Turner, B.W., Tréanton, J.A., Slatt, R.M., 2016. The use of chemostratigraphy to refine ambiguous sequence stratigraphic correlations in marine mudrocks. An example from the Woodford Shale, Oklahoma, USA. J. Geol. Soc. 173, 854–868. https://doi.org/10.1144/jgs2015-125

Turner, B.W., Tréanton, J.A., Slatt, R.M., 2016. The use of chemostratigraphy to refine ambiguous sequence stratigraphic correlations in marine mudrocks. An example from the Woodford Shale, Oklahoma, USA. J. Geol. Soc. 173, 854–868. https://doi.org/10.1144/jgs2015-125

Tyson, R.V., Pearson, T.H., 1991. Modern and ancient continental shelf anoxia: an overview. Geol. Soc. Lond., Spec. Publ. 58 (1), 1–24. http://dx.doi.org/10.1144/GSL.SP.1991.058.01.01

Van der Weijden, C.H., 2002. Pitfalls of normalization of marine geochemical data using a common divisor. Mar. Geol. 184, 167–187. https://doi.org/10.1016/S0025-3227(01)00297-3

Van Wagoner, J.C., Posamentier, H.W., Mitchum, R.M.J., Vail, P.R., Sarg, J.F., Loutit, T.S., Hardenbol, J., 1988. An overview of the fundamentals of sequence stratigraphy and key definitions, in: Wilgus, C.K., Hastings, B.S., Kendall, C.G.S., Posamentier, H.W., Ross, C.A., Van Wagoner, J.C. (Eds.), Sea Level Changes–An Integrated Approach, pp. 39–45 SEPM (Society for Sedimentary Geology) Special Publication 42. https://doi.org/10.1016/S0025-3227(01)00297-3

Ver Straeten, C.A., Brett, C.E., Sageman, B.B., 2011. Mudrock sequence stratigraphy: A multi-proxy (sedimentological, paleobiological and geochemical) approach, Devonian Appalachian Basin. Palaeogeogr. Palaeoclimat. Palaeoecol. 304 (1–2), 54–73. https://doi.org/10.1016/j.palaeo.2010.10.010

Voss, M., Deutsch, B., Elmgren, R., Humborg, C., Kuuppo, P., Pastuszak, M., Rolff, C., Schulte, U., 2006. Source identification of nitrate by means of isotopic tracers in the Baltic Sea catchments. Biogeosciences 3, 663–676. https://doi.org/10.5194/bg-3-663-2006

Wada, E., Kabaya, Y., Tsuru, K., Ishiwatari, R., 1990. 13C and 15N abundance of sedimentary organic matter in estuarine areas of Tokyo Bay, Japan. Mass Spectrosc. 38, 307–318.

Walliser, O.H., 1996. Global Events in the Devonian and Carboniferous, in: Walliser, O.H. (Ed.), Global Events and Event Stratigraphy in the Phanerozoic. Springer Berlin Heidelberg, pp. 225–250.

Wang, F., Guan, J., Feng, W., Bao, L., 2013. Evolution of Overmature Marine Shale Porosity and Implication to the Free Gas, vol. 40. Petroleum Exploration and Development, pp. 819–824. https://doi.org/10.1016/S1876-3804(13)60111-1

Wang, W.-L., Moore, J.K., Martiny, A.C., Primeau, F.W., 2019. Convergent estimates of marine nitrogen fixation. Nature 566, 205–211. https://doi.org/10.1038/s41586-019-0911-2

Wanty, R.B., Goldhaber, M.B., 1992. Thermodynamics and kinetics of reactions involving vanadium in natural systems: accumulation of vanadium in sedimentary rocks. Geochim. Cosmochim. Acta 56 (4), 1471–1483. https://doi.org/10.1016/0016-7037(92)90217-7

Ward, B.A., Dutkiewicz, S., Moore, C.M., Follows, M.J., 2013. Iron, phosphorus, and nitrogen supply ratios define the biogeography of nitrogen fixation. Limnol. Oceanogr. 58, 2059–2075. https://doi.org/10.4319/lo.2013.58.6.2059

Wedepohl, K.H., 1971. Environmental influences on the chemical composition of shales and clays. Phys. Chem. Earth 8, 307–333. https://doi.org/10.1016/0079-1946(71)90020-6

Wehausen, R., Brumsack, H.-J., 1999. Cyclic variations in the chemical composition of eastern Mediterranean Pliocene sediments: a key for understanding sapropel formation. Mar. Geol. 153, 161–176. https://doi.org/10.1016/S0025-3227(98)00083-8

Wignall, P.B., 1994. Black shales (No. 30). Oxford: Clarendon Press.

Wignall, P.B., Newton, R., 1998. Pyrite framboid diameter as a measure of oxygen deficiency in ancient mudrocks. Am. J. Sci. 298, 537–552. https://doi.org/10.2475/ajs.298.7.537

Wignall, P.B., Twitchett, R.J., 1996. Oceanic anoxia and the end Permian mass extinction. Science 272 (5265), 1155–1158. https://doi.org/10.1126/science.272.5265.1155

Wilde, P., Quinby-Hunt, M.S., Erdtmann, B.D., 1996. The whole-rock cerium anomaly: a potential indicator of eustatic sea-level changes in shales of the anoxic facies. Sediment. Geol. 101 (1–2), 43–53. https://doi.org/10.1016/0037-0738(95)00020-8

Williams, C.J., Hesselbo, S.P., Jenkyns, H.C., Morgans-Bell, H.S., 2001. Quartz silt in mudrocks as a key to sequence stratigraphy (Kimmeridge Clay Formation, Late Jurassic, Wessex Basin, UK). Terra Nova 13, 449–455. https://doi.org/10.1046/j.1365-3121.2001.00378.x

Williams, L.A., Crerar, D.A., 1985. Silica diagenesis; II, General mechanisms. J. Sediment. Res. 55 (3), 312–321. https://doi.org/10.1306/212F86B1-2B24-11D7-8648000102C1865D

Williams, L.B., Ferrell, R.E., Hutcheon, I., Bakel, A.J., Walsh, M.M., Krouse, H.R., 1995. Nitrogen isotope geochemistry of organic matter and minerals during diagenesis and hydrocarbon migration. Geochim. Cosmochim. Acta 59, 765–779. https://doi.org/10.1016/0016-7037(95)00005-K

Wilson, G.P., Lamb, A.L., Leng, M.J., Gonzalez, S., Huddart, D., 2005. Variability of organic δ13C and C/N in the Mersey Estuary, U.K. and its implications for sea-level reconstruction studies. Estuar. Coast. and Shelf Sci. 64, 685–698. https://doi.org/10.1016/j.ecss.2005.04.003

Wilson, R.D., Schieber, J., 2015. Sedimentary facies and depositional environment of the Middle Devonian Geneseo Formation of New York, USA. J. Sediment. Res. 85 (11), 1393–1415. https://doi.org/10.2110/jsr.2015.88

Wyrtki, K., 1962. The oxygen minima in relation to ocean circulation. Deep-Sea Res. Oceanogr. Abstr. 9 (1-2), 11–23. https://doi.org/10.1016/0011-7471(62)90243-7

Yamashita, Y., Takahashi, Y., Haba, H., Enomoto, S., Shimizu, H., 2007. Comparison of reductive accumulation of Re and Os in seawater–sediment systems. Geochim. Cosmochim. Acta 71 (14), 3458–3475. https://doi.org/10.1016/j.gca.2007.05.003

Yang, R., He, S., Yi, J., Hu, Q., 2016. Nano-scale pore structure and fractal dimension of organic-rich Wufeng-Longmaxi shale from Jiaoshiba area, Sichuan Basin: investigations using FE-SEM, gas adsorption and helium pycnometry. Mar. Petrol. Geol. 70, 27–45. https://doi.org/10.1016/j.marpetgeo.2015.11.019

Yang, Y., Aplin, A.C., 2007. Permeability and petrophysical properties of 30 natural mudstones. J. Geophys. Res. Solid Earth 112, 1–14. https://doi.org/10.1029/2005JB004243

Yassin, M.R., Begum, M., Dehghanpour, H., 2017. Organic shale wettability and its relationship to other petrophysical properties: a Duvernay case study. Int. J. Coal Geol. 169, 74–91. https://doi.org/10.1016/j.coal.2016.11.015

Yassin, M.R., Dehghanpour, H., Begum, M., Dunn, L., 2018. Evaluation of imbibition oil recovery in the Duvernay Formation. Soc. Petrol. Eng. 21 (2), 257–272. https://doi.org/10.2118/185065-PA

Yose, L.A., Brown, S., Davis, T.L., Eiben, T., Kompanik, G.S., Maxwell, S.R., 2001. 3-D geologic model of a fractured carbonate reservoir, Norman Wells Field, NWT, Canada. Bull. Can. Pet. Geol. 49, 86–116. https://doi.org/10.2113/49.1.86

Zambito, J.J., Brett, C.E., Baird, G.C., 2012. The Late Middle Devonian (Givetian) Global Taghanic Biocrisis in Its Type Area (Northern Appalachian Basin): Geologically Rapid Faunal Transitions Driven by Global and Local Environmental Changes, in: Talent, J.A. (Ed.), Earth and Life: Global Biodiversity, Extinction Intervals and Biogeographic Perturbations through Time. Springer Netherlands.

Zhang, J.-Z., Millero, F.J., 1993. The chemistry of anoxic waters in the Cariaco Trench. Deep Sea Res. Part Oceanogr. Res. Pap. 40, 1023–1041. https://doi.org/10.1016/0967-0637(93)90088-K

Zhang, J., Zeng, Y., Slatt, R., 2019. XRF (X-ray fluorescence) applied to characterization of unconventional Woodford Shale (Devonian, USA) lateral well heterogeneity. Fuel 254, 115565. https://doi.org/10.1016/j.fuel.2019.05.148

Zhang, X., Joachimski, M.M., Over, D.J., Ma, K., Huang, C., Gong, Y., 2019. Late Devonian carbon isotope chemostratigraphy: A new record from the offshore facies of South China. Glob. Planet. Change 182, 103024. https://doi.org/10.1016/j.gloplacha.2019.103024

Zhang, X., Sigman, D.M., Morel, F.M.M., Kraepiel, A.M.L., 2014. Nitrogen isotope fractionation by alternative nitrogenases and past ocean anoxia. Proc Natl Acad Sci USA 111, 4782–4787. https://doi.org/10.1073/pnas.1402976111

Zhou, C., Jiang, S.Y., 2009. Palaeoceanographic redox environments for the lower Cambrian Hetang Formation in South China: evidence from pyrite framboids, redox sensitive trace elements, and sponge biota occurrence. Palaeogeogr. Palaeoclimatol. Palaeoecol. 271 (3–4), 279–286. https://doi.org/10.1016/j.palaeo.2008.10.024

Zhou, L., Su, J., Huang, J., Yan, J., Xie, X., Gao, S., Dai, M., 2011. A new paleoenvironmental index for anoxic events—Mo isotopes in black shales from Upper Yangtze marine sediments. Sci. China Earth Sci., 54(7), 1024-1033. https://doi.org/10.1007/s11430-011-4188-z

Appendix 1. Supplementary Information for Chapter 2

SI Table 1.1 Total organic carbon (TOC) for samples from the Husky Little Bear N-09 and ConocoPhillips Mirror Lake N-20 cores.

Core	Group	Formation	Member	Depth (m)	TOC (wt. %)
N-20	Undefined	Imperial	Undefined	1900.44	1.31
N-20	Undefined	Imperial	Undefined	1909.45	2.63
N-20	Undefined	Imperial	Undefined	1918.86	1.78
N-20	Undefined	Imperial	Undefined	1925.86	1.88
N-20	Undefined	Imperial	Undefined	1927.58	1.57
N-20	Undefined	Imperial	Undefined	1936.02	2.88
N-20	Undefined	Imperial	Undefined	1936.71	2.51
N-20	Undefined	Imperial	Undefined	1942.71	2.11
N-20	Undefined	Imperial	Undefined	1945.86	1.60
N-20	Undefined	Imperial	Undefined	1947.07	1.29
N-20	Undefined	Imperial	Undefined	1954.76	1.46
N-20	Undefined	Imperial	Undefined	1955.08	1.66
N-20	Undefined	Imperial	Undefined	1963.07	1.69
N-20	Undefined	Imperial	Undefined	1963.66	2.48
N-20	Undefined	Imperial	Undefined	1966.11	2.64
N-20	Undefined	Imperial	Undefined	1969.32	3.23
N-20	Undefined	Imperial	Undefined	1971.9	3.42
N-20	Undefined	Imperial	Undefined	1972.85	4.41
N-20	Horn River Group	Canol	Dodo Canyon	1976.04	5.18
N-20	Horn River Group	Canol	Dodo Canyon	1979.61	4.59
N-20	Horn River Group	Canol	Dodo Canyon	1981.17	5.07
N-20	Horn River Group	Canol	Dodo Canyon	1985.11	3.67
N-20	Horn River Group	Canol	Dodo Canyon	1990.32	4.16
N-20	Horn River Group	Canol	Dodo Canyon	1990.87	3.70

N-20	Horn River Group	Canol	Dodo Canyon	1993.99	3.73
N-20	Horn River Group	Canol	Dodo Canyon	1997.04	4.07
N-20	Horn River Group	Canol	Dodo Canyon	1999.85	3.38
N-20	Horn River Group	Canol	Dodo Canyon	2002.41	4.03
N-20	Horn River Group	Canol	Vermillion Creek	2004.69	4.61
N-20	Horn River Group	Canol	Vermillion Creek	2008.09	2.78
N-20	Horn River Group	Canol	Vermillion Creek	2010.67	3.45
N-20	Horn River Group	Canol	Vermillion Creek	2013.38	3.57
N-20	Horn River Group	Canol	Vermillion Creek	2016.14	3.62
N-20	Horn River Group	Canol	Vermillion Creek	2017.76	4.26
N-20	Horn River Group	Canol	Vermillion Creek	2021.24	2.34
N-20	Horn River Group	Canol	Vermillion Creek	2025.4	4.14
N-20	Horn River Group	Canol	Vermillion Creek	2028	4.80
N-20	Horn River Group	Canol	Vermillion Creek	2030.05	4.81
N-20	Horn River Group	Canol	Vermillion Creek	2034.47	4.21
N-20	Horn River Group	Canol	Vermillion Creek	2035.67	4.39
N-20	Horn River Group	Canol	Vermillion Creek	2038.03	5.97
N-20	Horn River Group	Canol	Vermillion Creek	2040.17	7.46
N-20	Horn River Group	Canol	Vermillion Creek	2043.21	7.29
N-20	Horn River Group	Canol	Vermillion Creek	2044.85	6.69
N-20	Horn River Group	Canol	Vermillion Creek	2048.28	4.42
N-20	Horn River Group	Canol	Vermillion Creek	2051.31	6.22
N-20	Horn River Group	Hare Indian	Prohibition Creek	2053.85	6.14
N-20	Horn River Group	Hare Indian	Prohibition Creek	2055.44	5.85

N-20	Horn River Group	Hare Indian	Prohibition Creek	2059.02	5.19
N-20	Horn River Group	Hare Indian	Prohibition Creek	2062.38	5.02
N-20	Horn River Group	Hare Indian	Prohibition Creek	2063.73	4.05
N-20	Horn River Group	Hare Indian	Prohibition Creek	2067.98	1.55
N-20	Horn River Group	Hare Indian	Francis Creek	2071.52	3.81
N-20	Horn River Group	Hare Indian	Francis Creek	2074.3	3.04
N-20	Horn River Group	Hare Indian	Francis Creek	2078.8	4.19
N-20	Horn River Group	Hare Indian	Bluefish	2080.85	4.75
N-20	Horn River Group	Hare Indian	Bluefish	2086.94	2.26
N-20	Horn River Group	Hare Indian	Bluefish	2089.21	5.59
N-20	Horn River Group	Hare Indian	Bluefish	2091.08	0.69
N-20	Horn River Group	Hare Indian	Bluefish	2097.36	0.17
N-20	Horn River Group	Hare Indian	Bluefish	2101.49	0.15
N-09	Undefined	Imperial	Undefined	1670.82	3.09
N-09	Undefined	Imperial	Undefined	1672.46	5.57
N-09	Undefined	Imperial	Undefined	1675.34	1.58
N-09	Undefined	Imperial	Undefined	1678.51	1.57
N-09	Undefined	Imperial	Undefined	1687.87	1.54
N-09	Horn River Group	Canol	Dodo Canyon	1697.31	2.93
N-09	Horn River Group	Canol	Dodo Canyon	1699.77	3.55
N-09	Horn River Group	Canol	Dodo Canyon	1701.91	5.48
N-09	Horn River Group	Canol	Dodo Canyon	1703.64	5.00
N-09	Horn River Group	Canol	Dodo Canyon	1705.7	4.21
N-09	Horn River Group	Canol	Dodo Canyon	1706.58	3.99
N-09	Horn River Group	Canol	Dodo Canyon	1707.49	6.31
N-09	Horn River Group	Canol	Dodo Canyon	1708.56	5.61
N-09	Horn River Group	Canol	Dodo Canyon	1711.23	5.22
N-09	Horn River Group	Canol	Dodo Canyon	1713.88	3.86
N-09	Horn River Group	Canol	Dodo Canyon	1717.17	3.86

N-09	Horn River Group	Canol	Dodo Canyon	1719.63	5.14
N-09	Horn River Group	Canol	Dodo Canyon	1722.36	6.48
N-09	Horn River Group	Canol	Dodo Canyon	1725.83	4.70
N-09	Horn River Group	Canol	Dodo Canyon	1728.62	3.98
N-09	Horn River Group	Canol	Dodo Canyon	1732.16	3.46
N-09	Horn River Group	Canol	Dodo Canyon	1734.54	4.43
N-09	Horn River Group	Canol	Dodo Canyon	1736.63	7.37
N-09	Horn River Group	Canol	Vermillion Creek	1740.78	4.10
N-09	Horn River Group	Canol	Vermillion Creek	1742.61	4.23
N-09	Horn River Group	Canol	Vermillion Creek	1745.06	3.43
N-09	Horn River Group	Canol	Vermillion Creek	1747.35	4.86
N-09	Horn River Group	Canol	Vermillion Creek	1749.21	3.92
N-09	Horn River Group	Canol	Vermillion Creek	1754.68	4.53
N-09	Horn River Group	Canol	Vermillion Creek	1757.59	7.58
N-09	Horn River Group	Canol	Vermillion Creek	1759.49	6.08
N-09	Horn River Group	Canol	Vermillion Creek	1761.5	6.63
N-09	Horn River Group	Canol	Vermillion Creek	1762.95	6.25
N-09	Horn River Group	Canol	Vermillion Creek	1767.52	5.19
N-09	Horn River Group	Canol	Vermillion Creek	1768.93	4.59
N-09	Horn River Group	Canol	Vermillion Creek	1772.19	8.63
N-09	Horn River Group	Canol	Vermillion Creek	1775.97	7.43
N-09	Horn River Group	Canol	Vermillion Creek	1777.48	7.73
N-09	Horn River Group	Canol	Vermillion Creek	1781.14	7.73
N-09	Horn River Group	Canol	Vermillion Creek	1784.14	6.16
N-09	Horn River Group	Canol	Vermillion Creek	1785.74	6.65

N-09	Horn River Group	Hare Indian	Prohibition Creek	1788.18	4.23
N-09	Horn River Group	Hare Indian	Prohibition Creek	1789.98	3.87
N-09	Horn River Group	Hare Indian	Prohibition Creek	1793.98	5.38
N-09	Horn River Group	Hare Indian	Prohibition Creek	1796.05	4.08
N-09	Horn River Group	Hare Indian	Prohibition Creek	1798.67	5.07
N-09	Horn River Group	Hare Indian	Prohibition Creek	1800.5	3.38
N-09	Horn River Group	Hare Indian	Prohibition Creek	1802.62	4.16
N-09	Horn River Group	Hare Indian	Francis Creek	1807.35	4.05
N-09	Horn River Group	Hare Indian	Francis Creek	1812.42	4.15
N-09	Horn River Group	Hare Indian	Bluefish	1813.76	2.43
N-09	Horn River Group	Hare Indian	Bluefish	1814.67	6.54
N-09	Horn River Group	Hare Indian	Bluefish	1816.92	2.26
N-09	Horn River Group	Hare Indian	Bluefish	1823.52	5.33
N-09	Horn River Group	Hare Indian	Bluefish	1826.95	5.67

SI Table 1.2 Vitrinite reflectance results with depth in both the N-09 and N-20 cores. Definitions: % Ro–percent reflectance in oil immersion.

Core	Group	Formation	Member	Sample Depth (m)	Vitrinite Reflectance (% Ro)
N-09	Horn River Group	Canol	Dodo Canyon	1738.45	1.02
N-09	Horn River Group	Canol	Vermillion Creek	1765.07	1.07
N-09	Horn River Group	Canol	Vermillion Creek	1779.04	1.29
N-09	Horn River Group	Hare Indian	Prohibition Creek	1805.38	1.06
N-09	Horn River Group	Hare Indian	Bluefish	1820	1.21
N-20	Undefined	Imperial	Undefined	1900.44	0.17
N-20	Undefined	Imperial	Undefined	1909.45	1.16
N-20	Undefined	Imperial	Undefined	1918.86	0.99
N-20	Undefined	Imperial	Undefined	1925.86	1.05
N-20	Undefined	Imperial	Undefined	1927.58	0.98
N-20	Undefined	Imperial	Undefined	1936.02	1.28
N-20	Undefined	Imperial	Undefined	1936.71	1.14
N-20	Undefined	Imperial	Undefined	1942.71	1.17
N-20	Undefined	Imperial	Undefined	1945.86	1.01
N-20	Undefined	Imperial	Undefined	1947.07	0.11
N-20	Undefined	Imperial	Undefined	1954.76	0.04
N-20	Undefined	Imperial	Undefined	1955.08	1.16
N-20	Undefined	Imperial	Undefined	1963.07	0.99
N-20	Undefined	Imperial	Undefined	1963.66	1.14
N-20	Undefined	Imperial	Undefined	1966.11	1.26
N-20	Undefined	Imperial	Undefined	1969.32	1.26
N-20	Undefined	Imperial	Undefined	1971.9	1.28
N-20	Undefined	Imperial	Undefined	1972.85	1.34
N-20	Horn River Group	Canol	Dodo Canyon	1976.04	1.23
N-20	Horn River Group	Canol	Dodo Canyon	1979.61	1.34
N-20	Horn River Group	Canol	Dodo Canyon	1981.17	1.25
N-20	Horn River Group	Canol	Dodo Canyon	1985.11	1.25

N-20	Horn River Group	Canol	Dodo Canyon	1990.32	1.34
N-20	Horn River Group	Canol	Dodo Canyon	1990.87	1.26
N-20	Horn River Group	Canol	Dodo Canyon	1993.99	1.32
N-20	Horn River Group	Canol	Dodo Canyon	1997.04	1.32
N-20	Horn River Group	Canol	Dodo Canyon	1999.85	1.46
N-20	Horn River Group	Canol	Dodo Canyon	2002.41	1.32
N-20	Horn River Group	Canol	Vermillion Creek	2004.69	1.34
N-20	Horn River Group	Canol	Vermillion Creek	2008.09	1.34
N-20	Horn River Group	Canol	Vermillion Creek	2010.67	1.32
N-20	Horn River Group	Canol	Vermillion Creek	2013.38	1.28
N-20	Horn River Group	Canol	Vermillion Creek	2016.14	1.3
N-20	Horn River Group	Canol	Vermillion Creek	2017.76	1.28
N-20	Horn River Group	Canol	Vermillion Creek	2021.24	1.3
N-20	Horn River Group	Canol	Vermillion Creek	2025.4	1.34
N-20	Horn River Group	Canol	Vermillion Creek	2028	1.34
N-20	Horn River Group	Canol	Vermillion Creek	2030.05	1.34
N-20	Horn River Group	Canol	Vermillion Creek	2034.47	1.39
N-20	Horn River Group	Canol	Vermillion Creek	2035.67	1.25
N-20	Horn River Group	Canol	Vermillion Creek	2038.03	1.44
N-20	Horn River Group	Canol	Vermillion Creek	2040.17	1.34
N-20	Horn River Group	Canol	Vermillion Creek	2043.21	1.39
N-20	Horn River Group	Canol	Vermillion Creek	2044.85	1.34
N-20	Horn River Group	Canol	Vermillion Creek	2048.28	1.34

N-20	Horn River Group	Hare Indian	Prohibition Creek	2051.31	1.34
N-20	Horn River Group	Hare Indian	Prohibition Creek	2053.85	1.43
N-20	Horn River Group	Hare Indian	Prohibition Creek	2055.44	1.39
N-20	Horn River Group	Hare Indian	Prohibition Creek	2059.02	1.3
N-20	Horn River Group	Hare Indian	Prohibition Creek	2062.38	1.37
N-20	Horn River Group	Hare Indian	Prohibition Creek	2063.73	1.28
N-20	Horn River Group	Hare Indian	Prohibition Creek	2067.98	0.2
N-20	Horn River Group	Hare Indian	Prohibition Creek	2071.52	1.3
N-20	Horn River Group	Hare Indian	Francis Creek	2074.3	1.28
N-20	Horn River Group	Hare Indian	Francis Creek	2078.8	1.41
N-20	Horn River Group	Hare Indian	Bluefish	2080.85	1.35
N-20	Horn River Group	Hare Indian	Bluefish	2086.94	1.41
N-20	Horn River Group	Hare Indian	Bluefish	2089.21	1.44
N-20	Horn River Group	Hare Indian	Bluefish	2091.08	0.87
N-20	Horn River Group	Hare Indian	Bluefish	2097.36	0.22
N-20	Horn River Group	Hare Indian	Bluefish	2101.49	0.24

Appendix 2. Supplementary Information for Chapter 3

Extended Methods

a. Compositional Analysis

X-ray diffraction (XRD) analysis on 59 core samples was performed by Core Laboratories Canada. Each sample was prepared using a mortar and pestle before isopropyl alcohol was added

to 5 g of the resulting powder for further pulverization in a McCrone micronizing mill. Samples were then dried and packed into aluminum sample holders for whole-rock mounts. Samples were analyzed using a Philips automated powder diffractometer with a copper source (40 kV and 40 mA) using an angular range of 2–60º 2**θ** and a scan rate of 1º/min for whole-rock samples and an angular range of 2–50º 2**θ** at a rate of 1.5º/minute for clay samples. Semi-quantitative determination of mineral abundance was performed using integrated peak areas and empirical reference intensity ratio factors.

Total Organic Carbon (TOC) measurements were collected for 55 samples with a LECO analyzer by Core Laboratories Canada. Sample preparation involved sample pulverization to approximately 100 μm, followed by an extraction using organic solvents to remove potential contamination by oil-based drilling mud. To achieve this, an extraction was first performed using an azeotrophic mixture of chloroform-methanol for 24 hours, and next, an azeotrophic mixture of dicholoromethane-methanol was used for Soxhlet extraction over a 48-hour period. Once extractions were complete, samples were dried in a low-temperature friction air oven. The final step in sample preparation involved sample treatment with hydrochloric acid (HCl) to remove inorganic carbon present in carbonates. In this process, samples were immersed in HCl for 12–24 hours with periodic stirring and upon completion, the samples were rinsed with distilled water and dried. To determine TOC, prepared samples were combusted with a LECO SC-632 analyzer at 1400 ºC that measured the amount of CO_2 produced with an infrared cell. To monitor analytical precision, selected samples were analyzed in duplicate with precision usually better than ±0.1 wt. %.

b. Thermal Maturity

A description of the organic molecule used to measure vitrinite reflectance for each of the seven samples analyzed can be found in SI Table 2.1.

SI Table 2.1 Organic molecule used to measure vitrinite reflectance.

Sample depth (m)	Organic molecule used.
1692.58	Vitrinite.
1710.08	Vitrinite.
1738.45	Bitumen.
1765.07	Graptolite.
1779.04	Vitrinite.
1805.38	Graptolite.
1820.00	Vitrinite.

c. Porosimetry

Porosity was measured by Core Laboratories Canada for 64 samples following the Gas Research Institute (GRI) methodology (e.g., Luffel & Guidry, 1993). The GRI porosity measurement was completed in 2012, shortly after the core was extracted. This technique measures the bulk volume of a preserved 1" x 1" x 1" whole core piece through Hg immersion. In 2012, the fissility of the core was lower than at present and extracting the necessary core pieces did not pose a problem. Next, samples were crushed (20/35 US mesh size) and subjected to fluid extraction following the Dean Stark method and vacuum oven drying at 105ºC, followed by grain volume measurement with an Ultrapore-300 helium gas expansion porosimeter. Bulk porosity is calculated with Equation 1, where V_b is bulk volume, and V_g represents grain volume:

$$\phi = (V_b - V_g)/V_b \quad \text{(Eq. SI 2.1)}$$

Ten additional core samples were selected for low-pressure N_2 adsorption measurements (Table 1). Sample preparation consisted of Dean Stark solvent extraction using a mixture of methanol (23 wt. %), acetone (30 wt. %), and chloroform (47 wt. %) and then oven drying at 130 ºC for approximately 16 hours. Following this, core pieces were outgassed for 2–3 hours and then enveloped in pressurized nitrogen for 7–8 hours. Nitrogen adsorption and desorption was quantified using a Quantachrome Autosorb-IQ instrument at a temperature of 77 K. Equivalent surface areas were determined using the Brunauer–Emmett–Teller (BET) method (Brunauer et al., 1938) and pore size distributions were calculated following Density Functional Theory (DFT; e.g., Olivier et al., 1994).

d. Sampling Strategy

Two representative samples from each of the five lithofacies were selected for SEM and N_2 adsorption. The GRI porosity, TOC, XRD, vitrinite, and Rock-Eval pyrolysis datasets were donated to us by the company Husky Energy. For GRI porosity, TOC, XRD, the company chose to sample the Horn River Group at an interval typically ranging from approximately 1–3 m, to cover a range of core facies and petrophysical responses. Sample depths for vitrinite reflectance and rock-eval were selected by Husky Energy throughout the core, with a lower sampling interval typically ranging from 10 – 30 m.

Extended Results

a. Nitrogen Adsorption and Desorption Isotherms

Adsorption hysteresis describes a deviation of the adsorption isotherm from the desorption isotherm (Sing, 1982). The International Union of Pure and Applied Chemistry recognizes four types of hysteresis loops: type H1 is observed in materials with cylindrical-like pores or fairly uniform spherical pores (SI Fig. 2.1 A), type H2 is associated with disordered materials in which pore shape is not well-defined (SI Fig. 2.1 B), hysteresis type H3 is typically indicative of slit-shaped pores (SI Fig. 2.1 C), and materials with narrow slit-shaped pores often produce hysteresis type H4 (SI Fig. 2.1 H) (Alothman, 2012). The adsorption and desorption isotherms for all ten samples (Fig. 3.16) show a similar isotherm shape to hysteresis loop type H3 (SI Fig. 2.1 C).

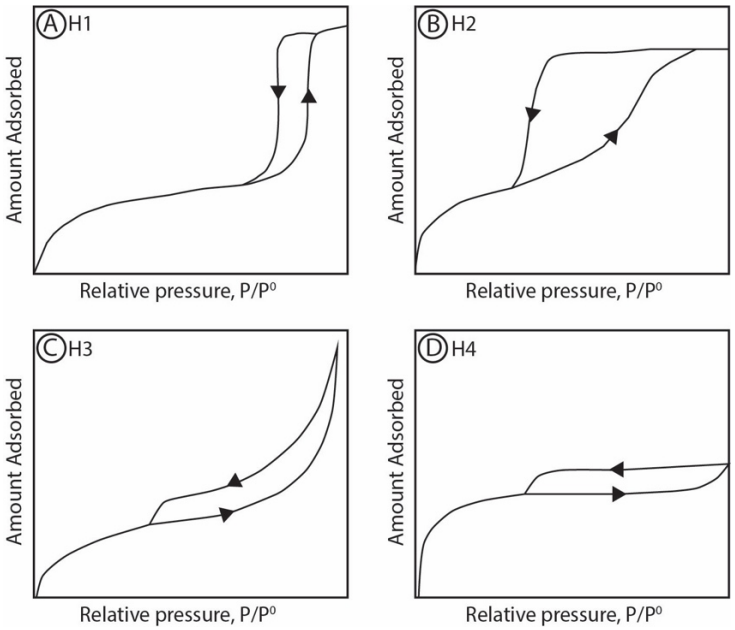

SI Figure 2.1 The four types of hysteresis loops recognized by the International Union of Pure and Applied Chemistry (IUPAC) after (Alothman, 2012). (A) Type H1 is observed in materials with cylindrical-like pores or fairly uniform spherical pores, (B) type H2 is associated with disordered materials in which pore shape is not well-defined, (C) hysteresis type H3 is typically

indicative of slit-shaped pores, and (D) materials with narrow slit-shaped pores often produce hysteresis type H4. Acronyms and definitions: STP – standard temperature and pressure, p^o – saturation pressure of N_2 at 77 K.

Appendix 3. Supplementary Information for Chapter 5

SI Table 3.1 Locations coordinates of all outcrops and wells

Well/Outcrop Name	Location
MGM Shell East Mackay I-78 well	64°47'42.00" N, 125°43'19.20" W
Husky Little Bear N-09 well	64°58’55.2" N, 126°31’20.2" W
ConocoPhillips Mirror Lake N-20 well	64°59'40.55" N, 126°48'14.83" W
ConocoPhillips Loon Creek O-06 well	65°05’51.50" N, 127°00’30.70" W
Carcajou River outcrop	64°46'35.72" N, 126°49'28.56" W
Dodo Creek outcrop	65° 0'7.20" N, 127°20'45.60" W
Powell Creek outcrop	65°16'37.20" N,128°46'26.40" W
Turnabout Creek outcrop	65°19'30.00" N, 129°38'45.60" W
Rumbly Creek outcrop	65°17'27.57" N, 131°18'32.90" W

SI Table 3.2 Summary statistics from X-ray fluorescence (XRF) data.

Core/Outcrop	Element	Mean (ppm)	Standard Deviation (ppm)	Coefficient of Variation (%)
I-78 Core	Al	54839	22836	42
N-09 Core	Al	51619	28410	55
N-20 Core	Al	68352	36638	54

O-06 Core	Al	52498	24336	46
Caracjou River Outcrop	Al	45565	19323	42
Dodo Creek Outcrop	Al	32946	13282	40
Powell Creek Outcrop	Al	39602	26000	66
Mountain River Outcrop	Al	44342	24720	56
Rumbly Creek	Al	32910	8187	25
Maximum				66
Minimum				25
Average				47

I-78 Core	Mo	44	29	65
N-09 Core	Mo	41	24	60
N-20 Core	Mo	31	24	77
O-06 Core	Mo	20	16	79
Caracjou River Outcrop	Mo	26	12	45
Dodo Creek Outcrop	Mo	30	13	42
Powell Creek Outcrop	Mo	10	18	174
Mountain River Outcrop	Mo	25	25	103
Rumbly Creek	Mo	24	8	35
Maximum				174
Minimum				35
Average				76

I-78 Core	Si	337135	101585	30
N-09 Core	Si	358215	88645	25
N-20 Core	Si	390654	97586	25
O-06 Core	Si	306722	103255	34
Caracjou River Outcrop	Si	368250	54133	15
Dodo Creek Outcrop	Si	382727	55928	15
Powell Creek Outcrop	Si	245226	132647	54
Mountain River Outcrop	Si	293596	118123	40
Rumbly Creek	Si	386803	48139	12
Maximum				54
Minimum				12
Average				28
I-78 Core	Ti	2356	944	40
N-09 Core	Ti	2220	1104	50
N-20 Core	Ti	2736	1353	49
O-06 Core	Ti	1358	663	49
Caracjou River Outcrop	Ti	2437	976	40
Dodo Creek Outcrop	Ti	1756	760	43
Powell Creek Outcrop	Ti	2438	1801	74
Mountain River Outcrop	Ti	2295	1232	54

Rumbly Creek	Ti	1938	544	28
Maximum				74
Minimum				28
Average				47
I-78 Core	V	324	219	68
N-09 Core	V	321	202	63
N-20 Core	V	362	197	54
O-06 Core	V	246	161	65
Caracjou River Outcrop	V	404	217	54
Dodo Creek Outcrop	V	331	156	47
Powell Creek Outcrop	V	257	315	122
Mountain River Outcrop	V	319	268	84
Rumbly Creek	V	211	79	37
Maximum				122
Minimum				37
Average				66